UTS UNIVERSITY OF TECHNOLOGY SYDNEY

Characterisation of Chronic Obstructive Pulmonary Disease Using Advanced Ventilation Imaging

by Edward Jeagal

Thesis submitted in fulfilment of the requirements for the degree of

Doctor of Philosophy

under the supervision of Distinguished Professor Brian Oliver

University of Technology Sydney
Faculty of Science

October 2024

Certificate of original authorship

I, Edward Jeagal, declare that this thesis is submitted in fulfilment of the requirements for the award of Doctor of Philosophy, in the Faculty of Science at the University of Technology Sydney.

This thesis is wholly my own work unless otherwise referenced or acknowledged. In addition, I certify that all information sources and literature used are indicated in the thesis. This document has not been submitted for qualifications at any other academic institution.

This research was supported by an Australian Government Research Training Program (RTP) Scholarship doi.org/10.82133/C42F-K220.

Signature: Production Note:
Signature removed prior to publication.

Date: 07/04/2026

Table of contents

Declaration ii

Acknowledgements iv

Glossary of abbreviations v

Thesis abstract vii

Chapter 1 – Introduction and Literature Review

1.1 Thesis Overview & Chapter Descriptions 2

1.2 What is chronic obstructive pulmonary disease 5

1.3 The burden of chronic obstructive pulmonary disease 5

1.4 Disease management 7

1.5 Assessing the severity of a heterogeneous disease 11

1.6 A small airways disease and looking beyond spirometry 16

1.7 Phenotyping a heterogenous disease 20

1.8 Quantitative computed tomography imaging analysis in COPD 26

1.9 Quantitative three-dimensional ventilation single photon emission computed tomography analysis in COPD 40

1.10 Inadequacies with current ventilation imaging analysis methods for single photon emission computed tomography 47

1.11 Quantitative three-dimensional magnetic resonance imaging analysis in COPD 53

1.12 Ventilation imaging & bronchodilator responsiveness in COPD 56

1.13 Airway hyperresponsiveness in COPD 60

1.14 Summary and aims of the thesis 63

1.15 References 66

Chapter 2 – Comparison of threshold techniques for determining ventilation using Single Photon Emission Computed Tomography

2.1 Abstract 84

2.2 Introduction 85

2.3 Methods 88

2.3.1 Lung phantom models 88

2.3.2 COPD participants 93

2.3.3 VSPECT/CT imaging 93

2.3.4 Imaging reconstruction and registration 94

2.3.5 Imaging analyses 95

2.3.6 Statistical analyses 101

2.4 Results 103

2.4.1 Validation of parameters for curve-fitting method 103

2.4.2 CT and true volume comparison 105

2.4.3 Comparison of accuracy of threshold methods 107

2.4.4 Effect of non-ventilation on threshold methods 110

2.4.5 Effect of ‘hot spots’ on thresholds 112

2.4.6 Applying thresholds on human lungs 114

2.5 Discussion 119

2.5.1 15% of maximum activity value threshold method 119

2.5.2 50% of the mean of 5 – 80% of maximum activity value threshold method 121

2.5.3 Otsu’s method 123

2.5.4 Curve-fitting threshold method 125

2.5.5 Threshold methods in human scans 127

2.5.6 Size dependent errors in threshold methods 128
2.5.7 Limitations 128
2.5.8 Conclusion 131
2.6 References 136

Chapter 3 – Relationships between non-ventilated volume and ‘hot spots' from Single Photon Emission Computed Tomography imaging and baseline lung function in COPD

3.1 Abstract 135
3.2 Introduction 136
3.3 Methods 138
3.3.1 Participants and study design 138
3.3.2 Lung function testing 139
3.3.3 Ventilation imaging 140
3.3.4 Image reconstruction and registration 141
3.3.5 Imaging analysis 142
3.3.6 Statistical analysis 143
3.4 Results 147
3.4.1 Participant demographics and lung function 147
3.4.2 Relationship between non-ventilated volume and hot spots 147
3.4.3 Correlations between imaging and demographics and lung function .. 150
3.5 Discussion 157
3.5.1 Non-ventilated volume 157
3.5.2 Hot spots 160
3.5.3 Non-ventilated volume versus hot spots 160

3.5.4 Limitations 163
3.5.5 Conclusions 164
3.6 References 165
Chapter 4 – Effects of bronchodilator on Ventilation Single Photon Emission Computed Tomography Imaging in COPD
4.1 Abstract 170
4.2 Introduction 171
4.3 Methods 173
4.3.1 Participants and study design 173
4.3.2 Lung function testing 175
4.3.3 Ventilation imaging 176
4.3.4 Image reconstruction and registration 177
4.3.5 Imaging analysis 178
4.3.6 Statistical analysis 179
4.4 Results 180
4.4.1 Participant demographics 180
4.4.2 Effect of bronchodilator on lung function and imaging parameters 182
4.4.3 Relationships between changes in non-ventilated volume and hot spots 185
4.4.4 Relationships between changes in imaging parameters and lung function 185
4.4.5 Relationships between baseline imaging parameters and changes in imaging parameters and lung function 191
4.4.6 Relationships between changes in imaging parameters and baseline lung function 191

4.5 Discussion 194
4.5.1 The effect of bronchodilator on non-ventilated volume 194
4.5.2 The effect of bronchodilator on hot spots count 201
4.5.3 Limitations 202
4.5.4 Conclusion 203
4.6 References 204

Chapter 5 – Effects of methacholine on Ventilation Single Photon Emission Computed Tomography Ventilation Imaging in COPD

5.1 Abstract 209
5.2 Introduction 210
5.3 Methods 213
5.3.1 Participants and study design 213
5.3.2 Lung function testing 214
5.3.3 Methacholine challenge test 215
5.3.4 Ventilation imaging 215
5.3.5 Image reconstruction and registration 217
5.3.6 Imaging analysis 218
5.3.7 Statistical analysis 220
5.4 Results 221
5.4.1 Participant demographics 221
5.4.2 Airway hyperresponsiveness and changes in lung function, non-ventilated volume, and hot spots 223
5.4.3 Relations between imaging parameters and airway hyperresponsiveness and closing index 227

5.4.4 Relationships between changes in imaging parameters and lung function 227
5.4.5 Predictors of changes in non-ventilated and hot spots 235
5.4.6 Relationships between baseline imaging parameters and changes in lung function 239
5.5 Discussion 242
5.5.1 The effects of methacholine on non-ventilated volume 243
5.5.2 The effects of methacholine on hot spots 245
5.5.3 Predictors of change in non-ventilated volume 247
5.5.4 Limitations 249
5.5.5 Conclusion 250
5.6 References 251

Chapter 6 – General discussion & conclusion

6.1 Results summary 255
6.2 The utility of measuring global estimates of non-ventilated volume and ‘hot spots’ count
6.2.1 Non-ventilated volume in COPD and possible utility 258
6.2.2 Hot spots in COPD and possible utility 258
6.3 Future directions for quantitative ventilation imaging analysis 259
6.3.1 Possible improvements to the measurement of non-ventilation 261
6.3.2 Possible improvements to the measurement of hot spots 262
6.3.3 Ventilation heterogeneity and analysis without thresholds 266
6.4 Conclusion 268
6.5 References 269

Acknowledgements

I would like to thank my primary supervisor Dist. Prof. Brian Oliver and my co-supervisor, Dr Alen Faiz, for supporting me throughout the tumultuous COVID years of my PhD. Of course, I owe so much to my external supervisor, Dr David Chapman, who had once been my primary supervisor prior to his new occupation at the Respiratory Investigation Unit, Royal North Shore Hospital. I cannot begin to express my gratitude towards you. All my wonderful years in research began when you took in that timid student under your wing all those years ago. You have supported and guided me throughout the entirety of my PhD journey by dealing with every concern and bringing my anxieties to rest. It is frankly impossible to thank you enough, and I am so happy to have met you.

I would also like to acknowledge Dr Kaj Blokland and Dr Troy Cross, both external supervisors, who have consistently been joyful and knowledgeable experts to turn to. Although I have known Dr Blokland for only a year or so, he has made a tremendous impact on me. I already miss our daily conversations. I must profess my deepest thanks towards Prof. Gregory King. You have always kept a watchful eye over me and directed me towards critical goals. Last year, I have learnt so much from you, and those long conversations into the night allowed me to make tremendous progress. Please know that I will be mulling over your words of advice and ways of thinking over many years to come.

So much of my positive memories and intact mental health is attributable to all of those who I have spent so much time with at the Woolcock and Royal North Shore Hospital. You have brought an innumerable number of smiles and laughter into my life. I know these riches will not be found anywhere else in the world. I would like to particularly thank Cindy, David, Faz, Fei, Kieran, Maria, Patrick, Rita, Ryan, Sandra, Sabine, and Tanya. I wish you all the best.

My acknowledgements would not be complete without me thanking Hooria. As we journeyed throughout the PhD, we both experienced similar hardships and joys in research. However, I was always astounded by your resilience and growth and wisdom. Thank you for making such a potentially difficult path into such a memorably happy one.

Finally, I wish to express my undying gratitude to my parents and my sister, Michelle. Your constant love, devotion, and support continue to hold me up to this day. I will spend the rest of my life thanking you all for your love.

Glossary of abbreviations

^{99m}Tc	99m-Technetium
AHR	Airway hyperresponsiveness
BDR	Bronchodilator responsiveness
BMI	Body mass index
CAT	COPD Assessment Test
COPD	Chronic obstructive pulmonary disease
CT	Computed tomography
D_{LCO}	Diffusing capacity for carbon monoxide
DRS, DRS_{FEV1}, DRS_{G5}, DRS_{R5}	Dose response slope for FEV1, G5, and R5
FEV1	Forced expiratory volume in 1 second
FOT	Oscillometry
FRC	Functional residual capacity
FVC	Forced vital capacity
G5	Respiratory system conductance at 5 Hz
GOLD	Global Initiative for Obstructive Lung Disease
IC	Inspiratory capacity
K_{CO}	Carbon monoxide transfer coefficient
LABA	Long-acting beta-adrenoceptor agonist
LAMA	Long-acting muscarinic antagonist
$Mask_{CT}$	CT-derived binary mask
MRI	Magnetic resonance imaging
R5	Respiratory system resistance at 5 Hz
RV	Residual volume

SPECT	Single-photon emission computed tomography
TLC	Total lung capacity
Thr_15%Max	15% of maximum activity threshold method
$Thr_50\%Mean_{5\text{-}80}$	50% of mean activity of 5 – 80% of maximum activity threshold method
Thr_Slope	Curve-fitting threshold threshold
Thr_Otsu	Otsu's method
VA	Alveolar volume
$Vent_{Vol}$	Ventilated volume
$Vent_{Non}$	Non-ventilated volume
VSPECT	Ventilation single-photon emission computed tomography

Thesis abstract

Background: Chronic obstructive pulmonary disease (COPD) is a complex and heterogenous disease. Conventional markers of disease severity such as spirometric parameters and demographics struggle to adequately characterise the disease due to their insensitivity. There have been efforts at COPD phenotyping by utilising complementary lung function tests and imaging techniques. Ventilation single photon computed tomography (VSPECT) may be utilised to quantitatively analyse ventilation defects. Qualitative VSPECT studies have long noted there to be poorer ventilation in patients with more severe disease. Due to advancements in imaging technology and analysis software, quantitative imaging analysis is more accessible than ever. Unfortunately, quantitative VSPECT has seldom been used to investigate COPD and available analysis techniques remain unvalidated.

Aims: Validate three existing analysis methods and a novel method that objectively define non-ventilated volume in VSPECT. Investigate the relationships between quantitative VSPECT parameters and various lung function measurements in COPD patients. Additionally, examine the effects of bronchodilator and bronchoconstriction on ventilation as measured with VSPECT.

Methods: Quantitative VSPECT parameters were global estimations of non-ventilated volume and ‘hot spots’ count. Lung function tests consisted of spirometry, body plethysmography, gas transfer, and oscillometry.

Results: The novel analysis method was demonstrated to be superior in accuracy and robustness compared to existing methods. Whilst increased non-ventilated volume correlated with lung function measurements indicating greater emphysema severity, increased ‘hot spots’ count correlated with greater ventilation heterogeneity, hyperinflation, gas trapping, and airflow limitation. The VSPECT parameters did not correlate with each other. There were no significant changes in either non-ventilated volume or ‘hot spots’ count following bronchodilation or bronchoconstriction. However, the responses in both VSPECT parameters were variable.

Conclusion: This thesis demonstrated that COPD patients with greater abnormalities in lung function possess increased non-ventilated volume and ‘hot spots’ count, confirming the observations made in older qualitative VSPECT studies. They also appeared to provide complementary information. However, the utility of either of these VSPECT parameters for more specific COPD characterisation or measuring response to bronchodilator treatment is likely to be limited. For future VSPECT studies, utilising topographical analysis or measuring ventilation heterogeneity may be of greater use for COPD characterisation

Chapter 1 – Introduction and Literature Review

1.1 Thesis Overview & Chapter Descriptions

The thesis was organised into a total of six chapters.

- The first chapter is an introduction to this thesis, and it provides a literature review on chronic obstructive pulmonary disease (COPD), disease burden of COPD, history of disease severity classification, and general disease management strategies. Chapter 1 also reviews the complex heterogeneity of COPD and the difficulties associated with assessing such a disease. Whilst conventional lung function measurement techniques such as spirometry and body plethysmography are discussed and compared to less conventional lung function techniques such as oscillometry, the primary focus of the literature review were quantitative imaging techniques, both computed tomography (CT) and ventilation imaging, particularly magnetic resonance imaging (MRI) and ventilation single photon emission computed tomography (VSPECT). Specifically, limitations and issues with these imaging modalities and analysis techniques, such as the lack of validation studies on 'thresholds' for ventilated activity in VSPECT, have been highlighted. However, Chapter 1 also stressed the potential in ventilation imaging techniques for phenotyping and investigating airway hyperresponsiveness and bronchodilator response in COPD.

- Chapter 2 is a lung phantom study that aimed to compare and assess various ventilation analysis methods that were noted in Chapter 1 in addition to a novel method that was dubbed the 'curve-fitting' threshold method. The physical lung phantoms, albeit conventional in design with static containers

filled with tracer solution and water and foam beads, sought to simulate ventilated and non-ventilated lung volumes as well as ‘hot spots’, which are commonly seen in Technegas VSPECT. In addition to lung phantoms, the threshold methods were also tested on lung scans from COPD participants, but no investigations into lung function parameters and their relationships with imaging parameters were conducted.

- Chapter 3 is a study that applied the novel ‘curve-fitting’ threshold method to primarily investigate relationships between the imaging parameters, non-ventilated volume ($Vent_{Non}$) and total ‘hot spots’ count, and lung function parameters, which were obtained from tests such as spirometry, body plethysmography, and oscillometry, in COPD participants. $Vent_{Non}$ and ‘hot spots’ count were hypothesised to be related to emphysema and ventilation heterogeneity, respectively. As noted in Chapter 2, no modifications were made to the ‘curve-fitting’ threshold method when it was applied to human participants.

- Chapter 4 sought to examine the effects of bronchodilator in COPD with both VSPECT imaging and lung function testing, which consisted of spirometry and oscillometry. Like Chapter 3, the imaging parameters were $Vent_{Non}$ and ‘hot spots’ count. Furthermore, the relationships between imaging and lung function parameters were also assessed, and the objectives of the study included investigating whether baseline imaging parameters could predict the change in lung function parameters post-bronchodilator and vice versa.

- Chapter 5, instead of examining the effects of bronchodilator, investigated the effects of bronchoconstriction in COPD. Again, the same VSPECT imaging parameters and lung function tests, spirometry and oscilliometry, were used in this study. However, due to the study's inclusion criteria, only a limited number of 10 participants were included.

- Chapter 6 consists of this thesis's general discussion and conclusion. Within it, brief descriptions of each chapter and their relevant findings are summarised. The primary focus of this chapter's discussion can be categorised into two sections. The first section discussed the utility of global imaging measurements used in this thesis, $Vent_{Non}$ and 'hot spots' count. The second section noted the limitations with these measurements and thus, suggested possible improvements and modifications in addition to potential new avenues to explore with VSPECT imaging.

1.2 What is chronic obstructive pulmonary disease

Chronic obstructive pulmonary disease (COPD) is a progressive respiratory disease that is characterised by partially reversible airflow obstruction, chronic bronchitis, emphysema, and the loss of elastic recoil (1). Typical symptoms include cough, dyspnoea, and reduced exercise capacity. COPD involves a variety of pathological changes. Aside from emphysematous destruction of the lung parenchyma, which reduces radial traction (2), there is an increased number of macrophages and lymphocytes in the airways. Mucus hypersecretion occurs as a result of goblet cell hyperplasia (3). Abnormalities in the airways include airway narrowing, obstruction, and obliteration (4, 5). The primary lung function test for diagnosis of COPD and management is spirometry. According to the Global Initiative for Chronic Obstructive Lung Disease (GOLD), a “forced expiratory volume 1 (FEV1)/forced vital capacity (FVC) < 0.7 post-bronchodilation” confirms the diagnosis of COPD (6).

1.3 The burden of chronic obstructive pulmonary disease

The global prevalence of COPD between 1990 – 2019 is reported to have increased by 97 million (7), but prevalence of COPD in Western world countries such as the United States between 2011 – 2021 (6.1% – 6.0%) (8) and Australia between 2011 – 2022 (2.4% – 2.5%) (9) are reported to be steady. Although COPD cases in China between 1990 – 2019 had increased by 1.58 million (10), COPD cases within East Asia are projected to decrease by 2050, and sub-Saharan Africa is instead projected to become the most prevalent COPD region (11).

In 2019, the disease was reported as the third leading cause of death worldwide (7), and the global number of cases was estimated to be 212 million (12). According to Adeloye et al., the top three countries with highest prevalence of COPD cases were

in Asia: China, India, and Indonesia (13). In Australia, 464,000 people aged 45 and over are diagnosed with COPD, and throughout 2021 – 2022, there had been 53,000 reported hospitalisations, and $831.6 million was spent on treatment and management (14). The primary cause of death depends on the severity of disease. Respiratory failure is the primary cause of death in patients with more severe disease (15), and for patients with mild or moderate disease severity, lung cancer and cardiovascular disease are noted to be the primary causes of death (16). Risk factors for death include diabetes, older age, sex (male), greater airflow obstruction severity, worse health status, underweight body mass index (BMI), and a history of exacerbations (17-20).

Smoking is long recognised to be the primary risk factor for COPD (21, 22), but evidence has revealed additional risk factors such as alpha-1 antitrypsin deficiency (23), sex (female) (24), and environmental pollution (25), including household air pollution from indoor gas cooking with biomass (26, 27). According to Chung et al. (24) and Sorheim et al. (28), it has been observed that female smokers were more likely to develop COPD and progress to more severe COPD. Regarding environmental pollution, Safiri et al. have suggested that excessive exposure to air pollution resulting from poor regulation of air quality in addition to the relatively recent introduction of automobiles were likely responsible for high death rates from COPD in developing countries such as Nepal (12). Multiple studies have also revealed a substantial incidence of COPD patients who have never smoked, particularly among females, and the proportion of these ‘non-smoker’ COPD patients range between 7 – 25% (29-32).

1.4 Disease management

The mainstay for COPD pharmacological therapy are inhaled bronchodilators, particularly long-acting β_2-agonists (LABA) and long-acting muscarinic antagonists (LAMA). For COPD patients with minimal symptoms and 0 – 1 exacerbations with no prior hospitalisations, the GOLD 2024 report recommends initial treatment with either a short-acting bronchodilator such as salbutamol or if available and affordable, LABA/LAMA monotherapy (6). For patients with worse presentation, such as more severe dyspnoea and a history of exacerbations or exacerbation-related hospitalisations, LABA/LAMA combination therapy is recommended instead. Compared to monotherapy, various studies have observed the superior ability of LABA/LAMA combination therapy in significantly reducing dyspnoea, exacerbations, and hospitalisation rates in more symptomatic COPD patients (33-36). Regarding initial treatment with either LABA or LAMA in less severe COPD patients, LAMA monotherapy appears to provide superior clinical outcomes, such as significantly lower incidence of exacerbation and non-serious adverse events (37). There are conflicting findings concerning whether bronchodilator therapy can significantly affect long-term decline of lung function (38-40). Recent evidence suggests disease progression can be delayed by early bronchodilator intervention in younger patients with milder severity (41, 42).

In addition to inhaled bronchodilators, inhaled corticosteroids (ICS) form another approach to initial pharmacological therapy, but its use is controversial. Although ICS cannot significantly affect long-term decline of lung function (as measured with spirometry) (40, 43), some studies have shown that ICS in conjunction with LABA therapy can decrease respiratory symptoms and use of health care services (44) and

reduce risk of future exacerbations and decline in health status (43, 45). Conversely, the use of ICS is also associated with increased risk of adverse advents, which include pneumonia (46, 47) and tuberculosis (48, 49), and there appears to be no significant reduction in mortality (50, 51). Compared to ICS/LABA combination therapy, which was once recommended by the GOLD 2017 report (52), LABA/LAMA combination therapy was found to be superior overall due to significantly greater improvement in health status and lung function and reduced risk of pneumonia (53). Furthermore, the withdrawal of ICS for most patients does not result in exacerbations (54). However, for a particular subgroup of symptomatic COPD patients who respond poorly to LABA/LAMA combination therapy, the use of ICS in addition to LABA/LAMA combination therapy is able to reduce the risk of exacerbation (55) without increasing risk of pneumonia (56). For this subgroup, the withdrawal of ICS, whilst continuing LABA/LAMA combination therapy, can lead to a greater decline of lung function (57). These patients who receive the greatest benefit from ICS treatment are associated with increased eosinophilic inflammation (58, 59). Therefore, the most recent GOLD report recommends the tailored use of ICS/LABA/LAMA triple therapy for patients with ≥ 2 moderate exacerbations or ≥ 1 exacerbation that led to a hospitalisation and a blood eosinophil count ≥ 300 cells/μL (6). A summary of these initial pharmacological treatment options according to GOLD are shown in Figure 1.

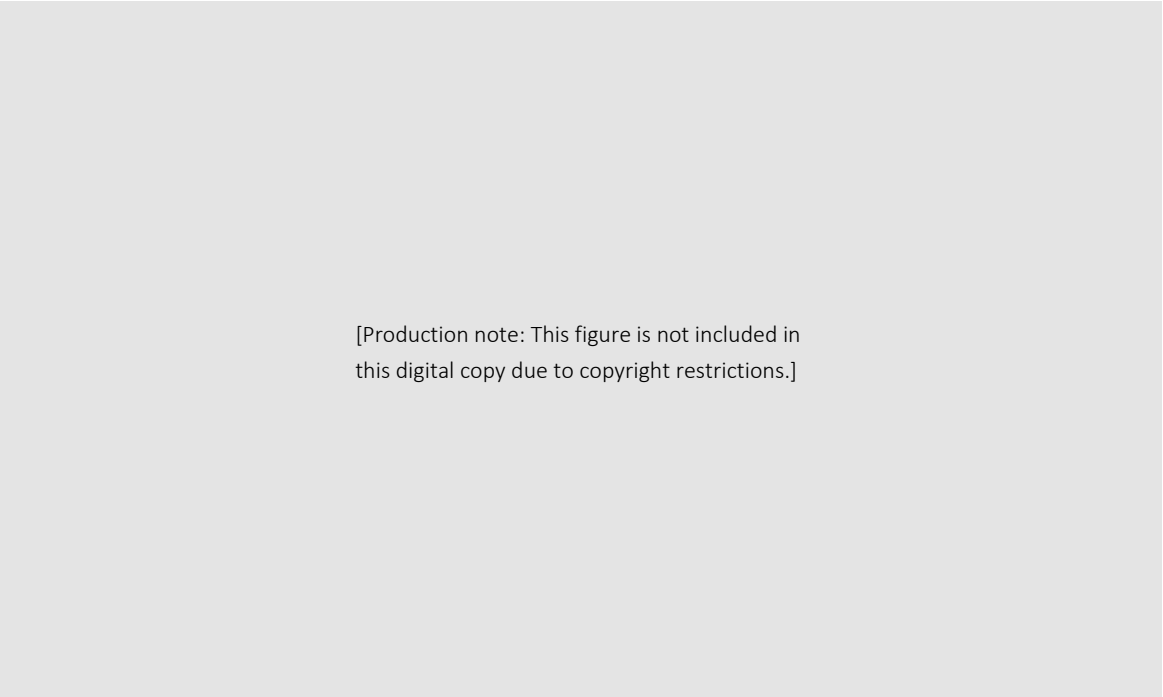


Figure 1: Reproduced figure detailing the recommended initial pharmacological treatment according to the 2024 Global Initiative for Chronic Obstructive Lung Disease (GOLD) report (6). LABA = long-acting β_2-agonists; LAMA = long-acting muscarinic antagonists; mMRC = modified Medical Research Council dyspnoea questionnaire; CAT = chronic obstructive pulmonary disease assessment test.

For follow-up pharmacological therapy, COPD patients who continue to experience exacerbations despite the use of LABA/LAMA/ICS triple therapy, adding either roflumilast, an anti-inflammatory drug that selectively inhibits phosphodiesterase-4, or azithromycin is recommended by GOLD (6). Roflumilast has been shown in multiple studies to significantly reduce exacerbation rate in COPD patients who are already treated with LABA/LAMA and ICS (60-62). Azithromycin was also demonstrated to decrease exacerbation rate and improve quality of life in COPD patients who frequently exacerbate (63-65). Antibiotic resistance (63) and increased risk of cardiovascular death in patients with high risk of cardiovascular disease (66), such as COPD patients, must be considered by the clinician before administering long-term azithromycin.

The most critical aspect of non-pharmacological therapy is smoking cessation. In COPD patients, smoking cessation has been associated with decreased risk of mortality (67), reduced respiratory symptoms (68), decreased risk of hospitalisation (69), and reduced rate of lung function decline at all stages of disease severity compared to COPD smokers (42, 70, 71), even with bronchodilator therapy (72). However, 30% - 40% of COPD patients continue to smoke (24, 73), and COPD smokers have increased tobacco consumption and nicotine dependence than non-COPD smokers (74). Furthermore, smoking cessation is observed to be infrequently advised by physicians (75). Current evidence suggests that combining both behavioural counselling and pharmacological intervention, such as nicotine replacement therapy and antidepressants, is the most effective at ceasing smoking entirely for COPD patients (76-78).

1.5 Assessing the severity of a heterogeneous disease

Classification methods of disease severity have varied over time. Initially, disease severity was graded almost solely by FEV1 thresholds. The first GOLD report in 2001 listed three stages of COPD severity: mild, moderate, and severe (79). Mild was defined by FEV1/FVC < 70% and FEV1 ≥ 80% of predicted; moderate was defined by FEV1/FVC < 70% and 30% of predicted ≤ FEV1 ≤ 80% of predicted; and severe was defined by FEV1/FVC < 70% and FEV1 < 30% of predicted. Other markers of disease severity were noted, but this simply consisted of symptom presentation, such as dyspnoea, and presence of respiratory or cardiac failure. This FEV1 centric grading system of disease severity persisted in the 2006 GOLD Report (80).

Since 2011, the assessment of disease severity has become more complicated (81). Instead of FEV1 predominately dictating disease severity, greater emphasis was placed on measuring the level of dyspnoea with the modified Medical Research Council dyspnoea scale (mMRC) (82, 83), health status, which is assessed with the COPD Assessment Test (CAT) (84), and risk of exacerbation by noting previous exacerbations and hospitalisations. At first, these additional parameters and FEV1 thresholds were simultaneously used to grade disease severity, and the GOLD 2011 report listed 4 grades of COPD severity: GOLD A, B, C, and D (81) (Figure 2). However, the role of spirometry lessened even further in the subsequent GOLD 2017 report (85) as the thresholds had been entirely removed from the assessment of disease severity (Figure 3). Since then, FEV1 has been used exclusively to diagnose COPD and assess the severity of airflow obstruction.



Figure 2: Reproduced figure for the assessment of COPD severity according to the Global Initiative for Chronic Obstructive Pulmonary Disease (GOLD) 2011 report (81). The GOLD report classified airflow limitation severity as follows: GOLD 1 or mild = forced expiratory volume in 1 second (FEV1) ≥ 80% predicted; GOLD 2 or moderate = 50% ≤ FEV1 < 80% predicted; GOLD 3 or severe = 30% ≤ FEV1 < 50% predicted; GOLD 4 or very severe = FEV_1 < 30% predicted. FEV1 = forced expiratory volume in 1 second; mMRC = modified Medical Research Council dyspnoea questionnaire; CAT = chronic obstructive pulmonary disease assessment test.

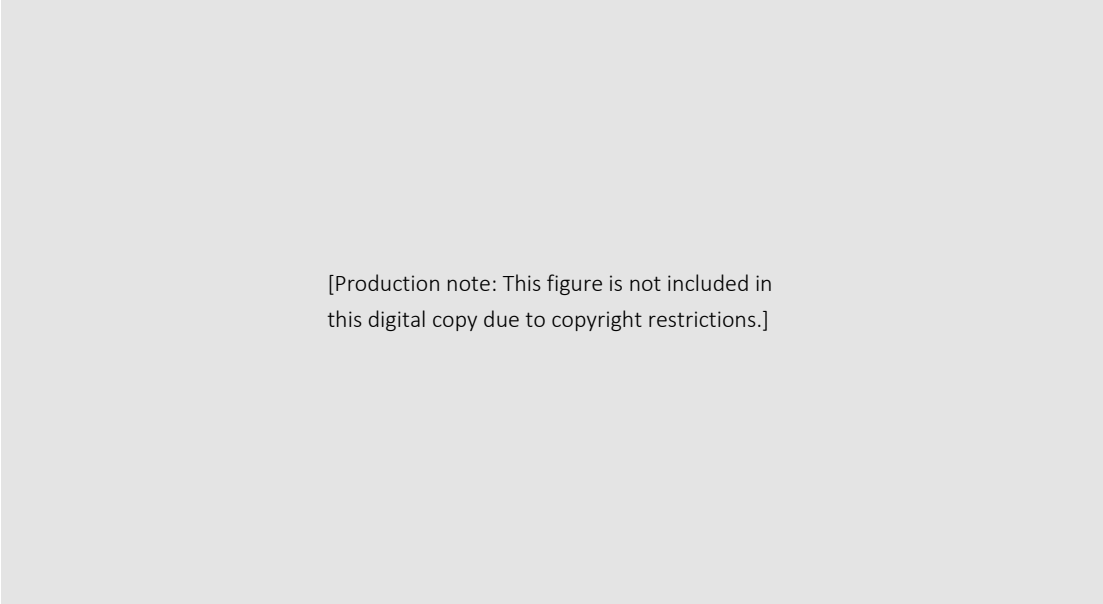


Figure 3: Reproduced figure for assessment of COPD severity according to the Global Initiative for Chronic Obstructive Pulmonary Disease (GOLD) 2017 report (85). Unlike the GOLD 2011 report, the GOLD classifications for severity of airflow limitation with forced expiratory volume 1 thresholds are separated from the ABCD assessment on COPD symptoms and exacerbation risk. FEV1 = forced expiratory volume in 1 second = FEV1; FVC = forced vital capacity; mMRC = modified Medical Research Council dyspnoea questionnaire; CAT = chronic obstructive pulmonary disease assessment test.

The receding role of spirometry in disease assessment can be explained by its limitations regarding solely characterising disease severity, guiding treatment, and predicting adverse events. Indeed, correlations between airflow obstruction severity and other important disease manifestations such as exacerbation history, symptom severity, and quality of life are weak (86). Spirometry is also found to be a poor predictor of future exacerbations (87), which indicates a subgroup of patients with 'mild' airflow obstruction but possess a high risk of exacerbations. 5-year survival is predicted significantly better by the level of dyspnoea than FEV1 (88). Following treatment, studies have shown only weak associations between improved FEV1 and reduced exacerbation risk (89) or improved quality of life, as determined by the St George's Respiratory Questionnaire (SGRQ) (90).

It may be unreasonable to expect spirometry or any other single test to accurately assess, characterise, or prognosticate a disease as complex and heterogeneous as COPD (91), in which there is considerable variability in progression (92) and presentation such as the presence of systematic inflammation (93). Indeed, reliable parameters such as exacerbation history is unable to account for future COPD exacerbators with no prior exacerbations or limited history (94). Although long term decline of lung function is indeed characteristic of COPD, Vestbo et al. (95) observed substantial heterogeneity in the changes of lung function over time. Whilst 23% of patients experienced changes in FEV1 ranging from -20 mL – 20 mL per year over a three-year study period, 38% had a FEV1 decrease of more than 40 mL per year (95). Symptoms are highly variable, and again, there is substantial heterogeneity in the probabilities for the occurrence of symptoms such as dyspnoea and wheeze (interquartile range of probabilities for dyspnoea and wheeze: 0.19 – 0.81 and 0.13 –

0.78, respectively). Cough was noted to be particularly unpredictable as correlations between cough frequency and spirometry and conventional patient characteristics, which include age, sex, smoking history, and BMI, were reportedly weak (96). The heterogeneity of COPD also extends to exacerbations (97), with substantial between-individual variability in exacerbation rate and exacerbation severity and no significant association between rate and severity (98).

Despite moving away from FEV1 to grade COPD severity exclusively, there are conflicting reports on the efficacy of these more complex systems compared to simpler systems. Developed in 2004, the body mass index, degree of airflow obstruction, dyspnoea, and exercise capacity (BODE) index is a well-known example, and it was demonstrated to be a significantly better predictor of risk of death, exacerbation rate, and exacerbation severity than FEV1 alone (99, 100). However, when the BODE index was compared to the GOLD 2006 grading system, which incorporates FEV1 thresholds and presence of respiratory failure, the clinical utility in predicting exacerbation risk was reportedly similar (101). Similarly, the predictive abilities of GOLD 2011 regarding hospitalisations and mortality were similar to the simpler GOLD 2006 system (102). Furthermore, Kim et al reported that the GOLD 2006 system predicted lung function decline significantly better than the GOLD 2011 system (103). These findings highlight the difficulties involved in the assessment and characterisation of COPD, even when accounting for multiple factors. But rather than disregarding complex, multipronged approaches entirely, it is possible that other important factors were ignored, or unnecessary parameters had been included, and a streamlined approach could prove to be more optimal. Indeed, the simpler dyspnoea, airflow obstruction, smoking status, and exacerbation history

(DOSE) index (104) predicted exacerbations better than either the more complex BODE and simpler age, dyspnoea, and obstruction (ADO) (105) indexes (106). Furthermore, the simpler GOLD 2017 system, which excludes FEV1 thresholds entirely and instead relies on health status, dyspnoea severity, and exacerbation history, was found to predict mortality and respiratory hospitalisations better than either the GOLD 2011 and 2007 systems, whilst maintaining similar predictive ability to the more complex BODE index (107).

1.6 A small airways disease and looking beyond spirometry

Peripheral or “small” airways are typically defined as non-cartilaginous airways with an internal diameter < 2 mm (108), beginning at the 8th out of the 23 airway generations from the trachea to the alveolar sacs (109). It is the function in these small airways instead of the larger proximal airways that are predominately affected in COPD. In 1968, Hogg et al. (110) noted that resistance in peripheral airways 2 – 3 mm in diameter, measured with a small catheter, from excised emphysematous lungs were four to forty times larger than healthy lungs without emphysema. However, central airways resistance in the emphysematous lungs were still mostly normal. Hogg et al. then utilised bronchography and histology to reveal that increased peripheral airways resistance was due to a combination of airway narrowing, obliteration, and mucus plugging. Peripheral airways resistance had contributed less than 25% to total airways resistance. Thus, Hogg et al. noted that unless total airways resistance became substantially affected by small airways disease, spirometric measurements on airflow limitation would be unable to detect abnormalities in small airway function. Instead, changes in ventilation distribution or

gas exchange were suggested as alternative measurements. Yanai et al. (111) later reported similar findings. By inserting a catheter-tipped micromanometer in the right lower lobe of a 3 mm bronchus in awake participants, Yanai et al. also observed significantly greater peripheral airways resistance in asthmatic patients with airflow obstruction and COPD patients compared to healthy participants. Total airways resistance in these patients with airflow obstruction were not significantly increased, but the ratio of peripheral airways resistance to total airways resistance was significantly increased. Airways ≤ 3 mm diameter were suggested by Yanai et al. to be the predominant site of airflow obstruction. In more recent years, multi-detector computed tomography (CT) and micro-CT (4, 112), which can assess small airways 2 mm in diameter and much smaller terminal bronchioles with an average diameter of 0.42 mm in healthy controls respectively (112), revealed that small airway narrowing and obliteration occur prior to the onset of emphysematous destruction. According to Hogg et al. (4), micro-CT indicated a 10 fold reduction in the number of terminal bronchioles and a 100-fold reduction in their minimal cross-sectional lumen area in lungs from COPD patients. Using both multi-detector CT and micro-CT, McDonough et al. (112) also reported a correlation between reduced count of terminal bronchioles and greater GOLD 2006 disease severity as determined by FEV1.

As mentioned previously by Hogg et al. as early as 1968 (110) and Meade in 1970 (113), spirometry is not a sensitive test for small airway disease. Spirometric measurements of airflow limitation are largely reflective airflow in the larger, proximal airways. Aside from CT imaging analysis of small airway count and airway lumen area, two alternative lung function tests appear to be more suitable for measuring

small airway dysfunction. Oscillometry, a supplementary lung function, is becoming more popular in use, and it appears to be a promising tool for assessing small airways disease. By applying flow oscillations at the mouth during tidal breathing, oscillometry measures respiratory system impedance, which is an assessment of the "relationship between pressure and flow changes" in and out of the respiratory system (114). Respiratory system impedance can be expressed as two different components, respiratory system resistance (Rrs) and respiratory system reactance (Xrs). Rrs can be surmised as the sum of lung resistance and resistance to chest wall tissue deformation, and the former can also be surmised as the sum of airway resistance, both intra- and extra-thoracic, and lung parenchymal tissue resistance. Similarly, Xrs reflects elasticity of the respiratory system, which like Rrs, includes chest wall and the lungs, composed of both airways and parenchymal tissue. By penetrating more peripheral airways, Rrs and Xrs at low frequencies such as 5 Hz can assess both peripheral airway and central airway dysfunction (115-117). In eighty smokers with preserved spirometry, Jetmalani et al. (118) observed that 51% of participants possessed abnormal Rrs at 5 Hz (R5). Wheeze was also found to be related with increased R5. Similar findings regarding abnormal oscillometric parameters in asymptomatic smokers (119), non-smokers with respiratory symptoms and no diagnosed respiratory disease (120), and participants exposed to dust and fumes (121), all of whom possess normal spirometry, have been reported. Clement et al. also noted oscillometry to be a more sensitive tool than spirometry for distinguishing between healthy people and people with mild or absent airflow obstruction as the latter group had increased Rrs and decreased Xrs (122). A recent study by Rath et al. (123) revealed that small airway dysfunction, as measured with Rrs 5-19 Hz (R5 – R19 Hz) and Xrs at 5 Hz (X5), was present within all GOLD

stages of COPD severity. Furthermore, the prevalence of small airway dysfunction positively correlated with GOLD COPD severity, and the presence of small airway dysfunction was associated with worse symptoms, reduced gas transfer, increased hyperinflation, increased airflow limitation, and reduced exercise capacity. Recently, Ribeiro et al. (124) reported significant correlations between increased Rrs at 4 Hz and reduced functional capacity for physical activity and reduced muscle strength. Thus, measuring small airway dysfunction with oscillometry may assist in assessing disease severity for COPD.

Another test for assessing small airway dysfunction is the multiple breath nitrogen washout test. Multiple breath nitrogen washout involves the patient inhaling 100% oxygen at approximately 1 L tidal volumes with a respiratory rate of 8 – 12 breaths per minute until tidal nitrogen concentration drops below a threshold. Although more difficult to perform in COPD patients than oscillometry, the test measures the degree of overall ventilation heterogeneity, which is expressed as the lung clearance index (LCI) (125). In a general population of men, Zaigham et al. reported that greater overall ventilation heterogeneity was associated with the future development of airflow obstruction and greater incidence of COPD-related hospitalisations (126). Ventilation heterogeneity in the small airways can also be assessed. Ventilation heterogeneity within more proximal airways at the entrance to the acinar, with gas transport dependent on convection, and more peripheral small airways, with gas transport dependent on diffusion, are represented by S_{cond} and S_{acin}, respectively (127). Within a cohort of 172 smokers, multiple breath nitrogen washout detected increased S_{cond} and S_{acin} in smokers with a 10-pack year history compared to never smokers (128). In comparison, spirometry could only identify abnormalities in

smokers with a pack year history of at least 20 years. Furthermore, the presence of emphysema was associated with greater increases in S_{acin} than S_{cond}, indicating the relationship between parenchymal damage, airway loss and ventilation heterogeneity. According to Verbanck et al. (129), COPD participants possess increased S_{cond} and S_{acin}, with the former ranging from 1 – 5 times and the latter ranging from 3 – 10 times the average normal values. Furthermore, increased S_{cond} was linked with reduced FEV1 and S_{acin} was linked with poorer gas diffusion. In a different study by Verbanck et al. (130), the authors investigated the relationship between the loss of terminal bronchioles and S_{acin} with a reference model, which was initially composed of 27,500 acini. This model was then "pruned" of its acini. As ventilation was forcibly distributed to an increasingly fewer number of acini, S_{acin} unsurprisingly increased. Multiple breath nitrogen washout could be particularly useful for an earlier diagnosis of COPD or for the characterisation of a 'pre-COPD'/'at risk' patient subgroup, which was previously suggested in the 2001 GOLD report (40).

1.7 Phenotyping a heterogeneous disease

As previously mentioned, assessing the clinical severity of disease remains a challenge. Staging COPD must consider not only lung function but also other markers such as exacerbation history, symptom severity, and quality of life, and of course, disease severity allows us to ascertain the risk of worse clinical outcomes. These outcomes can vary between increased risk of mortality and hospitalisations and deterioration of quality of life. The complexity of assessing COPD severity is reflected by the numerous updates to GOLD guidelines. The utility of spirometry,

which again, predominately reflects airflow within the larger, proximal airways, instead of the small airways beyond diagnosis is unclear. To clear up the heterogeneous nature of COPD, there have been efforts to phenotype the disease. Simply, phenotyping involves categorising patients into separate subgroups with unique clinical features (131). The end goal of phenotyping is to provide a more personalised approach to therapy and management, so that a patient's future risks may be accurately predicted and prevented with new therapeutics or strategies more complex than ICA/LABA/LAMA combinations (132, 133).

It must be noted that COPD phenotypes are not a recent invention. Although currently antiquated, the 'pink puffer' and 'blue bloater' terms were once used to characterise COPD patients into two phenotypes as either predominately emphysematous or predominately bronchial, respectively (134). Other than the presence of emphysema, which had been assessed with a plain radiograph, the 'pink puffer' phenotype was characterised by underweight BMI, hyperinflated lungs, and hyperventilation, and the 'blue bloater' phenotype was characterised by chronic bronchitis, overweight – obese BMI, chronic cough, and hypoxemia (135). More recent studies into the 'pink puffer' or emphysematous phenotype show it to be associated with poorer health status and reduced capacity and lacking response to ICS therapy (136), and the non-emphysematous phenotype to be associated with increased risk of diabetes and hypertension (137). However, Makita et al. (138) observed that chronic bronchial symptoms, which should uniquely characterise the 'blue bloater' or bronchial phenotype, were equally prevalent in the 'pink puffer' or emphysematous phenotype, and the utility of the predominately bronchial phenotype was thought to be questionable.

COPD phenotyping has since moved beyond the dichotomous ‘pink puffer’/’blue bloater’ classifications, and of course, the complexity of this disease makes it difficult to strictly characterise patients with only two phenotypes. Thus, there have been attempts at identifying additional or more precise COPD phenotypes. A widely acknowledged example would be the ‘frequent exacerbator’ phenotype. As the name suggests, it describes a subgroup of patients who experience frequent exacerbations (e.g., ≥ 2 exacerbations per year) despite optimal bronchodilator treatment (139). Aside from exacerbation history, this phenotype has been characterised with increased airway inflammation (140) and increased blood eosinophil cell count (141, 142) and chronic bronchitis (143). ‘Frequent exacerbator’ patients are also associated with worse clinical outcomes such as greater mortality (144), increased number of cardiovascular events (145), and poorer health status compared to patients who do not frequently exacerbate (146). Inhaled corticosteroids or oral anti-inflammatory drugs appear to be particularly beneficial to ‘frequent exacerbators’ by significantly reducing exacerbation rate (147, 148) and all-cause mortality (149). Thus, recent GOLD reports specifically recommend ICS/LABA/LAMA triple therapy in patients that present with ‘frequent exacerbator’ phenotype traits (previous exacerbations and blood eosinophil count ≥ 300 cells/μL) (6).

In 2014, the Spanish Guideline for COPD introduced two subcategories or ‘subphenotypes’ to the ‘frequent exacerbator’ phenotype by combining it with characteristics from the older ‘pink puffer’ and ‘blue bloater’ phenotypes: ‘frequent exacerbator with emphysema’ and ‘frequent exacerbator with chronic bronchitis’

(150). Additionally, the guideline recognised two other phenotypes: ‘asthma-COPD overlap’ and ‘non-exacerbator’. The prevalence for the ‘frequent exacerbator with emphysema’ phenotype is generally lower than the ‘frequent exacerbator with chronic bronchitis’ phenotype (approximately 5 – 19% and 12 – 40%, respectively) (151, 152), and there is limited information regarding the clinical relevance of these frequent exacerbator ‘sub-phenotypes’. A retrospective study conducted by Golpe et al (153) revealed that patients with the ‘frequent exacerbator with emphysema’ phenotype had the highest risk of death resulting from an exacerbation or COPD progression compared to the other three phenotypes. Furthermore, patients with this phenotype had also died more frequently from exacerbations or disease progression. Conversely, the ‘asthma-COPD’ overlap phenotype was associated with the best-long term prognosis (153). According to Chai et al. (152), patients with ‘frequent exacerbator with chronic bronchitis’ phenotype was found to possess the worst health status and more severe symptoms, particularly cough, phlegm, chest tightness, and dyspnoea, than the other phenotypes. Interestingly, despite increased mortality risk, patients with the ‘frequent exacerbator with emphysema’ phenotype was found to have similar levels of health status and symptom severity with the ‘non-exacerbator’ phenotype. The utility of the frequent exacerbator ‘sub-phenotypes’ is still relatively limited, and further investigations will be required to determine whether different pharmacological intervention strategies could alter health outcomes.

The ‘asthma-COPD’ overlap phenotype is another well-recognised phenotype (150), and Hardin et al. (154) observed that patients of this phenotype were younger with a reduced smoking history compare to non-overlap COPD patients. This is conflicted by findings from De Marco et al. (155) and Lee et al. (156) as they observed greater

prevalence in the elderly who had increased smoking history. However, the differences may be explained by patient populations. Specifically, the studies from De Marco et al. (155) and Lee et al. (156) examined predominately Caucasian and Northeast Asian patient populations, respectively. On the other hand, approximately 18% of the participants in the study from Hardin et al. (154) were of African American descent, who have greater prevalence of asthma than Caucasian and Asian populations (157, 158). Nonetheless, the 'asthma-COPD' overlap phenotype has been consistently associated with poorer health status, greater symptom severity, and reduced exercise capacity (154-156, 159), and although GOLD no longer recognises a distinct 'asthma-COPD' overlap phenotype, it does recommend the combined use of asthmatic and COPD pharmacotherapy guidelines, i.e. ICS and LABA/LAMA (6).

However, these newer phenotypes share a similar flaw to the older 'pink puffer'/'blue bloater' classification: non-specific clinical traits. Due to the heterogeneous nature of COPD, patients often present with a variety of clinical features, and 'unique' characteristics such as frequent exacerbations, emphysema, asthma overlap, and bronchitis can be observed across multiple phenotypes. Indeed, Hardin et al. (154) had observed similar extents of emphysema between the 'asthma-COPD' overlap and non-overlap phenotypes, and frequent exacerbations were also associated with 'asthma-COPD' overlap patients. Furthermore, both Hardin et al. (154) and Lee et al. (156) reported the presence of increased gas trapping and hyperinflation in patients with the 'asthma-COPD' phenotype. These traits have been used to define different phenotypes such as the 'frequent exacerbator' and the 'emphysematous' or 'emphysematous – hyperinflation' phenotypes (139, 160). With 'generic' traits such

as emphysema extent, exacerbations, and increased BMI, there could be potentially an exceedingly large number of phenotypes, sub-phenotypes, and combinations (e.g., asthma-COPD overlap with frequent exacerbations but no emphysema, asthma-COPD overlap non-exacerbator with emphysema, etc…). Therefore, it appears that the viability of traditional pathophysiological traits alone such as emphysema as precise phenotypical markers is limited.

Thus, other traits will need to be identified for better phenotype characterisation, and we must look at features beyond clinical presentation used in GOLD disease assessment or spirometry. These features may include genetic, environmental, inflammatory, and physiological factors. For a physiological approach to phenotyping, the aforementioned lung function tests sensitive to small airway dysfunction, ocillometry and multiple breath nitrogen washout, may be of tremendous use. Various studies have examined the utility of lung volume measurements. In 1978, Corbin et al. (161) conducted a four-year follow up study on a cohort of smokers, ex-smokers, and non-smokers. Between the first and second visits, there were no significant changes to either FEV1 or FEV1/FVC in any of the participants. However, measurements of total lung capacity (TLC), functional residual capacity (FRC)/TLC ratio, which represents hyperinflation, and residual volume/TLC ratio, which represents gas trapping, had all significantly increased in the smoker's group. The inspiratory capacity (IC)/TLC ratio, which is measured with body plethysmography, is representative of static hyperinflation. The IC/TLC ratio has been demonstrated to strongly correlate with dyspnoea (162) and predict decline of exercise capacity, increased risk of death, and exacerbations (163-165).

Imaging is an especially promising resource for COPD characterisation, and there has been significant progress within the realm of quantitative analysis techniques. Various pathophysiological changes in COPD such as airways disease, emphysema, gas trapping, and ventilation impairment can be assessed with either computed tomography (CT) or ventilation imaging techniques.

1.8 Quantitative computed tomography imaging analysis in COPD

Although quantitative CT analysis is beyond this thesis's objectives, it should be noted that a substantial amount of work towards COPD characterisation and phenotyping has been completed with CT. This section on various quantitative CT imaging analysis techniques briefly reviews the progression from global estimations on the extent of abnormal lung regions (e.g., emphysema) to more complex techniques, which assess airway narrowing, emphysema patterns, and structural heterogeneity. Due to the nature of CT, this form of imaging has been primarily reserved for assessing structural abnormalities and not lung function. The latter is typically reserved for ventilation imaging techniques. However, this section will also briefly describe recent innovations that have allowed CT to measure lung function as well. All these techniques have allowed us to better identify COPD patients at increased risk of poor clinical outcomes and distinct subgroups. Of course, whilst imaging techniques can differ greatly from each other, there can be similarities in image analysis methods (i.e., applying a global threshold to the image data). Some approaches in quantitative CT imaging analysis, such as investigating both gas

trapping and airway abnormalities, may potentially be applied to other ventilation imaging techniques.

Quantitative CT imaging analysis has been typically used to examine the extent of emphysema, hyperinflation, and other parenchymal abnormalities. The most common techniques involve measuring mean lung density and estimating areas of low attenuation in the lung (LAA). LAA is typically defined with a predetermined Hounsfield unit (HU) threshold on the image data and then expressed as a percentage of total CT lung volume (LAA%) (166). The most common predetermined HU threshold to assess emphysematous regions is -950 HU. This threshold can be attributed to a study from Gevenois et al. (167), which showed that a HU threshold of -950 HU threshold produced the strongest correlations between both macroscopic and microscopic measurements of emphysema (167, 168). Although alternative threshold techniques have since been proposed (169, 170), the -950 HU threshold remains the more predominant threshold due to “interests of balancing sensitivity and specificity” (171). A supplementary HU threshold can also be applied to assess lung regions affected with gas trapping and airflow obstruction instead of emphysema. According to Schroeder et al. (172), LAA defined with the -856 HU correlated with airflow obstruction more strongly than LAA defined with -950 HU threshold.

LAA% analysis has been used to identify patients with emphysema and non-obstructive lung function measurements (173) and predict greater risk of death (174) and exacerbations (175) and lung function decline (95). Dirksen et al. demonstrated

LAA% analysis to be a more sensitive technique for measuring treatment outcomes in COPD patients with α1-antitrypsin deficiency than health status assessed by SGRQ or spirometry (176). However, it should be noted that global LAA% analysis alone is unlikely to be sufficient for more precise physiological phenotyping. As noted previously, similar global extents of emphysema can be observed across supposedly distinct phenotypes. According to the findings from Gietema et al. (177), visual estimates of emphysema take additional factors in account such predominant emphysema type, abnormal patterns, legion sizes, and the presence of airways disease. In comparison to the Fleischer Society classification system, which comprehensively identifies different emphysema patterns and presence of airway diseases and abnormal features such as pulmonary vascular disease (178), LAA% analysis is reported to be less sensitive to smoking related injuries such as lung cancer (179-181).

There have been efforts to supplement LAA% analysis with complementary techniques so that information beyond global estimates is acquired. One example would be the combination of LAA analysis with fractal analysis, which was initially developed to quantitatively evaluate heterogeneity in size and shape of natural objects (182). Within the context of LAA analysis for CT imaging, fractal analysis can provide information concerning the heterogeneity and complexity of LAA regions within the lung. Mishima et al. reported that in seemingly non-emphysematous COPD patients who possessed similar total LAA% to healthy patients (< 30% of total CT lung volume), the number and complexity of small LAA clusters was decreased, and had been suggested to reflect the enlargement and reducing complexity of terminal airspace geometry in early emphysema (183). A study from Tanabe et al.,

who utilised similar LAA – fractal analysis techniques, reported that exacerbations could accelerate the progression of emphysema by both enlarging and adjoining existing LAA regions possibly as a result of further alveolar wall destruction (184). Additionally, LAA – fractal analysis has been shown to be sensitive to emphysematous changes to diffusing capacity in currently smoking COPD patients over a period of five years (185).

Recently, a completely alternative approach to quantitative CT analysis for emphysema has also been developed referred to as ‘texture analysis’. This analysis technique assesses a variety of CT image properties such as spatial relationships between areas of different intensity counts and size or patterns of low attenuation areas within a region of interest (ROI) in the lung. Unlike LAA% analysis, which has been generally standardised with the -950 HU threshold method, ‘texture analysis’ is far more complicated, and a variety of different algorithms have been proposed. The ‘adaptive multiple feature method’ (AWFM), which assesses various first and second order features such as mean intensity, variance, and non-uniformity within a ROI, has been used to evaluate emphysema (186). AWFM is also demonstrated to recognise different regional lung disease patterns on CT scans such as honeycomb lung tissue in pulmonary fibrosis, ‘ground glass opacities’ in pneumonia, and emphysema as well as experienced human observers (187).

In comparison to LAA%, emphysema severity as measured with AWFM and other ‘texture analysis’ methods correlate significantly better with lung function tests, such as spirometry and diffusing capacity for carbon monoxide (188, 189). According to

Sørensen et al., ‘texture analysis’ may be utilised to identify COPD patients with increased risk of rapid lung function decline. More recent ‘texture analysis’ methods such as the automated ‘gray-level run-length’ and ‘gray-level gap-length’ methods were able to successfully distinguish between healthy lungs, centrilobular emphysematous lungs, and lungs with respiratory bronchiolitis from non-emphysematous smokers (190). One limitation to the ‘texture analysis’ algorithms are their relative complexity and high computational cost compared to LAA% analysis. Therefore Mendoza et al. (191) proposed a simpler quantitative method for emphysema pattern analysis. In their study, Mendoza et al. hypothesised that rather than including spatial analysis, measuring local variations in pixel intensity alone would be sufficient to distinguish six CT lung tissue patterns: normal tissue, paraseptal emphysema, panlobular emphysema, and mild/moderate/severe centrilobular emphysema. By estimating intensity probability distribution functions for each lung tissue pattern with kernel density estimation (192), Mendoza et al. (191) reported that the simpler intensity distribution method classified emphysema patterns more successfully than the more complex ‘texture analysis’ method that incorporated both intensity and spatial analysis. LAA% analysis via the traditional -950 HU threshold and the intensity distribution method were later utilised by Castaldi et al. (193) to examine the relationships between emphysema patterns and demographics and measurements of lung function and symptoms in 9313 smokers. In comparison to -950 HU LAA% analysis, areas of low attenuation as assessed by the intensity distribution method (e.g., severe centrilobular emphysema) were more predictive of airflow obstruction, dyspnoea severity, exercise capacity, and exacerbations.

Although there have been numerous advancements and refinements to quantitative CT analysis of emphysema, emphysematous destruction is only one, important facet to COPD pathophysiology. Other anatomical and physiological manifestations such as airway wall thickening or small airways disease have been extensively examined with quantitative CT imaging analysis. Nakano et al. utilised a -500 HU threshold and an automatic algorithm that fanned out 128 rays over 360º from the centroid point of the lumen to estimate the airway wall area and thickness of the apical bronchus of the right upper lobe. They demonstrated that in smokers with airflow obstruction both airway wall area and thickness were significantly increased compared to smokers without airflow obstruction. These measurements had also correlated with worse airflow obstruction and gas trapping as determined by FEV1 and residual volume/total lung capacity ratio, respectively. There was no correlation between the outer area of the apical bronchus and severity of airflow obstruction. Thus, the authors suggested that airway wall thickening in COPD may be mostly characterised with internal encroachment towards the lumen rather than outward airway wall expansion. In patients with similar airflow obstruction severity, patients with greater emphysema (as assessed by LAA%) had thinner airway walls than patients with reduced or minimal emphysema. This was thought to indicate two COPD phenotypes, predominately emphysematous and predominately airways disease (194).

Subsequently, Nakano et al. developed a more complex software that was capable of placing seed points in the lumen of all larger airways that were visible on CT scans (195). By projecting 64 rays from the seed points within the lumens, the total airway area, luminal area, airway wall area, and wall area percentage of total airway

area were measured and compared with quantitative morphology of excised human lungs. After initially finding that the CT measurements were overestimated, the morphology data was used to correct the algorithm, and the average errors were reduced by 23% and 7% for airway lumina area and wall area, respectively. In a different study, Nakano et al. used the corrected algorithm and reported that the mean dimensions (e.g., internal perimeter and square root of airway wall area) of the smaller conducting airways with an internal diameter of 1.27 mm could be predicted by the dimensions of the larger airways, provided the minimum internal perimeter was 0.75 cm (196). However, it is important to note that while there was a correlation between measurements obtained from this algorithm and histological measurements, the former had again overestimated the airway wall area.

The algorithm from Nakano et al. that could predict the dimensions of small airways from larger CT visible airways were subsequently used in a multitude of COPD studies in conjunction with LAA% emphysema analysis. In a study by Patel et al., one of the objectives were to examine whether the contributions of airway wall thickness and emphysema to COPD severity were independent (197). To quantitively assess airway wall thickness from high resolution CT scans, Patel et al. had utilised the algorithm developed by Nakano et al. (195) to predict the square root of airway wall area of a ‘theoretical’ airway with an internal perimeter of 10 mm (AWT-Pi10), which conforms to an internal diameter > 2 mm. They reported that airway wall thickness and emphysema did indeed make independent contributions to airflow obstruction in COPD. Furthermore, the development of emphysema and airway wall thickening had distinctly clustered within families, and this possibly suggested genetic susceptibility to either the predominately emphysematous or predominately

airways disease phenotypes. However, it is important to note two potential limitations of this study. Firstly, AWT-Pi10 assesses the dimensions of a theoretical airway with an internal diameter > 2 mm, but as the authors themselves also note, the major site of airflow narrowing in COPD patients are instead in airways with an internal diameter < 2 mm. The second potential limitation with AWT-Pi10 and the algorithm from Nakano et al. in general (195) is its inability to consider the dynamics of airway wall thickness, particularly with airway smooth muscle contraction, narrowing, and dilation. Noble et al. utilised both histology and a fibre optic anatomical optical coherence tomography (aOCT) probe in 6 dissected pig airways to examine changes in internal diameter of the airway and airway wall movements induced by airway smooth muscle contraction (198). The authors reported that during contraction, airway diameter and the inner airway wall, comprising of both mucosa and airway smooth muscle, reduced and increased, respectively. Thus, neither airway wall area nor airway diameter remain static. As stated previously, the algorithm essentially calculates the dimensions of an airway wall from a seed point placed within the airway lumen and the rays projected from this seed point to the outer perimeter. It is unlikely that complex airway wall dynamics in contraction or dilation are accounted for, particularly when small airway wall dimensions are predicted from larger airways.

Grydeland et al. (199) investigated the relationships between quantitative CT measurements of airway wall thickness (as measured by AWT-Pi10), emphysema (as measured by LAA%), and clinical characteristics such as age, sex, smoking history, and degree of current smoking in COPD patients. The extent of emphysema was increased in patients who were older, ex-smokers with greater smoking pack years. Conversely, airway wall thickness had decreased with age and increased with

the degree of current smoking. In another quantitative CT study, Grydeland et al. (200) reported that whilst both emphysema (LAA%) and airway wall thickening (AWT-Pi10) independently related to the severity of dyspnoea in COPD patients, cough and wheezing were best predicted by AWT-Pi10. Thus, increased AWT-Pi10 was thought to be indicative of various pathological changes to the airways such as airway inflammation, hyperplasia of goblet cells, and mucus hypersecretion. Increased AWT-Pi10 positively correlated with diffusing capacity for carbon monoxide (DLCO) in COPD, while LAA%, unsurprisingly, negatively correlated with DLCO (201).

As noted previously, the classic ‘pink puffer’ and ‘blue bloater’ phenotypes are traditionally associated with muscle wasting and increased BMI, respectively. Utilising both LAA% and AWT-Pi10 techniques, Rutten et al. examined the associations between the quantitative CT parameters and measurements of body composition (202). Although decreased skeletal muscle mass was found to be significantly associated with a greater extent of emphysema, it was not found to be discriminatory for the predominately emphysematous phenotype. Additionally, increased wall thickness had significantly correlated with fat mass index in both COPD and healthy participants. Whilst the utility of traditional phenotypical markers such as body composition and BMI were somewhat questionable, the findings were supportive of the use of quantitative CT measurements as potential phenotyping traits.

AWT-Pi10 has also been demonstrated to be significantly associated with important clinical outcomes. According to Kahnert et al. (203), increased AWT-Pi10, and thus greater airway wall thickening, was associated with a history of myocardial infarction, greater annual decline of FVC, and increase of gas trapping over 6 years in COPD patients. AWT-Pi10 was shown to be a significant predictor of mortality. Furthermore, COPD patients receiving triple LABA/LAMA/ICS therapy had significantly decreased AWT-Pi10, and this was suggested by the authors to indicate morphological benefits in more severe patients with increased rate and severity of exacerbations. In participants without cardiovascular disease or prevalent chronic lower respiratory diseases such as asthma, COPD, or chronic bronchitis, increased AWT-Pi10 predicted incidence of COPD, greater lung function decline, and increased risk of mortality and respiratory-related hospitalisations (204). In a recent study by Chaudhary et al. (205), the authors developed a predictive model that included AWT-Pi10 and AMFM texture analysis, spirometry, and patient characteristics such as age, race, and BMI to identify COPD patients with a high risk of a severe exacerbation. The quantitative CT parameters were reported to be significantly better at predicting future severe exacerbations in 3 years than either exacerbation history or the BODE index.

Rather than analysing emphysema and small airways disease separately with LAA% and AWT-Pi10 respectively, Galbán et al. (206) sought to examine both and spatially display abnormal lung regions. To do so, the authors adapted and modified the “parametric response map” (PRM) technique for inspiratory and expiratory CT lung scans. It had been originally developed by Moffat et al. (207) for magnetic resonance imaging (MRI) scans from cancer patients to identify early therapeutic response on

tumours. The modified PRM technique by Galbán et al. (206) classified the image voxels into three different lung tissue categories: emphysema was defined by a -950 HU threshold on full inspiration, “functional small airways disease” or gas trapping was defined by a -856 HU threshold on expiration, and healthy lung tissue was defined either by a ≥-856 HU threshold on expiration or ≥-950 HU threshold on inspiration. The distribution of voxels in an emphysema (inspiration) – healthy lung tissue (inspiration) – functional small airways disease (expiration) – healthy lung tissue (expiration) quadrant indicated an airway to emphysema disease progression in COPD. This had not been previously observed with other quantitative CT imaging analysis techniques. Unlike AWT-Pi10 analysis, PRM can display the three different lung tissue categories three-dimensionally. This would potentially allow for regional tissue analysis.

Quantitative analysis with micro-computed tomography (micro-CT) may also be used to better characterise and phenotype COPD. Unlike CT, micro-CT allows for the visual identification of small airways with an internal diameter < 2mm from ex-vivo human lungs. Regarding COPD pathophysiology, this imaging technique has shown small airway narrowing and destruction occurring prior to the onset of emphysema (112). Additionally, micro-CT revealed that total small airway count and mean lumen diameter of the small airways are lowest in COPD patients with centrilobular emphysema, which is generally associated with cigarette smoking (4). This may indicate a more destructive structural process than COPD patients with alpha-1 antitrypsin deficiency and panlobular emphysema. Tanabe et al. (208) applied CT airway wall measurement techniques from Nakano et al. (194, 195) on micro-CT scans of ex-vivo 95 human lung tissue samples to measure the dimensions of the

small airways one generation proximal to the terminal bronchioles. They had also measured the number of alveolar attachments with a technique originally designed for histology (209), interalveolar distances for emphysema quantification, and length of the “pre-terminal” airways along the centreline with ImageJ (National Institutes of Health, Bethesda, MD). It was observed that in comparison to the control lungs, lungs with either centrilobular or panlobular emphysema had significantly decreased wall volume, total airway volume, alveolar attachments, and airway length. However, lungs with centrilobular emphysema had more severe and heterogeneous airway wall thickening and airway narrowing than lungs with panlobular emphysema. This again aligns with the findings from Hogg et al. that suggested a more destructive structural progress in smoking COPD patients (4).

Various machine learning tools have recently been utilised with CT lung scans. One example would be the Subtype and Stage Interference (SuStaIn) machine learning tool, and it was first developed by Young et al. to examine heterogeneity in neurodegenerative diseases (210). However, Young et al. subsequently applied SuStaIn to examine distinct patterns of disease progressions in COPD from CT lung data such as airway wall thickness and emphysema (211). They reported two distinct patterns of disease progression. The most predominant pattern (approximately 70% of patients) was defined by small airway wall changes and emphysema preceding large airway wall changes, and this pattern, named ‘Tissue to Airway’ (TA), appears to be aligned with the findings obtained from the micro-CT scans (small airways changes occurring first) (112). However, the less prevalent pattern (approximately 30% of patients) was characterised by large airway wall changes preceding small airway wall changes and emphysema, and this was named the ‘Airway to Tissue’

pattern (AT). TA patients had significantly greater extent of emphysema (LAA%) and tissue damage than AT patients. Conversely, AT patients had significantly greater airway wall thickness (AWT-Pi10) than TA patients. Interestingly, patients with the predominant ‘Tissue to Airway’ pattern possessed characteristics that resembled the classic ‘pink puffer’ phenotype: significantly lower BMI and a greater extent of emphysema. Conversely, the ‘Airway to Tissue’ pattern was associated with increased incidence of chronic bronchitis symptoms and greater airway wall thickening. Another characteristic of the ‘Airway to Tissue’ pattern was a greater decline of lung function during the earlier stages of disease severity (211).

Whilst CT is predominately used to assess abnormalities in lung structure such as emphysema and airway wall thickness, there have been several innovative techniques that aimed to examine lung function (i.e. ventilation) instead. Ventilation CT can be broadly categorised into two groups: tracer and non-tracer agent methods. The former generally utilises xenon (Xe) gas, which is mixed in a fixed ratio (e.g. 30%) with oxygen during wash-in periods, as a tracer or contrast agent and dual energy CT, and this allows the differentiation of Xe from lung tissue (212). There are a large variety of quantitative analysis methods available. One notable example, particularly relevant for COPD, is from Park et al. (213). They divided dual energy CT lung scans of 38 COPD participants into three areas based on HU thresholds: whole lung = -1024 – -500 HU; normal attenuating lung = -950 – -500HU; and low attenuating lung = -1024 – -950 HU. The presence of Xe was defined with a HU threshold range of 1 – 50 HU, and pixels with attenuation > 50 were regarded as noise. This threshold of 50 HU was reportedly based on their phantom data. Furthermore, the presence and concentration of Xe was measured in both wash-in

and wash-out periods. The authors reported positive and inverse correlations between spirometric indices (FEV1, FEV1/FVC) and Xe presence in normal attenuating and low attenuating lung regions, respectively. Furthermore, positive and inverse correlations between DLCO and Xe presence in normal attenuating and low attenuating lung regions, respectively, were observed. This technique can allow for visualisation, mapping, and quantification of ventilation within distinct regions of emphysematous and normal lung tissue. However, the high cost and concerns with radiation exposure appear to be this technique's primary limitations (214), and Xe dual CT ventilation imaging studies that measure other phenotypical markers such as lung volumes or negative clinical outcomes or with treatment in COPD participants remain sparse.

Assessing lung function, without the expense and radiation concerns associated with Xe dual CT imaging is a highly attractive option. The general steps with non-tracer ventilation CT consist of the following: 1) multiple images are acquired at different levels of inflation (e.g. from TLC to either FRC or RV); 2) the lung CT images are segmented, and a non-rigid algorithm is used to register the lung CT images at different levels of inflation to each other (215); and 3) specific changes in air volume are calculated to estimate regional ventilation. This form of functional CT imaging, particularly with improved air volume calculation methods, has been shown to significantly correlate with Xe CT based measurements of ventilation (216). Furthermore, significant associations between ventilation defects, as measured by CT, and reduced FEV1 and increased FEV1/FVC in COPD participants have been reported (217). Similar to the Xe CT ventilation study from Park et al. (213), who mapped and compared ventilation in emphysematous and normal lung regions,

Yamamoto et al. demonstrated with non-tracer CT that emphysematous regions to have consistently lower ventilation than non-emphysematous regions (218).

There has been a vast amount of progress made in quantitative CT analysis. Although global estimations on emphysematous regions via LAA% are too simplistic for precise phenotyping, various modifications with supplementary thresholds have been proposed over the years to better analyse emphysematous subtypes and categorise abnormal lung tissue. Quantitative CT has also been used extensively to examine pathological airway changes in COPD. Analysing both abnormal lung parenchyma and airways has allowed to identify various patient subgroups who are at increased risk of adverse clinical outcomes with different disease progressions. CT had historically been unable to assess lung function, hence the use of non-CT ventilation imaging. However, recent innovations in technology and analysis techniques have allowed CT to measure ventilation defects as well. CT imaging has been demonstrated to be an invaluable tool for COPD characterisation.

1.9 Quantitative three-dimensional ventilation single photon emission computed tomography analysis in COPD

Non-CT three-dimensional ventilation imaging shows promise in COPD characterisation and phenotyping. This form of imaging technique has generally been the primary method for viewing and assessing the ventilatory consequences of airway obstruction, small airway dysfunction, and emphysema. It may also be used to identify COPD patients with unremarkable spirometric parameters (e.g., FEV1 or FEV1/FVC) or demographics (e.g., smoking history) who nonetheless possess poor

ventilation. Another promising avenue for ventilation imaging analysis is the investigation of pharmacological treatment, which can potentially provide new treatment endpoints in clinical studies. This imaging technique could be used to better understand how bronchodilators work in COPD and examine whether these drugs are capable of reventilating previously unventilated lung regions. COPD patients who respond or don't to pharmacological treatment may also be identified. The improvements made to image resolution, scanner technology, analysis software, and cost make quantitative ventilation imaging analysis more accessible than ever.

Three-dimensional ventilation imaging is predominantly performed with either single photon computed tomography (SPECT) or hyperpolarised magnetic resonance imaging (MRI). For ventilation SPECT (VSPECT), it requires the participant to inhale radioactive aerosols, and common examples would be either Technegas, which are ultrafine Technetium-99m nanoparticles with a diameter of approximately 100 nm, or 99m-Technecium-labelled diethylene triamine pentaacetic acid (DTPA). Jögi et al. (219) compared these two agents. To summarise, Technegas is overall superior to DTPA, as the former was shown to deposit more evenly and peripherally in participants with both obstructive and non-obstructive airways disease. Although exaggerated deposition of aerosols, which create 'hot spots' (Figure 4), occur in both agents, DTPA is far more susceptible of the two. 'Hot spots' are thought to form due to turbulent airflow (i.e. deviating streamlines) in partially narrowed airways impacting aerosol particles onto the airway wall. In more severely narrowed or peripheral airways with consequently reduced or non-turbulent airflow, aerosol impaction should be minimised. Additionally, the likelihood of aerosol deposition is naturally higher with larger particles, hence the superiority of Technegas. Whether with DTPA or

Technegas, proximal airways and bifurcation points appear to be the predominant location of ‘hot spots’ in COPD patients (220). Another advantage of VSPECT and Technegas is the radioactive agent’s ability to adhere to lung structure for approximately twenty minutes after inhalation (221). Therefore, if the participant inhales tidal volumes of Technegas from FRC in a seated position, the supine VSPECT scan should reflect tidal ventilation distribution at the seated position. This is a unique advantage to VSPECT as hyperpolarised MRI scans are typically performed with a 1 L inhalation and breath hold manoeuvre from FRC. Although not a true gas, Technegas has been observed to disperse and penetrate peripheral lung spaces in a manner similar to gas, even in patients with severe airflow obstruction (222). However, whether Technegas deposition is reflective of diffusive flow in alveolar or collateral ventilation is unknown. In recent years, registration of SPECT and CT scans (SPECT/CT) has allowed for the examination of ventilation or non-ventilation within accurately defined lung borders (Figure 5) (223). It was previously difficult to distinguish the lung border with VSPECT alone if peripheral lung regions were poorly ventilated.

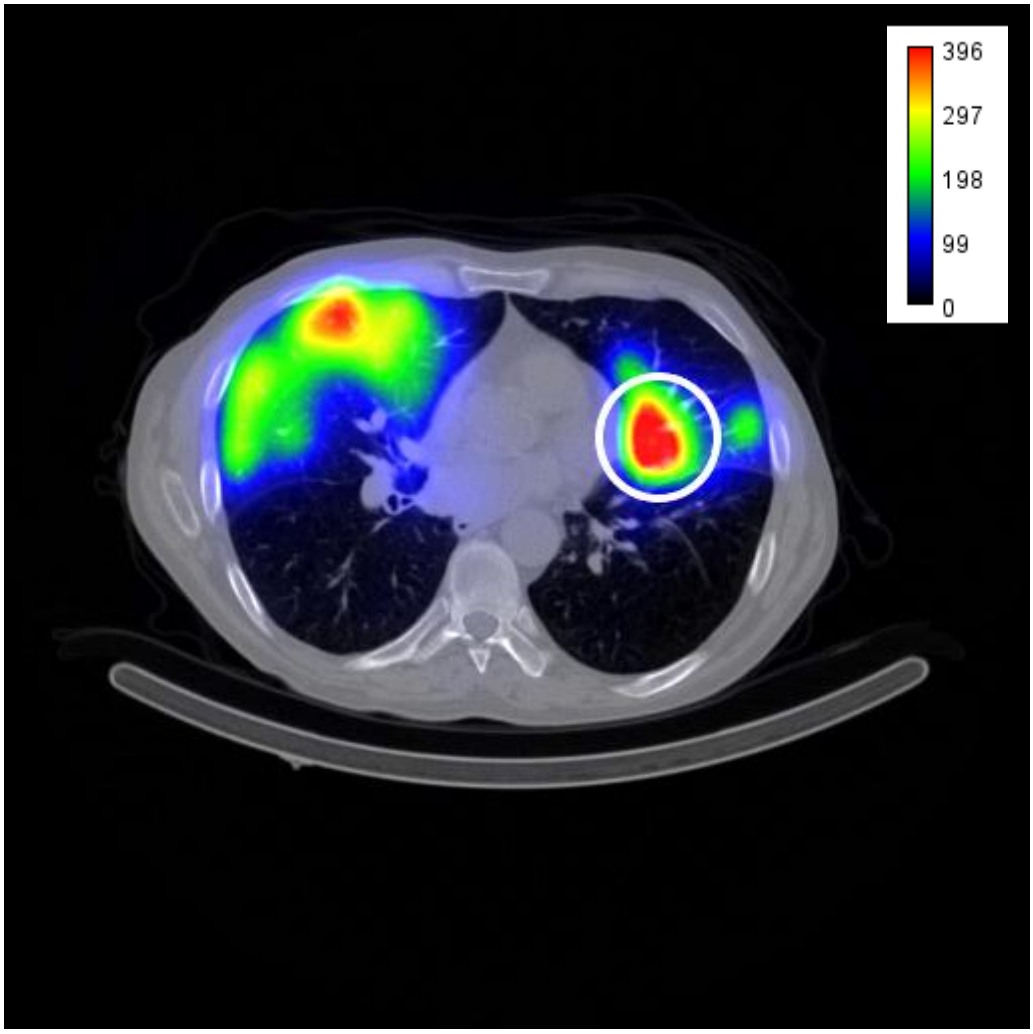


Figure 4: Technegas ventilation single photon computed tomography/computed tomography (VSPECT/CT) axial image of a 72-year-old COPD patient. A ‘hot spot’, a region with increased deposition of Technegas, is indicated with a white circle.

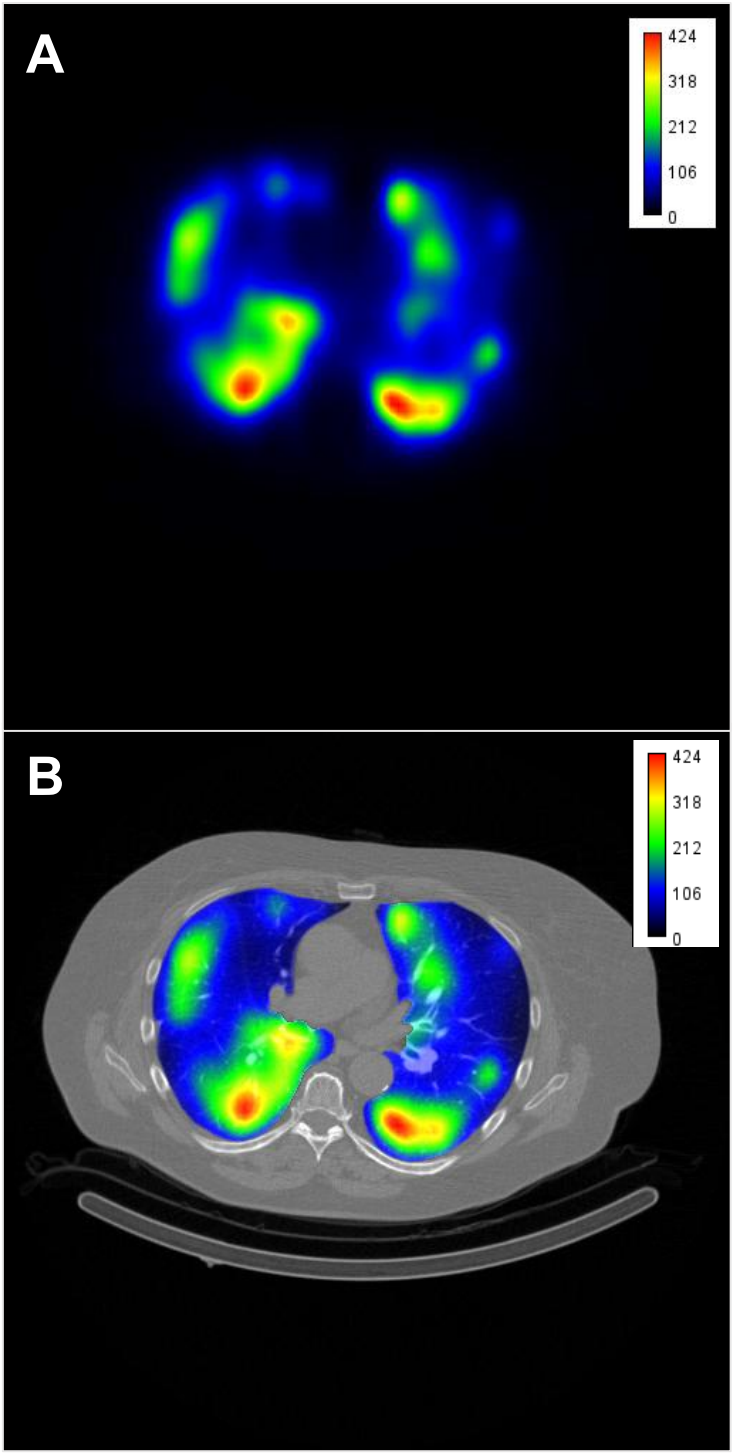


Figure 5: Technegas ventilation single photon computed tomography (VSPECT) axial images of a 74-year-old COPD patient with and without computed tomography (CT) registration. (A) VSPECT scan; (B) VSPECT/CT registered scan.

Despite the unique advantages of VSPECT to portray seated tidal ventilation, there have been minimal investigations involving global measurements of non-ventilated volume in COPD patients. However, VSPECT studies have long since demonstrated there to be limited ventilation in COPD patients with more severe disease. In a novel study, Cuna et al. (224) reported that a cohort of five COPD patients, those with more severe airflow limitation as measured by FEV1 had increased non-ventilated volume. Unfortunately, no other lung function tests were performed. In a recent VSPECT and hyperpolarised gas MRI comparison study in a mixed cohort of asthma, COPD, and non-obstructed patients by Radadia et al. (225), the authors observed that increased non-ventilated volume in the VSPECT scans correlated significantly with poorer gas transfer (D_{LCO}) and increased airflow obstruction (FEV1/FVC). COPD patients possessed significantly increased non-ventilated volume compared to both asthma and non-obstructed patients. This could indicate that VSPECT is sensitive to the effects on ventilation from parenchymal damage and airway abnormalities such as mucus plugging and obliteration. However, this study from Radadia et al. (225) did not examine lung volume measurements of gas trapping or hyperinflation nor oscillometric parameters related to small airway dysfunction. An older VSPECT and high resolution CT study by Stavngaard et al. (226) applied both quantitative and qualitative analysis techniques on non-ventilated volume in COPD patients. Qualitative assessment for non-ventilation consisted of visual scoring. The quantitative estimate for increased non-ventilated volume correlated with reduced FEV1 and reduced gas transfer (D_{LCO}). There were no associations between non-ventilated volume and RV or LAA% as measured with high resolution CT. Interestingly, qualitative scores indicating increased non-ventilation correlated with reduced FEV1, reduced D_{LCO}, increased RV, and

increased emphysema extent, despite both visual assessment and quantitative estimations correlating with each other. This discrepancy and the limited number of studies may have been due to the limitation and inadequacies of VSPECT quantitative techniques, but this will be covered in more detail later. Currently, there is only one VSPECT study that has investigated the effects of bronchodilator therapy on non-ventilation in COPD patients (227). According to Diba et al. (227), LAMA did not decrease non-ventilated volume. However, it should be noted that this study involved a small number of COPD patients (10), and quantitative analysis was performed with an unvalidated technique.

Whilst analysing non-ventilated volume has remained the primary focus of quantitative VSPECT studies, some studies have opted to examine ‘hot spots’ as well. As mentioned previously, ‘hot spots’ (Figure 4) occur from exaggerated deposition of the radioactive agent in lung regions with turbulent flow (e.g. narrowed airways) and/or at bifurcation points. To our knowledge there has been only one quantitative VSPECT study that analysed total ‘hot spots’ count but none for COPD. Pellegrino et al. (228) observed that following bronchoconstriction in asthma patients, the number of ‘hot spots’ in two-dimensional scintigraphic VSPECT images had increased, particularly in proximal lung regions. Qualitative VSPECT studies have consistently noted there to be more numerous and brighter ‘hot spots’ (from increased agent deposition) in more severe COPD patients (220). Bajc et al. (229) reported there to be both poorer overall ventilation and increased ‘hot spots’ count, both visually assessed, in patients affected with emphysema. The authors speculated that increased ‘hot spots’ count in more peripheral lungs regions resulted from small airways disease. Scores from visual grading systems that assess non-

ventilation and ‘hot spots’ count together has been shown to correlate with GOLD 2013’s COPD severity grades and to distinguish healthy participants from long-time smokers without COPD (230). A few qualitative studies have also examined the effect of interventions on ‘hot spots’. Paludan et al. (231) presented a qualitative VSPECT case report in which they examined the effects of continuous positive airway pressure (CPAP) therapy on two COPD patients. On the ventilation scans, they observed that either ‘hot spots’ count decreased or ‘hot spots’ occurred in more peripheral lung regions following CPAP therapy. This may have been due to reduced expiratory flow limitation and/or removed mucus plugs or clots through increased mucus mobilisation. Imai et al. (232) demonstrated that following lung volume reduction surgery in emphysematous patients, the number of ‘hot spots’ count reduced, and there was a correlation between improvement in spirometry and visually assessed scores for non-ventilation and ‘hot spots’. For a quantitative approach to ‘hot spot’ analysis, applying a ‘hot spot’ threshold in conjunction with a non-ventilation threshold would be simple to perform.

1.10 Inadequacies with current ventilation imaging analysis methods for single photon emission computed tomography

Much like the use of the -950 HU threshold in CT imaging analysis, measuring the extent of non-ventilated volume with VSPECT is also done with a threshold to the imaging data. In a three-dimensional VSPECT image, the intensity (i.e., ‘brightness’) of the three-dimensional pixels or ‘voxels’ ranges from zero or low in areas with no agent deposition (e.g., areas outside the lung or non-ventilation regions) to very high in areas with exaggerated agent deposition (i.e., ‘hot spots’). Applying an intensity

threshold to VSPECT data would classify the voxels above or below the intensity into either ventilated or non-ventilated categories. However, unlike the -950 HU threshold, which is demonstrated to correlate with macroscopic and microscopic measurements of emphysema (167, 168), none of the currently existing threshold techniques for VSPECT are validated. The primary challenge for quantitatively measuring non-ventilated volume with VSPECT is the unpredictable, heterogeneous range of voxel intensities that are found in patients with respiratory diseases such as COPD (Figure 6). ‘Hot spots’, particularly in patients with more severe obstructive lung disease, can produce voxels with substantially increased intensities from concentrated Technegas deposition within a small lung region. This will consequently increasing data heterogeneity and complicate imaging analysis. The range of voxel intensities would also be dependent on the radioactivity of the agent inhaled by the participant, which typically varies between 1.5 – 2.0 kilocounts. The intensity threshold for non-ventilation in a participant who inhales 1.3 kilocounts would be lower than the non-ventilation threshold in another participant who inhales 2.2 kilocounts.

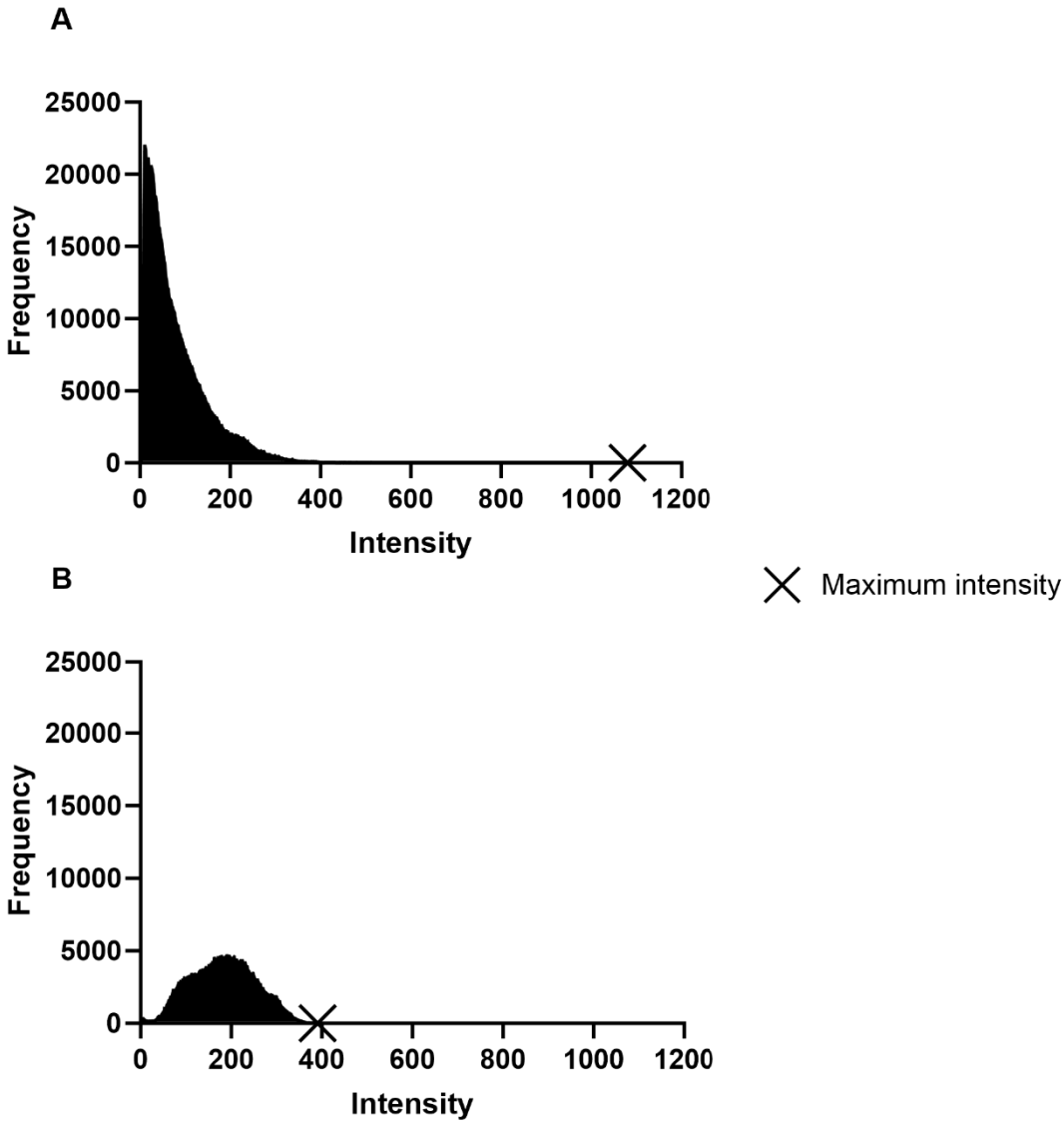


Figure 6: Two voxel frequency – voxel intensity plots from ventilation single-photon computed tomography/computed tomography (VSPECT/CT) scans of two different COPD patients. Both the frequency or number of voxels and the range of voxel intensities differ between the VSPECT/CT scans. The maximum intensity from each scan has been marked with an X.

Despite the variability in maximum voxel intensities, VSPECT studies have traditionally opted for a percentage of maximum threshold. In a systematic review of fifteen SPECT studies of lung cancer patients, the authors reported the percentage of maximum thresholds for VSPECT had widely ranged from 30% to 70% (233). According to Cuña et al, in which various percentages of maximum thresholds were assessed in five patients COPD, a threshold of 27% of maximum correlated best with FEV1 (224). However, heterogeneous maximum intensities in patients with varying severity of airflow obstruction is a significant issue for the traditional threshold method. A ‘fixed’ percentage of maximum threshold may accurately determine non-ventilated activity in one patient and inaccurately determine it in a different patient with substantially increased or decreased Technegas deposition in a ‘hot spot’. This problem has been noted by Nagao et al. (234) as they had attempted to adapt the same percentage of maximum threshold from a different VSPECT study but then noted that it had ‘defined’ ventilation in regions outside the lung.

To overcome this issue of variable maximum intensities, an alternative ‘adaptive’ threshold method was developed by Farrow et al. (223) for their VSPECT study on patients with asthma. Rather than solely relying on the maximum count to determine the threshold for non-ventilated activity, the authors used the mean activity as it would be relatively less affected by ‘hot spots’, which possess high intensities but a small amount of voxels. Specifically, their threshold was calculated by multiplying the mean count of the voxels between 5% and 80% of the maximum intensity by 50%. The 5% – 80% of maximum intensity was chosen to exclude extremely high and low intensities from ‘hot spots’ and non-ventilated regions, respectively. Farrow et al. (223) reported there to be no systematic differences between this method’s

measurement of ventilated volume at tidal breathing and FRC as measured with multiple breath nitrogen washout. So far, this threshold method has only been used in one VSPECT study that included COPD patients, and this was the aforementioned VSPECT and hyperpolarised gas MRI comparison study by Radadia et al. (225). Whilst no complications with the adaptive threshold technique from Farrow et al. were reported (223), it is still unknown whether the technique is accurate and robust enough for the heterogenous voxel data encountered in COPD.

In the broader realm of computer vision, there are a plethora of widely used automatic threshold techniques that may be suitable for VSPECT imaging analysis due to their robustness to data heterogeneity. Such examples include Otsu's method (235) (Figure 7), which determines its threshold by maximising variance between two different categories of voxel activity, and the IsoData method (236), which iteratively updates its threshold until the threshold value is larger than the average of the average intensities of the two voxel categories. Otsu's method has found use in CT imaging analysis for the purposes of segmentation of organ volumes (237), but it is yet to be utilised in VSPECT studies.

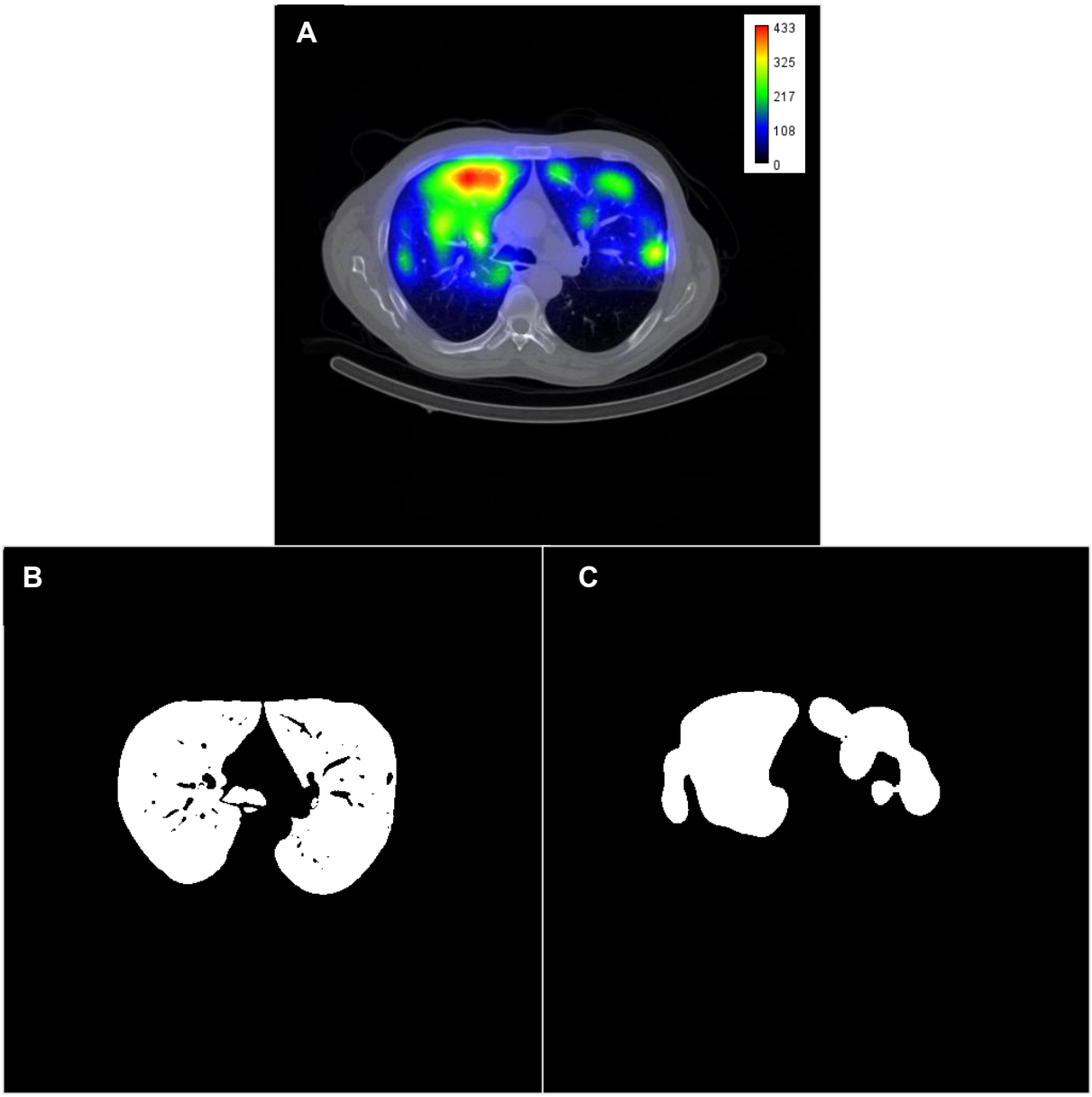


Figure 7: Otsu's method applied to Technegas ventilation single photon computed tomography/CT (VSPECT/CT) axial images of a 75-year-old COPD patient. (A) VSPECT/CT axial scan without Otsu's method thresholding; (B) Otsu's method thresholding to CT scan, categorising the lungs (and bronchus) and chest into binary classes. (C) Otsu's method thresholding to VSPECT scan, categorising Technegas voxel intensities into binary classes. This may be applied to identify ventilation/non-ventilated regions.

1.11 Quantitative three-dimensional magnetic resonance imaging analysis in COPD

As mentioned previously, another common example of three-dimensional ventilation imaging is hyperpolarised MRI, which involves the inhalation of a noble gas such as helium-3 or xenon-129. For hyperpolarised MRI, helium-3 possesses a stronger MRI signal than xenon-129, and so, most ventilation MRI studies were initially completed with helium-3 as its noble gas agent. However, helium-3 is also scarce (238) and expensive (239) due to it being exclusively sourced from the radioactive decay of tritium. Conversely, xenon-129 is cheaper and more abundant. Due to innovations in xenon-129 polarisation technology, such as increased production of highly polarised xenon-129 (240) and optimisation of the production process (241), in addition to improved MRI imaging technology (242), the use of xenon-129 for ventilation MRI studies have since increased in recent years. For measuring ventilation defects, it should be noted that there are differences between helium-3 and xenon-129 MRI scans. Two studies from Kirby et al. compared the volume and homogeneity of ventilation defects in COPD patients as measured with hyperpolarised helium-3 and xenon-129 MRI scans (243, 244). They observed that ventilation defects were both larger and more heterogeneous in xenon-129 MRI scans, and this most likely resulted from the relatively reduced diffusivity of xenon-129 compared to helium-3. Thus, xenon-129 may penetrate peripheral and/or diseased lung regions more slowly than helium-3, and helium-3 may also be a superior indicator of collateral ventilation. The inhalation technique for hyperpolarised MRI requires the participant to inhale 1 L of the noble gas and then hold their breath in a supine position throughout the scan.

Despite hyperpolarised MRI being more expensive than VSPECT, there are a greater number of ventilation imaging studies that have utilised the former method to assess COPD. A critical study by Kirby et al. (245) examined 91 COPD patients over a 5-year period with lung function tests, SGRQ, six-minute walk tests, quantitative CT, and helium-3 MRI. The authors reported that increased non-ventilated volume percentage of total lung volume (VDP%) significantly related to quantitative CT measurements of emphysema (LAA%) and airway wall thickening (airway wall area). Increased VDP% was speculated to represent functional consequences from both emphysema and airways disease, and so, it may assist in characterising the mixed airways-emphysematous COPD phenotype. In all COPD patients, the risk of hospitalisations throughout the 5-year period were not related to FEV1 or diffusing capacity (D_{LCO}). Instead, history of prior hospitalisations, exercise capacity, LAA%, and VDP% were significantly related to hospitalisation risk. In mild – moderate COPD patients specifically, increased VDP% was found to be the sole predictor of hospitalisation risk. Increased VDP% is also found in patients with worse airflow obstruction (FEV1/FVC) and gas diffusion (D_{LCO}) and greater smoking pack year history (225). In patients with mild – moderate COPD, baseline VDP% can predict minimum clinically important changes in health status, measured with SGRQ scores, throughout a 30-month period (246). Furthermore, VDP% changes within this time correlated with SGRQ scores. According to Davis et al. (247), increased VDP% correlates with COPD severity and increased ventilation heterogeneity as measured with the alveolar volume/total lung capacity ratio. Young et al. (248) reported a correlation between increased VDP% and poorer quality of life in COPD patients. Furthermore, there was also a significant association between increased small airways resistance heterogeneity due to heterogeneous airway narrowing in the lung

periphery (R5 – R19 Hz) and increased VDP% in COPD patients. Another common quantitative analysis technique for hyperpolarised MRI, either with helium-3 or xenon-129 (249), is apparent diffusion coefficient (ADC) of the noble gas agent. ADC is reflective of the restriction of the diffusion of noble gas atoms within an airspace. Compared to explanted healthy lungs, ADC in emphysematous lungs is reported to be significantly increased due to enlarged airspaces, resulting in less restriction of gas atom diffusion (250). Additionally, ADC appears to be a useful tool in detecting early lung damage as increased ADC is reported to be increased in both asymptomatic smokers (251) and participants exposed to second hand smoke (252). Regarding correlations with lung function measurements, increased ADC is significantly related to worse airflow obstruction, gas trapping, and DLCO in COPD patients (249, 253), and ADC was reported by Tafti et al. to have similar diagnostic performance to quantitative CT (254). Furthermore, in a case report by Kirby et al. on a 77-year-old COPD ex-smoker over a four-year period, they observed that six months prior to an acute exacerbation, both VDP% and ADC were increased by 13% and 0.34 cm^2/s compared to results from two and a half years prior. However, FEV1 was paradoxically increased by 6%. Following treatment, both VDP% and ADC returned to similar levels to four years prior.

Quantitative ventilation imaging techniques, primarily with MRI, have been extensively utilised to investigate physiological abnormalities in COPD, such as emphysema and airways disease. Objective imaging parameters were shown to be associated with important clinical outcomes such as hospitalisations, progression, and mortality. Such parameters can be helpful in either identifying patients with increased risk of poor clinical outcomes or defining more specific COPD phenotypes.

1.12 Ventilation imaging & bronchodilator responsiveness in COPD

Although there is a growing body of literature showing correlations between ventilation imaging parameters and a wide variety of measurements on lung function, clinical outcomes, and symptoms, very few quantitative ventilation imaging studies have studied the effects of bronchodilator treatment in COPD. But hyperpolarised MRI has revealed significant reductions in non-ventilated and poorly ventilated volumes following salbutamol (255) and dual LABA/LAMA therapy (256). As noted previously, VSPECT has not been used to investigate bronchodilators in COPD, but this technique possesses numerous advantages. These include its relatively lower cost to hyperpolarised MRI, easier inhalation technique (only tidal breaths and no breath holds throughout the scan), Technegas's ability to adhere to lung structure during seated inhalation, and the visualisation of tidal ventilation distribution. The physiological effects on ventilation in COPD patients with clinically significant bronchodilator responsiveness (BDR), a somewhat contentious phenotypical trait, has not been extensively examined with quantitative ventilation imaging.

Clinically significant BDR has traditionally been once regarded as diagnostic marker for asthma, and it is defined with a spirometric response to a known dose of SABA such as salbutamol. According to the most recent American Thoracic Society/European Respiratory Society (ATS/ERS) guideline, a positive BDR is defined by a ≥ 10% change in the predicted FEV1 value (257). The previous ATS/ERS guideline from 2005 defined positive BDR as a change of ≥ 12% and ≥ 200 mL in either FEV1 or FVC (258).

Whether defining BDR along 2005 or 2021 ATS/ERS guidelines, the prevalence of the ‘asthmatic’ trait in COPD patients is to range between 22.9% – 44.6% (259, 260). According to a recent study by Beasley et al. (261), the prevalence of BDR in asthma, mixed asthma/COPD, and COPD patients were 19.7%, 29.6%, and 24.7%, respectively. Although it is frequently observed, the utility of BDR, defined conventionally with spirometry, as a prognostic or phenotypical marker has been controversial. In asthma patients, positive BDR is associated with increased responsiveness to inhaled corticosteroids (262). Positive BDR in COPD has been speculated to indirectly reflect a variety of physiological responses, such as relaxation of airway smooth muscle tone, improved small airway function, reduced inflammation, and lung volume recruitment (260, 263, 264).

The associations between positive BDR in COPD and important clinical outcomes remain mixed. According to a study by Vestbo et al., in which changes in FEV1 over a three-year period were analysed in 2163 COPD patients, increased rate of FEV1 decline was observed in patients with positive BDR, alongside current smokers and emphysematous patients (95). Marín et al. investigated the impact of BDR on a variety of long-term clinical outcomes, which included time to hospitalisation, hospital visits, and mortality, in 1203 COPD patients without significant comorbidities. They reported that positive BDR was associated with an increased time to hospitalisation, reduced risk of hospitalisation, and reduced all-cause mortality (265). This connection between BDR and less severe clinical outcomes is supported by a study from Kim et al. (266), as they had also found a significant association between positive BDR and a reduced risk of acute exacerbations in COPD patients.

In COPD patients classified as ‘airways-predominant’ due to asthma-like symptoms and minimal emphysema severity as assessed with CT, positive BDR is significantly more common than ‘emphysema-predominant’ COPD patients (267). A high-resolution CT study from Kitaguchi et al. proposed three COPD phenotypes based on visually assessed emphysema severity and bronchial wall thickening: absent or minimal emphysema with or without bronchial wall thickening (group A), emphysema without bronchial wall thickening (group E), and emphysema with bronchial wall thickening (group M). In concordance with Marín et al., one of the characteristic traits for group A was greater prevalence of BDR, and there was a significant association between increased eosinophil count in sputum (268). Contrary to these findings that support BDR as phenotypical tool, Choi et al. (269) observed no significant differences in exacerbation rate or FEV1 decline over a three year period between positive and negative BDR COPD patients, despite the former group possessing patients with reduced BMI and increased symptom severity. A study by Albert et al. observed that in 1831 COPD patients, those with consistent BDR had no significantly different rates of mortality, exacerbation, or hospitalisations in one year than non-BDR patients once adjusted for differences in baseline FEV1 (270). BDR status was also shown to vary with repeated testing. Due to the temporal variability of the BDR status and lack of any associations to clinical outcomes, the authors surmised BDR to be an unreliable phenotypical marker. Janson et al. observed that whilst BDR in asthma was associated with wheeze, atopy, and higher exhaled nitric oxide, BDR in COPD was not associated with symptom burden, exacerbation, or health status (271). Due to the contentious status of BDR as prognostic marker or phenotypical trait, GOLD currently recommends against it as tool to inform therapeutic decisions (6).

Thus, BDR in COPD is still far from understood and the utility of this trait for COPD phenotyping or characterisation remains unknown. However, the reduction of airflow obstruction, as measured with spirometry, may not be the most suitable method of assessing bronchodilator response in COPD. As already mentioned, spirometry is an insensitive lung function test. Alternative tests that assess small airway dysfunction, hyperinflation, or ventilation distribution may help us further understand BDR in COPD. Indeed, instead of accompanying increased forced expiratory airflow, bronchodilator may predominately induce reduced static hyperinflation. According to Ramsdell and Tisi, approximately 19% of participants with airflow obstruction had a significant increase in vital capacity and decrease in functional residual capacity without change to FEV1/FVC (272). The finding of decreased hyperinflation and increased inspiratory capacity following bronchodilator in patients with COPD and airflow obstruction has been consistently shown (273-275). Donnell et al. (276) observed that even in patients with ‘irreversible emphysema’ and absent BDR can nonetheless experience significantly reduced hyperinflation following bronchodilator, and the changes were greatest in patents with more severe COPD. Aside from body plethysmography, oscillometry has been used to examine other physiological responses to bronchodilator such as reduced total mechanical load (277) and reduced respiratory system resistance and increased respiratory system reactance (278, 279). Ventilation imaging techniques may also be used to investigate changes in ventilated volume and distribution. A study from Kirby et al. (255) revealed significant improvements in VDP% following salbutamol administration in COPD patients. Furthermore, the authors reported there to be no significant differences in the change in VDP% between positive and negative BDR, as defined by spirometry, in COPD patients (255).

1.13 Airway hyperresponsiveness in COPD

AHR is characterised as excessive airway narrowing or closure in response to inhaled stimulus, and it is defined with a 20% FEV1 reduction in response to a specific bronchoconstrictor dose such as ≤ 4 μmol of methacholine or with the dose response slope. AHR has traditionally been associated with asthma, and is used as a clinical marker for diagnosis, severity, treatment management, and prognosis. For example, greater AHR severity is associated with increased risk of asthma exacerbation during ICS dose reduction (280). An asthma treatment strategy centred on reducing AHR was demonstrated to decrease exacerbation rate by 1.8-fold and significantly improve FEV1 compared to the 1995 Global Initiative for Asthma (GINA) strategy, which primarily assesses symptom severity and FEV1 exclusively (281).

Like BDR, AHR is again not traditionally considered a characteristic of COPD. However, the prevalence of AHR in COPD has been shown to range between 23% to 50% (282, 283). A greater proportion of female COPD patients have AHR, and there is a significant relationship between AHR and baseline FEV1 (284). Tkacova et al. (285) used data from two studies, Groningen Leiden Universities Corticosteroids in Obstructive Lung Disease (GLUCOLD) and Lung Health Study cohort (LHS), to investigate the relationships between AHR and lung function decline, respiratory mortality, and systematic inflammation. According to their findings, COPD patients with AHR were at a 2-fold increased risk of respiratory mortality and AHR patients from the larger LHS cohort experienced significantly greater lung function decline. Thus, the authors suggested AHR to be a possible characteristic for the asthma-COPD patient subgroup who are in urgent need of disease modification. Similar

findings of increased mortality risk in COPD with more AHR and/or more severe AHR have been reported by Vestbo et al. (286) and Teferra et al. (287). AHR is also reported to be associated with increased sputum eosinophils, worse symptoms, and increased exacerbations (288). In a cohort of 114 COPD participants from the GLUCOLD study, Berge et al. (289) noted that gas trapping, as measured by RV/TLC, was increased in COPD patients with greater AHR severity. Furthermore, improvement in AHR following ICS treatment were not associated with the reduction of airflow obstruction, as assessed by FEV1. Interestingly, improvement was instead associated with the reduction of gas trapping, possibly through dilating closed airways (290). Changes in gas trapping from airway dilation, and thus ventilation distribution, should also be measurable with VSPECT.

Currently, there are no VSPECT studies that examine airway closure following bronchoprovocation and AHR in COPD. However, VSPECT imaging has been used to investigate AHR in asthma. During induced bronchoconstriction, greater increase in non-ventilated volume independently correlated with more severe AHR and increased ventilation heterogeneity in convective-dependent airways (S_{cond}) (223). Asthma patients with more severe AHR also possessed increased non-ventilated volume at baseline. According to computational model simulations of smooth muscle activation in the airway tree from Venegas et al. (291), the formation of poorly ventilation lung regions after smooth muscle contraction are exacerbated by heterogeneity, which may either be structural (e.g., airway wall thickness) or functional (ventilation heterogeneity) in nature. However, it should be noted that there are noted differences between AHR in asthma and COPD. For example, AHR in asthma is predominately associated with eosinophilic airway inflammation (292).

However, AHR in COPD is associated with airway inflammation marked by increased neutrophils, lymphocytes, and macrophages (289) and reduced airway calibre (68). When Hardaker et al. (293) examined AHR in both older age-matched asthma and COPD patients, they observed that increased peripheral ventilation heterogeneity in the diffusive-dependent lung regions (S_{acin}) and increased RV predicted AHR in asthma. This was consistent with the model simulations from Venegas et al. (291). However, despite increased S_{acin} correlating with worse gas diffusion (D_{LCO}) in COPD patients, AHR was conversely predicted by reduced S_{acin} and decreased FVC. Thus, the authors speculated that COPD-specific processes such as parenchymal destruction, reducing tethering forces, and airway obliteration may put COPD patients with the emphysematous phenotype at reduced risk of AHR. Instead, COPD patients with a predominately airways disease phenotype may possess an increased AHR risk. From these findings, it is reasonable to assume there to be a different response in ventilation, as measured with VSPECT, to bronchoconstriction in COPD.

1.14 Summary and aims of the thesis

COPD has long been recognised as a highly heterogeneous disease, with variable symptom presentations, progression, and responses to treatment. Although disease characterisation or phenotypes are hardly a novel concept, efforts in identifying patient subgroups are complicated by non-specific traits. The path for more precise COPD phenotyping will require a variety of parameters beyond conventional clinical markers and spirometry. Quantitative ventilation imaging is a promising technique that can be used to investigate the extent of non-ventilated volume resulting from parenchymal destruction and airway closure in COPD patients. VSPECT is especially attractive due to its comparatively lower cost and easier preparation than ventilation MRI and its unique ability to visualise tidal ventilation. From the limited number of previous VSPECT studies, it is apparent that COPD patients with more severe disease are less ventilated. However, even fewer COPD studies have investigated correlations between non-ventilated volume and lung function tests beyond spirometry. There has yet to be any analysis into the relationships between non-ventilated volume and small airways disease, as measured by oscillometry, or lung volume measurements of hyperinflation.

For some time, VSPECT studies have noted seemingly more numerous ‘hot spots’ in patients with greater COPD severity. Increased ‘hot spots’ count and extent of non-ventilation have been previously used to visually grade ventilation impairment in COPD studies. However, the relationships between the total number of ‘hot spots’ and lung function measurements, such as lung volumes and oscillometry or FEV1, and non-ventilated volume remain unknown.

Whilst ventilation MRI studies demonstrated decreased non-ventilated volume post-bronchodilator in COPD patients, there is a gap in the literature regarding bronchodilator response in COPD patients as measured with quantitative VSPECT. Due to differences in techniques between VSPECT and MRI, the bronchodilator response on ventilation is also likely to differ between the two. Furthermore, no VSPECT studies have examined the relationships between changes in oscillometric parameters and imaging parameters post-bronchodilator. Whilst VSPECT has been used to investigate AHR and bronchoconstriction following a methacholine challenge in asthma patients, there are currently no VSPECT studies that examine AHR and ventilation in COPD. Current literature suggests there to be different physiological mechanisms behind AHR to each disease.

Finally, there have been a few different threshold techniques for quantitative ventilation SPECT analysis, but none are currently validated. The accuracy of these threshold techniques in differentiating non-ventilated activity from ventilated activity and their robustness to image data heterogeneity from ‘hot spots’ or areas with low intensities remain unexamined. Thus, it is paramount to validate these existing threshold techniques and develop an accurate, robust technique if existing techniques are problematic.

The primary aim of this thesis is to examine COPD patients with the use of the VSPECT/CT parameters, global non-ventilated volume and ‘hot spots’ count, at baseline, post-bronchodilator, and post-methacholine. Furthermore, we aim to examine the relationships between these VSPECT/CT parameters and lung function measurements. Prior to these investigations, we also aim to validate existing threshold techniques and assess a novel threshold technique for VSPECT.

The specific aims of the thesis are as follows:

1. Validate and assess existing threshold techniques in addition to a novel technique with physical lung phantom models for VSPECT.
2. Examine the relationships between non-ventilated volume and ‘hot spots’ and various lung function measurements in COPD patients at baseline.
3. Examine the changes in VSPECT parameters, non-ventilated volume and ‘hot spots’, following the administration of bronchodilator in COPD patients.
4. Examine the effects of bronchoconstriction on non-ventilated volume and ‘hot spots’ count in COPD patients with ventilation SPECT and the relationship between the imaging parameters and AHR.

1.15 References

1. Verbeken EK, Cauberghs M, Mertens I, Clement J, Lauweryns JM, Van de Woestijne KP. The senile lung. Comparison with normal and emphysematous lungs. 2. Functional aspects. Chest. 1992;101(3):800-9.
2. West J. Pulmonary Pathophyiology: The Essentials, vol. 52. Lippincott Williams and Wilkins, Baltimore, MD, USA; 2007.
3. Li K, Song Z, Yue Q, Wang Q, Li Y, Zhu Y, Chen H. Disease-specific transcriptional programs govern airway goblet cell metaplasia. Heliyon. 2024;10(13).
4. Hogg JC, McDonough JE, Sanchez PG, Cooper JD, Coxson HO, Elliott WM, Naiman D, Pochettino M, et al. Micro-computed tomography measurements of peripheral lung pathology in chronic obstructive pulmonary disease. Proc Am Thorac Soc. 2009;6(6):546-9.
5. Kirby M, Smith BM, Tanabe N, Hogg JC, Coxson HO, Sin DD, Bourbeau J, Tan WC. Computed tomography total airway count predicts progression to COPD in at-risk smokers. ERJ Open Research. 2021;7(4):00307-2021.
6. (GOLD) GIfCOLD. Global strategy for the diagnosis, management, and prevention of chronic obstructive lung disease (2024 Report) 2024 [Available from: https://goldcopd.org/2024-gold-report/.
7. Vos T, Lim SS, Abbafati C, Abbas KM, Abbasi M, Abbasifard M, Abbasi-Kangevari M, Abbastabar H, et al. Global burden of 369 diseases and injuries in 204 countries and territories, 1990–2019: a systematic analysis for the Global Burden of Disease Study 2019. The Lancet. 2020;396(10258):1204-22.
8. Liu Y, Carlson SA, Watson KB, Xu F, Greenlund KJ. Trends in the Prevalence of Chronic Obstructive Pulmonary Disease Among Adults Aged ≥18 Years - United States, 2011-2021. MMWR Morb Mortal Wkly Rep. 2023;72(46):1250-6.
9. Statistics ABo. Chronic Obstructive Pulmonary Disease 2022 [Available from: https://www.abs.gov.au/statistics/health/health-conditions-and-risks/chronic-obstructive-pulmonary-disease/latest-release.
10. Li M, Hanxiang C, Na Z, Ping Z, Shengnan D, Taihua W, Yuanyuan Y, Ni Y. Burden of COPD in China and the global from 1990 to 2019: a systematic analysis for the Global Burden of Disease Study 2019. BMJ Open Respir Res. 2023;10(1).
11. Boers E, Barrett M, Su JG, Benjafield AV, Sinha S, Kaye L, Zar HJ, Vuong V, et al. Global Burden of Chronic Obstructive Pulmonary Disease Through 2050. JAMA Network Open. 2023;6(12):e2346598-e.
12. Safiri S, Carson-Chahhoud K, Noori M, Nejadghaderi SA, Sullman MJM, Ahmadian Heris J, Ansarin K, Mansournia MA, et al. Burden of chronic obstructive pulmonary disease and its attributable risk factors in 204 countries and territories, 1990-2019: results from the Global Burden of Disease Study 2019. Bmj. 2022;378:e069679.
13. Adeloye D, Song P, Zhu Y, Campbell H, Sheikh A, Rudan I. Global, regional, and national prevalence of, and risk factors for, chronic obstructive pulmonary disease (COPD) in 2019: a systematic review and modelling analysis. Lancet Respir Med. 2022;10(5):447-58.
14. Health AIo, Welfare. Chronic obstructive pulmonary disease. Canberra: AIHW; 2023.
15. Zielinski J, MacNee W, Wedzicha J, Ambrosino N, Braghiroli A, Dolensky J, Howard P, Gorzelak K, et al. Causes of death in patients with COPD and chronic respiratory failure. Monaldi Arch Chest Dis. 1997;52(1):43-7.
16. Anthonisen NR, Skeans MA, Wise RA, Manfreda J, Kanner RE, Connett JE. The effects of a smoking cessation intervention on 14.5-year mortality: a randomized clinical trial. Ann Intern Med. 2005;142(4):233-9.

17. Park SC, Kim DW, Park EC, Shin CS, Rhee CK, Kang YA, Kim YS. Mortality of patients with chronic obstructive pulmonary disease: a nationwide populationbased cohort study. Korean J Intern Med. 2019;34(6):1272-8.
18. Gudmundsson G, Gislason T, Lindberg E, Hallin R, Ulrik SC, Brøndum E, Nieminen MM, Aine T, et al. Mortality in COPD patients discharged from hospital: the role of treatment and co-morbidity. Respiratory Research. 2006;7(1):109.
19. Mannino DM, Buist AS, Petty TL, Enright PL, Redd SC. Lung function and mortality in the United States: data from the First National Health and Nutrition Examination Survey follow up study. Thorax. 2003;58(5):388-93.
20. Guo Y, Zhang T, Wang Z, Yu F, Xu Q, Guo W, Wu C, He J. Body mass index and mortality in chronic obstructive pulmonary disease: A dose-response meta-analysis. Medicine (Baltimore). 2016;95(28):e4225.
21. Vogelmeier CF, Criner GJ, Martinez FJ, Anzueto A, Barnes PJ, Bourbeau J, Celli BR, Chen R, et al. Global Strategy for the Diagnosis, Management, and Prevention of Chronic Obstructive Lung Disease 2017 Report. GOLD Executive Summary. Am J Respir Crit Care Med. 2017;195(5):557-82.
22. Cohen BH. Is pulmonary dysfunction the common denominator for the multiple effects of cigarette smoking? Lancet. 1978;2(8098):1024-7.
23. Larsson C. Natural history and life expectancy in severe alpha1-antitrypsin deficiency, Pi Z. Acta Med Scand. 1978;204(5):345-51.
24. Chung C, Lee KN, Han K, Shin DW, Lee SW. Effect of smoking on the development of chronic obstructive pulmonary disease in young individuals: a nationwide cohort study. Front Med (Lausanne). 2023;10:1190885.
25. Wu Y, Song P, Lin S, Peng L, Li Y, Deng Y, Deng X, Lou W, et al. Global Burden of Respiratory Diseases Attributable to Ambient Particulate Matter Pollution: Findings From the Global Burden of Disease Study 2019. Front Public Health. 2021;9:740800.
26. Chan KH, Kurmi OP, Bennett DA, Yang L, Chen Y, Tan Y, Pei P, Zhong X, et al. Solid Fuel Use and Risks of Respiratory Diseases. A Cohort Study of 280,000 Chinese Never-Smokers. Am J Respir Crit Care Med. 2019;199(3):352-61.
27. Chapman RS, He X, Blair AE, Lan Q. Improvement in household stoves and risk of chronic obstructive pulmonary disease in Xuanwei, China: retrospective cohort study. Bmj. 2005;331(7524):1050.
28. Sørheim IC, Johannessen A, Gulsvik A, Bakke PS, Silverman EK, DeMeo DL. Gender differences in COPD: are women more susceptible to smoking effects than men? Thorax. 2010;65(6):480-5.
29. Vogelmeier CF, Criner GJ, Martinez FJ, Anzueto A, Barnes PJ, Bourbeau J, Celli BR, Chen R, et al. Global Strategy for the Diagnosis, Management, and Prevention of Chronic Obstructive Lung Disease 2017 Report. GOLD Executive Summary. American Journal of Respiratory and Critical Care Medicine. 2017;195(5):557-82.
30. Terzikhan N, Verhamme KM, Hofman A, Stricker BH, Brusselle GG, Lahousse L. Prevalence and incidence of COPD in smokers and non-smokers: the Rotterdam Study. Eur J Epidemiol. 2016;31(8):785-92.
31. Mahmood T, Singh RK, Kant S, Shukla AD, Chandra A, Srivastava RK. Prevalence and etiological profile of chronic obstructive pulmonary disease in nonsmokers. Lung India. 2017;34(2):122-6.
32. Chronic obstructive pulmonary disease among adults--United States, 2011. MMWR Morb Mortal Wkly Rep. 2012;61(46):938-43.
33. Mammen MJ, Pai V, Aaron SD, Nici L, Alhazzani W, Alexander PE. Dual LABA/LAMA Therapy versus LABA or LAMA Monotherapy for Chronic Obstructive Pulmonary Disease. A Systematic Review and Meta-analysis in Support of the American Thoracic Society Clinical Practice Guideline. Ann Am Thorac Soc. 2020;17(9):1133-43.

34. Rogliani P, Calzetta L, Braido F, Cazzola M, Clini E, Pelaia G, Rossi A, Scichilone N, et al. LABA/LAMA fixed-dose combinations in patients with COPD: a systematic review. Int J Chron Obstruct Pulmon Dis. 2018;13:3115-30.
35. Aziz MIA, Tan LE, Wu DB, Pearce F, Chua GSW, Lin L, Tan PT, Ng K. Comparative efficacy of inhaled medications (ICS/LABA, LAMA, LAMA/LABA and SAMA) for COPD: a systematic review and network meta-analysis. Int J Chron Obstruct Pulmon Dis. 2018;13:3203-31.
36. Miravitlles M, Urrutia G, Mathioudakis AG, Ancochea J. Efficacy and safety of tiotropium and olodaterol in COPD: a systematic review and meta-analysis. Respir Res. 2017;18(1):196.
37. Koarai A, Sugiura H, Yamada M, Ichikawa T, Fujino N, Kawayama T, Ichinose M. Treatment with LABA versus LAMA for stable COPD: a systematic review and meta-analysis. BMC Pulmonary Medicine. 2020;20(1):111.
38. Burge PS, Calverley PM, Jones PW, Spencer S, Anderson JA, Maslen TK. Randomised, double blind, placebo controlled study of fluticasone propionate in patients with moderate to severe chronic obstructive pulmonary disease: the ISOLDE trial. Bmj. 2000;320(7245):1297-303.
39. Celli BR, Anderson JA, Cowans NJ, Crim C, Hartley BF, Martinez FJ, Morris AN, Quasny H, et al. Pharmacotherapy and Lung Function Decline in Patients with Chronic Obstructive Pulmonary Disease. A Systematic Review. Am J Respir Crit Care Med. 2021;203(6):689-98.
40. Pauwels RA, Löfdahl CG, Laitinen LA, Schouten JP, Postma DS, Pride NB, Ohlsson SV. Long-term treatment with inhaled budesonide in persons with mild chronic obstructive pulmonary disease who continue smoking. European Respiratory Society Study on Chronic Obstructive Pulmonary Disease. N Engl J Med. 1999;340(25):1948-53.
41. Singh D, Litewka D, Páramo R, Rendon A, Sayiner A, Tanni SE, Acharya S, Aggarwal B, et al. DElaying Disease Progression In COPD with Early Initiation of Dual Bronchodilator or Triple Inhaled PharmacoTherapy (DEPICT): A Predictive Modelling Approach. Adv Ther. 2023;40(10):4282-97.
42. Welte T, Vogelmeier C, Papi A. COPD: early diagnosis and treatment to slow disease progression. Int J Clin Pract. 2015;69(3):336-49.
43. Burge PS, Calverley PMA, Jones PW, Spencer S, Anderson JA, Maslen TK. Randomised, double blind, placebo controlled study of fluticasone propionate in patients with moderate to severe chronic obstructive pulmonary disease: the ISOLDE trial. BMJ. 2000;320(7245):1297-303.
44. Wise R, Connett J, Weinmann G, Scanlon P, Skeans M. Effect of inhaled triamcinolone on the decline in pulmonary function in chronic obstructive pulmonary disease. N Engl J Med. 2000;343(26):1902-9.
45. Yang IA, Clarke MS, Sim EH, Fong KM. Inhaled corticosteroids for stable chronic obstructive pulmonary disease. Cochrane Database Syst Rev. 2012;2012(7):Cd002991.
46. Kew KM, Seniukovich A. Inhaled steroids and risk of pneumonia for chronic obstructive pulmonary disease. Cochrane Database Syst Rev. 2014;2014(3):Cd010115.
47. Crim C, Calverley PMA, Anderson JA, Celli B, Ferguson GT, Jenkins C, Jones PW, Willits LR, et al. Pneumonia risk in COPD patients receiving inhaled corticosteroids alone or in combination: TORCH study results. European Respiratory Journal. 2009;34(3):641-7.
48. Lee C-H, Kim K, Hyun MK, Jang EJ, Lee NR, Yim J-J. Use of inhaled corticosteroids and the risk of tuberculosis. Thorax. 2013;68(12):1105-13.
49. Park JW, Hong Y, Rhee CK, Choi HS, Kim K, Yoo KH, Jung KS, Park JH. The Impact of Inhaled Corticosteroids on the Prognosis of Chronic Obstructive Pulmonary Disease. Int J Chron Obstruct Pulmon Dis. 2023;18:733-43.
50. Vestbo J, Anderson JA, Brook RD, Calverley PM, Celli BR, Crim C, Martinez F, Yates J, et al. Fluticasone furoate and vilanterol and survival in chronic obstructive pulmonary disease with heightened cardiovascular risk (SUMMIT): a double-blind randomised controlled trial. Lancet. 2016;387(10030):1817-26.
51. Calverley PM, Anderson JA, Celli B, Ferguson GT, Jenkins C, Jones PW, Yates JC, Vestbo J. Salmeterol and fluticasone propionate and survival in chronic obstructive pulmonary disease. N Engl J Med. 2007;356(8):775-89.

52. Disease GIfCOL. Global Initiative for Chronic Obstructive Lung Disease 2017 Report 2017 [Available from: https://goldcopd.org/wp-content/uploads/2017/02/wms-GOLD-2017-FINAL.pdf.
53. Horita N, Goto A, Shibata Y, Ota E, Nakashima K, Nagai K, Kaneko T. Long-acting muscarinic antagonist (LAMA) plus long-acting beta-agonist (LABA) versus LABA plus inhaled corticosteroid (ICS) for stable chronic obstructive pulmonary disease (COPD). Cochrane Database of Systematic Reviews. 2017(2).
54. Patel S, Dickinson S, Morris K, Ashdown HF, Chalmers JD. A descriptive cohort study of withdrawal from inhaled corticosteroids in COPD patients. npj Primary Care Respiratory Medicine. 2022;32(1):25.
55. Harries TH, Rowland V, Corrigan CJ, Marshall IJ, McDonnell L, Prasad V, Schofield P, Armstrong D, et al. Blood eosinophil count, a marker of inhaled corticosteroid effectiveness in preventing COPD exacerbations in post-hoc RCT and observational studies: systematic review and meta-analysis. Respiratory Research. 2020;21(1):3.
56. Papi A, Vestbo J, Fabbri L, Corradi M, Prunier H, Cohuet G, Guasconi A, Montagna I, et al. Extrafine inhaled triple therapy versus dual bronchodilator therapy in chronic obstructive pulmonary disease (TRIBUTE): a double-blind, parallel group, randomised controlled trial. Lancet. 2018;391(10125):1076-84.
57. Magnussen H, Disse B, Rodriguez-Roisin R, Kirsten A, Watz H, Tetzlaff K, Towse L, Finnigan H, et al. Withdrawal of inhaled glucocorticoids and exacerbations of COPD. N Engl J Med. 2014;371(14):1285-94.
58. Cheng SL. Blood eosinophils and inhaled corticosteroids in patients with COPD: systematic review and meta-analysis. Int J Chron Obstruct Pulmon Dis. 2018;13:2775-84.
59. Bafadhel M, McKenna S, Terry S, Mistry V, Reid C, Haldar P, McCormick M, Haldar K, et al. Acute Exacerbations of Chronic Obstructive Pulmonary Disease. American Journal of Respiratory and Critical Care Medicine. 2011;184(6):662-71.
60. Martinez FJ, Calverley PM, Goehring UM, Brose M, Fabbri LM, Rabe KF. Effect of roflumilast on exacerbations in patients with severe chronic obstructive pulmonary disease uncontrolled by combination therapy (REACT): a multicentre randomised controlled trial. Lancet. 2015;385(9971):857-66.
61. Rennard SI, Calverley PM, Goehring UM, Bredenbröker D, Martinez FJ. Reduction of exacerbations by the PDE4 inhibitor roflumilast--the importance of defining different subsets of patients with COPD. Respir Res. 2011;12(1):18.
62. Fabbri LM, Calverley PM, Izquierdo-Alonso JL, Bundschuh DS, Brose M, Martinez FJ, Rabe KF. Roflumilast in moderate-to-severe chronic obstructive pulmonary disease treated with longacting bronchodilators: two randomised clinical trials. Lancet. 2009;374(9691):695-703.
63. Albert RK, Connett J, Bailey WC, Casaburi R, Cooper JA, Jr., Criner GJ, Curtis JL, Dransfield MT, et al. Azithromycin for prevention of exacerbations of COPD. N Engl J Med. 2011;365(8):689-98.
64. Uzun S, Djamin RS, Kluytmans JAJW, Mulder PGH, van't Veer NE, Ermens AAM, Pelle AJ, Hoogsteden HC, et al. Azithromycin maintenance treatment in patients with frequent exacerbations of chronic obstructive pulmonary disease (COLUMBUS): a randomised, double-blind, placebo-controlled trial. The Lancet Respiratory Medicine. 2014;2(5):361-8.
65. Herath SC, Poole P. Prophylactic antibiotic therapy for chronic obstructive pulmonary disease (COPD). Cochrane Database Syst Rev. 2013(11):Cd009764.
66. Ray WA, Murray KT, Hall K, Arbogast PG, Stein CM. Azithromycin and the risk of cardiovascular death. N Engl J Med. 2012;366(20):1881-90.
67. Doo JH, Kim SM, Park YJ, Kim KH, Oh YH, Kim JS, Park SM. Smoking cessation after diagnosis of COPD is associated with lower all-cause and cause-specific mortality: a nationwide population-based cohort study of South Korean men. BMC Pulmonary Medicine. 2023;23(1):237.
68. Kanner RE, Connett JE, Williams DE, Buist AS. Effects of randomized assignment to a smoking cessation intervention and changes in smoking habits on respiratory symptoms in smokers with early chronic obstructive pulmonary disease: the Lung Health Study. Am J Med. 1999;106(4):410-6.

69. Godtfredsen NS, Vestbo J, Osler M, Prescott E. Risk of hospital admission for COPD following smoking cessation and reduction: a Danish population study. Thorax. 2002;57(11):967-72.
70. Anthonisen NR, Connett JE, Murray RP. Smoking and lung function of Lung Health Study participants after 11 years. Am J Respir Crit Care Med. 2002;166(5):675-9.
71. Burchfiel CM, Marcus EB, Curb JD, Maclean CJ, Vollmer WM, Johnson LR, Fong KO, Rodriguez BL, et al. Effects of smoking and smoking cessation on longitudinal decline in pulmonary function. Am J Respir Crit Care Med. 1995;151(6):1778-85.
72. Anthonisen NR, Connett JE, Kiley JP, Altose MD, Bailey WC, Buist AS, Conway WA, Jr., Enright PL, et al. Effects of smoking intervention and the use of an inhaled anticholinergic bronchodilator on the rate of decline of FEV1. The Lung Health Study. Jama. 1994;272(19):1497-505.
73. Tashkin DP, Celli B, Senn S, Burkhart D, Kesten S, Menjoge S, Decramer M. A 4-Year Trial of Tiotropium in Chronic Obstructive Pulmonary Disease. New England Journal of Medicine. 2008;359(15):1543-54.
74. Jiménez-Ruiz CA, Masa F, Miravitlles M, Gabriel R, Viejo JL, Villasante C, Sobradillo V. Smoking characteristics: differences in attitudes and dependence between healthy smokers and smokers with COPD. Chest. 2001;119(5):1365-70.
75. Stead M, Angus K, Holme I, Cohen D, Tait G. Factors influencing European GPs' engagement in smoking cessation: a multi-country literature review. Br J Gen Pract. 2009;59(566):682-90.
76. van Eerd EAM, van der Meer RM, van Schayck OCP, Kotz D. Smoking cessation for people with chronic obstructive pulmonary disease. Cochrane Database of Systematic Reviews. 2016(8).
77. Warnier MJ, Riet EESv, Rutten FH, Bruin MLD, Sachs APE. Smoking cessation strategies in patients with COPD. European Respiratory Journal. 2013;41(3):727-34.
78. van der Meer RM, Wagena EJ, Ostelo RW, Jacobs JE, van Schayck CP. Smoking cessation for chronic obstructive pulmonary disease. Cochrane Database Syst Rev. 2003;2003(2):Cd002999.
79. PAUWELS RA, BUIST AS, CALVERLEY PMA, JENKINS CR, HURD SS. Global Strategy for the Diagnosis, Management, and Prevention of Chronic Obstructive Pulmonary Disease. American Journal of Respiratory and Critical Care Medicine. 2001;163(5):1256-76.
80. Rabe KF, Hurd S, Anzueto A, Barnes PJ, Buist SA, Calverley P, Fukuchi Y, Jenkins C, et al. Global strategy for the diagnosis, management, and prevention of chronic obstructive pulmonary disease: GOLD executive summary. Am J Respir Crit Care Med. 2007;176(6):532-55.
81. Vestbo J, Hurd SS, Agustí AG, Jones PW, Vogelmeier C, Anzueto A, Barnes PJ, Fabbri LM, et al. Global strategy for the diagnosis, management, and prevention of chronic obstructive pulmonary disease: GOLD executive summary. Am J Respir Crit Care Med. 2013;187(4):347-65.
82. Fletcher C. Standardised questionnaire on respiratory symptoms: a statement prepared and approved by the MRC Committee on the Aetiology of Chronic Bronchitis (MRC breathlessness score). Bmj. 1960;2(2):1665.
83. Surveillance for respiratory hazards in the occupational setting [American Thoracic Society]. Am Rev Respir Dis. 1982;126(5):952-6.
84. Jones PW, Harding G, Berry P, Wiklund I, Chen WH, Kline Leidy N. Development and first validation of the COPD Assessment Test. Eur Respir J. 2009;34(3):648-54.
85. Vogelmeier CF, Criner GJ, Martinez FJ, Anzueto A, Barnes PJ, Bourbeau J, Celli BR, Chen R, et al. Global Strategy for the Diagnosis, Management, and Prevention of Chronic Obstructive Lung Disease 2017 Report: GOLD Executive Summary. European Respiratory Journal. 2017;49(3):1700214.
86. Chai CS, Ng DL, Bt Mos S, Ibrahim MAB, Tan SB, Pang YK, Liam CK. COPD exacerbations and patient-reported outcomes according to post-bronchodilator FEV(1) - a post-hoc analysis of pooled data. BMC Pulm Med. 2023;23(1):150.
87. SEEMUNGAL TAR, DONALDSON GC, PAUL EA, BESTALL JC, JEFFRIES DJ, WEDZICHA JA. Effect of Exacerbation on Quality of Life in Patients with Chronic Obstructive Pulmonary Disease. American Journal of Respiratory and Critical Care Medicine. 1998;157(5):1418-22.
88. Nishimura K, Izumi T, Tsukino M, Oga T. Dyspnea is a better predictor of 5-year survival than airway obstruction in patients with COPD. Chest. 2002;121(5):1434-40.

89. Zhudenkov K, Palmér R, Jauhiainen A, Helmlinger G, Stepanov O, Peskov K, Eriksson UG, Wählby Hamrén U. Longitudinal FEV(1) and Exacerbation Risk in COPD: Quantifying the Association Using Joint Modelling. Int J Chron Obstruct Pulmon Dis. 2021;16:101-11.
90. Jones PW, Bosh TK. Quality of life changes in COPD patients treated with salmeterol. Am J Respir Crit Care Med. 1997;155(4):1283-9.
91. Agusti A, Calverley PMA, Celli B, Coxson HO, Edwards LD, Lomas DA, MacNee W, Miller BE, et al. Characterisation of COPD heterogeneity in the ECLIPSE cohort. Respiratory Research. 2010;11(1):122.
92. Coxson HO, Dirksen A, Edwards LD, Yates JC, Agusti A, Bakke P, Calverley PM, Celli B, et al. The presence and progression of emphysema in COPD as determined by CT scanning and biomarker expression: a prospective analysis from the ECLIPSE study. The lancet Respiratory medicine. 2013;1(2):129-36.
93. Agustí A, Edwards LD, Rennard SI, MacNee W, Tal-Singer R, Miller BE, Vestbo J, Lomas DA, et al. Persistent systemic inflammation is associated with poor clinical outcomes in COPD: a novel phenotype. PloS one. 2012;7(5):e37483.
94. Kellerer C, Kahnert K, Trudzinski FC, Lutter J, Berschneider K, Speicher T, Watz H, Bals R, et al. COPD maintenance medication is linked to left atrial size: Results from the COSYCONET cohort. Respir Med. 2021;185:106461.
95. Vestbo J, Edwards LD, Scanlon PD, Yates JC, Agusti A, Bakke P, Calverley PM, Celli B, et al. Changes in forced expiratory volume in 1 second over time in COPD. N Engl J Med. 2011;365(13):1184-92.
96. Johnson KM, Safari A, Tan WC, Bourbeau J, FitzGerald JM, Sadatsafavi M, Study O. Heterogeneity in the respiratory symptoms of patients with mild-to-moderate COPD. Int J Chron Obstruct Pulmon Dis. 2018;13:3983-95.
97. Hurst JR, Vestbo J, Anzueto A, Locantore N, Müllerova H, Tal-Singer R, Miller B, Lomas DA, et al. Susceptibility to exacerbation in chronic obstructive pulmonary disease. N Engl J Med. 2010;363(12):1128-38.
98. Sadatsafavi M, Sin DD, Zafari Z, Criner G, Connett JE, Lazarus S, Han M, Martinez F, et al. The Association Between Rate and Severity of Exacerbations in Chronic Obstructive Pulmonary Disease: An Application of a Joint Frailty-Logistic Model. Am J Epidemiol. 2016;184(9):681-9.
99. Celli BR, Cote CG, Marin JM, Casanova C, Montes de Oca M, Mendez RA, Pinto Plata V, Cabral HJ. The body-mass index, airflow obstruction, dyspnea, and exercise capacity index in chronic obstructive pulmonary disease. N Engl J Med. 2004;350(10):1005-12.
100. Marin JM, Carrizo SJ, Casanova C, Martinez-Camblor P, Soriano JB, Agusti AG, Celli BR. Prediction of risk of COPD exacerbations by the BODE index. Respir Med. 2009;103(3):373-8.
101. Faganello MM, Tanni SE, Pelegrino NRG, Lucheta PA, Godoy I, Sanchez FF. BODE Index and GOLD Staging as Predictors of 1-Year Exacerbation Risk in Chronic Obstructive Pulmonary Disease. The American Journal of the Medical Sciences. 2010;339(1):10-4.
102. Johannessen A, Nilsen RM, Storebø M, Gulsvik A, Eagan T, Bakke P. Comparison of 2011 and 2007 Global Initiative for Chronic Obstructive Lung Disease Guidelines for Predicting Mortality and Hospitalization. American Journal of Respiratory and Critical Care Medicine. 2013;188(1):51-9.
103. Kim J, Yoon HI, Oh Y-M, Lim SY, Lee J-H, Kim T-H, Lee SY, Lee JH, et al. Lung function decline rates according to GOLD group in patients with chronic obstructive pulmonary disease. International Journal of Chronic Obstructive Pulmonary Disease. 2015;10(null):1819-27.
104. Jones RC, Donaldson GC, Chavannes NH, Kida K, Dickson-Spillmann M, Harding S, Wedzicha JA, Price D, et al. Derivation and Validation of a Composite Index of Severity in Chronic Obstructive Pulmonary Disease. American Journal of Respiratory and Critical Care Medicine. 2009;180(12):1189-95.
105. Puhan MA, Garcia-Aymerich J, Frey M, ter Riet G, Antó JM, Agustí AG, Gómez FP, Rodríguez-Roisín R, et al. Expansion of the prognostic assessment of patients with chronic obstructive pulmonary disease: the updated BODE index and the ADO index. Lancet. 2009;374(9691):704-11.

106. Motegi T, Jones RC, Ishii T, Hattori K, Kusunoki Y, Furutate R, Yamada K, Gemma A, et al. A comparison of three multidimensional indices of COPD severity as predictors of future exacerbations. Int J Chron Obstruct Pulmon Dis. 2013;8:259-71.
107. Lee SJ, Yun SS, Ju S, You JW, Cho YJ, Jeong YY, Kim JY, Kim HC, et al. Validity of the GOLD 2017 classification in the prediction of mortality and respiratory hospitalization in patients with chronic obstructive pulmonary disease. Int J Chron Obstruct Pulmon Dis. 2019;14:911-9.
108. Ranga V, Kleinerman J. Structure and function of small airways in health and disease. Arch Pathol Lab Med. 1978;102(12):609-17.
109. Weibel ER. Principles and methods for the morphometric study of the lung and other organs. Lab Invest. 1963;12:131-55.
110. Hogg JC, Macklem PT, Thurlbeck WM. Site and Nature of Airway Obstruction in Chronic Obstructive Lung Disease. New England Journal of Medicine. 1968;278(25):1355-60.
111. Yanai M, Sekizawa K, Ohrui T, Sasaki H, Takishima T. Site of airway obstruction in pulmonary disease: direct measurement of intrabronchial pressure. J Appl Physiol (1985). 1992;72(3):1016-23.
112. McDonough JE, Yuan R, Suzuki M, Seyednejad N, Elliott WM, Sanchez PG, Wright AC, Gefter WB, et al. Small-Airway Obstruction and Emphysema in Chronic Obstructive Pulmonary Disease. New England Journal of Medicine. 2011;365(17):1567-75.
113. Mead J. The lung's "quiet zone". N Engl J Med. 1970;282(23):1318-9.
114. King GG, Bates J, Berger KI, Calverley P, Melo PLd, Dellacà RL, Farré R, Hall GL, et al. Technical standards for respiratory oscillometry. European Respiratory Journal. 2020;55(2):1900753.
115. Shi Y, Aledia AS, Tatavoosian AV, Vijayalakshmi S, Galant SP, George SC. Relating small airways to asthma control by using impulse oscillometry in children. Journal of Allergy and Clinical Immunology. 2012;129(3):671-8.
116. Peslin R, Fredberg JJ. Oscillation Mechanics of the Respiratory System. Comprehensive Physiology. p. 145-77.
117. Frantz ID, Close RH. Alveolar Pressure Swings during High Frequency Ventilation in Rabbits. Pediatric Research. 1985;19(2):162-6.
118. Jetmalani K, Thamrin C, Farah CS, Bertolin A, Chapman DG, Berend N, Salome CM, King GG. Peripheral airway dysfunction and relationship with symptoms in smokers with preserved spirometry. Respirology. 2018;23(5):512-8.
119. Pisi R, Aiello M, Frizzelli A, Calzetta L, Marchi L, Bertorelli G, Pisi G, Chetta A. Detection of Small Airway Dysfunction in Asymptomatic Smokers with Preserved Spirometry: The Value of the Impulse Oscillometry System. Int J Chron Obstruct Pulmon Dis. 2021;16:2585-90.
120. Li L-Y, Yan T-S, Yang J, Li Y-Q, Fu L-X, Lan L, Liang B-M, Wang M-Y, et al. Impulse oscillometry for detection of small airway dysfunction in subjects with chronic respiratory symptoms and preserved pulmonary function. Respiratory Research. 2021;22(1):68.
121. Oppenheimer BW, Goldring RM, Herberg ME, Hofer IS, Reyfman PA, Liautaud S, Rom WN, Reibman J, et al. Distal airway function in symptomatic subjects with normal spirometry following World Trade Center dust exposure. Chest. 2007;132(4):1275-82.
122. Clément J, Làndsér FJ, Van de Woestijne KP. Total Resistance and Reactance in Patients with Respiratory Complaints with and without Airways Obstruction. Chest. 1983;83(2):215-20.
123. Rath AK, Sahu D, De S. Oscillometry-Defined Small Airway Dysfunction in Patients with Chronic Obstructive Pulmonary Disease. Tuberc Respir Dis (Seoul). 2024;87(2):165-75.
124. Ribeiro CO, Lopes AJ, de Melo PL. Respiratory Oscillometry in Chronic Obstructive Pulmonary Disease: Association with Functional Capacity as Evaluated by Adl Glittre Test and Hand Grip Strength Test. Int J Chron Obstruct Pulmon Dis. 2022;17:1017-30.
125. Robinson PD, Latzin P, Verbanck S, Hall GL, Horsley A, Gappa M, Thamrin C, Arets HG, et al. Consensus statement for inert gas washout measurement using multiple- and single- breath tests. Eur Respir J. 2013;41(3):507-22.

126. Zaigham S, Wollmer P, Engström G. The Association of Lung Clearance Index with COPD and FEV1 Reduction in 'Men Born in 1914'. COPD: Journal of Chronic Obstructive Pulmonary Disease. 2017;14(3):324-9.
127. Crawford AB, Makowska M, Paiva M, Engel LA. Convection- and diffusion-dependent ventilation maldistribution in normal subjects. J Appl Physiol (1985). 1985;59(3):838-46.
128. Verbanck S, Schuermans D, Meysman M, Paiva M, Vincken W. Noninvasive Assessment of Airway Alterations in Smokers. American Journal of Respiratory and Critical Care Medicine. 2004;170(4):414-9.
129. VERBANCK S, SCHUERMANS D, VAN MUYLEM A, MELOT C, NOPPEN M, VINCKEN W, PAIVA M. Conductive and Acinar Lung-zone Contributions to Ventilation Inhomogeneity in COPD. American Journal of Respiratory and Critical Care Medicine. 1998;157(5):1573-7.
130. Verbanck S, King GG, Paiva M, Schuermans D, Vanderhelst E. The Functional Correlate of the Loss of Terminal Bronchioles in Chronic Obstructive Pulmonary Disease. American Journal of Respiratory and Critical Care Medicine. 2018;197(12):1633-5.
131. Han MK, Agusti A, Calverley PM, Celli BR, Criner G, Curtis JL, Fabbri LM, Goldin JG, et al. Chronic obstructive pulmonary disease phenotypes: the future of COPD. Am J Respir Crit Care Med. 2010;182(5):598-604.
132. Galas DJ, Hood L. Systems biology and emerging technologies will catalyze the transition from reactive medicine to predictive, personalized, preventive and participatory (P4) medicine. Interdisciplinary Bio Central. 2009;1(2):6.1-6.4.
133. Stolz D, Mkorombindo T, Schumann DM, Agusti A, Ash SY, Bafadhel M, Bai C, Chalmers JD, et al. Towards the elimination of chronic obstructive pulmonary disease: a Lancet Commission. The Lancet. 2022;400(10356):921-72.
134. Burrows B, Fletcher CM, Heard BE, Jones NL, Wootliff JS. THE EMPHYSEMATOUS AND BRONCHIAL TYPES OF CHRONIC AIRWAYS OBSTRUCTION: A Clinicopathological Study of Patients in London and Chicago. The Lancet. 1966;287(7442):830-5.
135. Filley GF, Beckwitt HJ, Reeves JT, Mitchell RS. Chronic obstructive bronchopulmonary disease: II. Oxygen transport in two clinical types. The American Journal of Medicine. 1968;44(1):26-38.
136. Lee JH, Lee YK, Kim EK, Kim TH, Huh JW, Kim WJ, Lee JH, Lee SM, et al. Responses to inhaled long-acting beta-agonist and corticosteroid according to COPD subtype. Respir Med. 2010;104(4):542-9.
137. Hersh CP, Make BJ, Lynch DA, Barr RG, Bowler RP, Calverley PM, Castaldi PJ, Cho MH, et al. Non-emphysematous chronic obstructive pulmonary disease is associated with diabetes mellitus. BMC Pulm Med. 2014;14:164.
138. Makita H, Nasuhara Y, Nagai K, Ito Y, Hasegawa M, Betsuyaku T, Onodera Y, Hizawa N, et al. Characterisation of phenotypes based on severity of emphysema in chronic obstructive pulmonary disease. Thorax. 2007;62(11):932-7.
139. Miravitlles M, Calle M, Soler-Cataluña JJ. Clinical Phenotypes of COPD: Identification, Definition and Implications for Guidelines. Archivos de Bronconeumología. 2012;48(3):86-98.
140. Bhowmik A, Seemungal TA, Sapsford RJ, Wedzicha JA. Relation of sputum inflammatory markers to symptoms and lung function changes in COPD exacerbations. Thorax. 2000;55(2):114-20.
141. Wu Y-K, Su W-L, Yang M-C, Chen S-Y, Wu C-W, Lan C-C. Characterization Associated with the Frequent Severe Exacerbator Phenotype in COPD Patients. International Journal of Chronic Obstructive Pulmonary Disease. 2021;16(null):2475-85.
142. Bélanger M, Couillard S, Courteau J, Larivée P, Poder TG, Carrier N, Girard K, Vézina FA, et al. Eosinophil counts in first COPD hospitalizations: a comparison of health service utilization. Int J Chron Obstruct Pulmon Dis. 2018;13:3045-54.
143. Kim V, Han MK, Vance GB, Make BJ, Newell JD, Hokanson JE, Hersh CP, Stinson D, et al. The chronic bronchitic phenotype of COPD: an analysis of the COPDGene Study. Chest. 2011;140(3):626-33.

144. Suissa S, Dell'Aniello S, Ernst P. Long-term natural history of chronic obstructive pulmonary disease: severe exacerbations and mortality. Thorax. 2012;67(11):957-63.
145. Soler JJ, Sánchez L, Román P, Martínez MA, Perpiñá M. Risk factors of emergency care and admissions in COPD patients with high consumption of health resources. Respir Med. 2004;98(4):318-29.
146. Seemungal TA, Donaldson GC, Paul EA, Bestall JC, Jeffries DJ, Wedzicha JA. Effect of exacerbation on quality of life in patients with chronic obstructive pulmonary disease. Am J Respir Crit Care Med. 1998;157(5 Pt 1):1418-22.
147. Calverley PMA, Anderson JA, Celli B, Ferguson GT, Jenkins C, Jones PW, Yates JC, Vestbo J. Salmeterol and Fluticasone Propionate and Survival in Chronic Obstructive Pulmonary Disease. New England Journal of Medicine. 2007;356(8):775-89.
148. Calverley PMA, Sanchez-Toril F, McIvor A, Teichmann P, Bredenbroeker D, Fabbri LM. Effect of 1-Year Treatment with Roflumilast in Severe Chronic Obstructive Pulmonary Disease. American Journal of Respiratory and Critical Care Medicine. 2007;176(2):154-61.
149. Sin DD, Wu L, Anderson JA, Anthonisen NR, Buist AS, Burge PS, Calverley PM, Connett JE, et al. Inhaled corticosteroids and mortality in chronic obstructive pulmonary disease. Thorax. 2005;60(12):992-7.
150. Miravitlles M, Soler-Cataluña JJ, Calle M, Molina J, Almagro P, Quintano JA, Riesco JA, Trigueros JA, et al. Spanish guideline for COPD (GesEPOC). Update 2014. Arch Bronconeumol. 2014;50 Suppl 1:1-16.
151. Cosio BG, Soriano JB, López-Campos JL, Calle M, Soler JJ, de-Torres JP, Marín JM, Martínez C, et al. Distribution and Outcomes of a Phenotype-Based Approach to Guide COPD Management: Results from the CHAIN Cohort. PLoS One. 2016;11(9):e0160770.
152. Chai CS, Liam CK, Pang YK, Ng DL, Tan SB, Wong TS, Sia JE. Clinical phenotypes of COPD and health-related quality of life: a cross-sectional study. Int J Chron Obstruct Pulmon Dis. 2019;14:565-73.
153. Golpe R, Suárez-Valor M, Martín-Robles I, Sanjuán-López P, Cano-Jiménez E, Castro-Añón O, Pérez de Llano LA. Mortality in COPD patients according to clinical phenotypes. Int J Chron Obstruct Pulmon Dis. 2018;13:1433-9.
154. Hardin M, Silverman EK, Barr RG, Hansel NN, Schroeder JD, Make BJ, Crapo JD, Hersh CP. The clinical features of the overlap between COPD and asthma. Respir Res. 2011;12(1):127.
155. de Marco R, Pesce G, Marcon A, Accordini S, Antonicelli L, Bugiani M, Casali L, Ferrari M, et al. The coexistence of asthma and chronic obstructive pulmonary disease (COPD): prevalence and risk factors in young, middle-aged and elderly people from the general population. PLoS One. 2013;8(5):e62985.
156. Lee HY, Kang JY, Yoon HK, Lee SY, Kwon SS, Kim YK, Rhee CK. Clinical characteristics of asthma combined with COPD feature. Yonsei Med J. 2014;55(4):980-6.
157. Moorman JE, Zahran H, Truman BI, Molla MT. Current asthma prevalence - United States, 2006-2008. MMWR Suppl. 2011;60(1):84-6.
158. Akinbami LJ, Moorman JE, Bailey C, Zahran HS, King M, Johnson CA, Liu X. Trends in asthma prevalence, health care use, and mortality in the United States, 2001-2010. NCHS Data Brief. 2012(94):1-8.
159. Miravitlles M, Soriano JB, Ancochea J, Muñoz L, Duran-Tauleria E, Sánchez G, Sobradillo V, García-Río F. Characterisation of the overlap COPD-asthma phenotype. Focus on physical activity and health status. Respir Med. 2013;107(7):1053-60.
160. Casanova C, Cote C, Torres JPd, Aguirre-Jaime A, Marin JM, Pinto-Plata V, Celli BR. Inspiratory-to-Total Lung Capacity Ratio Predicts Mortality in Patients with Chronic Obstructive Pulmonary Disease. American Journal of Respiratory and Critical Care Medicine. 2005;171(6):591-7.
161. Corbin RP, Loveland M, Martin RR, Macklem PT. A four-year follow-up study of lung mechanics in smokers. Am Rev Respir Dis. 1979;120(2):293-304.

162. O'Donnell DE, Guenette JA, Maltais F, Webb KA. Decline of Resting Inspiratory Capacity in COPD: The Impact on Breathing Pattern, Dyspnea, and Ventilatory Capacity During Exercise. CHEST. 2012;141(3):753-62.
163. Cardoso J, Coelho R, Rocha C, Coelho C, Semedo L, Bugalho Almeida A. Prediction of severe exacerbations and mortality in COPD: the role of exacerbation history and inspiratory capacity/total lung capacity ratio. Int J Chron Obstruct Pulmon Dis. 2018;13:1105-13.
164. French A, Balfe D, Mirocha JM, Falk JA, Mosenifar Z. The inspiratory capacity/total lung capacity ratio as a predictor of survival in an emphysematous phenotype of chronic obstructive pulmonary disease. Int J Chron Obstruct Pulmon Dis. 2015;10:1305-12.
165. Ramon MA, Ferrer J, Gimeno-Santos E, Donaire-Gonzalez D, Rodríguez E, Balcells E, de Batlle J, Benet M, et al. Inspiratory capacity-to-total lung capacity ratio and dyspnoea predict exercise capacity decline in COPD. Respirology. 2016;21(3):476-82.
166. Müller NL, Staples CA, Miller RR, Abboud RT. "Density mask". An objective method to quantitate emphysema using computed tomography. Chest. 1988;94(4):782-7.
167. Gevenois PA, De Vuyst P, de Maertelaer V, Zanen J, Jacobovitz D, Cosio MG, Yernault JC. Comparison of computed density and microscopic morphometry in pulmonary emphysema. Am J Respir Crit Care Med. 1996;154(1):187-92.
168. Gevenois PA, Maertelaer Vd, Vuyst PD, Zanen J, Yernault JC. Comparison of computed density and macroscopic morphometry in pulmonary emphysema. American Journal of Respiratory and Critical Care Medicine. 1995;152(2):653-7.
169. Madani A, Zanen J, de Maertelaer V, Gevenois PA. Pulmonary emphysema: objective quantification at multi-detector row CT--comparison with macroscopic and microscopic morphometry. Radiology. 2006;238(3):1036-43.
170. Parr DG, Stoel BC, Stolk J, Stockley RA. Validation of computed tomographic lung densitometry for monitoring emphysema in alpha1-antitrypsin deficiency. Thorax. 2006;61(6):485-90.
171. Lynch DA, Al-Qaisi MA. Quantitative computed tomography in chronic obstructive pulmonary disease. J Thorac Imaging. 2013;28(5):284-90.
172. Schroeder JD, McKenzie AS, Zach JA, Wilson CG, Curran-Everett D, Stinson DS, Newell JD, Jr., Lynch DA. Relationships between airflow obstruction and quantitative CT measurements of emphysema, air trapping, and airways in subjects with and without chronic obstructive pulmonary disease. AJR Am J Roentgenol. 2013;201(3):W460-70.
173. Heussel CP, Herth FJ, Kappes J, Hantusch R, Hartlieb S, Weinheimer O, Kauczor HU, Eberhardt R. Fully automatic quantitative assessment of emphysema in computed tomography: comparison with pulmonary function testing and normal values. Eur Radiol. 2009;19(10):2391-402.
174. Johannessen A, Skorge TD, Bottai M, Grydeland TB, Nilsen RM, Coxson H, Dirksen A, Omenaas E, et al. Mortality by level of emphysema and airway wall thickness. Am J Respir Crit Care Med. 2013;187(6):602-8.
175. Han MK, Kazerooni EA, Lynch DA, Liu LX, Murray S, Curtis JL, Criner GJ, Kim V, et al. Chronic obstructive pulmonary disease exacerbations in the COPDGene study: associated radiologic phenotypes. Radiology. 2011;261(1):274-82.
176. Dirksen A, Piitulainen E, Parr DG, Deng C, Wencker M, Shaker SB, Stockley RA. Exploring the role of CT densitometry: a randomised study of augmentation therapy in alpha1-antitrypsin deficiency. Eur Respir J. 2009;33(6):1345-53.
177. Gietema HA, Müller NL, Fauerbach PV, Sharma S, Edwards LD, Camp PG, Coxson HO. Quantifying the extent of emphysema: factors associated with radiologists' estimations and quantitative indices of emphysema severity using the ECLIPSE cohort. Acad Radiol. 2011;18(6):661-71.
178. Lynch DA, Austin JH, Hogg JC, Grenier PA, Kauczor H-U, Bankier AA, Barr RG, Colby TV, et al. CT-definable subtypes of chronic obstructive pulmonary disease: a statement of the Fleischner Society. Radiology. 2015;277(1):192-205.

179. Lynch DA, Moore CM, Wilson C, Nevrekar D, Jennermann T, Humphries SM, Austin JHM, Grenier PA, et al. CT-based Visual Classification of Emphysema: Association with Mortality in the COPDGene Study. Radiology. 2018;288(3):859-66.
180. Wilson DO, Leader JK, Fuhrman CR, Reilly JJ, Sciurba FC, Weissfeld JL. Quantitative computed tomography analysis, airflow obstruction, and lung cancer in the Pittsburgh lung screening study. Journal of Thoracic Oncology. 2011;6(7):1200-5.
181. de Torres JP, Bastarrika G, Wisnivesky JP, Alcaide AB, Campo A, Seijo LM, Pueyo JC, Villanueva A, et al. Assessing the relationship between lung cancer risk and emphysema detected on low-dose CT of the chest. Chest. 2007;132(6):1932-8.
182. Mandelbrot BB, Mandelbrot BB. The fractal geometry of nature: WH freeman New York; 1982.
183. Mishima M, Hirai T, Itoh H, Nakano Y, Sakai H, Muro S, Nishimura K, Oku Y, et al. Complexity of terminal airspace geometry assessed by lung computed tomography in normal subjects and patients with chronic obstructive pulmonary disease. Proc Natl Acad Sci U S A. 1999;96(16):8829-34.
184. Tanabe N, Muro S, Hirai T, Oguma T, Terada K, Marumo S, Kinose D, Ogawa E, et al. Impact of exacerbations on emphysema progression in chronic obstructive pulmonary disease. Am J Respir Crit Care Med. 2011;183(12):1653-9.
185. Tanabe N, Muro S, Sato S, Oguma T, Sato A, Hirai T. Fractal analysis of low attenuation clusters on computed tomography in chronic obstructive pulmonary disease. BMC Pulm Med. 2018;18(1):144.
186. UPPALURI R, MITSA T, SONKA M, HOFFMAN EA, McLENNAN G. Quantification of Pulmonary Emphysema from Lung Computed Tomography Images. American Journal of Respiratory and Critical Care Medicine. 1997;156(1):248-54.
187. Uppaluri R, Hoffman EA, Sonka M, Hartley PG, Hunninghake GW, McLennan G. Computer recognition of regional lung disease patterns. Am J Respir Crit Care Med. 1999;160(2):648-54.
188. Sørensen L, Shaker SB, de Bruijne M. Quantitative analysis of pulmonary emphysema using local binary patterns. IEEE Trans Med Imaging. 2010;29(2):559-69.
189. Park YS, Seo JB, Kim N, Chae EJ, Oh YM, Lee SD, Lee Y, Kang SH. Texture-based quantification of pulmonary emphysema on high-resolution computed tomography: comparison with density-based quantification and correlation with pulmonary function test. Invest Radiol. 2008;43(6):395-402.
190. Ginsburg SB, Lynch DA, Bowler RP, Schroeder JD. Automated texture-based quantification of centrilobular nodularity and centrilobular emphysema in chest CT images. Acad Radiol. 2012;19(10):1241-51.
191. Mendoza CS, Washko GR, Ross JC, Diaz AA, Lynch DA, Crapo JD, Silverman EK, Acha B, et al. EMPHYSEMA QUANTIFICATION IN A MULTI-SCANNER HRCT COHORT USING LOCAL INTENSITY DISTRIBUTIONS. Proc IEEE Int Symp Biomed Imaging. 2012:474-7.
192. Botev ZI, Grotowski JF, Kroese DP. Kernel density estimation via diffusion. 2010.
193. Castaldi PJ, San José Estépar R, Mendoza CS, Hersh CP, Laird N, Crapo JD, Lynch DA, Silverman EK, et al. Distinct quantitative computed tomography emphysema patterns are associated with physiology and function in smokers. Am J Respir Crit Care Med. 2013;188(9):1083-90.
194. Nakano Y, Wong JC, de Jong PA, Buzatu L, Nagao T, Coxson HO, Elliott WM, Hogg JC, et al. The prediction of small airway dimensions using computed tomography. Am J Respir Crit Care Med. 2005;171(2):142-6.
195. Nakano Y, Whittall KP, Kalloger SE, Coxson HO, Flint J, Pare PD, English JC, editors. Development and validation of human airway analysis algorithm using multidetector row CT. Medical Imaging 2002: Physiology and Function from Multidimensional Images; 2002: SPIE.
196. Nakano Y, Wong JC, Jong PAd, Buzatu L, Nagao T, Coxson HO, Elliott WM, Hogg JC, et al. The Prediction of Small Airway Dimensions Using Computed Tomography. American Journal of Respiratory and Critical Care Medicine. 2005;171(2):142-6.

197. Patel BD, Coxson HO, Pillai SG, Agustí AG, Calverley PM, Donner CF, Make BJ, Müller NL, et al. Airway wall thickening and emphysema show independent familial aggregation in chronic obstructive pulmonary disease. Am J Respir Crit Care Med. 2008;178(5):500-5.
198. Noble PB, West AR, McLaughlin RA, Armstrong JJ, Becker S, McFawn PK, Williamson JP, Eastwood PR, et al. Airway narrowing assessed by anatomical optical coherence tomography in vitro: dynamic airway wall morphology and function. Journal of Applied Physiology. 2010;108(2):401-11.
199. Grydeland TB, Dirksen A, Coxson HO, Pillai SG, Sharma S, Eide GE, Gulsvik A, Bakke PS. Quantitative computed tomography: emphysema and airway wall thickness by sex, age and smoking. European Respiratory Journal. 2009;34(4):858-65.
200. Grydeland TB, Dirksen A, Coxson HO, Eagan TML, Thorsen E, Pillai SG, Sharma S, Eide GE, et al. Quantitative Computed Tomography Measures of Emphysema and Airway Wall Thickness Are Related to Respiratory Symptoms. American Journal of Respiratory and Critical Care Medicine. 2010;181(4):353-9.
201. Grydeland TB, Thorsen E, Dirksen A, Jensen R, Coxson HO, Pillai SG, Sharma S, Eide GE, et al. Quantitative CT measures of emphysema and airway wall thickness are related to D(L)CO. Respir Med. 2011;105(3):343-51.
202. Rutten EP, Grydeland TB, Pillai SG, Wagers S, Dirksen A, Coxson HO, Gulsvik A, Wouters EF, et al. Quantitative CT: Associations between Emphysema, Airway Wall Thickness and Body Composition in COPD. Pulm Med. 2011;2011:419328.
203. Kahnert K, Jörres RA, Kauczor HU, Alter P, Trudzinski FC, Herth F, Jobst B, Weinheimer O, et al. Standardized airway wall thickness Pi10 from routine CT scans of COPD patients as imaging biomarker for disease severity, lung function decline, and mortality. Ther Adv Respir Dis. 2023;17:17534666221148663.
204. Oelsner EC, Smith BM, Hoffman EA, Kalhan R, Donohue KM, Kaufman JD, Nguyen JN, Manichaikul AW, et al. Prognostic Significance of Large Airway Dimensions on Computed Tomography in the General Population. The Multi-Ethnic Study of Atherosclerosis (MESA) Lung Study. Ann Am Thorac Soc. 2018;15(6):718-27.
205. Chaudhary MFA, Hoffman EA, Guo J, Comellas AP, Newell JD, Jr., Nagpal P, Fortis S, Christensen GE, et al. Predicting severe chronic obstructive pulmonary disease exacerbations using quantitative CT: a retrospective model development and external validation study. Lancet Digit Health. 2023;5(2):e83-e92.
206. Galbán CJ, Han MK, Boes JL, Chughtai KA, Meyer CR, Johnson TD, Galbán S, Rehemtulla A, et al. Computed tomography-based biomarker provides unique signature for diagnosis of COPD phenotypes and disease progression. Nat Med. 2012;18(11):1711-5.
207. Moffat BA, Chenevert TL, Lawrence TS, Meyer CR, Johnson TD, Dong Q, Tsien C, Mukherji S, et al. Functional diffusion map: a noninvasive MRI biomarker for early stratification of clinical brain tumor response. Proc Natl Acad Sci U S A. 2005;102(15):5524-9.
208. Tanabe N, Vasilescu DM, McDonough JE, Kinose D, Suzuki M, Cooper JD, Paré PD, Hogg JC. Micro-Computed Tomography Comparison of Preterminal Bronchioles in Centrilobular and Panlobular Emphysema. Am J Respir Crit Care Med. 2017;195(5):630-8.
209. Nagai A, Yamawaki I, Takizawa T, Thurlbeck WM. Alveolar attachments in emphysema of human lungs. Am Rev Respir Dis. 1991;144(4):888-91.
210. Young AL, Marinescu RV, Oxtoby NP, Bocchetta M, Yong K, Firth NC, Cash DM, Thomas DL, et al. Uncovering the heterogeneity and temporal complexity of neurodegenerative diseases with Subtype and Stage Inference. Nat Commun. 2018;9(1):4273.
211. Young AL, Bragman FJS, Rangelov B, Han MK, Galbán CJ, Lynch DA, Hawkes DJ, Alexander DC, et al. Disease Progression Modeling in Chronic Obstructive Pulmonary Disease. American Journal of Respiratory and Critical Care Medicine. 2020;201(3):294-302.
212. Chae EJ, Seo JB, Goo HW, Kim N, Song K-S, Lee SD, Hong S-J, Krauss B. Xenon Ventilation CT with a Dual-Energy Technique of Dual-Source CT: Initial Experience. Radiology. 2008;248(2):615-24.

213. Park E-A, Goo JM, Park SJ, Lee HJ, Lee CH, Park CM, Yoo C-G, Kim JH. Chronic Obstructive Pulmonary Disease: Quantitative and Visual Ventilation Pattern Analysis at Xenon Ventilation CT Performed by Using a Dual-Energy Technique. Radiology. 2010;256(3):985-97.
214. Remy-Jardin M, Faivre JB, Pontana F, Hachulla AL, Tacelli N, Santangelo T, Remy J. Thoracic applications of dual energy. Radiol Clin North Am. 2010;48(1):193-205.
215. Cao K, Ding K, Christensen G, Reinhardt J. Tissue volume and vesselness measure preserving nonrigid registration of lung CT images: SPIE; 2010.
216. Ding K, Cao K, Fuld MK, Du K, Christensen GE, Hoffman EA, Reinhardt JM. Comparison of image registration based measures of regional lung ventilation from dynamic spiral CT with Xe-CT. Med Phys. 2012;39(8):5084-98.
217. Yamamoto T, Kabus S, Lorenz C, Mittra E, Hong JC, Chung M, Eclov N, To J, et al. Pulmonary ventilation imaging based on 4-dimensional computed tomography: comparison with pulmonary function tests and SPECT ventilation images. Int J Radiat Oncol Biol Phys. 2014;90(2):414-22.
218. Yamamoto T, Kabus S, Klinder T, Lorenz C, Von Berg J, Blaffert T, Loo BW, Keall PJ. Investigation of four-dimensional computed tomography-based pulmonary ventilation imaging in patients with emphysematous lung regions. Physics in Medicine & Biology. 2011;56(7):2279.
219. Jögi J, Jonson B, Ekberg M, Bajc M. Ventilation–Perfusion SPECT with ^{99m}Tc-DTPA Versus Technegas: A Head-to-Head Study in Obstructive and Nonobstructive Disease. Journal of Nuclear Medicine. 2010;51(5):735-41.
220. de Nijs R, Sijtsema ND, Kruis MF, Jensen CV, Iversen M, Perch M, Mortensen J. Comparison of 81mKrypton and 99mTc-Technegas for ventilation single-photon emission computed tomography in severe chronic obstructive pulmonary disease. Nucl Med Commun. 2021;42(2):160-8.
221. Amis TC, Crawford AB, Davison A, Engel LA. Distribution of inhaled 99mtechnetium labelled ultrafine carbon particle aerosol (Technegas) in human lungs. European Respiratory Journal. 1990;3(6):679.
222. Crawford AB, Davison A, Amis TC, Engel LA. Intrapulmonary distribution of 99mtechnetium labelled ultrafine carbon aerosol (Technegas) in severe airflow obstruction. Eur Respir J. 1990;3(6):686-92.
223. Farrow CE, Salome CM, Harris BE, Bailey DL, Bailey E, Berend N, Young IH, King GG. Airway closure on imaging relates to airway hyperresponsiveness and peripheral airway disease in asthma. J Appl Physiol (1985). 2012;113(6):958-66.
224. Cuña EG, Gambini JP, Servente L, Savio E, Engler HW, González GA, Alonso O. Quantitative comparison between single-photon emission computed tomography and positron emission tomography imaging of lung ventilation with (99m)Tc-technegas and (68)Ga-gallgas in patients with chronic obstructive pulmonary disease: A pilot study. World J Nucl Med. 2019;18(3):251-7.
225. Radadia N, Friedlander Y, Priel E, Konyer NB, Huang C, Jamal M, Farncombe T, Marriott C, et al. Comparison of ventilation defects quantified by Technegas SPECT and hyperpolarized 129Xe MRI. Frontiers in Physiology. 2023;14.
226. Stavngaard T, Søgaard LV, Mortensen J, Hanson LG, Schmiedeskamp J, Berthelsen AK, Dirksen A. Hyperpolarised 3He MRI and 81mKr SPECT in chronic obstructive pulmonary disease. European Journal of Nuclear Medicine and Molecular Imaging. 2005;32(4):448-57.
227. Diba C, Salome CM, Berend N, Harris B, Bailey D, King GG. Effect of Bronchodilator on Ventilation Heterogeneity in COPD. D28 IMAGING OBSTRUCTIVE LUNG DISEASES I. American Thoracic Society International Conference Abstracts: American Thoracic Society; 2009. p. A5577.
228. Pellegrino R, Biggi A, Papaleo A, Camuzzini G, Rodarte JR, Brusasco V. Regional expiratory flow limitation studied with Technegas in asthma. Journal of Applied Physiology. 2001;91(5):2190-8.
229. Bajc M, Chen Y, Wang J, Li XY, Shen WM, Wang CZ, Huang H, Lindqvist A, et al. Identifying the heterogeneity of COPD by V/P SPECT: a new tool for improving the diagnosis of parenchymal defects and grading the severity of small airways disease. Int J Chron Obstruct Pulmon Dis. 2017;12:1579-87.
230. Bajc M, Schümichen C, Grüning T, Lindqvist A, Le Roux P-Y, Alatri A, Bauer RW, Dilic M, et al. EANM guideline for ventilation/perfusion single-photon emission computed tomography (SPECT) for

diagnosis of pulmonary embolism and beyond. European Journal of Nuclear Medicine and Molecular Imaging. 2019;46(12):2429-51.
231. Paludan JPD, Andresen SR, Abrahamsen J, Petersen LJ, Høyer C. Improvement in image quality of Tc-99m-based ventilation/perfusion single-photon emission computed tomography in patients with chronic obstructive pulmonary disease through pretest continuous positive airway pressure treatment. World J Nucl Med. 2019;18(2):185-6.
232. Imai T, Sasaki Y, Shinkai T, Ohishi H, Nezu K, Nishimoto Y, Ichiba N, Yamane T, et al. Clinical evaluation of99mTc-Technegas SPECT in thoracoscopic lung volume reduction surgery in patients with pulmonary emphysema. Annals of Nuclear Medicine. 2000;14(4):263-70.
233. Lee SJ, Park HJ. Single photon emission computed tomography (SPECT) or positron emission tomography (PET) imaging for radiotherapy planning in patients with lung cancer: a meta-analysis. Sci Rep. 2020;10(1):14864.
234. Nagao M, Murase K, Yasuhara Y, Ikezoe J. Quantitative analysis of pulmonary emphysema: three-dimensional fractal analysis of single-photon emission computed tomography images obtained with a carbon particle radioaerosol. AJR Am J Roentgenol. 1998;171(6):1657-63.
235. Otsu N. A Threshold Selection Method from Gray-Level Histograms. IEEE Transactions on Systems, Man, and Cybernetics. 1979;9(1):62-6.
236. Picture Thresholding Using an Iterative Selection Method. IEEE Transactions on Systems, Man, and Cybernetics. 1978;8(8):630-2.
237. Högberg J, Andersén C, Rydén T, Lagerlöf JH. Comparison of Otsu and an adapted Chan-Vese method to determine thyroid active volume using Monte Carlo generated SPECT images. EJNMMI Phys. 2024;11(1):6.
238. Shea DA, Morgan DL. The helium-3 shortage: Supply, demand, and options for congress: Congressional Research Service Washington, DC; 2010.
239. Kramer D. For some, helium-3 supply picture is brightening. Physics Today. 2011;64(5):20-2.
240. Hersman FW, Ruset IC, Ketel S, Muradian I, Covrig SD, Distelbrink J, Porter W, Watt D, et al. Large production system for hyperpolarized 129Xe for human lung imaging studies. Acad Radiol. 2008;15(6):683-92.
241. Norquay G, Parnell SR, Xu X, Parra-Robles J, Wild JM. Optimized production of hyperpolarized 129Xe at 2 bars for in vivo lung magnetic resonance imaging. Journal of Applied Physics. 2013;113(4).
242. Stewart NJ, Norquay G, Griffiths PD, Wild JM. Feasibility of human lung ventilation imaging using highly polarized naturally abundant xenon and optimized three-dimensional steady-state free precession. Magn Reson Med. 2015;74(2):346-52.
243. Kirby M, Svenningsen S, Owrangi A, Wheatley A, Farag A, Ouriadov A, Santyr GE, Etemad-Rezai R, et al. Hyperpolarized 3He and 129Xe MR Imaging in Healthy Volunteers and Patients with Chronic Obstructive Pulmonary Disease. Radiology. 2012;265(2):600-10.
244. Kirby M, Svenningsen S, Kanhere N, Owrangi A, Wheatley A, Coxson HO, Santyr GE, Paterson NA, et al. Pulmonary ventilation visualized using hyperpolarized helium-3 and xenon-129 magnetic resonance imaging: differences in COPD and relationship to emphysema. J Appl Physiol (1985). 2013;114(6):707-15.
245. Kirby M, Pike D, Coxson HO, McCormack DG, Parraga G. Hyperpolarized (3)He ventilation defects used to predict pulmonary exacerbations in mild to moderate chronic obstructive pulmonary disease. Radiology. 2014;273(3):887-96.
246. Kirby M, Eddy RL, Pike D, Svenningsen S, Coxson HO, Sin DD, McCormack DG, Parraga G. MRI ventilation abnormalities predict quality-of-life and lung function changes in mild-to-moderate COPD: longitudinal TINCan study. Thorax. 2017;72(5):475-7.
247. Davis C, Sheikh K, Pike D, Svenningsen S, McCormack DG, O'Donnell D, Neder JA, Parraga G. Ventilation Heterogeneity in Never-smokers and COPD:: Comparison of Pulmonary Functional Magnetic Resonance Imaging with the Poorly Communicating Fraction Derived From Plethysmography. Academic Radiology. 2016;23(4):398-405.

248. Young HM, Guo F, Eddy RL, Maksym G, Parraga G. Oscillometry and pulmonary MRI measurements of ventilation heterogeneity in obstructive lung disease: relationship to quality of life and disease control. Journal of Applied Physiology. 2018;125(1):73-85.
249. Kaushik SS, Cleveland ZI, Cofer GP, Metz G, Beaver D, Nouls J, Kraft M, Auffermann W, et al. Diffusion-weighted hyperpolarized 129Xe MRI in healthy volunteers and subjects with chronic obstructive pulmonary disease. Magn Reson Med. 2011;65(4):1154-65.
250. Woods JC, Choong CK, Yablonskiy DA, Bentley J, Wong J, Pierce JA, Cooper JD, Macklem PT, et al. Hyperpolarized 3He diffusion MRI and histology in pulmonary emphysema. Magn Reson Med. 2006;56(6):1293-300.
251. Fain SB, Panth SR, Evans MD, Wentland AL, Holmes JH, Korosec FR, O'Brien MJ, Fountaine H, et al. Early emphysematous changes in asymptomatic smokers: detection with 3He MR imaging. Radiology. 2006;239(3):875-83.
252. Wang C, Mugler JP, 3rd, de Lange EE, Patrie JT, Mata JF, Altes TA. Lung injury induced by secondhand smoke exposure detected with hyperpolarized helium-3 diffusion MR. J Magn Reson Imaging. 2014;39(1):77-84.
253. Meng X-f, Lin Q-y, Yin H, Li Z-q. Hyperpolarized 3helium MRI measured apparent diffusion coefficient and its correlations with pulmonary functions tests in patients with chronic obstructive pulmonary disease: A meta-analysis. The Clinical Respiratory Journal. 2021;15(11):1185-93.
254. Tafti S, Garrison WJ, John P. Mugler I, Shim YM, Altes TA, Mata JF, Lange EEd, Gordon D. Cates J, et al. Emphysema Index Based on Hyperpolarized 3He or 129Xe Diffusion MRI: Performance and Comparison with Quantitative CT and Pulmonary Function Tests. Radiology. 2020;297(1):201-10.
255. Kirby M, Mathew L, Heydarian M, Etemad-Rezai R, McCormack DG, Parraga G. Chronic obstructive pulmonary disease: quantification of bronchodilator effects by using hyperpolarized ^{3}He MR imaging. Radiology. 2011;261(1):283-92.
256. Mummy DG, Coleman EM, Wang Z, Bier EA, Lu J, Driehuys B, Huang Y-C. Regional Gas Exchange Measured by 129Xe Magnetic Resonance Imaging Before and After Combination Bronchodilators Treatment in Chronic Obstructive Pulmonary Disease. Journal of Magnetic Resonance Imaging. 2021;54(3):964-74.
257. Stanojevic S, Kaminsky DA, Miller MR, Thompson B, Aliverti A, Barjaktarevic I, Cooper BG, Culver B, et al. ERS/ATS technical standard on interpretive strategies for routine lung function tests. Eur Respir J. 2022;60(1).
258. Pellegrino R, Viegi G, Brusasco V, Crapo RO, Burgos F, Casaburi R, Coates A, van der Grinten CPM, et al. Interpretative strategies for lung function tests. European Respiratory Journal. 2005;26(5):948.
259. Bhatt SP, Fortis S, Bodduluri S. New Guidelines for Bronchodilator Responsiveness in COPD: A Test in Search of a Use. Am J Respir Crit Care Med. 2022;206(8):1042-4.
260. Li Y, Lin J, Wang Z, Wang Z, Tan L, Liu S, Huang J, Gao Y, et al. Bronchodilator Responsiveness Defined by the 2005 and 2021 ERS/ATS Criteria in Patients with Asthma as Well as Chronic Obstructive Pulmonary Disease. Int J Chron Obstruct Pulmon Dis. 2022;17:2623-33.
261. Beasley R, Hughes R, Agusti A, Calverley P, Chipps B, Del Olmo R, Papi A, Price D, et al. Prevalence, Diagnostic Utility and Associated Characteristics of Bronchodilator Responsiveness. Am J Respir Crit Care Med. 2024;209(4):390-401.
262. Durack J, Lynch SV, Nariya S, Bhakta NR, Beigelman A, Castro M, Dyer A-M, Israel E, et al. Features of the bronchial bacterial microbiome associated with atopy, asthma, and responsiveness to inhaled corticosteroid treatment. Journal of allergy and clinical immunology. 2017;140(1):63-75.
263. Park JH, Lee JH, Kim HJ, Jeong N, Jang HJ, Kim HK, Park CS. Usefulness of impulse oscillometry for the assessment of bronchodilator response in elderly patients with chronic obstructive airway disease. J Thorac Dis. 2019;11(4):1485-94.
264. Tashkin DP, Celli B, Decramer M, Liu D, Burkhart D, Cassino C, Kesten S. Bronchodilator responsiveness in patients with COPD. European Respiratory Journal. 2008;31(4):742-50.

265. Marín JM, Ciudad M, Moya V, Carrizo S, Bello S, Piras B, Celli BR, Miravitlles M. Airflow reversibility and long-term outcomes in patients with COPD without comorbidities. Respiratory medicine. 2014;108(8):1180-8.
266. Kim J, Kim WJ, Lee C-H, Lee SH, Lee M-G, Shin K-C, Yoo KH, Lee J-H, et al. Which bronchodilator reversibility criteria can predict severe acute exacerbation in chronic obstructive pulmonary disease patients? Respiratory Research. 2017;18(1):107.
267. Hersh CP, Jacobson FL, Gill R, Silverman EK. Computed tomography phenotypes in severe, early-onset chronic obstructive pulmonary disease. Copd. 2007;4(4):331-7.
268. Kitaguchi Y, Fujimoto K, Kubo K, Honda T. Characteristics of COPD phenotypes classified according to the findings of HRCT. Respir Med. 2006;100(10):1742-52.
269. Choi JY, Kim SK, Lee JH, Jung K-S, Yoo KH, Hwang K-E, Lee JD, Kim Y-I, et al. Differences in clinical significance of bronchodilator responses measured by forced expiratory volume in 1 second and forced vital capacity. PLOS ONE. 2023;18(2):e0282256.
270. Albert P, Agusti A, Edwards L, Tal-Singer R, Yates J, Bakke P, Celli BR, Coxson HO, et al. Bronchodilator responsiveness as a phenotypic characteristic of established chronic obstructive pulmonary disease. Thorax. 2012;67(8):701-8.
271. Janson C, Malinovschi A, Amaral AFS, Accordini S, Bousquet J, Buist AS, Canonica GW, Dahlén B, et al. Bronchodilator reversibility in asthma and COPD: findings from three large population studies. European Respiratory Journal. 2019;54(3):1900561.
272. Ramsdell JW, Tisi GM. Determination of Bronchodilation in the Clinical Pulmonary Function Laboratory: Role of Changes in Static Lung Volumes. CHEST. 1979;76(6):622-8.
273. Newton MF, O'Donnell DE, Forkert L. Response of lung volumes to inhaled salbutamol in a large population of patients with severe hyperinflation. Chest. 2002;121(4):1042-50.
274. Celli B, ZuWallack R, Wang S, Kesten S. Improvement in resting inspiratory capacity and hyperinflation with tiotropium in COPD patients with increased static lung volumes. Chest. 2003;124(5):1743-8.
275. O'Donnell DE, Flüge T, Gerken F, Hamilton A, Webb K, Aguilaniu B, Make B, Magnussen H. Effects of tiotropium on lung hyperinflation, dyspnoea and exercise tolerance in COPD. European Respiratory Journal. 2004;23(6):832-40.
276. O'Donnell DE, Forkert L, Webb KA. Evaluation of bronchodilator responses in patients with “irreversible” emphysema. European Respiratory Journal. 2001;18(6):914-20.
277. da Costa GM, Faria ACD, Di Mango AMGT, Lopes AJ, Lopes de Melo P. Respiratory Impedance and Response to Salbutamol in Healthy Individuals and Patients with COPD. Respiration. 2014;88(2):101-11.
278. Dellacà RL, Pompilio PP, Walker PP, Duffy N, Pedotti A, Calverley PMA. Effect of bronchodilation on expiratory flow limitation and resting lung mechanics in COPD. European Respiratory Journal. 2009;33(6):1329-37.
279. Jetmalani K, Brown NJ, Boustany C, Toelle BG, Marks GB, Abramson MJ, Johns DP, James AL, et al. Normal limits for oscillometric bronchodilator responses and relationships with clinical factors. ERJ Open Res. 2021;7(4).
280. Leuppi JD, Salome CM, Jenkins CR, Anderson SD, Xuan W, Marks GB, Koskela H, Brannan JD, et al. Predictive markers of asthma exacerbation during stepwise dose reduction of inhaled corticosteroids. Am J Respir Crit Care Med. 2001;163(2):406-12.
281. Sont JK, Willems LN, Bel EH, van Krieken JH, Vandenbroucke JP, Sterk PJ. Clinical control and histopathologic outcome of asthma when using airway hyperresponsiveness as an additional guide to long-term treatment. The AMPUL Study Group. Am J Respir Crit Care Med. 1999;159(4 Pt 1):1043-51.
282. Cerveri I, Bruschi C, Zoia MC, Zanon P, Maccarini L, Grassi M, Rampulla C. Distribution of bronchial nonspecific reactivity in the general population. Chest. 1988;93(1):26-30.
283. Yan K, Salome CM, Woolcock AJ. Prevalence and nature of bronchial hyperresponsiveness in subjects with chronic obstructive pulmonary disease. Am Rev Respir Dis. 1985;132(1):25-9.

284. Tashkin DP, Altose MD, Bleecker ER, Connett JE, Kanner RE, Lee WW, Wise R. The lung health study: airway responsiveness to inhaled methacholine in smokers with mild to moderate airflow limitation. The Lung Health Study Research Group. Am Rev Respir Dis. 1992;145(2 Pt 1):301-10.
285. Tkacova R, Dai DLY, Vonk JM, Leung JM, Hiemstra PS, van den Berge M, Kunz L, Hollander Z, et al. Airway hyperresponsiveness in chronic obstructive pulmonary disease: A marker of asthma-chronic obstructive pulmonary disease overlap syndrome? J Allergy Clin Immunol. 2016;138(6):1571-9.e10.
286. Vestbo J, Hansen EF. Airway hyperresponsiveness and COPD mortality. Thorax. 2001;56(suppl 2):ii11-ii4.
287. Teferra AA, Vonk JM, Boezen HM. Longitudinal changes in airway hyperresponsiveness and COPD mortality. European Respiratory Journal. 2020;55(2):1901378.
288. Zanini A, Cherubino F, Zampogna E, Croce S, Pignatti P, Spanevello A. Bronchial hyperresponsiveness, airway inflammation, and reversibility in patients with chronic obstructive pulmonary disease. Int J Chron Obstruct Pulmon Dis. 2015;10:1155-61.
289. van den Berge M, Vonk JM, Gosman M, Lapperre TS, Snoeck-Stroband JB, Sterk PJ, Kunz LIZ, Hiemstra PS, et al. Clinical and inflammatory determinants of bronchial hyperresponsiveness in COPD. European Respiratory Journal. 2012;40(5):1098-105.
290. Berge Mvd, Vonk JM, Gosman M, Lapperre TS, Snoeck-Stroband JB, Sterk PJ, Kunz LIZ, Hiemstra PS, et al. Clinical and inflammatory determinants of bronchial hyperresponsiveness in COPD. European Respiratory Journal. 2012;40(5):1098-105.
291. Venegas JG, Winkler T, Musch G, Vidal Melo MF, Layfield D, Tgavalekos N, Fischman AJ, Callahan RJ, et al. Self-organized patchiness in asthma as a prelude to catastrophic shifts. Nature. 2005;434(7034):777-82.
292. Wardlaw AJ, Dunnette S, Gleich GJ, Collins JV, Kay AB. Eosinophils and mast cells in bronchoalveolar lavage in subjects with mild asthma. Relationship to bronchial hyperreactivity. Am Rev Respir Dis. 1988;137(1):62-9.
293. Hardaker KM, Downie SR, Kermode JA, Berend N, King GG, Salome CM. Ventilation heterogeneity is associated with airway responsiveness in asthma but not COPD. Respir Physiol Neurobiol. 2013;189(1):106-11.

Chapter 2 – Comparison of threshold techniques for determining ventilation using Single Photon Emission Computed Tomography

2.1 Abstract

Introduction: For quantitative VSPECT/CT analysis, there are a variety of threshold methods that can be used to define 'ventilated' and 'non-ventilated' volumes. Clinical application for such methods requires them to be optimised, but none have been validated. Our objective was to assess threshold methods and to develop a novel threshold method.

Methods: 10 phantom lung models were scanned with SPECT/CT. These 10 containers of known volume, packed with foam beads to simulate lungs, were filled with ^{99m}Tc solution, which simulated Technegas deposition. Smaller containers also of known volumes, with no radioactivity, were inserted to simulate non-ventilated regions. Small vials with increased ^{99m}Tc solution were attached to simulate 'hot spots'. We assessed four threshold methods: 15% of maximum activity (Thr_15%Max), weighted average intensity of all voxels between 5 – 80% of the maximum multiplied by 50% (Thr_50%Mean$_{5\text{-}80}$), Otsu's method (Thr_Otsu), and the curve-fitting method (Thr_Slope). The methods were also applied in 23 COPD participants.

Results: Thr_Slope provided the most accurate and robust measurements on non-ventilated volume as determined by Lin's concordance correlation ($\rho c = 0.988$), and it was the only method that had been unaffected by 'hot spot' vials. Thr_Slope produced significantly different measurements of non-ventilated volume compared to all other methods.

Conclusion: Thr_Slope is superior to existing threshold methods, and so, it is ideal for human VSPECT/CT studies.

2.2 Introduction

Airways diseases are characterised by severe airway narrowing and closure. With ventilation imaging, these airways can appear as an apparent absence of ventilation in lung regions. These regions of apparently absent ventilation are of interest because they represent airways and lung tissue that are most severely affected by disease, and they are potentially targets for tissue sampling and for treatment. A common 3-dimensional imaging method is single-photon emission computed tomography (SPECT), which generally uses ^{99m}Tc-labeled Technegas as its agent. SPECT has been used in respiratory research to investigate ventilation and perfusion, in asthma, chronic obstructive pulmonary disease (COPD) and COVID-19 (1-4). Fusion of SPECT with computed tomography images (SPECT/CT) also allows correlation of function with structural information. Accurate separation of ventilation versus non-ventilation requires accurate classification of voxels into presence or absence of radioactivity. There are several available methods to distinguish ventilated and non-ventilated lung regions on ventilation SPECT (VSPECT) images. However, no studies have assessed the accuracy of methods to measure ^{99m}Tc activity with physical lung phantom models of known volumes with and without ^{99m}Tc.

Distinguishing ventilated from non-ventilated voxel activity requires the use of a cut-off value to the image data, where voxels below the cut-off become classified as non-ventilation. This technique is referred to as a threshold method. It is important for a threshold method to be both accurate and robust, especially for images with highly variable data. Regarding VSPECT/CT, the image data is indeed often highly variable due to heterogeneous ventilation in subjects with asthma or COPD (5, 6).

Poor or absent ventilation results in large proportions of voxels with low activity i.e., ‘noise’. Conversely, voxels with extraordinarily high activity or ‘hot spots’ could also be present. These ‘hot spots’ are caused by deposits of Technegas at locations with uneven ventilation or severe airway narrowing (7). If ventilation and non-ventilation is to be accurately determined, then ideally the threshold method should be accurate and robust against non-ventilation and ‘hot spots’.

Traditionally, the presence of ventilation in VSPECT has been determined as an arbitrary percentage of the maximum activity, using thresholds values that can range from 10-70% of maximum activity (6, 8, 9). There is no consensus on the most optimal percentage of maximum activity threshold but Nagao et al. recommended a threshold no less than 15% of maximum activity (10). However, when the image data and hence maximum activity is highly variable within subjects, this method will almost certainly be inaccurate. Because of this problem, Farrow et al. developed a VSPECT/CT threshold method that was based on the average activity calculated from all voxels in the ‘middle part’ of the count range (counts between 5% and 80% of the maximum) (11). They reasoned that a threshold based on a large proportion of the lung pixels, rather than a single pixel, would be more accurate for heterogeneous ventilation scans in patients with asthma. Furthermore, they determined that multiplying that average activity value by 50%, resulted in unbiased measurements of ventilation volumes, when compared with the ‘gold standard’ lung function measurements.

The method of Otsu is also potentially suitable for VSPECT image analysis. It has been applied to picture segmentation e.g., separating water versus land in aerial photos or separating foreground objects from the bland background. It is an iterative statistical method which assumes that the background will be bland or relatively homogenous, compared with the foreground or object(s) of interest (12). Therefore, the method finds a threshold that splits the image dataset into two classes, background and foreground, where intraclass variance is minimal and interclass variance is maximal. It should be ideal for VSPECT image data, where non-ventilated lung (which is bland and has low variance), from ventilated lung (which would have a higher variance). Indeed, Otsu's method had superior performance in images with heterogeneous data when compared to other popular automatic threshold methods (8). The threshold is therefore based on the low, background count rates, rather than the commonly used percent of maximum count, and can also be automated.

In addition to these existing threshold methods, a new threshold could also be developed. Instead of basing the threshold on a variable data point such as the maximum activity value, which would be particularly sensitive to 'hot spots' and random variation, the method may choose a specific data point on a fitted curve of activity distribution. This could identify a consistent point across different VSPECT images regardless of ventilation heterogeneity i.e. random variation.

Our primary aim was to determine the most accurate threshold method for distinguishing ventilated from non-ventilated lung regions. Therefore, we used lung

phantom models of known volumes with and without varying concentrations of ^{99m}Tc solution to simulate non-ventilation, ventilation heterogeneity, and 'hot spots'. Four threshold methods were used: percent of maximum count, the method of Farrow et al. (based on 'middle range' counts), Otsu's method (based on low counts), and a novel method using curve-fitting of the voxel activity distribution. We compared the accuracy of each threshold method in estimating volumes with and without ^{99m}Tc solution. We had also applied all four threshold methods in COPD patients to determine whether they produced significantly different measurements of non-ventilated volume.

2.3 Methods

2.3.1 Lung phantom models

10 lung phantom models were constructed from 10 plastic containers of various sizes, which ranged from 0.4 to 5.1 L. True volumes of each lung phantom container were calculated from their measured dimensions.

The lung phantom containers had been tightly packed with foam beads, after which a premixed ^{99m}Tc solution, consisting of water and ^{99m}Tc eluted in saline, of a set concentration was poured. The phantom was thus mostly air contained within the foam beads, which were surrounded by water, thereby approximating the density of human lungs. 3 different concentrations of ^{99m}Tc solutions were used to simulate different levels of ^{99m}Tc activity observed in human studies. 4 lung phantoms had a

^{99m}Tc concentration of 0.04 mBq/mL; 3 lung phantoms had a concentration of 0.06 mBq/mL; the remaining 3 lung phantoms had a concentration of 0.08 mBq/mL.

Non-ventilated lung was simulated by inserting 1 – 2 smaller plastic containers, ranging from 0.07 – 2.5 L in size, into 8 out of the 10 lung phantoms. These had been filled with foam beads, but the spaces were filled with non-radioactive water, thus simulating non-ventilated lung regions. The volumes of each lung phantom container and their non-ventilated container(s) and ^{99m}Tc concentrations are displayed in Table 1.

'Hot spots' due to high, localised Technegas deposition, were simulated with 7.6 mL vials, filled with foam beads. They were filled with 0.18, 0.24, or 0.30 mBq/mL solutions of ^{99m}Tc which, given their high concentrations compared with the concentrations that filled the phantoms, would appear as localised 'hot spots'. These vials were placed on the exterior of all lung phantoms so that the lung phantoms could be analysed with and without 'hot spots'.

The protocol for the preparation of the ^{99m}Tc solutions consisted of the following. On the day of the scan, 4 doses of ^{99m}Tc, 1 mL in volume, were dispensed from a molybdenum-99 generator. The radioactivity of the 4 doses were 224, 204, 120, and 60 mBq. Fo the ^{99m}Tc solution concentration of 0.04 mBq/mL, the 204 mBq dose was mixed into a container with 3400 mL of water. For 0.06 mBq/mL, the 120 mBq dose was mixed into a container with 2000 mL of water. For 0.08 mBq/mL, the 224 mBq dose was mixed into a container with 2800 mL of water. These solutions were then

injected into their respective lung phantoms, which already contained ‘non-ventilated’ plastic containers with only water. For the ‘hot spot’ vials, the 60 mBq dose was initially mixed into a container with 59 mL of water to create a ^{99m}Tc solution concentration of 1 mBq/mL. For the 0.18 mBq/mL vial, 3.2 mL of 1 mBq/mL solution was mixed into a container with 14.8 mL of water. For the 0.24 mBq/mL vials, 4.3 mL of 1 mBq/mL solution was mixed into a container with 13.7 mL of water. For the 0.30 mBq/mL vials, 5.4 mL of 1 mBq/mL solution was mixed into a container with 12.6 mL of water. These solutions were then injected into their respective ‘hot spot’ vials. The timing from the initial preparation of the 4 ^{99m}Tc doses to the final scan was kept within 5 hours. The varying concentrations and therefore activities of the ^{99m}Tc solutions should not have changed radioactive decay characteristics of the tracer agent.

The lung phantoms and ‘hot spots’ were set up in 2 different configurations (Figure 1). 4 phantoms had ‘hot spot’ vials attached directly to the exterior (Figure 1A), and the remaining 6 phantoms were separated from ‘hot spot’ vials (Figure 1B). These 2 configurations simulated the presence of ‘hot spots’ near ventilated and non-ventilated lung. As shown in Figure 1, the ‘true’ ventilated volume ($Vent_{Vol}$) of the phantom which contained ^{99m}Tc was thus:

Container volume + ‘hot spot’ vial – volume of internal container(s) with no ^{99m}Tc

The ‘true’ non-ventilated volume ($Vent_{Non}$) was simply the volume of the internal non-radioactive container(s).

Table 1: Technetium-99m concentrations and true measurements of total volume, ventilated volume ($Vent_{Vol}$), and non-ventilated volume ($Vent_{Non}$).

Phantom lung #	Total volume (L)	$Vent_{Vol}$ (L)	$Vent_{Non}$ (L)	Concentration (mBq/mL)
1	5.13	4.34	0.79	0.04
2	4.44	2.57	1.79	0.04
3	1.25	1.00	0.25	0.04
4	0.41	0.39	0	0.04
5	5.13	2.66	2.47	0.06
6	1.38	1.38	0	0.06
7	0.66	0.45	0.21	0.06
8	5.13	3.16	1.98	0.08
9	2.86	2.49	0.37	0.08
10	0.93	0.86	0.08	0.08

L = litre; mL = millilitre; mBq = millibecquerel

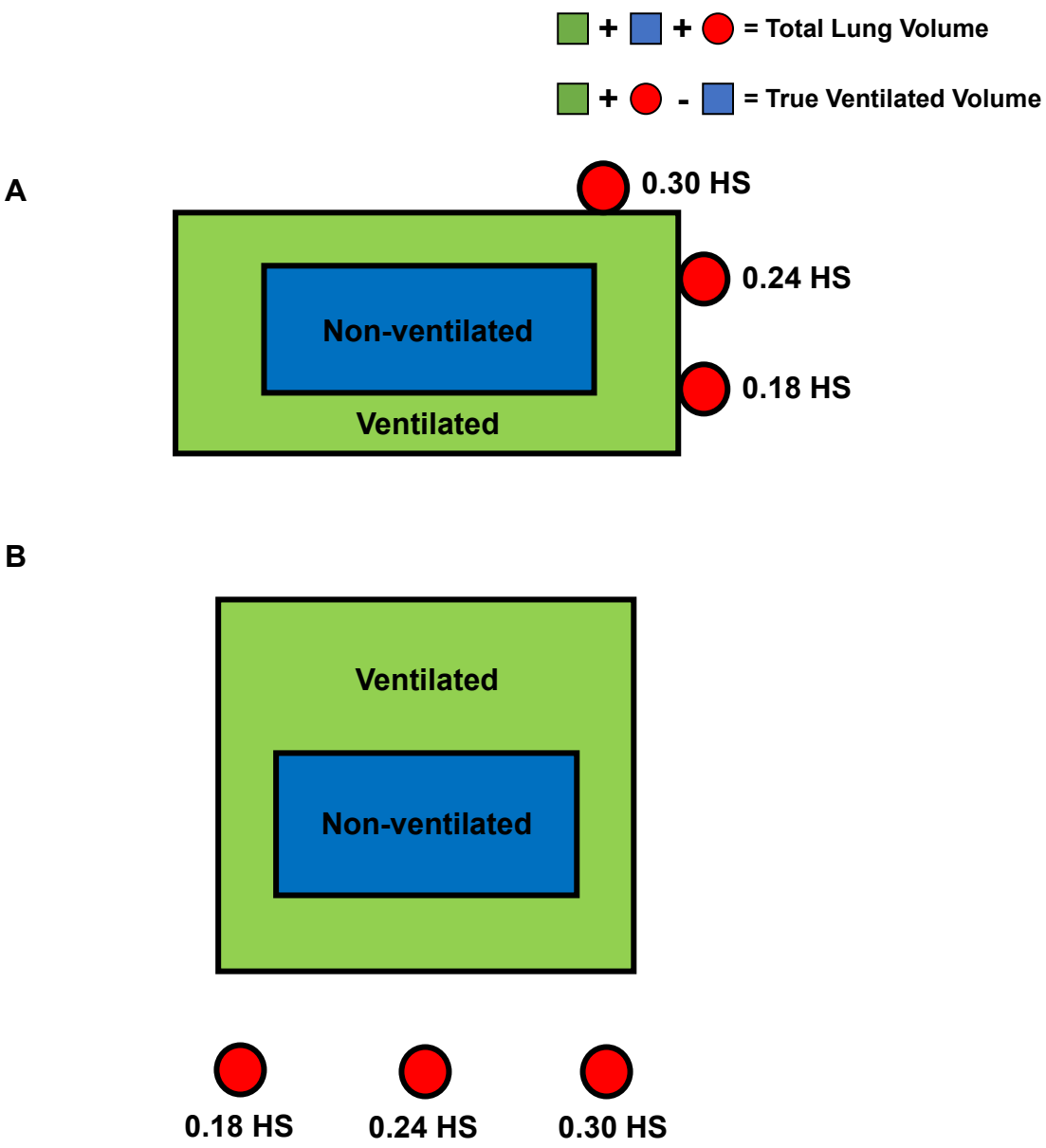


Figure 1: Configurations of lung pahntoms with simulated hot spots. Representation of lung phantom with vials attached to the exterior of the containing simulating 'hot spots' of 0.18 mBq/mL (0.18 HS), 0.24 mBq/mL (0.24 HS), and 0.30 mBq/mL (0.30 HS) (A). Lung phantom with unattached 'hot spot' vials (B).

2.3.2 COPD participants

23 participants with physician diagnosed COPD (13 men, 10 women) were recruited from the Department of Respiratory Medicine at Royal North Shore Hospital. The inclusion criteria were as follows: 18 – 80 years old, physician diagnosed COPD, and a smoking history of at least 10 pack years. Exclusion criteria were other active or chronic respiratory diseases, history of lung surgery, history of chronic kidney disease, significant cardiac disease, intensive care unit admissions in the last 12 months, and significant respiratory infection or documented exacerbation within the previous 6 weeks. All participants provided written, informed consent. The study was approved by the local Human Research Ethics Committee (Northern Sydney Local Health District, RESP/18/198).

For this study, a single visit was required. Prior to attending the visit, participants had withheld short-acting bronchodilators for 6 hours and LABA and/or LAMA medication for 24 hours.

2.3.3 VSPECT/CT imaging

VSPECT/CT imaging was conducted at the Department of Nuclear Medicine, Royal North Shore Hospital, using a Siemens Symbia T16 SPECT/CT system. To acquire the VSPECT/CT scans from COPD participants, the participants inhaled 500 – 700 mL of Technegas from functional residual capacity (FRC) at approximately 0.5 – 1 L/sec in a seated, upright position. The volume and flow rate of each inhalation was monitored with a MGC Diagnostics CPFS/D USB spirometer and MGC Breeze Suite interface (v. 8.6.0.56, MGC Diagnostics Corporation, Saint Paul). Two – four

inhalations were generally taken to achieve the required radioactivity of approximately 1.5 – 2.0 kilocounts/s. Approximately 40 mBq of Technegas was inhaled. For accurate VSPECT/CT registration, contrast bead markers, approximately 1 mm in diameter, were attached to the suprasternal notch, xiphisternum, and 12th ribs.

VSPECT and CT scans were acquired with a 128 x 128 matrix and 512 x 512 matrix respectively. VSPECT acquisitions employed the same settings used in previous human studies (11, 13, 14) of 60 stops x2 projections (total 120 projections), 15 seconds per stop, non-circular clockwise orbit and continuous acquisition). Low dose CT scans were acquired (30 mA, 110 kVp, pitch 1.5, slice thickness 3 mm). The count rates from each phantom also reproduced the activity seen in our previous human studies of at least 1.5 kilocounts/s. Four VSPECT/CT scans were needed to image all 10 lung phantoms. Prior to scanning, the count rate of the lung phantoms were measured and the scan times were adjusted for 1.8 – 2.0 counts/sec.

2.3.4 Imaging reconstruction and registration

Using 128 slices, VSPECT images were reconstructed with an ordered subset expectation maximization (OSEM) Siemens Flash 3D algorithm, CT-based attenuation correction, and a Gaussian filter. CT image reconstruction was completed with a 512 x 512 matrix and OSEM Siemens Flash 3D algorithm. Both VSPECT and CT images were converted to Digital Imaging and Communication in Medicine (DICOM) file format.

VSPECT scans had initially been registered to CT scans by using the known, fixed spatial relationship between the VSPECT and CT scanners. However, more accurate registration was performed using a HERMES (Nuclear Diagnostics, Stockholm, Sweden) workstation. Due to the disparity of matrix sizes between the VSPECT and CT images, the smaller 128 x 128 matrix of VSPECT was increased to 512 x 512, while preserving the original counts. Following this, registration of the lung phantoms was manually performed with HERMES's Multimodality software package (Nuclear Diagnostics) by visually confirming the correct alignment of the edges of the radioactive volumes of the lung phantom, with the edges of the containers on CT. Therefore, the voxel width and height and slice thickness of the final VSPECT and CT images were approximately 0.977 mm, 0.977 mm and 3 mm, respectively. As noted previously, the contrast bead markers were used to aid registration of the human VSPECT and CT images.

2.3.5 Imaging analyses

All imaging analyses, including the extraction of histogram VSPECT data, was performed with Fiji (National Institutes of Health, United States of America). Outlines of the phantom lungs, non-ventilation, and hot spots were manually defined from the CT images of the containers. From these outlines, a 'lung mask' was constructed, which included the total volume of each 'lung container' + external 'hot spot' vial. The volume of the 'CT derived lung mask' ($Mask_{CT}$) was calculated as total voxels x volume per voxel (0.003 mL). The $Mask_{CT}$ were then overlain onto the VSPECT images, and all voxel activity outside the mask were set to 0 (Figure 2).

Lung outlines from the human CT scans were defined differently. Instead of manual definition, a region growing algorithm (15), which had been implemented within a MATLAB script (R2019b, MathWorks, Natick) (16), was used. The script also produced binarized ‘lung masks’, similar to the lung phantoms. These ‘lung masks’ were then applied to the VSPECT images, setting all voxel activity outside the mask to 0. VSPECT voxel data within the mask were exported onto Microsoft Excel (2021, Microsoft, Redmond).

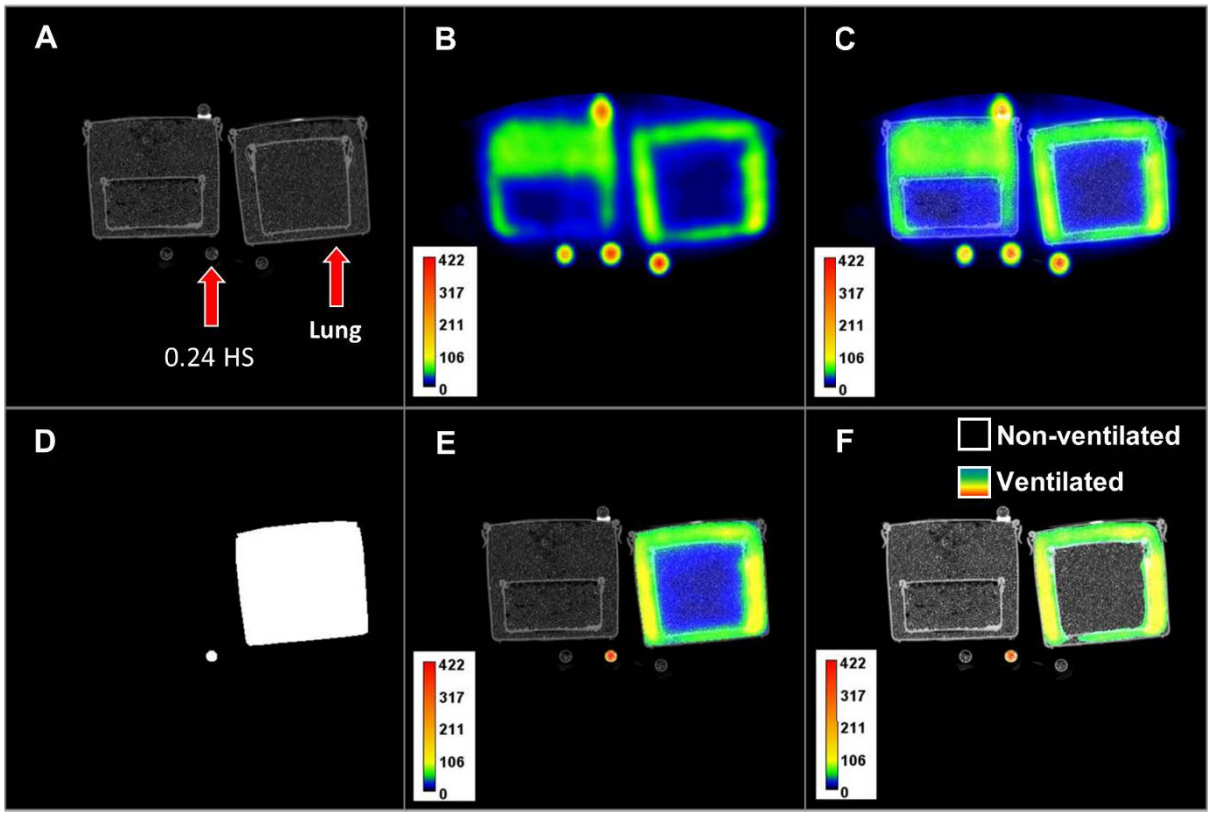


Figure 2: Imaging analysis process for lung phantom and hot spot vial. Images were modified to include the lung phantoms in 2 different hot spot configurations for visual purposes. (A) Computed tomography (CT) image of two lung phantoms and 'hot spots', arranged in two different configurations, with red arrows that indicate lung phantom and 'hot spot' selected for analysis; (B) single-photon emission computed tomography (SPECT) image of the same lung phantoms and 'hot spots'; (C) SPECT/CT fusion image with no CT mask applied; (D) CT masks of the selected lung phantom and 'hot spot'; (E) SPECT/CT fusion image with CT mask applied; (F) threshold applied to selected lung phantom and 'hot spot' vial. 0.24 HS = 0.24 mBq/mL 'hot spot' vial.

We calculated thresholds using 4 different methods to measure $Vent_{Vol}$ and $Vent_{Non}$.

1) “Thr_15%Max” threshold: The maximum count of the remaining voxels was determined and then multiplied by 15%. All voxels with values ≥ Thr_15%Max threshold were determined to contain ^{99m}Tc activity.

2) “Thr_50%$Mean_{5-80}$” threshold was calculated by the method of Farrow et al (11). The weighted average intensity of all voxels between 5 – 80% of the maximum was calculated. The threshold was determined as the average multiplied by 50%. All voxels with values ≥ Thr_50%$Mean_{5-80}$ threshold were determined as ventilated volume.

3) The “Thr_Otsu” threshold was calculated by the method of Otsu (12), using the threshold tool on Fiji. However, unlike other threshold methods, Thr_Otsu included the voxels with 0 activity outside of the lung phantom in its algorithm. The Fiji threshold tool cannot exclude voxel data. All voxels with values ≥ Thr_Otsu threshold were determined to contain ^{99m}Tc activity.

4) The curve-fitting threshold, “Thr_Slope”, was calculated by first obtaining the frequency for each voxel activity in the SPECT image. This was then followed by calculating the cumulative voxel frequency for each voxel activity, starting with the lowest activity, and this was expressed as a percentage of total voxel frequency. For example, voxels with an activity of 35 or lower and 80 or lower would constitute 60% and 90% of the total voxel frequency of a lung phantom, respectively. The

cumulative frequency was then plotted against voxel activity (Figure 3). From this plot, slopes of straight lines (cumulative frequency/voxel activity) between every sequential pair of data points ≥ 90% cumulative frequency (approximating the upper plateau) were calculated using the equation: slope = $(y_2 – y_1)/(x_2 – x_1)$. A specific slope cut-off value was then selected. The initial voxel activity ('x_2' in the slope equation) corresponding to a slope ≤ cut-off value was referred to as the 'slope point'. The voxel activity at 'slope point' was then multiplied by a fixed percentage to obtain the threshold voxel activity. All voxels with values ≥ threshold voxel activity were determined to contain ^{99m}Tc activity. To develop the most accurate version of Thr_Slope, a sensitivity analysis was conducted on slope cut-off values, which ranged from 0.001 – 1.000, and percentages of the 'slope point', ranging from 20 – 40%. The values that produced the most accurate measurements of $Vent_{Vol}$ and $Vent_{Non}$ compared to their corresponding true measurements from all lung phantoms, including 'hot spots' (Table 1) were used for Thr_Slope when it was assessed and compared to the previously noted threshold methods. The same 'slope point' and % of 'slope point' values would then be used for the human VSPECT/CT scans.

Threshold measured $Vent_{Vol}$ was calculated by multiplying the number of voxels ≥ the threshold x volume/voxel (0.003 mL). Conversely, threshold measured $Vent_{Non}$ was calculated by multiplying the number of voxels < the threshold x volume/voxel (0.003 mL).

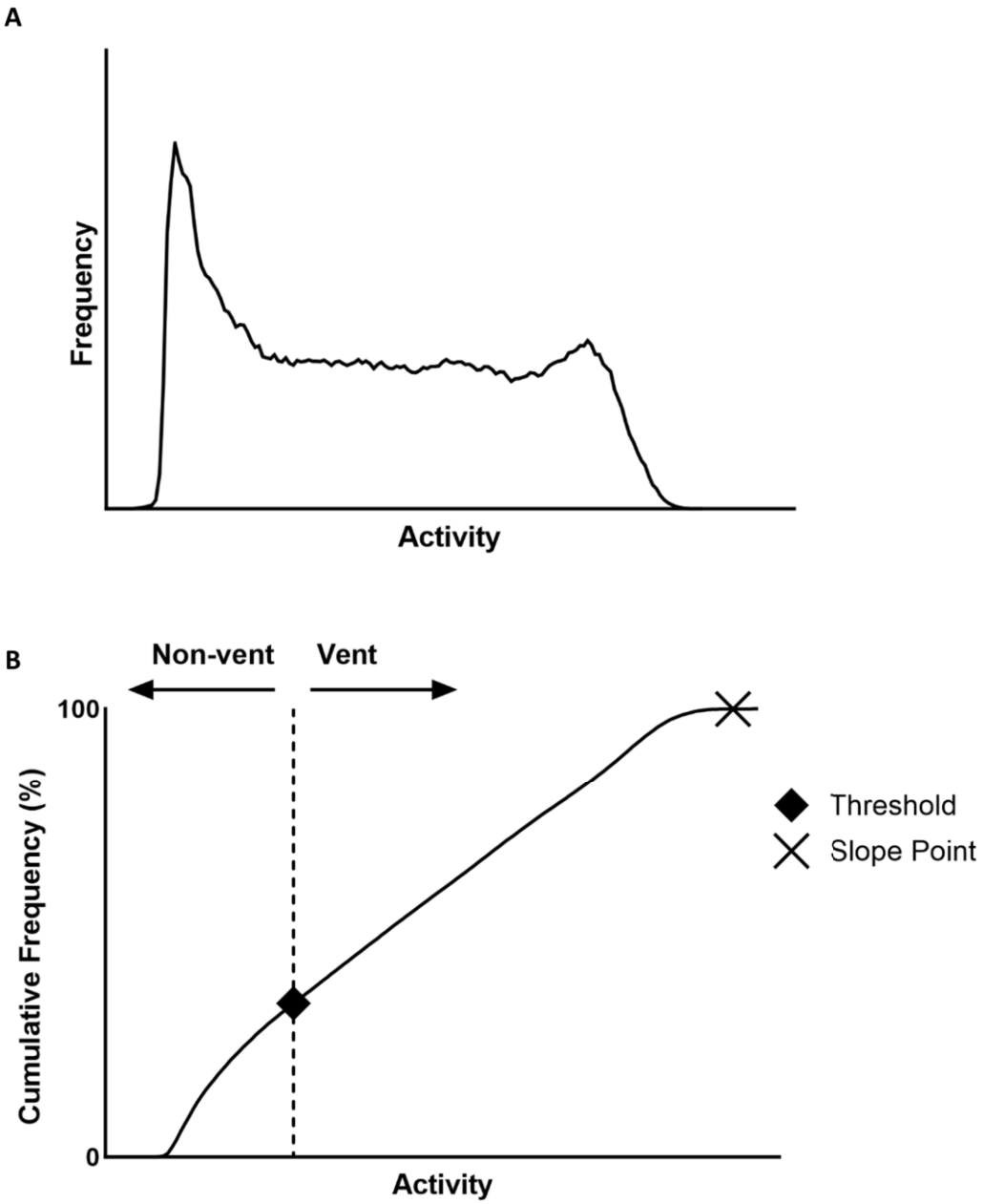


Figure 3: Voxel frequency – activity histogram from a masked lung phantom with no hot spot (A), and plot of cumulative frequency – activity from the same lung phantom with curve fitting threshold method (B). (B) This plot is an example of the curve-fitting threshold method that multiplied the 'slope point' voxel activity with ≤ 0.010 slope by 30%. The unit of a threshold is voxel activity. In this lung phantom, the threshold was 45 voxel activity, and it corresponded to 34% cumulative frequency. Different slope points and percentages were assessed to determine the most ideal threshold method; Vent = ventilated activity; Non-vent = non-ventilated activity.

2.3.6 Statistical analyses

GraphPad Prism version 10.0.2 was used to analyse data and generate graphs, except when assessing strength of agreement between true and threshold calculated $Vent_{Vol}$ and $Vent_{Non}$. This was done by calculating Lin's concordance correlation coefficient (ρ_c) (17) on IBM SPSS Statistics 27. The ρ_c syntax for SPSS had been sourced from Nass et al. (18). The equation for ρ_c was:

$$\rho_c = \frac{2\rho\sigma_x\sigma_y}{\sigma^2_x + \sigma^2_y + (\mu_x - \mu_y)}$$

- ρ_c = Lin's concordance correlation coefficient
- ρ = Pearson's correlation coefficient
- σ_x, σ_y = standard deviation of methods 'x' (threshold method) and 'y' (true measuements)
- σ^2_x, σ^2_y = variances of methods 'x' and 'y'
- μ_x, μ_y = means of methods 'x' and 'y'

To summarise, ρ_c is a measurement of the agreement between two sets of variables, typically between a 'gold standard' method and a 'new' method, and it evaluates how closely the variables from the new method cluster around a theoretical 'perfect' 45º line of concordance with the 'gold standard' method. In this study, the 'gold standard' were the true $Vent_{Vol}$ and $Vent_{Non}$ measurements as measured from the lung phantoms (Table 1), and the new methods were $Vent_{Vol}$ and $Vent_{Non}$ as measured by the threshold methods. A perfect agreement between the true and threshold measurements will produce $\rho_c = 1$. As recommended by McBride, the strength of agreement for ρ_c was determined as follows: < 0.90 indicated poor strength, 0.90 – 0.95 indicated moderate strength, 0.95 – 0.99 indicated substantial strength, and > 0.99 indicated near perfect strength (19). This form of agreement analysis was

performed to confirm the optimal values of ‘slope point’ and % of ‘slope point’ for Thr_Slope with lung phantom $Vent_{Vol}$ and $Vent_{Non}$ measurements. Additionally, the ρ_c of the three other threshold methods were also calculated. The same values were used in human VSPECT/CT scans. Furthermore, the accuracy of the four threshold methods were also assessed with ρ_c.

The errors in volume measurements of $Mask_{CT}$, $Vent_{Vol}$, and $Vent_{Non}$ were also assessed using methods of Bland-Altman. The effect of ‘hot spots’ on threshold values was examined using either repeat measures one-way ANOVA for parametric variables or Friedman test for nonparametric variables, with post-hoc Dunnett’s multiple comparisons test for both. Friedman’s tests compared $Vent_{Non}$ measurements from human participant VSPECT/CT scans. Data are presented as mean ± SD unless otherwise stated. Statistical significance was p-value < 0.05.

.

2.4 Results

2.4.1 Validation of parameters for curve-fitting threshold method

To determine the optimal curve-fitting parameters for the slope threshold method we compared the ρ_c between the true measurements of $Vent_{Vol}$ and $Vent_{Non}$ and Thr_Slope measured $Vent_{Vol}$ and $Vent_{Non}$ using different values for the curve fitting parameters (Tables 2 and 3). Compared to other slope values, using the slope value of 0.010 for 'slope point' possessed the greatest strengths of agreement, with near-perfect strength for $Vent_{Vol}$ ($\rho_c = 0.997$) and substantial strength for $Vent_{Non}$ ($\rho_c = 0.988$). Furthermore, multiplying the 0.010 'slope point' by 30% produced the most accurate $Vent_{Vol}$ and $Vent_{Non}$ measurements.

Table 2: Strengths of agreement analysis for 30% of slope 0.001 – 1.000 measurements of ventilated ($Vent_{Vol}$) and non-ventilated volume ($Vent_{Non}$).

	$Vent_{Vol}$ (L)	$Vent_{Non}$ (L)
30% of Slope 0.001	0.984	0.967
30% of Slope 0.010	**0.997**	**0.988**
30% of Slope 0.100	0.994	0.978
30% of Slope 1.000	0.978	0.927

Data presented as Lin's concordance correlation coefficient, with the strongest coefficients in bold.

Table 3: Strengths of agreement analysis for 20 – 40% of slope 0.010 measurements of ventilated ($Vent_{Vol}$) and non-ventilated volume ($Vent_{Non}$).

	$Vent_{Vol}$ (L)	**$Vent_{Non}$ (L)**
20% of Slope 0.010	0.953	0.837
25% of Slope 0.010	0.984	0.987
30% of Slope 0.010	**0.997**	**0.988**
35% of Slope 0.010	0.994	0.987
40% of Slope 0.010	0.970	0.955

Data presented as Lin's concordance correlation coefficient, with the strongest coefficients in bold.

2.4.2 CT and true volume comparison

The mean difference between $Mask_{CT}$ and true total volumes of the lung phantom containers and ‘hot spot’ vials was -0.001 ± 0.06 L (Figure 4). No significant size dependent error was detected ($p = 0.06$).

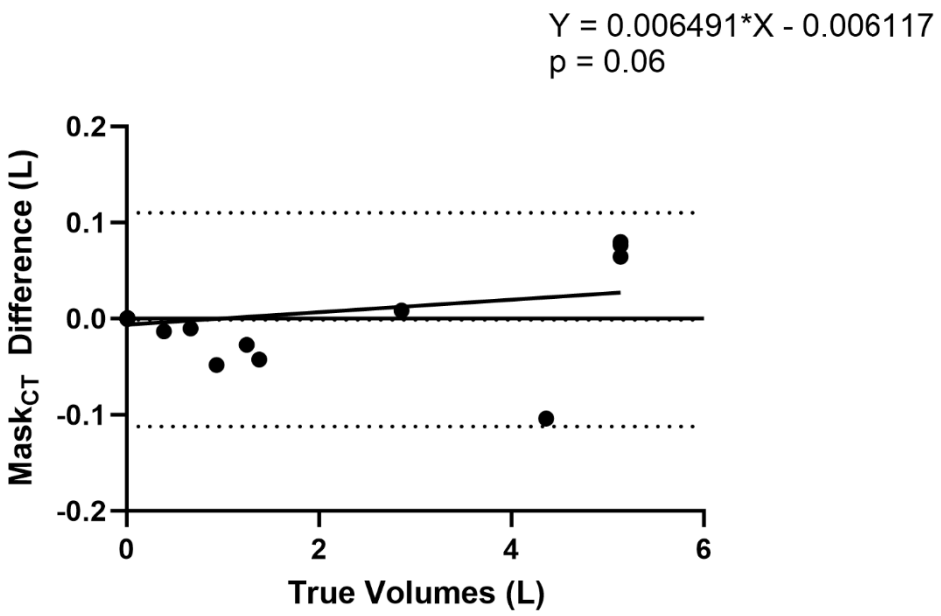


Figure 4: Bland-Altman plot of true and computed tomography mask ($Mask_{CT}$) measurements of lung phantoms and 'hot spot' vials volumes, expressed in litres (L). Data plotted as true volumes minus $Mask_{CT}$ volumes versus true volumes. Mean difference and 95% limits of agreement are displayed in dotted lines. No significant size dependent error was found (p-value = 0.06).

2.4.3 Comparison of accuracy of threshold methods for measuring ventilated and non-ventilated volumes

The ρ_c between true and threshold measured $Vent_{Vol}$ and $Vent_{Non}$ are displayed in Figures 5 and 6, respectively. For $Vent_{Vol}$, Thr_15%Max had poor strength of agreement (ρ_c = 0.874), both Thr_50%$Mean_{5-80}$ and Thr_Otsu had substantial strength of agreement (ρ_c = 0.969 and 0.994, respectively), and Thr_Slope had near perfect strength of agreement (ρ_c = 0.997). For $Vent_{Non}$, both Thr_15% and Thr_50%$Mean_{5-80}$ possessed poor strength of agreement (ρ_c = 0.774 and 0.897, respectively), while Thr_Otsu and Thr_Slope had substantial strength of agreement (ρ_c = 0.980 and 0.988 respectively). Overall, Thr_Slope provided the most accurate measurements for $Vent_{Vol}$ and $Vent_{Non}$.

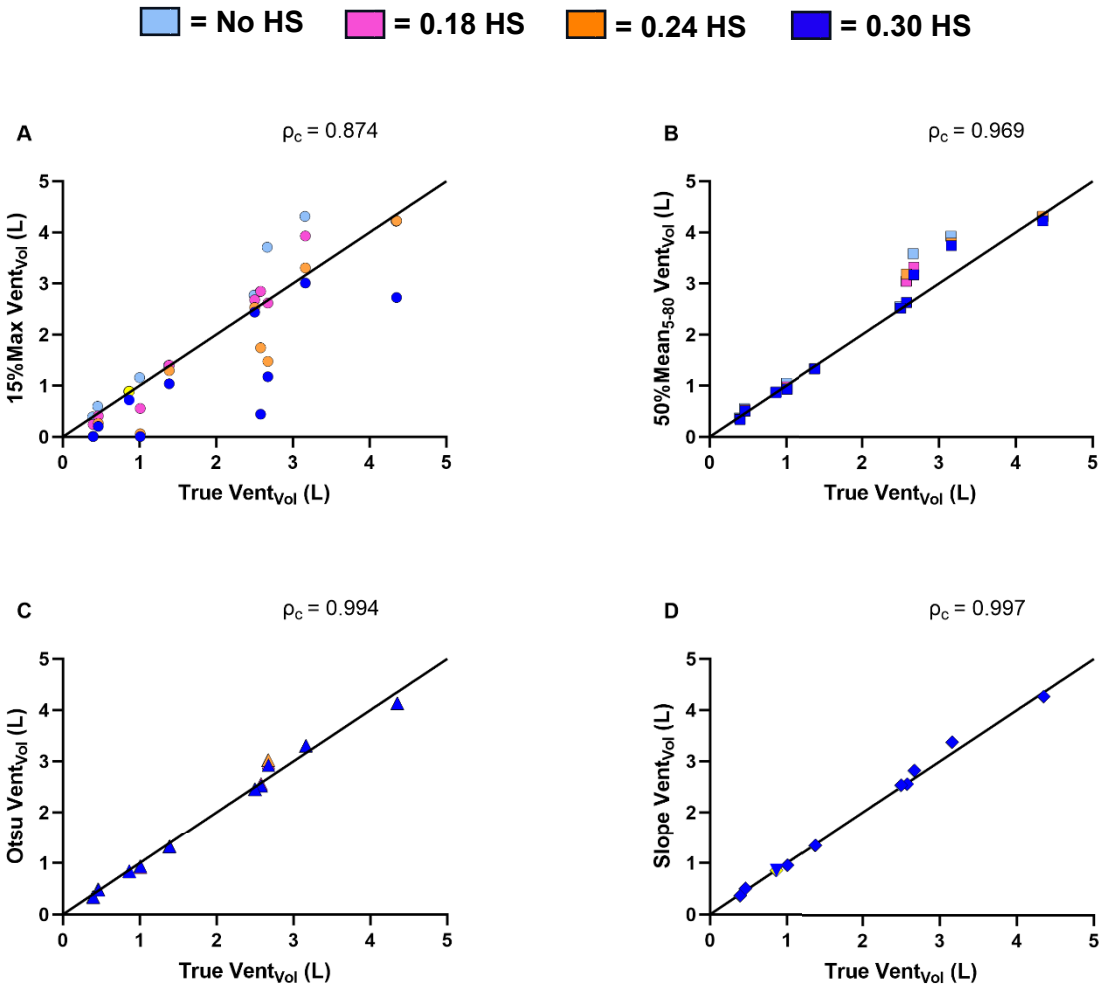


Figure 5: Relationships and Lin's concordance correlation coefficients (ρ_c) between true and threshold measurements of ventilated volume ($Vent_{Vol}$), expressed in litres (L). (A) 15% of maximum threshold method (15%Max); (B) 50% of the mean activity of 5 – 80% of maximum activity threshold method ($50\%Mean_{5-80}$); (C) Otsu's method (Otsu); (D) Slope threshold method (Slope). ρ_c = Lin's concordance correlation coefficient; No HS = no 'hot spot' included in analysis; 0.18 HS = 0.18 mBq/mL 'hot spot' vial included in analysis; 0.24 HS = 0.24 mBq/mL 'hot spot' vial included in analysis; 0.30 HS = 0.30 mBq/mL 'hot spot' vial included in analysis.

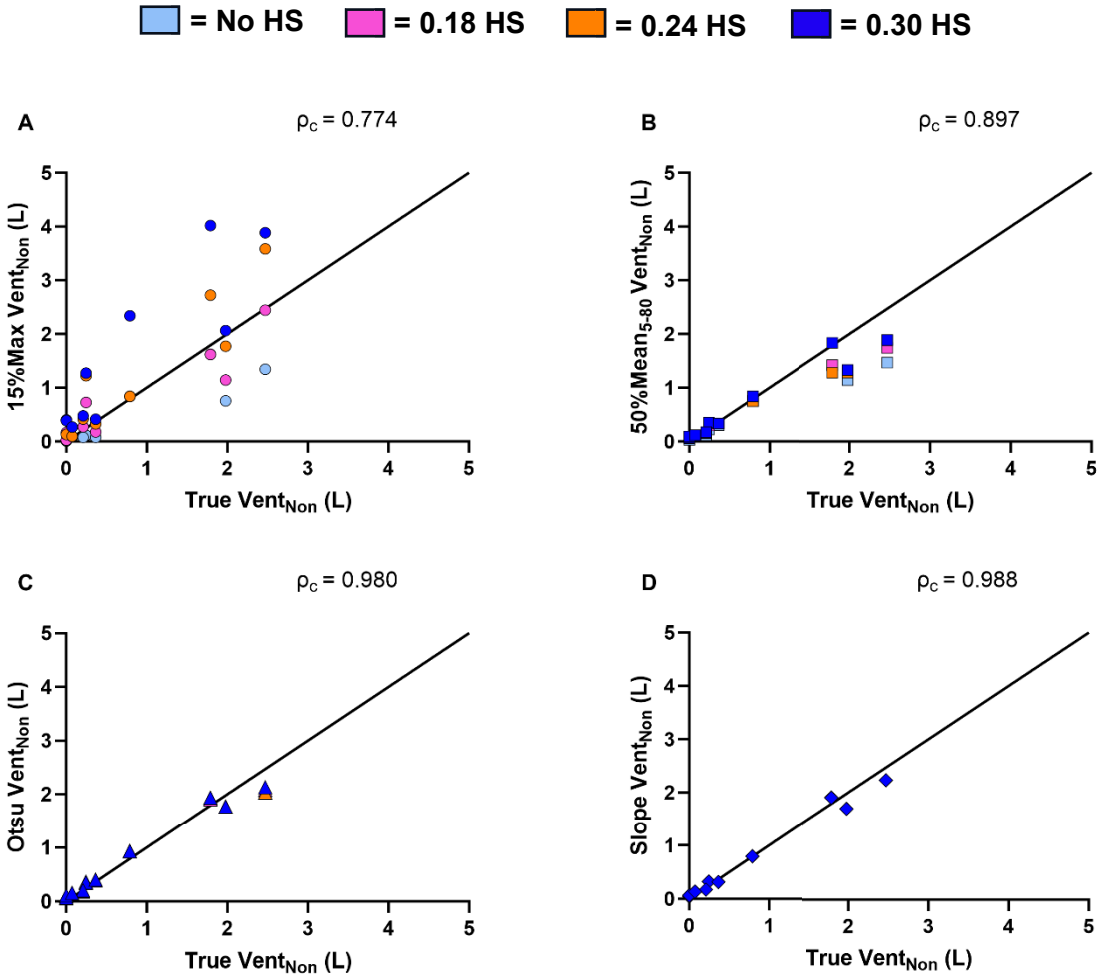


Figure 6: Relationships between true and threshold measurements of non-ventilated volume ($Vent_{Non}$), expressed in litres (L). (A) 15% of maximum threshold method (15%Max); (B) 50% of the mean activity of 5 – 80% of maximum activity threshold method ($50\%Mean_{5-80}$); (C) Otsu's method (Otsu); (D) Slope threshold method (Slope). ρ_c = Lin's concordance correlation coefficient; No HS = no 'hot spot' included in analysis; 0.18 HS = 0.18 mBq/mL 'hot spot' vial included in analysis; 0.24 HS = 0.24 mBq/mL 'hot spot' vial included in analysis; 0.30 HS = 0.30 mBq/mL 'hot spot' vial included in analysis.

2.4.4 Effect of non-ventilation on threshold methods

Bland-Altman plots of the differences between true and threshold measurements of $Vent_{Non}$ are shown in Figure 7. The mean difference ± SD between true $Vent_{Non}$ and Thr_15M, Thr_50%$Mean_{5-80}$, Thr_Otsu, and Thr_Slope $Vent_{Non}$ were -0.196 ± 0.653, 0.160 ± 0.316, -0.006 ± 0.168, 0.02 ± 0.129, respectively. Aside from Thr_15M ($p = 0.96$), significant size dependent errors were found in the other 3 threshold methods. Specifically, larger non-ventilated containers had been underestimated by Thr_50%$Mean_{5-80}$, Thr_Otsu, and Thr_Slope. According to the linear regression slopes for these 3 threshold methods, Thr_50%$Mean_{5-80}$ was most affected by true $Vent_{Non}$ volume ($m = 0.319$) and Thr_Slope was the least affected ($m = 0.094$).

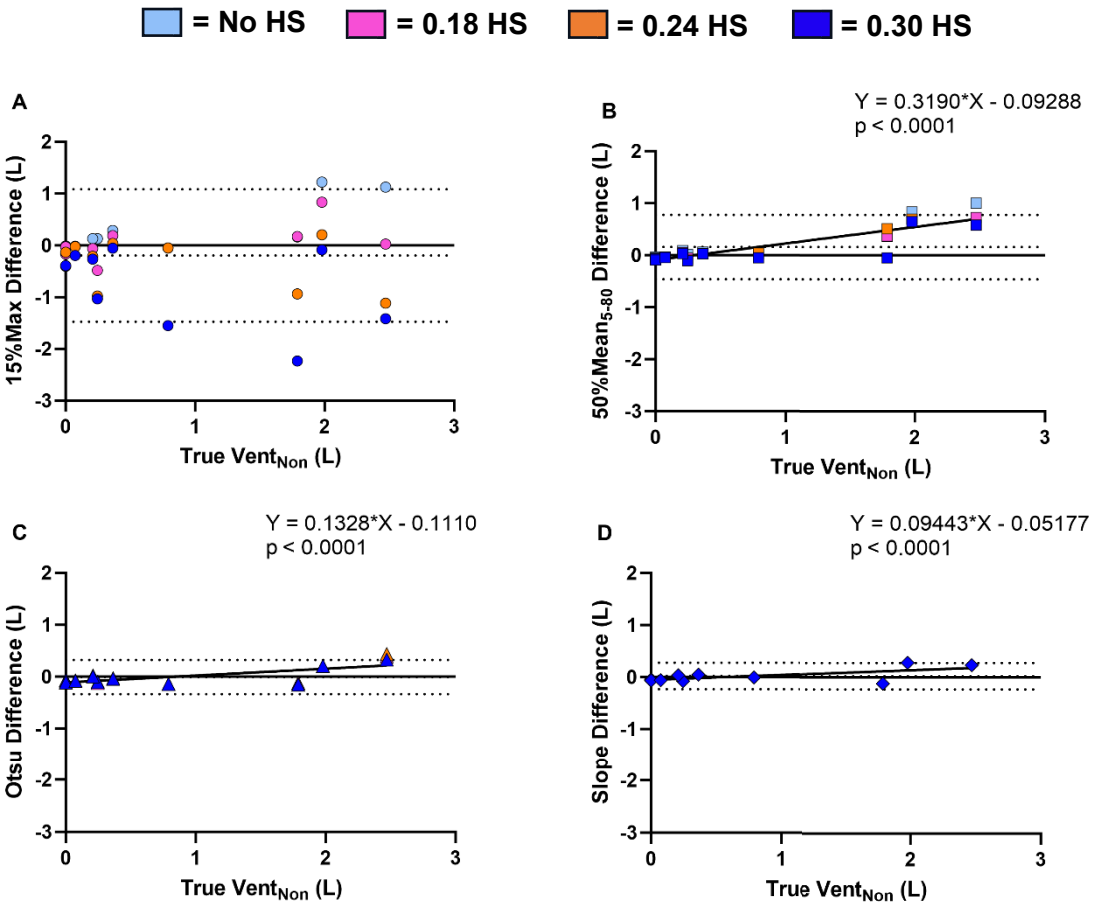


Figure 7: Bland-Altman plots of non-ventilated volume measurements from true and threshold methods. Data plotted as true minus threshold measured non-ventilated, expressed as absolute difference versus true non-ventilated volume. Mean difference and 95% limits of agreement shown in dotted lines. (A) 15% of maximum activity threshold method (15%Max); (B) 50% of the mean activity between 5-80% of maximum activity threshold method (50%Mean$_{5-80}$); (C) Otsu's method (Otsu); (D) slope threshold method. Significant size dependent errors were found for 50%Mean$_{5-80}$ ($p < 0.0001$), Otsu ($p < 0.0001$), and Slope ($p < 0.0001$), but not for 15%Max ($p = 0.96$).

2.4.5 Effect of 'hot spots' on thresholds

The threshold cut-off values from all methods are displayed in Figure 8. For Thr_15%Max, the thresholds for lung phantoms with a 0.24 mBq/mL or a 0.30 mBq/mL 'hot spot' vial were significantly increased ($p = 0.0097$ and < 0.0001, respectively) from the thresholds calculated from the lung phantoms with no 'hot spot' vials. Thr_50%Mean$_{5\text{-}80}$'s thresholds for lung phantoms with either a 0.18 mBq/mL or a 0.30 mBq/mL 'hot spot' vial were significantly increased ($p = 0.0097$ and < 0.0001, respectively) from the method's thresholds for the lung phantoms with no 'hot spot' vials. Thr_Otsu had calculated significantly increased threshold cut-off values for lung phantoms with a 0.30 mBq/mL 'hot spot' vial from lung phantoms with no 'hot spot' vials ($p = 0.03$). When using Thr_Slope, 'hot spot' vials had no significant effect on threshold cut-off values ($p = 0.34$).

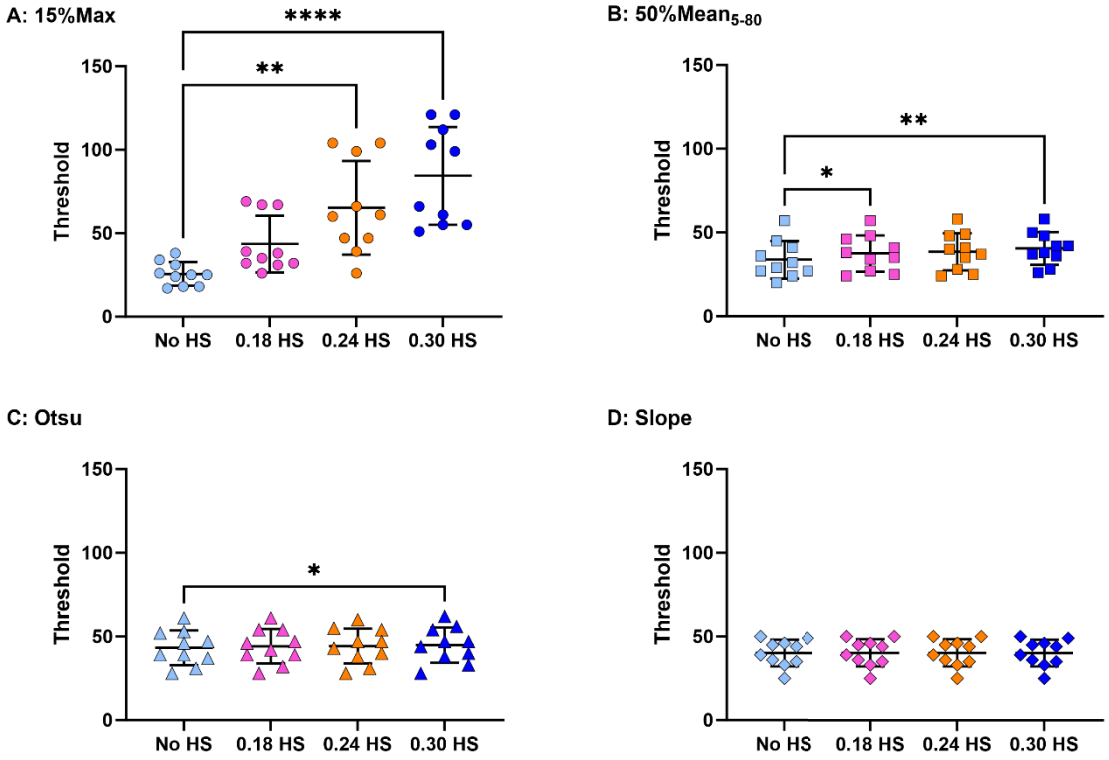


Figure 8: Threshold cut-off values in lung phantoms with no hot spots (No HS), with a 0.18 mBq/mL ^{99m}Tc 'hot spot' vial (0.18 HS), 0.24 mBq/mL ^{99m}Tc 'hot spot' vial (0.24 HS), and 0.30 mBq/mL ^{99m}Tc 'hot spot' vial (0.30 HS) calculated by different threshold methods. (A) Threshold cut-off values as calculated by 15% of maximum threshold method (15%Max); (B) threshold cut-off values as calculated by 50% of the mean activity between 5-80% of maximum activity threshold method (50%Mean$_{5-80}$); (C) threshold cut-off values as calculated by Otsu's method (Otsu); (D) threshold cut-off values as calculated by slope threshold method (Slope). Comparisons of threshold cut-off values for 15%Max were carried out with Friedman's test. For the other threshold methods, RM one-way ANOVA was used for comparisons of threshold cut-off values. Post-hoc analysis for all threshold methods was done with Dunnett's multiple comparisons test. *$p < 0.05$; ** $p < 0.01$; **** $p < 0.0001$.

2.4.6 Applying thresholds in human lungs

For all threshold methods, the same steps used in the lung phantoms were taken (Figures 9). Thus, the 'slope point' and % of 'slope point' for Thr_Slope were 0.01 and 30%, respectively For Thr_Slope, voxel frequency – activity histograms and cumulative frequency – activity plots with corresponding 'slope points' and thresholds for four lung phantoms (two with and two without hotspots) and four COPD participants are shown in Figures 10 and 11, respectively. $Vent_{Non}$ for human VSPECT/CT scans was expressed as a % of total CT lung volume. Although lung phantoms with 'hot spots' possessed a longer tail at the end of the cumulative frequency – activity plot than lung phantoms without 'hot spots', the 'slope points' were unaffected. The varying volumes of $Vent_{Vol}$/$Vent_{Non}$ volumes in the lung phantoms also seemed to have minimal effect on the 'slope points'. These two observations in the lung phantoms can also be seen in the human cumulative frequency – activity plots as well. Not only were the human plots similar in shape to the lung phantoms, the 'slope points' and thresholds appeared to be little affected.

The mean ± SD $Vent_{Non}$ as measured with Thr_Slope, Thr_Otsu, $Thr_Mean_{5\text{-}80}$, and Thr_15%Max were 49.29 ± 21.14, 39.27 ± 19.37, 31.00 ± 15.97, and 37.14 ± 26.06, respectively (Figure 12). There were significant differences in $Vent_{Non}$ as measured with Thr_Slope compared to all other threshold methods ($p = 0.0097$, < 0.0001, < 0.0001 for Thr_Otsu, $Thr_50\%Mean_5$, and Thr_15%Max, respectively). Thr_Otsu produced significantly different $Vent_{Non}$ measurements from $Thr_Mean_{5\text{-}80}$ ($p = 0.0097$) but not from Thr_15%Max. $Vent_{Non}$ measurements between $Thr_Mean_{5\text{-}80}$ and Thr_15%Max were not significantly different.

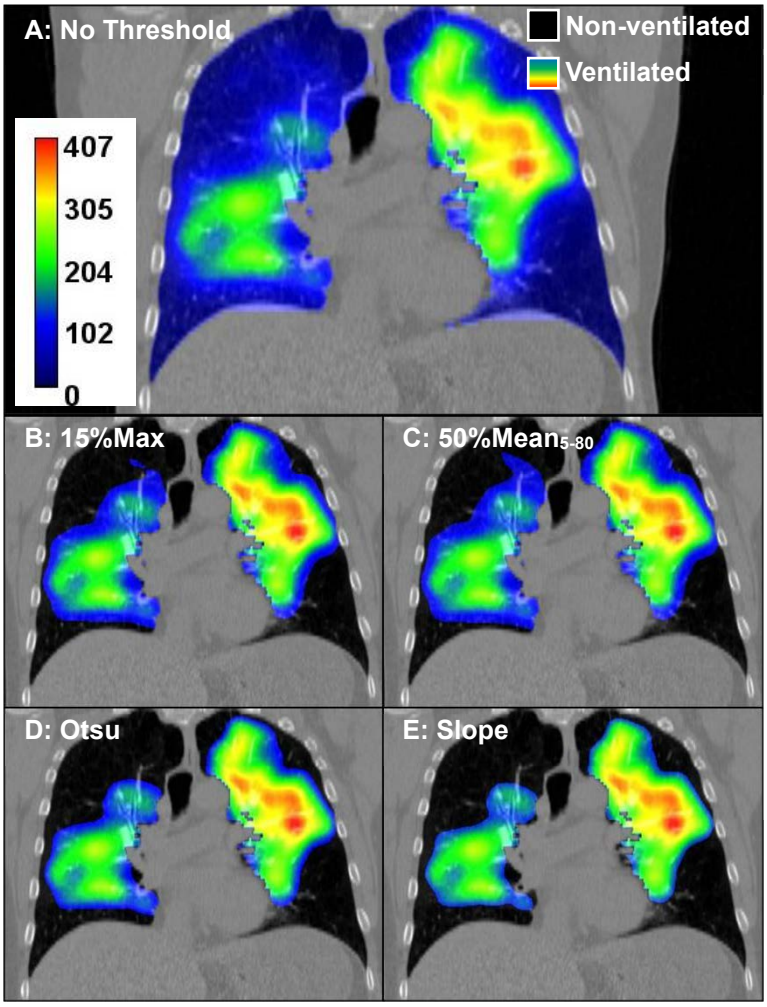


Figure 9: Masked single-photon emission tomography (SPECT)/computed tomography (CT) scan of a 59-year-old COPD participant with no applied threshold (A) and applied thresholds (B – E). Technegas activity is shown by the colour scale from dark blue (lowest activity) to red (highest activity). Non-ventilation is represented by the colour black; (B) SPECT/CT image with threshold calculated by 15% of maximum activity threshold method (15%Max); (C) SPECT/CT image with threshold calculated by 50% of the mean activity between 5-80% of maximum activity threshold method (50%Mean$_{5-80}$); (D) SPECT/CT image with threshold calculated by Otsu's method (Otsu); (E) SPECT/CT image with threshold calculated by slope threshold method (Slope).

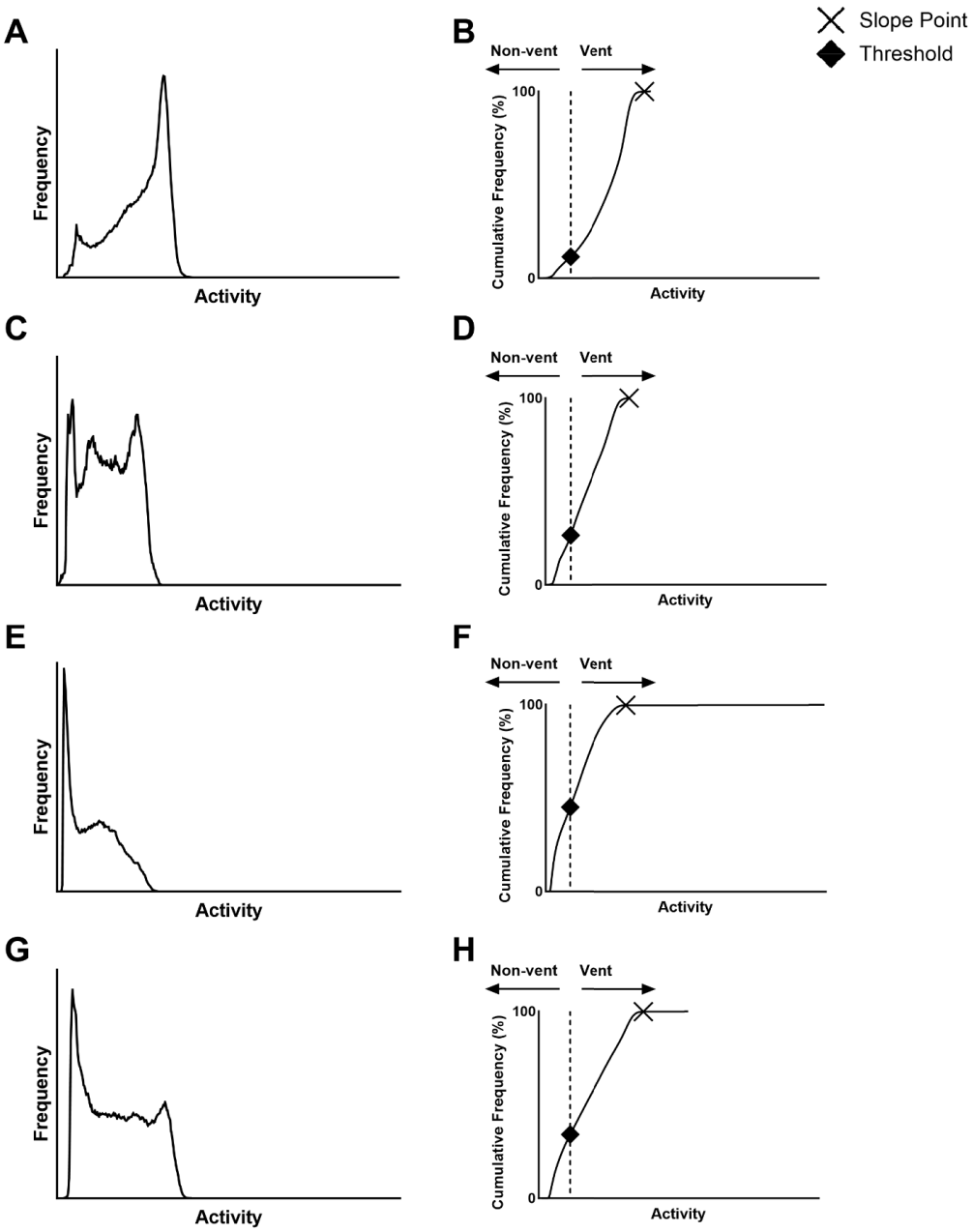


Figure 10: Voxel frequency – activity histograms from two lung phantoms without hot spots (A, C) and two lung phantoms with hot spots (E, G) and their respective cumulative frequency – activity plots (no hot spots: B, D; with hot spots: F, H). Both the 'slope points' and the thresholds, which was obtained by multiplying the voxel activity at the 'slope point' by 30%, are displayed on the cumulative frequency – activity plots. Vent = ventilated activity; Non-vent = non-ventilated activity.

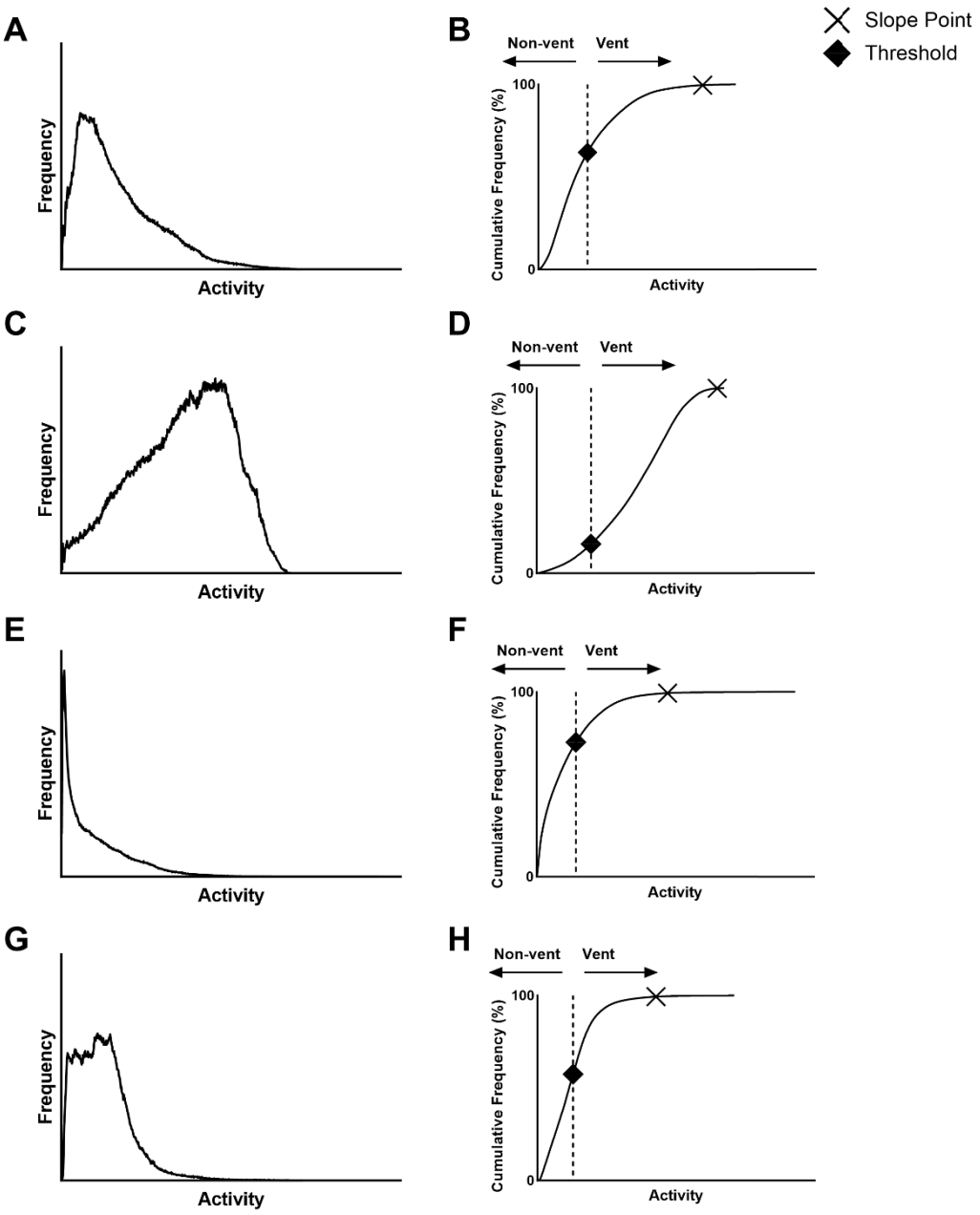


Figure 11: Voxel frequency – activity histograms from four COPD participants (A, C, E, G) and their respective cumulative frequency – activity plots (B, D, F, H). Both the 'slope points' and the thresholds, which was obtained by multiplying the voxel activity at the 'slope point' by 30%, are displayed on the cumulative frequency – activity plots. Vent = ventilated activity; Non-vent = non-ventilated activity.

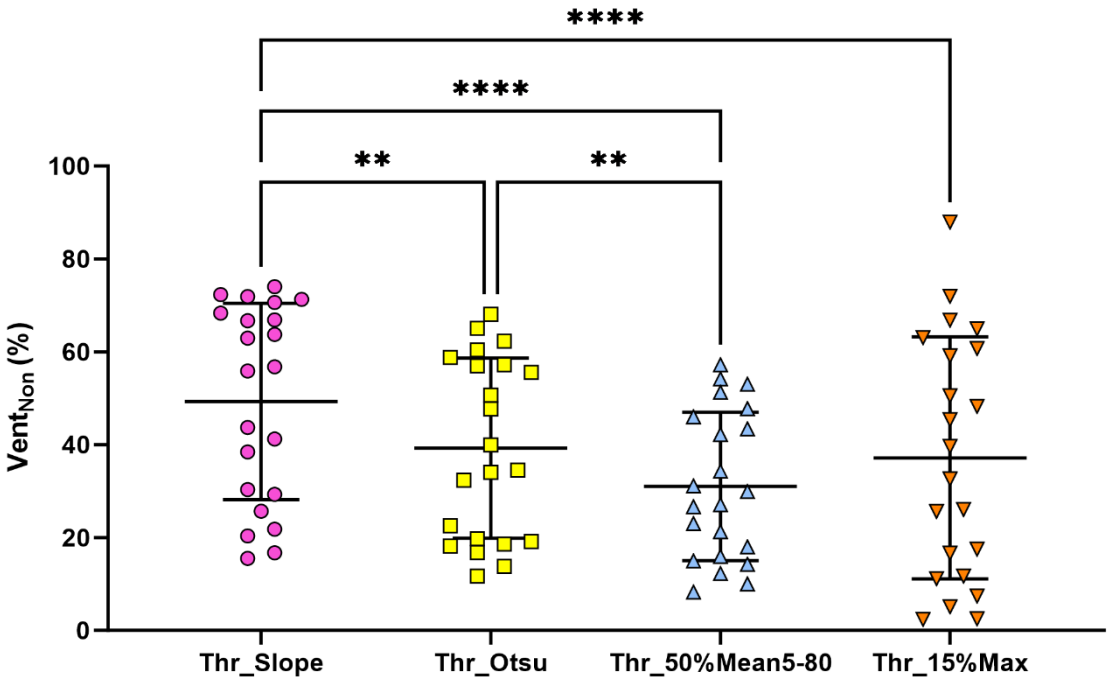


Figure 12: Non-ventilated volume ($Vent_{Non}$) as measured with slope threshold method (Thr_Slope), Otsu's method (Thr_Otsu), 50% of the mean activity between 5-80% of maximum activity threshold method ($Thr_50\%Mean_{5-80}$), and 15% of maximum threshold method (Thr_15%Max). Comparisons of $Vent_{Non}$ between threshold methods were carried out with Friedman's test. Post-hoc analysis was done with Dunnett's multiple comparisons test. ** $p < 0.01$; **** $p < 0.0001$.

2.5 Discussion

We are the first study to address the need for accurately defined volumes with and without ^{99m}Tc in SPECT by assessing 4 different threshold methods in physical lung phantoms. A novel analysis method utilising the slope of the cumulative frequency graph (Thr_Slope) was the most accurate method for measuring $Vent_{Vol}$ and $Vent_{Non}$, with the highest ρ_c values and strongest strengths of agreement, which were near-perfect for $Vent_{Vol}$ and substantial for $Vent_{Non}$. In contrast, defining ventilation based on a standard threshold of 15% of maximal intensity (Thr_15%) performed the worst with poor strength of agreement for both $Vent_{Vol}$ and $Vent_{Non}$. All threshold methods, excluding Thr_15%Max, significantly underestimated $Vent_{Non}$ in lung phantoms with larger non-ventilated containers. However, out of these 3 methods, $Thr_50\%Mean_{5-80}$ was the most affected by true $Vent_{Non}$ and Thr_Slope was the least affected. It was also observed that Thr_15%Max, $Thr_50\%Mean_{5-80}$, and Thr_Otsu had been significantly affected by ‘hot spots’, leading to significant increases in threshold cut-off values. Only Thr_Slope remained unaffected by 'hot spots’.

2.5.1 15% of maximum activity value threshold method

As noted previously, Thr_15%Max produced the most inaccurate measurements in this study. These results are generalisable to other percentage values (e.g. 5%, 20%, etc…) since any “fixed” percentage of a maximum activity value would still be susceptible to ‘hot spots’.

Although the ^{99m}Tc concentrations of the lung phantoms and 'hot spot' vials were controlled, the maximum activity value was nonetheless unpredictable and inconsistent. Various issues such as photon scatter from nearby 'hot spot' vials and other lung phantoms and the heterogeneous deposition of ^{99m}Tc solution in the foam beads meant that the maximum activity value was highly variable. Consequently, Thr_15%Max measurements of both $Vent_{Vol}$ and $Vent_{Non}$ were also variable, even in ideal conditions when 'hot spots' were excluded for analysis. Furthermore, as the threshold cut-off value was dictated solely by the maximum activity value, Thr_15%Max calculated significantly increased threshold cut-off values in lung phantoms with 'hot spots' vials. This method's overall poor accuracy, high variability, and susceptibility to 'hot spots' explains why no size dependent error was found.

In human VSPECT imaging, 'hot spots' from airway narrowing or uneven ventilation and variable activities from heterogeneous ^{99m}Tc deposition are common in disease such as asthma and COPD (5, 20). Naturally, the same issues responsible for poor accuracy and high variability for Thr_15%Max in this study would then be present in human scans as well. Indeed, difficulties with this method and other percentage values in human VSPECT studies have been reported. The same percentage of maximum activity threshold method that appeared to be suitable for one COPD study (6, 9) was observed by the authors to poorly delineate ventilated activity in a different COPD study (10). Lee et al. had similarly determined that a "fixed" percentage of maximum activity threshold used across different VSPECT images is unlikely to be viable for imaging analysis (21).

2.5.2 50% of the mean of 5 – 80% of maximum activity value threshold method

Instead of the traditional percentage of maximum activity threshold method, several studies have defined non-ventilated lung regions by multiplying the mean of 5 – 80% of the maximum activity value by 50% (1, 11, 14). This study has found two critical flaws to Thr_50%Mean$_{5\text{-}80}$, which were poor accuracy for measurements of Vent$_{Non}$ and susceptibility to 'hot spots'.

The inaccuracies in estimated Vent$_{Non}$ appears to arise from the abrupt underestimation of Vent$_{Non}$ in lung phantoms with ≥ 1.8 L true Vent$_{Non}$ (Figure 6B). The reason behind this phenomenon was the method's use of the average activity value to determine its threshold cut-off value. Greater proportions of voxels with low activity i.e., "noise" from large non-ventilated containers reduced the lung phantoms' average activity and consequently the threshold cut-off value. A low threshold cut-off value would incorrectly classify non-ventilated image data as Vent$_{Vol}$ and underestimate Vent$_{Non}$. If the mean activity between 5 – 80% of maximum activity was multiplied by a higher percentage than 50%, the threshold cut-off values would increase. Although this may produce more accurate Vent$_{Non}$ measurements in lung phantoms with large non-ventilated containers, the high threshold cut-off values would then result in poorer accuracy in lung phantoms with smaller non-ventilated containers i.e., larger average activities. Thus, both Thr_15%Max and Thr_50%Mean$_{5\text{-}80}$ share a common issue: multiplying an inconsistent value with a fixed percentage.

Farrow et al. (11) opted to rely on the average activity value with the reasoning that its threshold cut-off value should be based on voxel activities with the largest proportion instead of smaller ‘hot spots’. Theoretically, the threshold cut-off value would be representative of overall activity and robust against ‘hot spots’ that are common to diseases such as asthma (20). However, our study found that Thr_50%Mean$_{5\text{-}80}$ was nonetheless susceptible to ‘hot spots’. It calculated significantly increased threshold cut-off values in lung phantoms with a 0.18 mBq/mL and 0.30 mBq/mL ‘hot spot’ vial. This occurred because the range of activity when calculating the mean, in this case 5 – 80% of maximum activity, was still determined by the ‘hot spot’. As the ‘hot spots’ introduced larger maximum activities, the voxels within 5 – 80% of the maximum activity also changed, significantly increasing the threshold cut-off values.

Both flaws make Thr_50%Mean$_{5\text{-}80}$ unsuitable for VSPECT imaging analysis, particularly in diseases with poor or heterogeneous ventilation (22-24). In subjects with severe COPD, asthma, or lung cancer (25, 26), greater proportions of image noise from poorly ventilated lung regions would result in low threshold cut-off values and inaccurately defined non-ventilation. And like Thr_15%Max, the presence of ‘hot spots’ in human VSPECT scans can also affect the method’s accuracy.

2.5.3 Otsu's method

Thr_Otsu iteratively selects the threshold cut-off value with the greatest interclass variance between two classes of image data, which were non-ventilated and ventilated activity in our study. The reasoning behind this approach is that one class would generally be blander or more homogeneous and consequently distinct than the other. We find that Thr_Otsu to be superior at accurately measuring $Vent_{Vol}$ and $Vent_{Non}$ than existing SPECT threshold methods, Thr_15%Max and Thr_50%Mean[5-80].

The overall good performance of Thr_Otsu aligns with the findings from other threshold evaluation studies, which attest its high accuracy when measuring shape and uniformity in pictures (8, 27). However, Thr_Otsu relies on homogeneous backgrounds with a distinctly different foreground, meaning that this threshold method is particularly susceptible to heterogeneous backgrounds which cause a loss of the bimodal activity – frequency histogram (28). In images with non-bimodal distributions, Xu et al. observed that the threshold cut-off value for Thr_Otsu were biased towards the class with the larger variance (29). Therefore, increased background heterogeneity would reduce the threshold cut-off value from the optimal value, whereas a highly heterogeneous foreground would increase the threshold cut-off from the optimal value. Consistent with this, we report that the Otsu method the threshold cut-off values for lung phantoms with a 0.30 mBq/mL 'hot spot' vial were significantly increased (Figure 9C).

Nonetheless, Thr_Otsu managed to provide $Vent_{Vol}$ and $Vent_{Non}$ measurements with substantial strengths of agreement, and it was also more robust against 'hot spots' than either Thr_15%Max and Thr_50%$Mean_{5-80}$. Unlike Thr_50%$Mean_{6-80}$, the accuracy of Thr_Otsu was unaffected by the presence and volume of $Vent_{Non}$. This surprisingly accurate and robust performance of Thr_Otsu, despite its sensitivity to heterogeneity, is explained by how Fiji performs thresholding on default settings. As opposed to all other threshold methods in this study, which exclusively analysed the voxel data within the $Mask_{CT}$ of the lung phantoms, Thr_Otsu included all the voxels with 0 activity outside of the $Mask_{CT}$ in its algorithm. This ensured an ideal homogenous background with generally consistent variance for all lung phantoms, and thus, at least one class of activity possessed minimal intra-class variance. For ventilated activity, the small voxel frequencies of 'hot spot' vials meant that variance did not significantly increase until the activities of the 0.30 mBq/mL 'hot spot' vial was included. With multiple 'hot spots' or in potential lung phantom designs with greater image heterogeneity, which creates increased intra-class variance for $Vent_{Vol}$, it is likely that the accuracy of Thr_Otsu will be further affected by the greater variance of the $Vent_{Vol}$ class.

Unlike the other threshold methods in this study, Thr_Otsu is substantially more difficult to modify. We had used the base version of Thr_Otsu, which is readily available as one of the default threshold options in Fiji. Modifying this method's iterative thresholding that selects for maximum between-class variance through custom coding Fiji was beyond the scope of this study. However, like Thr_Slope, it is possible that with a more accurate and robust version of Thr_Otsu may be developed with if its iterative algorithm was optimised with sensitivity analysis.

Compared to existing VSPECT threshold methods, Thr_Otsu should undoubtedly be more accurate for human VSPECT imaging analysis, provided the algorithm replicates the default settings in Fiji. If the background outside of the lung borders is included for Thr_Otsu, this method is far less sensitive to noise and ‘hot spots’ that are common to diseased lungs.

2.5.4 Curve-fitting threshold method

Using the cumulative frequency – activity plot, Thr_Slope identified the ‘slope point’, which was the initial activity value ≥ 90% cumulative frequency with a specific slope cut-off value (cumulative frequency/voxel activity), and then multiplied it with a fixed percentage. We assessed different parameters for both the ‘slope point’ and percentage of ‘slope point’ with lung phantoms and confirmed the optimal values were a 0.010 slope and 30%, respectively.

Our results show Thr_Slope to be more accurate and robust at measuring $Vent_{Vol}$ and $Vent_{Non}$ than all other threshold methods in this study. It was the only method that had a near perfect strength of agreement for $Vent_{Vol}$. Furthermore, the threshold cut-off values remained uniquely unaffected when ‘hot spots’ vials were included for analysis. This can be primarily attributed to the identification of the ‘slope point’ as the basis for its threshold. Unlike maximum or average activity and class variance, which are susceptible to substantial changes from varying amounts of $Vent_{Vol}$ or ‘hot spots’ presence, the presence of a flat ‘tail’, with varying lengths, and its relative position on the cumulative frequency – activity plot remained consistent in both lung phantoms and human VSPECT/CT scans. All images, regardless of ‘hot spots’

presence or $Vent_{Vol}$ or $Vent_{Non}$ volumes, possessed a ‘tail’, in which voxel activity was very high and voxel frequency was very low. In a completely ‘ventilated’ lung phantom without ‘hot spots’, the onset of this tail (i.e. ‘slope point’) can be thought of as a precise border between the upper end of ‘ventilated’ activity, hence the minimal frequency, and the beginning of any ‘hot spot’ activity. Once ‘hot spots’ were included for analysis, the voxel activity of the ‘slope point’ did not significantly shift but the length of the tail increased instead due to larger voxel activities but still relatively minor voxel frequencies. $Vent_{Non}$ volume also failed to affect the ‘slope point’. This was expected as theoretically the upper end of ventilated activity has no relationship to the presence and volume of non-ventilated activity or noise.

The primary benefit of utilising sensitivity analysis with ρ_c was that it located the ‘slope point’ voxel activity on the cumulative frequency – activity plot that best aligned with the theoretical border between ‘ventilated’ and ‘hot spot’ activities. If the slope or ratio of vertical change was too high (e.g. 1.00), the ‘slope point’ preceded the onset of the tail, being instead placed within the upper end of ‘ventilated’ activity. Conversely, if the slope was too low (e.g. 0.001), the ‘slope point’ succeeded the onset of the tail as it was shifted towards ‘hot spot’ activity. The former had likely made the threshold sensitive to the heterogeneity of ventilated activity, and the latter was consequently sensitive to ‘hot spots’. Performing sensitivity analysis with either Thr_15%Max or $Thr_50\%Mean_{5\text{-}80}$ is unlikely to have resolved their accuracy issues. Maximum or mean voxel activities are inherently sensitive to ‘hot spots’ and ‘ventilated’ activity, respectively. Therefore, altering the percentages of maximum or mean values cannot desensitise either of these values to heterogeneity.

Regarding human VSPECT imaging analysis, the primary concern for accurate thresholds is data heterogeneity from issues such as poor ventilation or ‘hot spots’. As Thr_Slope is both highly accurate and insensitive to heterogeneity, even more so than Thr_Otsu in lung phantoms, it should be the ideal threshold method for analysing human VSPECT images. However, as Thr_Slope was optimised with only 10 lung phantoms that do not simulate the full spectrum of image heterogeneity found in human VSPECT/CT scans, it is possible that the most accurate ‘slope point’ and % of ‘slope point’ values for human scans are different to 0.010 slope and 30%, respectively. This can be explored in future studies with more complex lung phantom designs with greater image heterogeneity.

2.5.5 Threshold methods in human scans

Although we did not have a gold standard measure of true $Vent_{Non}$ in human VSPECT/CT images, there were some similar findings with the results from our lung phantoms. We observed no difficulties when applying Thr_Slope on human VSPECT images. Thr_Slope produced significantly different estimations of $Vent_{Non}$ from all other threshold methods. Like the lung phantoms, Thr_50%$Mean_{5\text{-}80}$ produced the smallest estimations of $Vent_{Non}$, which was expected as COPD participants tended to possess large lung regions of low activity voxels. Furthermore, Thr_Otsu calculated a significantly smaller $Vent_{Non}$ than Thr_Slope. This was consistent with the lung phantom results since Thr_Otsu was susceptible to increased noise and voxel activity heterogeneity.

2.5.6 Size dependent errors in threshold methods

Thr_50%Mean$_{5\text{-}80}$, Thr_Otsu, and Thr_Slope, had a size dependent error when measuring Vent$_{Non}$ (Figure 7). Thr_15%Max did not possess a size dependent error, but this was attributable to its very poor accuracy. The existence of the size dependent errors in threshold measurements of Vent$_{Non}$ can arise from two factors. One is a threshold method's sensitivity to increased proportions of low activity voxels, such as Thr_50%Mean$_{5\text{-}80}$. The second factor is photon scatter. True Vent$_{Non}$ of the non-ventilated contained included their exterior dimensions, such as the lid, handles, and outer plastic surface. However, photon scatter from the ventilated lung phantom and 'hot spots' resulted in ventilated activity around and within the thin 2 mm plastic exterior of the non-ventilated containers in the SPECT image. Therefore, SPECT images would appear to have "eroded" regions of non-ventilation and "dilated" ventilated regions when compared to CT images. Discrepancies between true Vent$_{Non}$ and SPECT Vent$_{Non}$ would increase in lung phantoms with larger non-ventilated containers. Since scatter is inherent to SPECT imaging, this error could not be completely remedied with a threshold method. But the size dependent error can be reduced in threshold methods that are less sensitive if not wholly insensitive to noise. In this study, we found Thr_Slope to have the smallest size dependent error.

2.5.7 Limitations

The primary limitation for this study was the design of the lung phantoms themselves. Our study opted for a conventional design by using plastic containers and polystyrene foam beads that were mixed with ^{99m}Tc solution. However, foam

beads have a higher density than either healthy or diseased lungs. Alternative lung phantom designs such as expanding polyurethane foam can better replicate healthy and diseased lung densities (30, 31). Another limitation related to the simple simulation of non-ventilation. For this study, the containers without any ^{99m}Tc solution acted as a broad surrogate for non-ventilated lung regions. However, in human lungs, poorly ventilated regions may still contain albeit markedly reduced depositions of ^{99m}Tc. Furthermore, as the lung phantoms were simply static containers of ^{99m}Tc solution, the effects of tidal breathing on motion blurring and regional ventilation on ^{99m}Tc delivery and deposition could not be replicated in this study.

Due to the labour-intensive process of preparing the ^{99m}Tc solutions and the lung phantoms, the time between the initial generation of the ^{99m}Tc doses and the final scan was approximately 5 hours. As the half-life for ^{99m}Tc is approximately 6 hours, there must have been substantial reduction in radioactivity, and the timing was not controlled. Compared to human VSPECT imaging, the time from Technegas generation to the scan was generally 15 minutes, and during inhalation, Technegas radioactivity was approximately 40 mBq. Whilst scan time for the lung phantoms was adjusted for 1.8 – 2.0 kilocounts/s, similar to human VSPECT/CT scanning, the substantial differences between human and lung phantom imaging in radioactivity at the time of scanning and the time from ^{99m}Tc generation to scanning were limitations in this study. It is possible that newer lung phantom designs that make use of expanding polyurethane foam may be prepared faster than conventional lung phantom designs, but this will need to be assessed. Another method for future lung phantom studies would be to dedicate only one or two lung phantoms for one scan

date. This should reduce the time between ^{99m}Tc generation and scanning to a minimum.

There was also another limitation related to lung phantom design, particularly the placement of the ‘hot spot’ vials. For convenience, all the ‘hot spot’ vials were all external to the lung phantoms (Figure 1). This allowed us to analyse the lung phantoms with and without direct ‘hot spot’ activity. However, this does not simulate human VSPECT/CT images as accurately as lung phantom designs with interior ‘hot spot’ vials. Interior ‘hot spot’ vials would have likely produced greater image heterogeneity, particularly from photon scatter contained entirely within the lung phantom mask, than external vials that emitted only partial photon scatter. Another limitation with the ‘hot spot’ vials were their unrealistic identical volumes. Larger ‘hot spots’ that introduce greater image heterogeneity and greater frequency of voxels with high activity were also not simulated. Finally, multiple ‘hot spots’ vials nor multiple lung phantom containers with varying ^{99m}Tc concentrations were not analysed in this study. Both should again introduce greater image heterogeneity and better simulate some human VSPECT/CT images. It is unknown how exactly greater image heterogeneity under these conditions would affect the threshold methods. We may presume that the accuracy issues with Thr_15%Max and Thr_50%Mean$_{5\text{-}80}$ would be exacerbated. Thr_Otsu should also be theoretically affected by greater image heterogeneity, as the method relies on the homogeneity of one class and distinct differences between the ventilated and non-ventilated classes of voxel activity. Future studies may explore how the ‘curve-fitting’ method may perform with more realistically simulated and more heterogenous lung phantoms.

2.5.8 Conclusion

In conclusion, current VSPECT/CT threshold methods such as Thr_15%Max or Thr_50%Mean$_{5\text{-}80}$ are demonstrably inadequate at classifying ventilated and non-ventilated volume in heterogeneously ventilated lungs. A new alternative method, Thr_Slope, can provide very accurate measurements, and it is generally robust against data heterogeneity in VSPECT/CT. This makes the novel threshold method developed in this study as an ideal analysis method for human VSPECT/CT imaging, particularly in patients with heterogenous ventilation.

2.6 References

1. Rutting S, Chapman DG, Thamrin C, Tang FSM, Dame Carroll JR, Bailey DL, Trifunovic M, Magnussen JS, et al. Effect of combination inhaled therapy on ventilation distribution measured by SPECT/CT imaging in uncontrolled asthma. J Appl Physiol (1985). 2021;131(2):621-9.
2. Jögi J, Ekberg M, Jonson B, Bozovic G, Bajc M. Ventilation/perfusion SPECT in chronic obstructive pulmonary disease: an evaluation by reference to symptoms, spirometric lung function and emphysema, as assessed with HRCT. Eur J Nucl Med Mol Imaging. 2011;38(7):1344-52.
3. Bajc M, Jonson B. Ventilation/Perfusion SPECT for Diagnosis of Pulmonary Embolism and Other Diseases. International Journal of Molecular Imaging. 2011;2011:682949.
4. Cobes N, Guernou M, Lussato D, Queneau M, Songy B, Bonardel G, Grellier JF. Ventilation/perfusion SPECT/CT findings in different lung lesions associated with COVID-19: a case series. Eur J Nucl Med Mol Imaging. 2020;47(10):2453-60.
5. Bajc M, Chen Y, Wang J, Li XY, Shen WM, Wang CZ, Huang H, Lindqvist A, et al. Identifying the heterogeneity of COPD by V/P SPECT: a new tool for improving the diagnosis of parenchymal defects and grading the severity of small airways disease. Int J Chron Obstruct Pulmon Dis. 2017;12:1579-87.
6. Satoh K, Tanabe M, Takahashi K, Kobayashi T, Nishiyama Y, Yamamoto Y, Honjo N, Sasaki M, et al. Assessment of technetium-99m Technegas scintigraphy for ventilatory impairment in pulmonary emphysema: comparison of planar and SPECT images. Ann Nucl Med. 1997;11(2):109-13.
7. Jobse BN, Rhem RG, McCurry CA, Wang IQ, Labiris NR. Imaging lung function in mice using SPECT/CT and per-voxel analysis. PLoS One. 2012;7(8):e42187.
8. Lee SU, Yoon Chung S, Park RH. A comparative performance study of several global thresholding techniques for segmentation. Computer Vision, Graphics, and Image Processing. 1990;52(2):171-90.
9. Zhang X, Hirano H, Yamamoto K, Kusaka Y, Sugimoto K, Kimoto T, Hayashi N, Ishii Y. Technegas ventilation SPECT for evaluating silicosis in comparison with computed tomography. Ann Nucl Med. 1996;10(2):165-70.
10. Nagao M, Murase K, Yasuhara Y, Ikezoe J. Quantitative analysis of pulmonary emphysema: three-dimensional fractal analysis of single-photon emission computed tomography images obtained with a carbon particle radioaerosol. AJR Am J Roentgenol. 1998;171(6):1657-63.
11. Farrow CE, Salome CM, Harris BE, Bailey DL, Bailey E, Berend N, Young IH, King GG. Airway closure on imaging relates to airway hyperresponsiveness and peripheral airway disease in asthma. J Appl Physiol (1985). 2012;113(6):958-66.
12. Otsu N. A Threshold Selection Method from Gray-Level Histograms. IEEE Transactions on Systems, Man, and Cybernetics. 1979;9(1):62-6.
13. Farrow CE, Salome CM, Harris BE, Bailey DL, Berend N, King GG. Peripheral ventilation heterogeneity determines the extent of bronchoconstriction in asthma. Journal of Applied Physiology. 2017;123(5):1188-94.
14. Rutting S, Mahadev S, Tonga KO, Bailey DL, Dame Carroll JR, Farrow CE, Thamrin C, Chapman DG, et al. Obesity alters the topographical distribution of ventilation and the regional response to bronchoconstriction. Journal of Applied Physiology. 2019;128(1):168-77.
15. Kroon D-J. Region Growing: MATLAB Central File Exchange; 2008 [Available from: https://au.mathworks.com/matlabcentral/fileexchange/19084-region-growing.
16. Koltai H. Novel 3D Segmentation Methods for SPECT Images of Airway Disease: The University of Sydney; 2021.
17. Lin LI. A concordance correlation coefficient to evaluate reproducibility. Biometrics. 1989;45(1):255-68.
18. Nass SA, Hossain I, Sanyang C, Baldeh B, Pereira DIA. Hemoglobin point-of-care testing in rural Gambia: Comparing accuracy of HemoCue and Aptus with an automated hematology analyzer. PLoS One. 2020;15(10):e0239931.

19. McBride G. A proposal for strength-of-agreement criteria for Lin's concordance correlation coefficient. NIWA client report: HAM2005-062. 2005;45:307-10.
20. Berend N, Salome CM, King GG. Mechanisms of airway hyperresponsiveness in asthma. Respirology. 2008;13(5):624-31.
21. Lee SJ, Park HJ. Single photon emission computed tomography (SPECT) or positron emission tomography (PET) imaging for radiotherapy planning in patients with lung cancer: a meta-analysis. Sci Rep. 2020;10(1):14864.
22. Harris RS, Winkler T, Tgavalekos N, Musch G, Melo MF, Schroeder T, Chang Y, Venegas JG. Regional pulmonary perfusion, inflation, and ventilation defects in bronchoconstricted patients with asthma. Am J Respir Crit Care Med. 2006;174(3):245-53.
23. King GG, Eberl S, Salome CM, Meikle SR, Woolcock AJ. Airway closure measured by a technegas bolus and SPECT. American Journal of Respiratory and Critical Care Medicine. 1997;155(2):682-8.
24. Amis TC, Crawford AB, Davison A, Engel LA. Distribution of inhaled 99mtechnetium labelled ultrafine carbon particle aerosol (Technegas) in human lungs. European Respiratory Journal. 1990;3(6):679.
25. Munawar I, Yaremko BP, Craig J, Oliver M, Gaede S, Rodrigues G, Yu E, Reid RH, et al. Intensity modulated radiotherapy of non-small-cell lung cancer incorporating SPECT ventilation imaging. Med Phys. 2010;37(4):1863-72.
26. Meng X, Frey K, Matuszak M, Paul S, Ten Haken R, Yu J, Kong FM. Changes in functional lung regions during the course of radiation therapy and their potential impact on lung dosimetry for non-small cell lung cancer. Int J Radiat Oncol Biol Phys. 2014;89(1):145-51.
27. Sahoo PK, Soltani S, Wong AKC. A survey of thresholding techniques. Computer Vision, Graphics, and Image Processing. 1988;41(2):233-60.
28. Kittler J, Illingworth J. On threshold selection using clustering criteria. IEEE Transactions on Systems, Man, and Cybernetics. 1985;SMC-15(5):652-5.
29. Xu X, Xu S, Jin L, Song E. Characteristic analysis of Otsu threshold and its applications. Pattern Recognition Letters. 2011;32(7):956-61.
30. Levine ZH, Li M, Reeves AP, Yankelevitz DF, Chen JJ, Siegel EL, Peskin A, Zeiger DN. A low-cost density reference phantom for computed tomography. Medical Physics. 2009;36(2):286-8.
31. Hoy CFO, Naguib HE, Paul N. Fabrication and characterization of polymeric cellular foams for low-density computed tomography phantom applications. Journal of Cellular Plastics. 2018;55(1):73-87.

Chapter 3 – Relationships between non-ventilated volume and ‘hot spots' from Single Photon Emission Computed Tomography imaging and baseline lung function in COPD

3.1 Abstract

Introduction: In COPD, VSPECT has long since shown the loss of ventilation in patients with more severe disease and emphysema. But the relationships between quantitative estimates on non-ventilated volume and 'hot spots' count, which depict regions of turbulent airflow, and lung function measurements beyond spirometry remain poorly understood. Thus, our objective was to examine the relationships between non-ventilated volume and 'hot spots' count and various lung function measurements in COPD.

Methods: 23 COPD participants underwent lung function testing, consisting of spirometry, body plethysmography, gas diffusion (D_{LCO}), and oscillometry, which was then followed by a VSPECT/CT scan. Non-ventilated volume ($Vent_{Non}$) and 'hot spots' were defined with the curve-fitting threshold method.

Results: Both VSPECT/CT parameters correlated with a multitude of lung function measurements. Increased $Vent_{Non}$ primarily correlated with worse FEV1/FVC ($r = -0.51$; $p = 0.01$) and measurements relating to worse emphysema (D_{LCO}: $r = -0.61$; $p = 0.003$). Increased 'Hot spots' count had correlated with reduced FEV1 ($r = -0.57$; $p = 0.005$), greater hyperinflation (FRC/TLC) ($r = 0.65$; $p = 0.001$), gas trapping (RV/TLC) ($r = 0.54$; $p = 0.009$), and ventilation heterogeneity (VA/TLC) ($r = -0.53$; $p = 0.01$). $Vent_{Non}$ did not correlate with 'hot spots' count.

Conclusion: $Vent_{Non}$ and 'hot spots' count provide complementary information on ventilation impairment in COPD, and they relate to different lung function measurements. Whether these parameters are sensitive to the effects of bronchodilator treatment or bronchoconstriction remains to be determined.

3.2 Introduction

Chronic obstructive pulmonary disease (COPD) is a progressive obstructive lung disease, characterized by partially reversible airflow obstruction and parenchymal lung destruction i.e., emphysema (1). The effects of these characteristics on ventilation can be visualized with three-dimensional ventilation techniques, such as single-photon emission computed tomography (SPECT) or magnetic resonance imaging (MRI). Ventilation SPECT (VSPECT), which generally uses Technegas (^{99m}Tc) as its ventilation agent, allows for the estimation of lung volumes with absent and reduced deposition of the ventilation agent at functional residual capacity (2, 3). Bajc et al. reported significant correlations between their qualitative estimation of unventilated and hypo-ventilated lung volume as visualised by VSPECT and airflow obstruction severity (4). In quantitative ventilation studies, whether completed with VSPECT or MRI, unventilated and hypo-ventilated lung volume is typically calculated as a percentage of total lung volume and reported simply as ventilation defect percentage (VDP) (5, 6). Both VSPECT and MRI measurements of VDP have been shown to correlate with airflow obstruction severity (7) in addition to gas diffusion (5). In our study, the term 'non-ventilated volume' ($Vent_{Non}$) is used as an alternative title for VDP.

Another parameter from VSPECT imaging is the presence of voxels with extremely high activity i.e., 'hot spots'. These 'hot spots' are suggested to represent an increased deposition of Technegas particles in narrowed airways or regions with turbulent ventilation (8, 9). Although 'hot spots' are usually determined qualitatively, increased number of 'hot spots' was found to be associated with worse airflow

obstruction and increased disease severity (10, 11). We recently developed a novel curve-fitting method for quantitatively defining non-ventilated volume. In our previous chapter, we demonstrated the method to be superior in accuracy to current methods. However, this curve fitting method may also be used to quantitatively define ‘hot spots’. It is currently unknown how both measurements, non-ventilated volume and ‘hot spots’ count, as defined by our novel method would relate to each other and lung function tests in COPD patients.

Aside from spirometry and other standard lung function tests, oscillometry provides complementary information on small airway function and respiratory mechanics such as respiratory system resistance and reactance. Small airways disease, which involve obstruction, remodelling, and obliteration of the small airways (12, 13), is one of the characteristic features of COPD, and it has been linked to disease progression (14) and poor clinical outcomes (15). Unlike spirometry (16), oscillometry is purported to be sensitive to small airways function and early changes in lung function (17, 18). Whether VSPECT is also sensitive to small airways function and respiratory mechanics is unknown.

Therefore, our primary research objective for this study was to examine the relationships between the two imaging parameters, non-ventilated volume and ‘hot spots’ count, and measurements of lung function and small airways in COPD. We hypothesized that 1) the extent of non-ventilated volume would be related to emphysema and 2) the presence of ‘hot spots’ to be related to ventilation heterogeneity.

3.3 Methods

3.3.1 Participants and Study Design

23 participants with physician diagnosed COPD (13 men, 10 women) were recruited from the Department of Respiratory Medicine at Royal North Shore Hospital. The inclusion criteria were as follows: 18 – 80 years old, physician diagnosed COPD, and a smoking history of at least 10 pack years. Exclusion criteria were other active or chronic respiratory diseases, history of lung surgery, history of chronic kidney disease, significant cardiac disease, intensive care unit admissions in the last 12 months, and significant respiratory infection or documented exacerbation within the previous 6 weeks. All participants provided written, informed consent. The study was approved by the local Human Research Ethics Committee (Northern Sydney Local Health District, RESP/18/198)

For this study, participants were required to attend a single visit. Prior to each visit, the participants withheld short-acting bronchodilators for 6 hours and LABA and/or LAMA medication for 24 hours. During the visit, participants completed the COPD Assessment Test (CAT) (19) and underwent lung function testing in this order: oscillometry (FOT), spirometry, body plethysmography, and single breath diffusing capacity. The visit was concluded with a VSPECT/CT scan.

3.3.2 Lung Function Testing

Spirometry, body plethysmography, and diffusing capacity had been performed with the Jaeger MS Body/Diff Master Screen (Jaeger, Hoechberg, Germany) according to American Thoracic Society (ATS)/European Respiratory Society (ERS) criteria (20-22).

FOT was performed with the tremoFlo C-100 oscillometry system (v. 1.0.43.44, Thorasys Thoracic Medical Systems Inc, Montreal) at 5 – 37 Hz. Device calibration was performed prior to the testing session. Following the ERS technical standards, participants underwent at least 3 breathing measurements. For each measurement, the participant was instructed to breathe tidally in a seated position and support their cheeks for 60 seconds, whilst wearing a nose clip. The mean resistance (R5) and reactance (X5), both at 5 Hz, were then obtained. Measurements with signs of leak, coughs, swallows, or incorrect technique were excluded for quality control. A R5 coefficient of variation ≤ 10% was required for each testing session.

The z-scores for spirometry, body plethysmography, and diffusing capacity were determined with reference equations from the Global Lung Initiative (GLI) (23-25). Reference equations from Brown et al. were used to calculate FOT z-scores (26) as one participant's weight was outside the range of the latter's reference equations. .

3.3.3 Ventilation Imaging

VSPECT/CT Imaging was conducted at the Department of Nuclear Medicine, Royal North Shore Hospital, using a Siemens Symbia T16 SPECT/CT system. Technegas, consisting of 100 nm Technetium (^{99m}Tc) carbon nanoparticles, was used as the ventilation agent. The inhaled distribution of Technegas has been demonstrated to resemble gas, even in participants with severe airway obstruction (27), and its distribution should also remain fixed for at least 20 minutes after inhalation (28, 29).

Participants were required to breathe in 500 – 700 mL of Technegas from functional residual capacity (FRC) at approximately 0.5 – 1 L/sec in a seated, upright position. The volume and flow rate of each inhalation was monitored with a MGC Diagnostics CPFS/D USB spirometer and MGC Breeze Suite interface (v. 8.6.0.56, MGC Diagnostics Corporation, Saint Paul). Two – four inhalations were generally taken to achieve the required radioactivity of approximately 1.5 – 2.0 kilocounts/s, and approximately 40 mBq of Technegas was inhaled. As VSPECT/CT scans from this study were compared to post-bronchodilator and post-methacholine scans in subsequent studies (Chapter 4 and 5), participants were administered with 400 µg of salbutamol. Contrast bead markers were then attached to their suprasternal notch, xiphisternum, and 12th ribs.

Supine VSPECT and low dose CT scans (30 mA, 110 kVp, pitch 1.5, slice thickness 3 mm) were acquired with a 128 x 128 matrix and 512 x 512 matrix, respectively. Participants breathed tidally throughout the VSPECT scan, but they were then instructed to hold their breath at FRC for the CT scan. Following the settings on

other human VSPECT studies (30-32), VSPECT acquisitions employed 60 stops x2 projections (total 120 projections), 15 seconds per stop, non-circular clockwise orbit and continuous acquisition.

3.3.4 Image Reconstruction and Registration

Using 128 slices, VSPECT images were reconstructed with an ordered subset expectation maximization (OSEM) Siemens Flash 3D algorithm, CT-based attenuation correction, and a Gaussian filter. CT image reconstruction was completed with a 512 x 512 matrix and OSEM Siemens Flash 3D algorithm. Both VSPECT and CT images were converted to Digital Imaging and Communication in Medicine (DICOM) file format.

VSPECT and CT scans were first registered using the known, fixed spatial relationship between the VSPECT and CT scanners. The DICOM files of both scans were then transferred onto a HERMES (Nuclear Diagnostics, Stockholm, Sweden) workstation. The matrix size of the VSPECT scan was increased from 128 x 128 matrix to 512 x 512, and the original counts remained preserved. Additional three-dimensional registration was completed with the multimodality software package on HERMES by visually aligning the markers on the VSPECT and CT scans.

3.3.5 Imaging Analysis

Lung outlines on the CT scans were defined through a region growing algorithm (33) that had been implemented within a MATLAB script (R2019b, MathWorks, Natick) (34). The script produced a binarized mask of the lung outlines, which was applied onto the VSPECT scan (Figure 1). All VSPECT voxel activity outside of the lung borders were set to 0. VSPECT voxel data within the mask were exported onto Microsoft Excel (2021, Microsoft, Redmond).

Definition of non-ventilated volume ($Vent_{Non}$) and 'hot spots' required the curve-fitting threshold method (Figure 2), as described in Chapter 2. To summarize, the cumulative voxel frequency was first plotted against activity, and the slopes of each data point were then calculated. The initial activity value ≥ 90% cumulative frequency with a slope ≤ 0.010 was selected as the 'slope point'. Voxels < 30% x the 'slope point' were determined to be $Vent_{Non}$. $Vent_{Non}$ was expressed as a percentage of total lung volume, which had been derived from the CT mask of the lungs. Voxels ≥ the 'slope point' were determined to be 'hot spot' activity. To count the number of 'hot spots' in three-dimensional space, the masked VSPECT image was first opened in Fiji (National Institutes of Health, United States of America). Secondly, the VSPECT image was binarized, in which all voxel activity < the 'slope point' was set to 0 and all voxel activity ≥ the 'slope point' was set to 255 i.e., the maximum activity in an 8-bit image. Finally, the 3D Objects Counter plugin had been used to count the number of 'hot spots' in three-dimensional space. Examples of both $Vent_{Non}$ and 'hot spot' counting are shown in Figure 3.

3.3.6 Statistical Analysis

GraphPad Prism version 10.0.2 was used to analyse data and generate graphs. All data were expressed as mean ± SD unless otherwise stated. Correlations between $Vent_{Non}$ and measurements of lung function and demographics were examined by Spearman correlation. A p-value of < 0.05 was considered statistically significant.

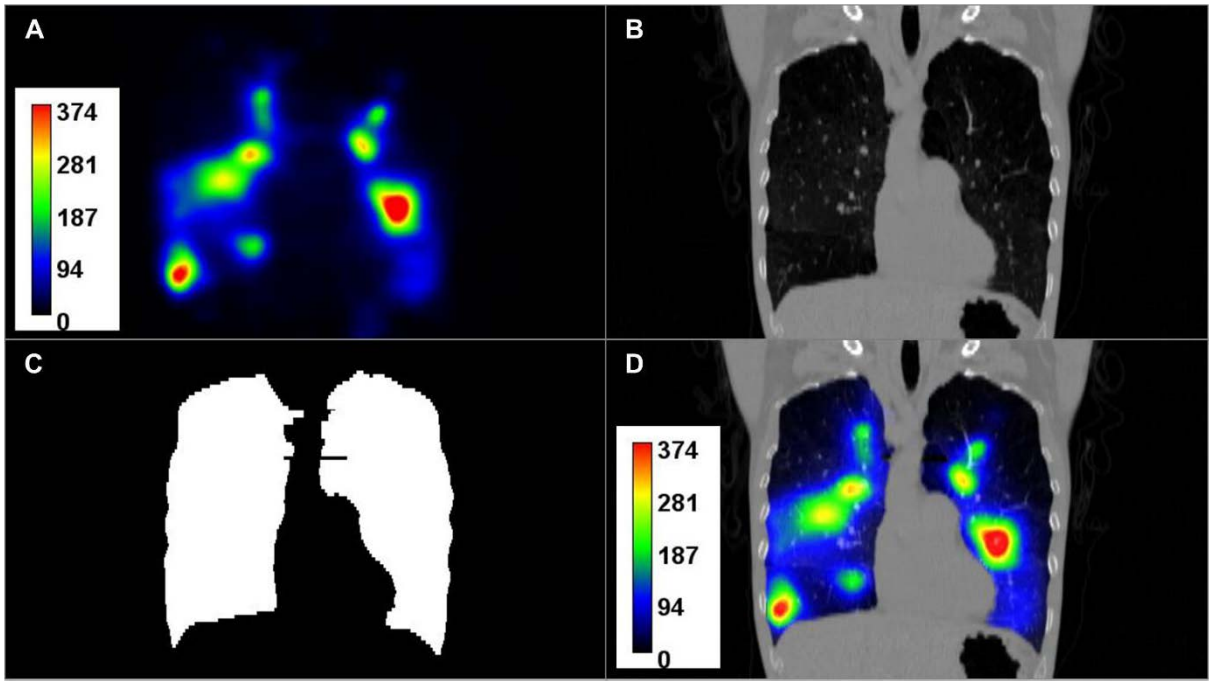


Figure 1: Masking for ventilation single-photon emission computed tomography (VSPECT)/computed tomography (CT) scan. (A) VSPECT scan; (B) CT scan; (C) binarised mask of lung outlines from CT scan; (D) fused VSPECT/CT scan with overlain mask, setting all activity outside lung borders to 0.

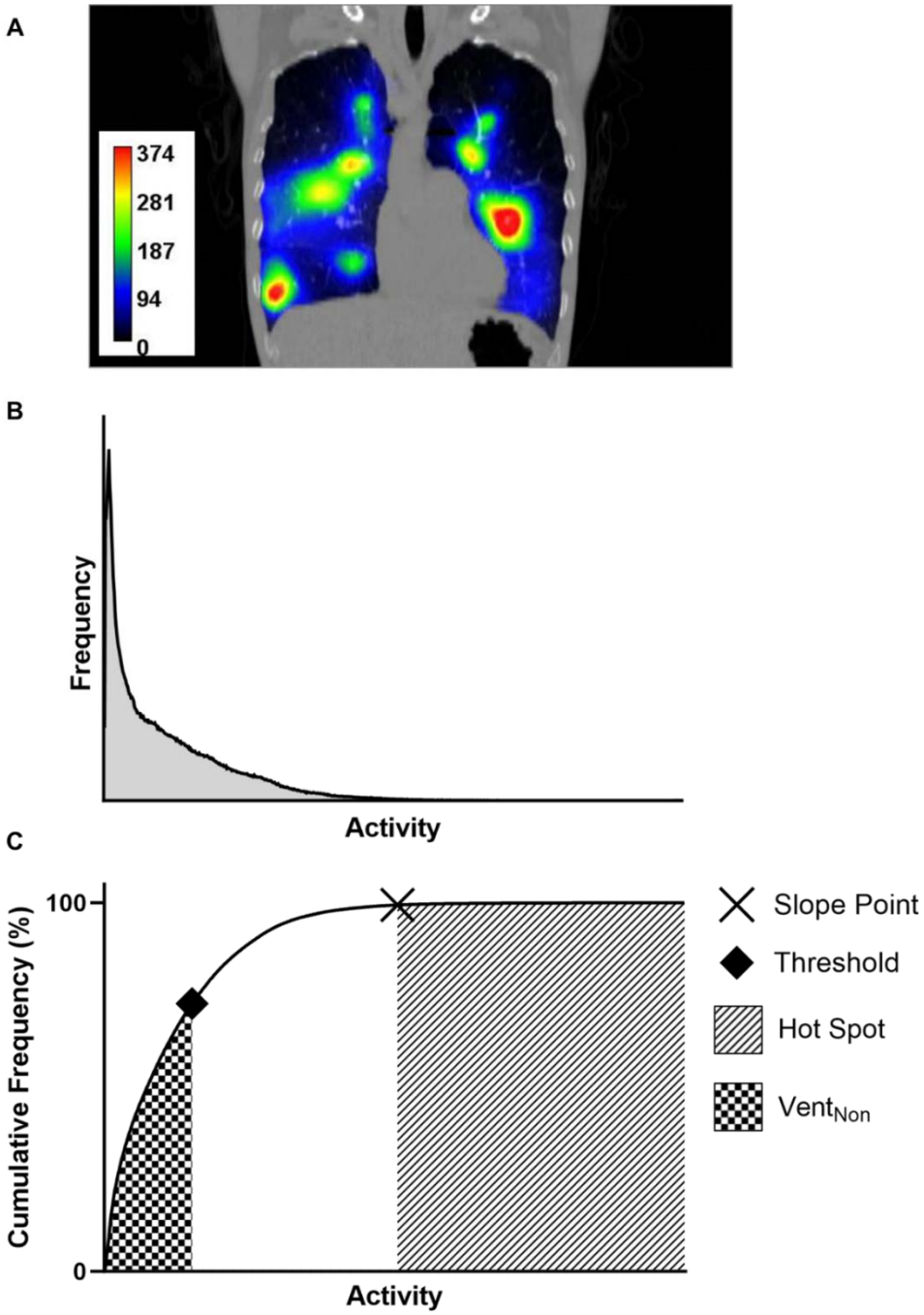


Figure 2: Curve-fitting threshold method for ventilation single-photon emission computed tomography (VSPECT)/computed tomography (CT) scan. (A) Fused and masked VSPECT/CT scan; (B) Voxel activity – frequency plot of masked VSPECT/CT scan; (C) Voxel activity – cumulative frequency plot with curve-fitting threshold method. Slope Point = initial activity value ≥ 90% cumulative frequency with ≤ 0.010 slope; Threshold = 30% x 'slope point'; $Vent_{Non}$ = non-ventilated volume

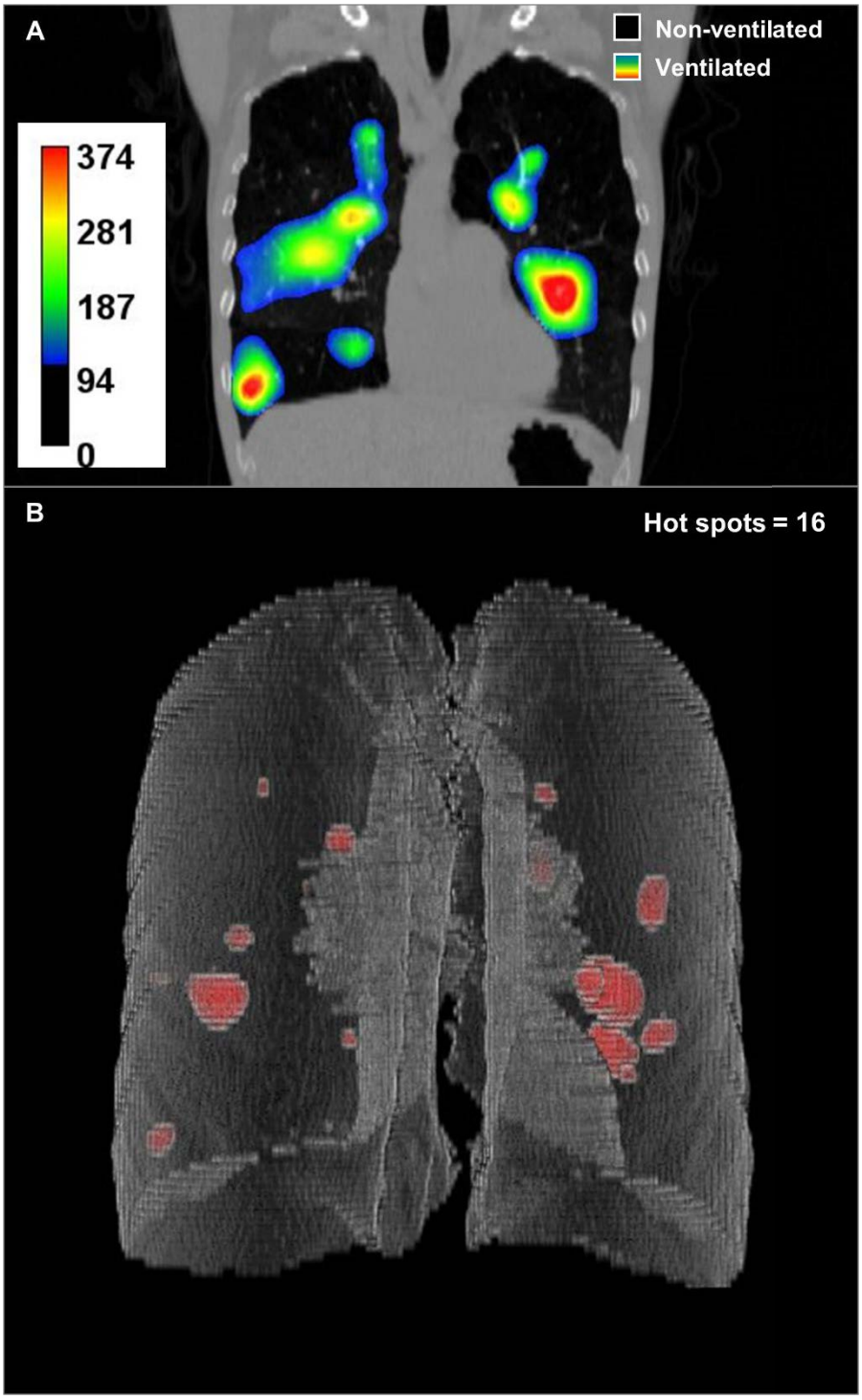


Figure 3: Measurement of non-ventilation (A) and number of hot spots (B) in ventilation single-photon emission computed tomography (VSPECT)/computed tomography scan.

3.4 Results

3.4.1 Participant Demographics and Lung Function

Participant demographics and lung function measurements are displayed in Table 1. 23 participants were recruited for this study, but 1 participant was unable to perform the Technegas inhalation manoeuvre correctly. On average, participants were overweight (BMI: 28.0 ± 6.2) and moderately impacted by the disease (CAT: 17.9 ± 6.9). Furthermore, participants overall had severe airway obstruction (FEV1/FVC z-score: -3.5 ± 1.0) with minimal hyperinflation (FRC/TLC z-score: 1.1 ± 1.4) and gas trapping (RV/TLC z-score: 1.7 ± 1.8). The mean D_{LCO} and K_{CO} z-scores indicated moderate impairment of gas diffusion (D_{LCO} and K_{CO} z-scores: -3.0 ± 2.4 and -2.2 ± 2.1, respectively). Although, mean R5 z-score was within the limits of normal, the mean X5 z-score was abnormal (-5.1 ± 3.5). For VSPECT parameters, mean ± SD $Vent_{Non}$ and 'hot spots' count were 49.3 ± 21.1 and 6 ± 3, respectively.

3.4.2 Relationship between non-ventilation and hot spots

The relationship between $Vent_{Non}$ and 'hot spot' count is plotted in Figure 4. There was no correlation between the two imaging parameters (p-value = 0.36).

Table 1: Participant demographics, lung function, and imaging parameters

Participants, *n*	23
Males/females, *n*	13/10
Age, years	67.3 ± 8.3
Height, m	1.7 ± 0.08
BMI, kg/m^2	28.0 ± 6.2
Smoking history, pack years	39.6 ± 25.5
CAT	17.9 ± 6.9
FEV1, z-score	-2.7 ± 1.0
FVC. z-score	-0.5 ± 1.1
FEV1/FVC, %	44.5 ± 12.4
FEV1/FVC, z-score	-3.5 ± 1.0
TLC, z-score	0.6 ± 1.3
IC, z-score	-0.8 ± 0.8
FRC, z-score	1.4 ± 1.5
RV, z-score	1.7 ± 1.8
FRC/TLC, %	63.5 ± 8.1
FRC/TLC, z-score	1.1 ± 1.4
RV/TLC, %	47.2 ± 9.5
RV/TLC, z-score	1.5 ± 1.4
D_{LCO}, z-score	-3.0 ± 2.4
K_{CO}, z-score	-2.2 ± 2.1
VA/TLC	0.8 ± 0.1
R5, z-score	1.4 ± 1.1
X5, z-score	-2.6 ± 0.7
$Vent_{Non}$, %	49.3 ± 29.1
Hot spots, n	6 ± 3

BMI = body mass index; CAT = chronic obstructive pulmonary disease assessment test; FEV1 = forced expiratory volume in 1 second; FVC = forced vital capacity; TLC = total lung capacity; IC = inspiratory capacity; FRC = functional residual capacity; RV = residual volume; DL_{CO} = diffusing capacity for carbon monoxide; K_{CO} = carbon monoxide transfer coefficient; VA = alveolar volume; R5 = respiratory system resistance measured at 5 Hz; X5 = respiratory system reactance measured at 5 Hz; $Vent_{Non}$ = non-ventilated volume

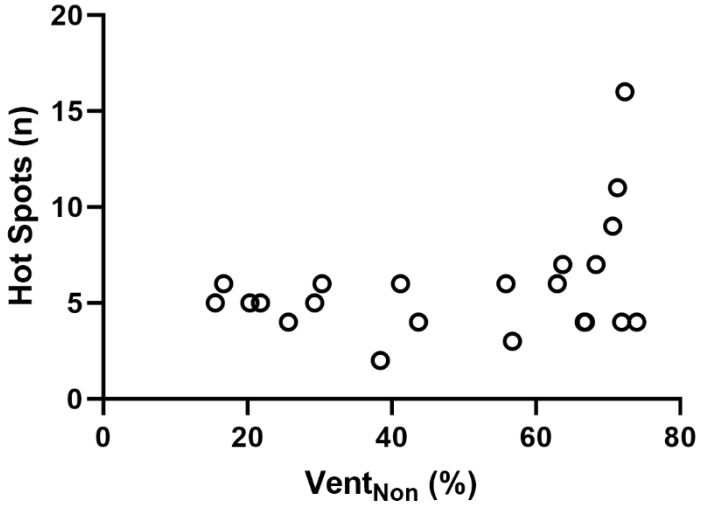


Figure 4: Relationship between non-ventilated volume ($Vent_{Non}$) and 'hot spots' count. The number of 'hot spots' did not correlate with $Vent_{Non}$ (r_s = 0.20, p = 0.36).

3.4.3 Correlations between imaging and demographics and lung function

Univariate correlations between the imaging parameters, $Vent_{Non}$ and 'hot spots' count, and demographics and lung function are shown in Table 2. $Vent_{Non}$ did not correlate with age, smoking history, or CAT, but decreased $Vent_{Non}$ correlated with increased BMI (r_s = -0.68, p-value = 0.0005), . There were no correlations between $Vent_{Non}$ and FEV1 z-score or FVC z-score. Increased $Vent_{Non}$ correlated with decreased absolute FEV1/FVC (r_s = -0.51, p-value = 0.01), but the strength of the correlation was lost when looked at FEV1/FVC z-score (r_s = -0.41, p-value = 0.06). Increased $Vent_{Non}$ correlated with multiple lung volume measurements; greater $Vent_{Non}$ was associated with greater TLC z-score (r_s = -0.58, p-value = 0.005), FRC z-score (r_s = -0.54, p-value = 0.009), and RV z-score (r_s = -0.49, p-value = 0.02). However, Ventnon was not correlated with IC z-score, FRC/TLC z-score, and RV/TLC z-score. $Vent_{Non}$ correlated with D_{LCO} z-score (r_s = -0.61, p-value = 0.003), K_{CO} z-score (r_s = -0.68, p-value = 0.0004), and VA/TLC (r_s = -0.74, p-value < 0.0001). There were no correlations between $Vent_{Non}$ and FOT measurements (R5, R5 z-score, X5, and X5 z-score).

'Hot spots' count did not correlate with age, BMI, smoking history, or CAT. For spirometry, increased 'hot spots' count was associated with a decreased FEV1 z-score (r_s = -0.57, p-value = 0.005), and a borderline significant correlation was seen with FVC (r_s = -0.42, p-value = 0.05). However, there were no correlations with either FEV1/FVC or FEV1/FVC z-scores. Increased 'hot spots' count was significantly associated with increased TLC z-score (r_s = 0.42, p-value = 0.05), FRC z-score (r_s = 0.50, p-value = 0.02), RV z-score (r_s = 0.56, p-value = 0.007), FRC/TLC z-score (r_s =

0.65, p-value = 0.001), and RV/TLC z-score (r_s = 0.54, p-value = 0.009). No correlations were found with IC z-score. ‘Hot spots’ count correlated with VA/TLC (r_s = -0.53, p-value = 0.01), but there were no significant relationships with either D_{LCO} z-score or K_{CO} z-score. Increased ‘hot spot’ count correlated with more abnormal (I.e. decreased) absolute X5 (r_s = -0.51, p-value = 0.01), but did not correlate with R5, R5 z-score, or X5 score.

Table 2: Univariate correlations between demographics, lung function, and non-ventilated volume.

	$Vent_{Non}$		Hot Spots	
	r_s	p-value	r_s	p-value
Age, years	0.26	0.24	-0.01	0.97
BMI, kg/m^2	**-0.68**	**0.0005**	-0.39	0.07
Smoking history, pack years	0.28	0.20	0.02	0.94
CAT	-0.03	0.88	0.31	0.16
FEV1, z-score	-0.22	0.32	**-0.57**	**0.005**
FVC, z-score	0.11	0.62	-0.42	0.05
FEV1/FVC, %	**-0.51**	**0.01**	-0.39	0.06
FEV/FVC, z-score	-0.41	0.06	-0.41	0.06
TLC, z-score	**0.58**	**0.005**	**0.42**	**0.05**
IC, z-score	0.11	0.62	-0.37	0.09
FRC, z-score	**0.54**	**0.009**	**0.50**	**0.02**
RV, z-score	**0.49**	**0.02**	**0.56**	**0.007**
FRC/TLC, z-score	0.22	0.32	**0.65**	**0.001**
RV/TLC, z-score	0.35	0.11	**0.54**	**0.009**
D_{LCO}, z-score	**-0.61**	**0.003**	-0.39	0.07
K_{CO}, z-score	**-0.68**	**0.0004**	-0.34	0.13
VA/TLC	**-0.74**	**<0.0001**	**-0.53**	**0.01**
R5, z-score	-0.27	0.22	0.22	0.32
X5, z-score	-0.41	0.06	-0.17	0.45

Univariate correlations between lung function and demographics and non-ventilated lung volume ($Vent_{Non}$) and ‘hot spots’ count using Spearman’s rank correlation. BMI = body mass index; CAT = chronic obstructive pulmonary disease assessment test; FEV1 = forced expiratory volume in 1 second; FVC = forced vital capacity; TLC = total lung capacity; FRC = functional residual capacity; RV = residual volume; DL_{CO} = diffusing capacity for carbon monoxide; K_{CO} = carbon monoxide transfer coefficient; VA = alveolar volume; R5 = respiratory system resistance measured at 5 Hz; X5 = respiratory system reactance measured at 5 Hz.

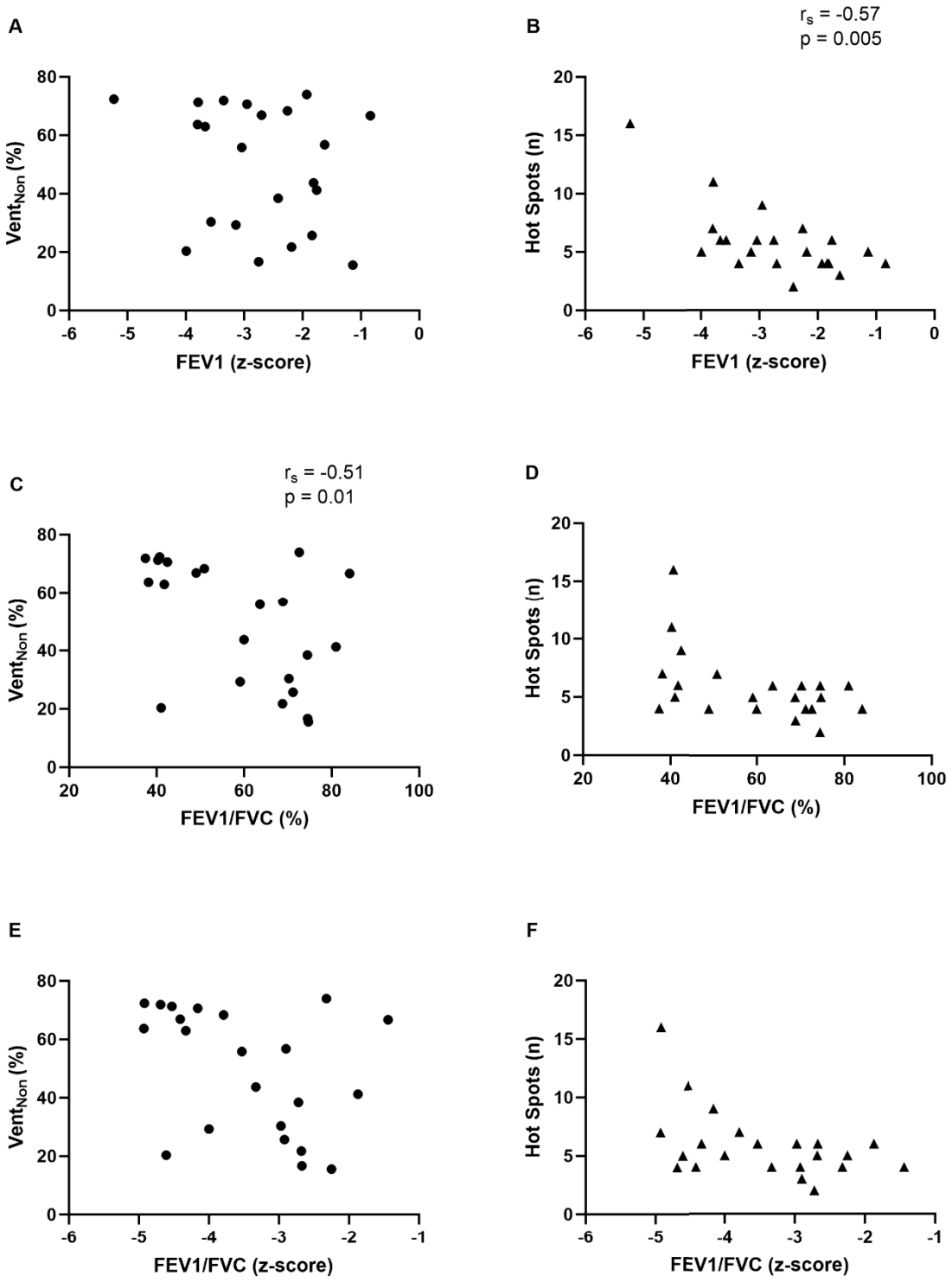


Figure 5: Relationships between non-ventilated volume ($Vent_{Non}$) and 'hot spots' count with spirometric measurements. FEV1 = forced expiratory volume in 1 second; FVC = forced vital capacity

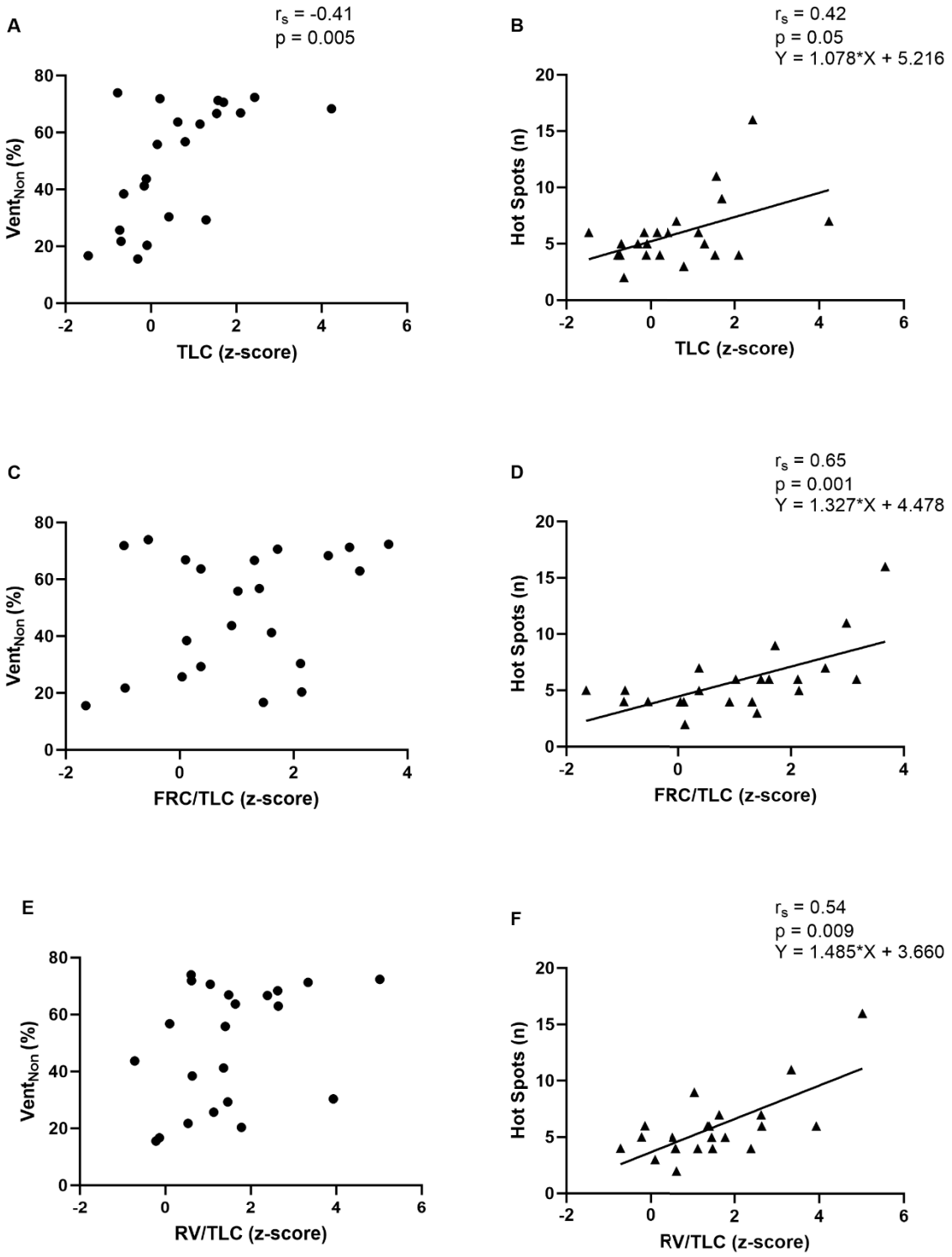


Figure 6: Relationships between non-ventilated volume ($Vent_{Non}$) and 'hot spots' count with lung volume measurements. Linear regression lines were plotted for B, D, and F. TLC = total lung capacity; FRC = functional residual capacity; RV = residual volume

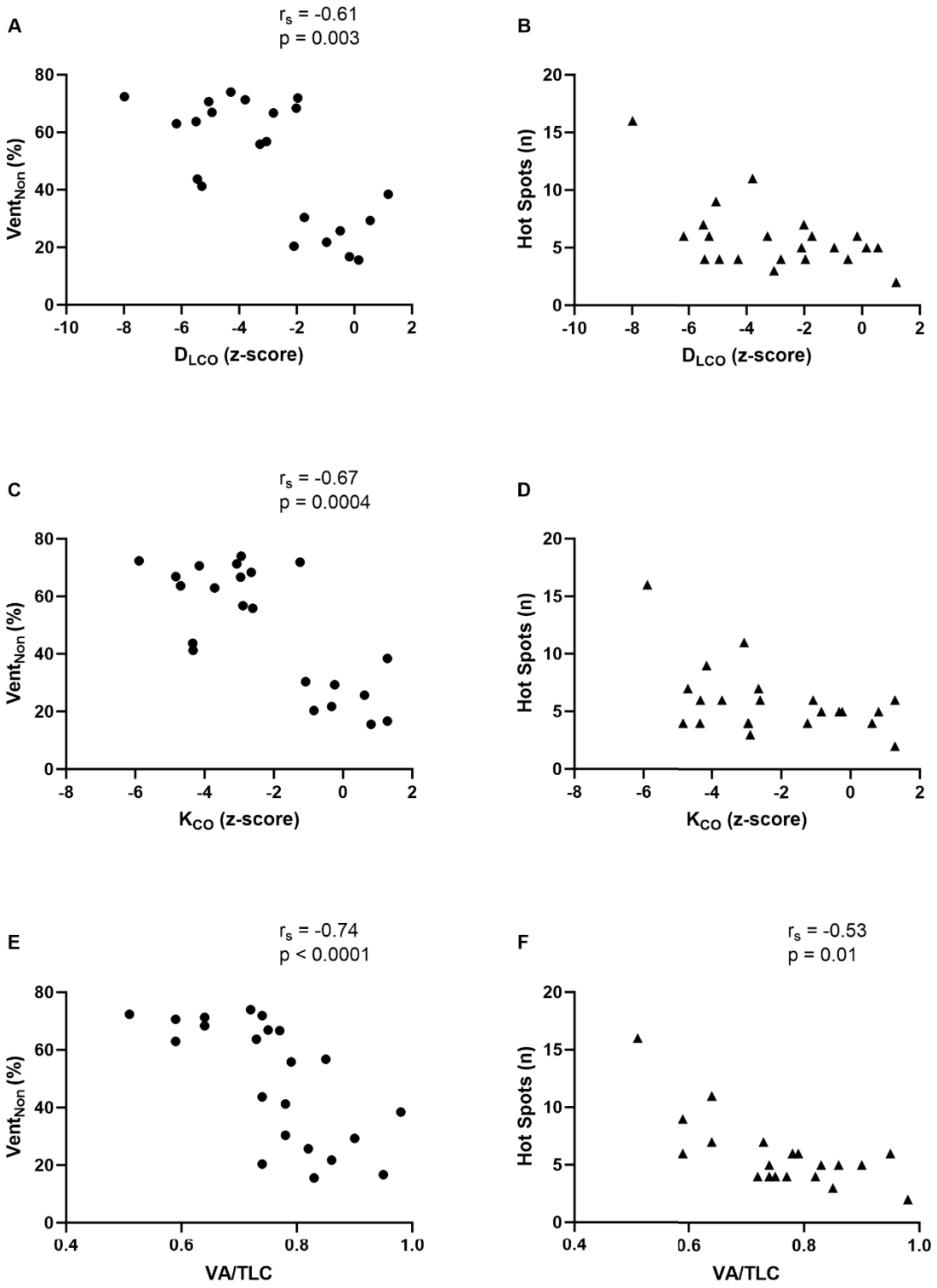


Figure 7: Relationships between non-ventilated volume ($Vent_{Non}$) and 'hot spots' count with diffusing capacity of the lung for carbon monoxide (D_{LCO}) z-score, carbon monoxide transfer coefficient (K_{CO}) z-score, and ratio of alveolar volume to total lung capacity (VA/TLC).

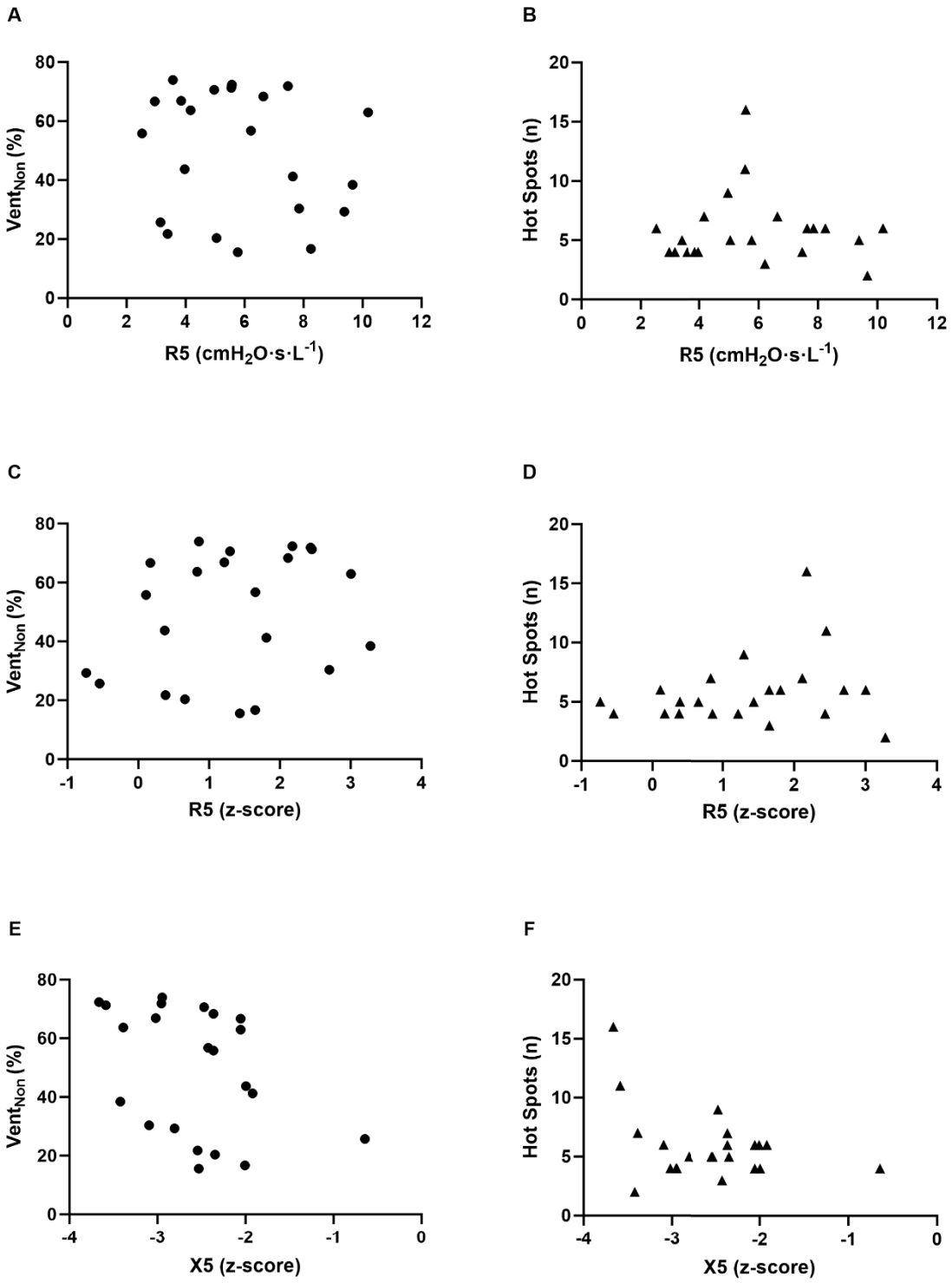


Figure 8: Relationships between non-ventilated volume ($Vent_{Non}$) and 'hot spots' count with oscillometry measurements. R5 = respiratory system resistance measured at 5 Hz; X5 = respiratory system reactance measured at 5 Hz.

3.5 Discussion

In this study, we demonstrated that the two imaging parameters, $Vent_{Non}$ and 'hot spots' count, were unrelated to each other. However, as hypothesized, they had correlated with different lung function measurements. Increased $Vent_{Non}$ was exclusively associated with poorer gas diffusion as measured by D_{LCO} and K_{CO} z-scores. Additional correlations with worse absolute hyperinflation and gas trapping indicate $Vent_{Non}$ to be mostly related to emphysema. Increased 'hot spots' count on the other hand had related to a low FEV1 z-score and worse relative hyperinflation and gas trapping, but no associations were found between 'hot spots' count and gas diffusion measurements. Interestingly, both $Vent_{Non}$ and 'hot spots' count correlated with ventilation heterogeneity. Our findings therefore suggest that increased 'hot spots' count is primarily indicative of airflow impairment and worse ventilation heterogeneity. Neither $Vent_{Non}$ and 'hot spots' count related with the oscillometric parameters, R5 and X5.

3.5.1 Non-ventilated volume

We observed $Vent_{Non}$ had correlated strongly with D_{LCO}, K_{CO}, and VA/TLC suggesting that this parameter is likely predominantly affected by emphysema in people with COPD. This is supported by the additional correlations with measurements of hyperinflation and gas trapping as well as airway obstruction. In a study by Radadia et al., increased $Vent_{Non}$ had also been associated with decreased FEV1/FVC and decreased D_{LCO}, albeit calculated as % of predicted (5). However, another study had shown a correlation not with FEV1/FVC, but with FEV1 instead (7). Although the reasons for this conflict are unclear, it may be contributed to the use of different

threshold methods. The former study opted for the method based on the mean activity by Farrow et al. (30) and the latter study utilised the maximum activity method, which we have shown both to be sensitive to noise or $Vent_{Non}$ and maximum activity or 'hot spots', respectively (Chapter 2). Specifically, greater volumes of $Vent_{Non}$ would cause the mean activity method to lower its threshold, and the presence of 'hot spots' would cause the maximum activity method to increase its threshold. This may explain the differences in our findings with these studies. A lower threshold, which consequently underestimates $Vent_{Non}$ volumes, could also be more sensitive to more peripheral alveolar regions with greater time constraints for Technegas filling, hence the correlation between D_{LCO} and $Vent_{Non}$ as measured by the mean threshold method. Conversely, a higher threshold that overestimates $Vent_{Non}$ volumes, such as the maximum activity method, may also be more sensitive to airways in central lung regions with limited time constraints for Technegas filling.

Due to the physical properties of Technegas, it is not surprising that $Vent_{Non}$ relates to parameters affected by emphysema. The small particle size of Technegas, which is approximately 100 nm in diameter, allows for the aerosol agent to penetrate peripheral lung spaces and into the alveoli beyond the conducting airways (35-37), even in patients with severe airflow obstruction (27, 28). Therefore, if Technegas deposition is reduced in COPD patients, increasing $Vent_{Non}$, then there must be a loss of accessible airways, either from complete obstruction or obliteration (38). For our study, we observed that in some participants, $Vent_{Non}$ was very high (≥ 70%), which indicates a significant loss of accessible airways. CT and micro-CT scans of emphysematous lungs reveal not only severely narrowed if not completely

obstructed small airways, but also a drastic loss in the number of terminal bronchioles (39), ranging up to 89% reduction in patients with severe COPD (13).

$Vent_{Non}$ also did not appear to be merely restricted to the peripheral lung regions, and we find it unlikely that physiological changes at the peripheral lung regions were solely responsible for the high $Vent_{Non}$ observed in our study. Indeed, Milne et al. (40) had proposed that the loss of proximal airways dependent on convective flow from parenchymal damage should significantly affect Technegas deposition. Therefore, the expansion of $Vent_{Non}$ into more proximal lung regions may be explained by two additional factors. The first factor is the destruction of larger, proximal airways. This has been corroborated by CT scans of COPD patients with emphysema and low D_{LCO} % of predicted (41) and another older study that reported a reduced count of macroscopic airways in emphysematous lungs (42). The second factor could be from either complete obstruction or mucous plugging in the larger airways, which was found to be characteristic of the emphysema COPD phenotype (43). These widespread changes involving obstructed airways and loss of airways, in both the peripheral and proximal lung regions, would explain why Technegas deposition was so largely reduced in our participants with worse gas diffusion, hyperinflation, gas trapping, and airway obstruction. Determining whether ventilation still occurs in these damaged regions through smaller collateral pathways (44, 45) in conjunction will require further examination.

3.5.2 Hot spots

We observed several relationships between ‘hot spots’ count and FEV1 z-score, lung volumes, and VA/TLC. These findings indicate a greater ‘hot spots’ count was particularly associated with airflow impairment and ventilation heterogeneity as measured by VA/TLC (46-48), but not with airway obstruction, which is defined with FEV1/FVC. Previous VSPECT studies with COPD participants noted correlations with ‘hot spots’ count and FEV1, FVC, and FEV1/FVC (4, 11). Unlike our methods, these studies assessed ventilatory impairment by 4 grades, in which an increased number of visible ‘hot spots’ and ventilation defects, both qualitatively defined, indicated more severe impairment. The precise number of ‘hot spots’ from these VSPECT images were not published, making comparisons of results difficult.

For aerosol ventilation agents like Technegas, ‘hot spots’ or particle aggregation is noted to occur primarily from two reasons. The first reason is inertial impaction of particles with the airway wall and at bifurcation points in lung regions with particularly increased airflow velocity such as the trachea. Inertial impaction is also observed in narrowed proximal airways, and it occurs more frequently with larger aerosol particles such as ^{99m}Tc-diethylenetriamine pentaacetate (approximately 0.5 – 2 μm in diameter) (2). The second reason is turbulent airflow, which may also occur when airways bifurcate or narrow (8). Previous VSPECT studies report ‘hot spots’, albeit qualitatively defined, form almost exclusively in proximal or central lung regions via inertial impaction or turbulent airflow, with minimal Technegas aggregation in peripheral lung regions due to reduced airflow velocity and alternate deposition mechanisms i.e., gravitational settling and random molecule collision i.e., Brownian

motion (49, 50). However, Crawford et al. reported that ‘hot spots’ could indeed form in peripheral lung regions, but whether this was from alternate mechanisms or whether they related to measurements of airflow obstruction or ventilation heterogeneity are unknown (27).

The strong association with FEV1 further indicates exaggerated Technegas aggregation being related to proximal airway narrowing and airflow impairment, as qualitative observations from VSPECT studies have previously suggested (28, 51). The relationship between VA/TLC and ‘hot spots’ count may also suggest that the imaging parameter is sensitive to ventilation heterogeneity between parallel sister airways that have heterogeneously narrowed (52). It is possible that Technegas aggregation and increased deposition occurs in the airway with greater airflow velocity and turbulence, even in the peripheral regions, Measurements of ventilation heterogeneity and peripheral airway narrowing are consistently shown to relate with each other (53-55). The absent relationships between ‘hot spots’ and oscillometric parameters challenges this idea since the latter’s parameters are also known to be sensitive to small airway narrowing and ventilation heterogeneity. However, R5 and X5 are global measurements of various other physiological mechanisms including chest-wall abnormalities (56), airway length (57), communicating lung volume (58), compliance across the entire airway ‘tree’ (59), and central airway shunting (60). ‘Hot spots’ count may exclusively reflect airway narrowing, but more studies are required to confirm this. Furthermore, oscillometry is performed during tidal breathing, and respiratory mechanics is unlikely to remain consistent when inhaling 500 mL – 700 mL of Technegas via the patient administration kit. Multiple breath nitrogen washout (MBNW) could provide insight on whether ‘hot spots’ count in COPD patients is

primarily dictated by ventilation heterogeneity across the entire lung, the larger conducting airways, or at the convective-diffusive front.

3.5.3 Non-ventilated versus hot spots

Interestingly, there was no relationship between $Vent_{Non}$ and 'hot spots' count despite each of these parameters correlating with similar lung function measurements such as TLC, FRC, and RV. This suggests that the aggregation of Technegas particles from turbulent or abnormal airflow is largely unrelated to the loss of lung regions from emphysema. Therefore, COPD patients with 'pruned' or plugged airways may not necessarily experience airway narrowing and poor ventilation heterogeneity as well. This suggests the possibility of at least two distinct COPD phenotypes: emphysematous and bronchitis subgroups. Additionally, the non-relationship between $Vent_{Non}$ and 'hot spots' count suggests that Technegas does not aggregate in completely obstructed airways with no airflow. Since both parameters provide complimentary information, they may be useful when phenotyping COPD and investigating response to treatment.

The imaging parameters also possessed different lung function correlations. $Vent_{Non}$ had unique relationships with gas diffusion measurements, as previously discussed, and FEV1/FVC. Conversely, 'hot spots' count uniquely correlated with FRC/TLC and RV/TLC. We speculate that the absent correlation between 'hot spots' count and FEV1/FVC may be due to some participants experiencing premature airway closure, thereby reducing FVC and increasing FEV1/FVC. Conversely, the relationship between $Vent_{Non}$ and FEV1/FVC could be driven primarily by BMI as $Vent_{Non}$ failed to

correlate with FEV1/FVC z-score. Whilst increased TLC is largely reflective of increased lung compliance from emphysema (61), increased FRC and RV relative to TLC may also be indicative of small airway narrowing. This has been proposed previously (62, 63) and indeed, increased FRC and RV correlated more strongly with distal airway inflammation than TLC (64).

3.5.4 Limitations

One limitation for our study was inconsistent Technegas inhalation. Despite training the participants on the required volumes and flow rate during inhalation, there was nonetheless variation in inhalation technique. Consequently, despite achieving the minimum radioactivity of 1.5 kilocounts/s for virtually all participants, Technegas deposition would be more central and aggregated in those who inhaled more quickly due to increased turbulent airflow and impaction. Another limitation was the lack of any direct measurement of emphysema through dosimetry of high-resolution CT scans. Regarding limitations in imaging analysis, it must be noted that both $Vent_{Non}$ and 'hot spots' do not contain any topographical information and the distances of $Vent_{Non}$ regions or 'hot spots' relative to proximal or peripheral lung regions were unknown. A potential approach is segmenting the CT masks into peripheral and proximal regions of interest. Generally, segmentation is an unstandardised technique (65), where regions are defined arbitrarily e.g., outer shell is 2/3 of total lung volume (66). More accurate definitions for these regions may instead be based on the generation of airways, which can be visualised and defined even with low dose CT scans (67). Airways beyond CT resolution such as $>12^{th}$ generation could then be segmented into a peripheral region of interest (68). Furthermore, masks or outlines

of the airways could also be obtained through automated algorithms (69, 70) to determine locations of $Vent_{Non}$ regions and ‘hot spots’.

3.5.5 Conclusions

In summary, our study observed that measurements of non-ventilation in VSPECT/CT correlated strongly with lung function parameters associated with emphysema whereas a greater number of ‘hot spots’ correlated with lung function parameters associated with airflow impairment and ventilation heterogeneity. Both imaging parameters were unrelated to each other, suggesting that these parameters provide distinct and complementary information in patients with COPD.

3.6 References

1. Piqueras MGC, Cosio MG. Disease of the airways in chronic obstructive pulmonary disease. European Respiratory Journal. 2001;18(34 suppl):41s.
2. Jögi J, Jonson B, Ekberg M, Bajc M. Ventilation–Perfusion SPECT with 99mTc-DTPA Versus Technegas: A Head-to-Head Study in Obstructive and Nonobstructive Disease. Journal of Nuclear Medicine. 2010;51(5):735.
3. Satoh K, Nakano S, Tanabe M, Nishiyama Y, Takahashi K, Kobayashi T, Honjo N, Sasaki M, et al. A clinical comparison between Technegas SPECT, CT, and pulmonary function tests in patients with emphysema. Radiat Med. 1997;15(5):277-82.
4. Bajc M, Chen Y, Wang J, Li XY, Shen WM, Wang CZ, Huang H, Lindqvist A, et al. Identifying the heterogeneity of COPD by V/P SPECT: a new tool for improving the diagnosis of parenchymal defects and grading the severity of small airways disease. Int J Chron Obstruct Pulmon Dis. 2017;12:1579-87.
5. Radadia N, Friedlander Y, Priel E, Konyer NB, Huang C, Jamal M, Farncombe T, Marriott C, et al. Comparison of ventilation defects quantified by Technegas SPECT and hyperpolarized 129Xe MRI. Frontiers in Physiology. 2023;14.
6. Kirby M, Svenningsen S, Owrangi A, Wheatley A, Farag A, Ouriadov A, Santyr GE, Etemad-Rezai R, et al. Hyperpolarized 3He and 129Xe MR Imaging in Healthy Volunteers and Patients with Chronic Obstructive Pulmonary Disease. Radiology. 2012;265(2):600-10.
7. Cuña EG, Gambini JP, Servente L, Savio E, Engler HW, González GA, Alonso O. Quantitative comparison between single-photon emission computed tomography and positron emission tomography imaging of lung ventilation with (99m)Tc-technegas and (68)Ga-gallgas in patients with chronic obstructive pulmonary disease: A pilot study. World J Nucl Med. 2019;18(3):251-7.
8. Jobse BN, Rhem RG, McCurry CA, Wang IQ, Labiris NR. Imaging lung function in mice using SPECT/CT and per-voxel analysis. PLoS One. 2012;7(8):e42187.
9. Santolicandro A, Ruschi S, Fornai E, Giuntini C. Imaging of ventilation in chronic obstructive pulmonary disease. J Thorac Imaging. 1986;1(2):36-53.
10. Jögi J, Ekberg M, Jonson B, Bozovic G, Bajc M. Ventilation/perfusion SPECT in chronic obstructive pulmonary disease: an evaluation by reference to symptoms, spirometric lung function and emphysema, as assessed with HRCT. Eur J Nucl Med Mol Imaging. 2011;38(7):1344-52.
11. Bajc M, Markstad H, Jarenbäck L, Tufvesson E, Bjermer L, Jögi J. Grading obstructive lung disease using tomographic pulmonary scintigraphy in patients with chronic obstructive pulmonary disease (COPD) and long-term smokers. Ann Nucl Med. 2015;29(1):91-9.
12. Hogg JC, Macklem PT, Thurlbeck WM. Site and Nature of Airway Obstruction in Chronic Obstructive Lung Disease. New England Journal of Medicine. 1968;278(25):1355-60.
13. McDonough JE, Yuan R, Suzuki M, Seyednejad N, Elliott WM, Sanchez PG, Wright AC, Gefter WB, et al. Small-Airway Obstruction and Emphysema in Chronic Obstructive Pulmonary Disease. New England Journal of Medicine. 2011;365(17):1567-75.
14. Hogg JC, Chu F, Utokaparch S, Woods R, Elliott WM, Buzatu L, Cherniack RM, Rogers RM, et al. The Nature of Small-Airway Obstruction in Chronic Obstructive Pulmonary Disease. New England Journal of Medicine. 2004;350(26):2645-53.
15. Pisi R, Aiello M, Zanini A, Tzani P, Paleari D, Marangio E, Spanevello A, Nicolini G, et al. Small airway dysfunction and flow and volume bronchodilator responsiveness in patients with chronic obstructive pulmonary disease. International Journal of Chronic Obstructive Pulmonary Disease. 2015;10(null):1191-7.
16. Johns DP, Walters JA, Walters EH. Diagnosis and early detection of COPD using spirometry. J Thorac Dis. 2014;6(11):1557-69.
17. Berger KI, Pradhan DR, Goldring RM, Oppenheimer BW, Rom WN, Segal LN. Distal airway dysfunction identifies pulmonary inflammation in asymptomatic smokers. ERJ Open Res. 2016;2(4).

18. Faria AC, Costa AA, Lopes AJ, Jansen JM, Melo PL. Forced oscillation technique in the detection of smoking-induced respiratory alterations: diagnostic accuracy and comparison with spirometry. Clinics (Sao Paulo). 2010;65(12):1295-304.
19. Jones PW, Harding G, Berry P, Wiklund I, Chen WH, Leidy NK. Development and first validation of the COPD Assessment Test. European Respiratory Journal. 2009;34(3):648.
20. Graham BL, Steenbruggen I, Miller MR, Barjaktarevic IZ, Cooper BG, Hall GL, Hallstrand TS, Kaminsky DA, et al. Standardization of Spirometry 2019 Update. An Official American Thoracic Society and European Respiratory Society Technical Statement. American Journal of Respiratory and Critical Care Medicine. 2019;200(8):e70-e88.
21. Graham BL, Brusasco V, Burgos F, Cooper BG, Jensen R, Kendrick A, MacIntyre NR, Thompson BR, et al. 2017 ERS/ATS standards for single-breath carbon monoxide uptake in the lung. European Respiratory Journal. 2017;49(1):1600016.
22. Wanger J, Clausen JL, Coates A, Pedersen OF, Brusasco V, Burgos F, Casaburi R, Crapo R, et al. Standardisation of the measurement of lung volumes. European Respiratory Journal. 2005;26(3):511-22.
23. Philip HQ, Sanja S, Tim JC, Xaver B, Graham LH, Bruce HC, Paul LE, John LH, et al. Multi-ethnic reference values for spirometry for the 3–95-yr age range: the global lung function 2012 equations. European Respiratory Journal. 2012;40(6):1324.
24. Graham LH, Nicole F, Gregg R, Tolu O, Bruce T, Jane K, Irene S, Brendan GC, et al. Official ERS technical standard: Global Lung Function Initiative reference values for static lung volumes in individuals of European ancestry. European Respiratory Journal. 2021;57(3):2000289.
25. “Official ERS technical standards: Global Lung Function Initiative reference values for the carbon monoxide transfer factor for Caucasians.” Sanja Stanojevic, Brian L. Graham, Brendan G. Cooper, Bruce R. Thompson, Kim W. Carter, Richard W. Francis and Graham L. Hall on behalf of the Global Lung Function Initiative T_{LCO} working group. Eur Respir J 2017; 50: 1700010. European Respiratory Journal. 2020;56(4):1750010.
26. Brown NJ, Xuan W, Salome CM, Berend N, Hunter ML, Musk AW, James AL, King GG. Reference equations for respiratory system resistance and reactance in adults. Respiratory Physiology & Neurobiology. 2010;172(3):162-8.
27. Crawford AB, Davison A, Amis TC, Engel LA. Intrapulmonary distribution of 99mtechnetium labelled ultrafine carbon aerosol (Technegas) in severe airflow obstruction. Eur Respir J. 1990;3(6):686-92.
28. Amis TC, Crawford AB, Davison A, Engel LA. Distribution of inhaled 99mtechnetium labelled ultrafine carbon particle aerosol (Technegas) in human lungs. European Respiratory Journal. 1990;3(6):679.
29. Lemb M, Oei T, Eifert H, Günther B. Technegas: a study of particle structure, size and distribution. European journal of nuclear medicine. 1993;20:576-9.
30. Farrow CE, Salome CM, Harris BE, Bailey DL, Bailey E, Berend N, Young IH, King GG. Airway closure on imaging relates to airway hyperresponsiveness and peripheral airway disease in asthma. J Appl Physiol (1985). 2012;113(6):958-66.
31. Farrow CE, Salome CM, Harris BE, Bailey DL, Berend N, King GG. Peripheral ventilation heterogeneity determines the extent of bronchoconstriction in asthma. Journal of Applied Physiology. 2017;123(5):1188-94.
32. Rutting S, Mahadev S, Tonga KO, Bailey DL, Dame Carroll JR, Farrow CE, Thamrin C, Chapman DG, et al. Obesity alters the topographical distribution of ventilation and the regional response to bronchoconstriction. Journal of Applied Physiology. 2019;128(1):168-77.
33. Kroon D-J. Region Growing: MATLAB Central File Exchange; 2008 [Available from: https://au.mathworks.com/matlabcentral/fileexchange/19084-region-growing.
34. Koltai H. Novel 3D Segmentation Methods for SPECT Images of Airway Disease: The University of Sydney; 2021.

35. Tim JS, Klaus HM, John Fitz G, william MB, Rodney JB, Christopher L, Graham AH. The Physical and Chemical Nature of Technegas. Journal of Nuclear Medicine. 1997;38(8):1327.
36. Burch WM, Sullivan PJ, McLaren CJ. Technegas--a new ventilation agent for lung scanning. Nucl Med Commun. 1986;7(12):865-71.
37. Isawa T, Teshima T, Anazawa Y, Miki M, Motomiya M. Technegas for inhalation lung imaging. Nucl Med Commun. 1991;12(1):47-55.
38. King GG, Harris B, Mahadev S. V/Q SPECT: Utility for Investigation of Pulmonary Physiology. Seminars in Nuclear Medicine. 2010;40(6):467-73.
39. Hogg JC, McDonough JE, Sanchez PG, Cooper JD, Coxson HO, Elliott WM, Naiman D, Pochettino M, et al. Micro-computed tomography measurements of peripheral lung pathology in chronic obstructive pulmonary disease. Proc Am Thorac Soc. 2009;6(6):546-9.
40. Milne S, King GG. Advanced imaging in COPD: insights into pulmonary pathophysiology. J Thorac Dis. 2014;6(11):1570-85.
41. Diaz AA, Valim C, Yamashiro T, Estépar RSJ, Ross JC, Matsuoka S, Bartholmai B, Hatabu H, et al. Airway Count and Emphysema Assessed by Chest CT Imaging Predicts Clinical Outcome in Smokers. Chest. 2010;138(4):880-7.
42. Scott KW, Steiner GM. Postmortem assessment of chronic airways obstruction by tantalum bronchography. Thorax. 1975;30(4):405-14.
43. Okajima Y, Come CE, Nardelli P, Sonavane SK, Yen A, Nath HP, Terry N, Grumley SA, et al. Luminal Plugging on Chest CT Scan: Association With Lung Function, Quality of Life, and COPD Clinical Phenotypes. Chest. 2020;158(1):121-30.
44. Morrell NW, Wignall BK, Biggs T, Seed WA. Collateral ventilation and gas exchange in emphysema. Am J Respir Crit Care Med. 1994;150(3):635-41.
45. Terry PB, Traystman RJ, Newball HH, Batra G, Menkes HA. Collateral Ventilation in Man. New England Journal of Medicine. 1978;298(1):10-5.
46. Ross JC, Ley GD, Krumholz RA, Rahbari H. A Technique for Evaluation of Gas Mixing in the Lung: Studies in Cigarette Smokers and Nonsmokers. American Review of Respiratory Disease. 1967;95(3):447-53.
47. Hughes JMB, Pride NB. Examination of the Carbon Monoxide Diffusing Capacity (DlCO) in Relation to Its Kco and Va Components. American Journal of Respiratory and Critical Care Medicine. 2012;186(2):132-9.
48. Roberts CM, MacRae KD, Seed WA. Multi-breath and single breath helium dilution lung volumes as a test of airway obstruction. Eur Respir J. 1990;3(5):515-20.
49. Carvalho TC, Peters JI, Williams RO. Influence of particle size on regional lung deposition – What evidence is there? International Journal of Pharmaceutics. 2011;406(1):1-10.
50. Le Roux PY, Schafer WM, Blanc-Beguin F, Tulchinsky M. Ventilation Scintigraphy With Radiolabeled Carbon Nanoparticulate Aerosol (Technegas): State-of-the-Art Review and Diagnostic Applications to Pulmonary Embolism During COVID-19 Pandemic. Clin Nucl Med. 2023;48(1):8-17.
51. Wollmer P. Aerosolised radionuclides for functional imaging in COPD/asthma. Clinical and Translational Imaging. 2014;2(5):403-13.
52. Carroll JRD, Magnussen JS, Berend N, Salome CM, King GG. Greater parallel heterogeneity of airway narrowing and airway closure in asthma measured by high-resolution CT. Thorax. 2015;70(12):1163-70.
53. Verbanck S, Schuermans D, Vincken W. Small airways ventilation heterogeneity and hyperinflation in COPD: response to tiotropium bromide. Int J Chron Obstruct Pulmon Dis. 2007;2(4):625-34.
54. Neder JA, O'Donnell CDJ, Cory J, Langer D, Ciavaglia CE, Ling Y, Webb KA, O'Donnell DE. Ventilation Distribution Heterogeneity at Rest as a Marker of Exercise Impairment in Mild-to-Advanced COPD. COPD: Journal of Chronic Obstructive Pulmonary Disease. 2015;12(3):252-9.

55. Pisi R, Aiello M, Calzetta L, Frizzelli A, Alfieri V, Bertorelli G, Pisi G, Chetta A. Ventilation Heterogeneity in Asthma and COPD: The Value of the Poorly Communicating Fraction as the Ratio of Total Lung Capacity to Alveolar Volume. Respiration. 2021;100(5):404-10.
56. Desiraju K, Agrawal A. Impulse oscillometry: The state-of-art for lung function testing. Lung India. 2016;33(4):410-6.
57. Gregory GK, Jason B, Kenneth IB, Peter C, Pedro LdM, Raffaele LD, Ramon F, Graham LH, et al. Technical standards for respiratory oscillometry. European Respiratory Journal. 2020;55(2):1900753.
58. Milne S, Jetmalani K, Chapman DG, Duncan JM, Farah CS, Thamrin C, King GG. Respiratory system reactance reflects communicating lung volume in chronic obstructive pulmonary disease. Journal of Applied Physiology. 2019;126(5):1223-31.
59. Bhansali PV, Irvin CG, Dempsey JA, Bush R, Webster JG. Human pulmonary resistance: effect of frequency and gas physical properties. J Appl Physiol Respir Environ Exerc Physiol. 1979;47(1):161-8.
60. Oostveen E, Peslin R, Duvivier C, Rotger M, Mead J. Airways impedance during single breaths of foreign gases. Journal of Applied Physiology. 1991;71(5):1813-21.
61. D. E O, Donnell, Laveneziana P. Physiology and consequences of lung hyperinflation in COPD. European Respiratory Review. 2006;15(100):61.
62. McNulty W, Usmani OS. Techniques of assessing small airways dysfunction. European Clinical Respiratory Journal. 2014;1(1):25898.
63. Usmani OS, Dhand R, Lavorini F, Price D. Why We Should Target Small Airways Disease in Our Management of Chronic Obstructive Pulmonary Disease. Mayo Clinic Proceedings. 2021;96(9):2448-63.
64. Turato G, Zuin R, Miniati M, Baraldo S, Rea F, Beghé B, Monti S, Formichi B, et al. Airway Inflammation in Severe Chronic Obstructive Pulmonary Disease. American Journal of Respiratory and Critical Care Medicine. 2002;166(1):105-10.
65. Biddiscombe MF, Meah SN, Underwood SR, Usmani OS. Comparing Lung Regions of Interest in Gamma Scintigraphy for Assessing Inhaled Therapeutic Aerosol Deposition. Journal of Aerosol Medicine and Pulmonary Drug Delivery. 2011;24(3):165-73.
66. Hannan W, Emmett P, Aitken R, Love R, Millar A, Muir A. Effective penetration of the lung periphery using radioactive aerosols: concise communication. Journal of Nuclear Medicine: Official Publication, Society of Nuclear Medicine. 1982;23(10):872-7.
67. Dijkstra AE, Postma DS, ten Hacken N, Vonk JM, Oudkerk M, van Ooijen PMA, Zanen P, Mohamed Hoesein FA, et al. Low-dose CT measurements of airway dimensions and emphysema associated with airflow limitation in heavy smokers: a cross sectional study. Respiratory Research. 2013;14(1):11.
68. Dijkstra AE, Postma DS, ten Hacken N, Vonk JM, Oudkerk M, van Ooijen PM, Zanen P, Mohamed Hoesein FA, et al. Low-dose CT measurements of airway dimensions and emphysema associated with airflow limitation in heavy smokers: a cross sectional study. Respir Res. 2013;14(1):11.
69. Mayer D, Bartz D, Fischer J, Ley S, del Río A, Thust S, Kauczor HU, Heussel CP. Hybrid segmentation and virtual bronchoscopy based on CT images. Acad Radiol. 2004;11(5):551-65.
70. Tschirren J, Hoffman EA, McLennan G, Sonka M. Intrathoracic airway trees: segmentation and airway morphology analysis from low-dose CT scans. IEEE Trans Med Imaging. 2005;24(12):1529-39.

Chapter 4 – Effects of bronchodilator on Ventilation Single Photon Emission Computed Tomography Imaging in COPD

4.1 Abstract

Introduction: COPD is a complex and heterogeneous disease, and the effects of bronchodilator remain unclear. Bronchodilator response is measured with spirometry, but the test is inadequate in assessing the complex pathophysiology of the disease. VSPECT/CT may provide greater insight on the effects of bronchodilator on ventilation in COPD. Our objective was to examine the effects of bronchodilator on non-ventilated volume and 'hot spots' count in COPD with VSPECT/CT.

Methods: 22 COPD participants underwent baseline lung function testing, consisting of spirometry, body plethysmography, gas diffusion (D_{LCO}), and oscillometry in the first visit. The first visit then concluded with a baseline VSPECT/CT scan. The second visit consisted of pre- and post-bronchodilator (400 µg salbutamol) spirometry and oscillometry and a post-bronchodilator VSPECT/CT scan. Non-ventilated volume ($Vent_{Non}$) and 'hot spots' were defined with the curve-fitting threshold method.

Results: Neither $Vent_{Non}$ nor 'hot spots' count significantly increased post-bronchodilator. However, the responses for both VSPECT/CT parameters were highly variable. There was a significant relationship between increased $Vent_{Non}$ and decreased resistance at 5 Hz (R5) post-bronchodilator ($r = -0.51$; $p = 0.02$).

Conclusion: VSPECT/CT appears to be sensitive to the effects of bronchodilator on ventilation. We speculate that the changes in $Vent_{Non}$ post-bronchodilator to possibly reflect airway recruitment and redistribution of ventilation. Alternative imaging analysis methods such as topographical analysis in peripheral lung regions should be examined.

4.2 Introduction

Chronic obstructive pulmonary disease (COPD) involves highly heterogeneous pathology including small airway narrowing, emphysema and mucus plugging. For both initial and long-term pharmacological therapy, bronchodilators are essential (1), and the response in lung function to bronchodilator is assessed with spirometry alone. However, bronchodilators are known to produce significant improvements beyond FEV1 such as symptoms (2), small airway function (3, 4), and lung volumes relating to hyperinflation and gas trapping (5, 6). The discordance between spirometry and other lung function tests is likely due to the former's measurements primarily reflecting the larger proximal airways as it is measured throughout the lung volume range. A three-dimensional imaging technique such as ventilation single-photon emission computed tomography/computed tomography (VSPECT/CT) can visualise and estimate the extent of non-ventilation and presence of ventilation abnormalities. Despite differing analysis methods, VSPECT parameters are shown to consistently relate with COPD disease severity (7-9). The use of VSPECT/CT may be able to provide additional insight into the responses in ventilation to bronchodilator in people with COPD.

Utilising our novel curve-fitting method, VSPECT/CT provides two complementary quantifiable parameters of lung function – non-ventilated volume and number of clusters of aggregated Technegas particles, termed hot spots. We have shown that increased non-ventilated volume related to lung function measurements associated with worse gas diffusion and gas trapping, whereas hot spots primarily related to lung function measurements associated with airflow impairment and ventilation

heterogeneity (Chapter 3). The effects of bronchodilator on ventilation in COPD have almost exclusively been examined with hyperpolarised noble gas magnetic resonance imaging (MRI), and results generally indicate that non-ventilated volume is significantly reduced post-bronchodilator (10-12). However, non-ventilated volume as measured by MRI significantly differ from VSPECT/CT measurements (7), and it is currently unknown if the latter ventilation imaging method is also sensitive to the effects of bronchodilator in COPD. 'Hot spots' are observed to occur more frequently in more severe COPD patients (8), and although the effects of bronchodilator have yet to be examined with 'hot spots' count, they have been previously noted to decrease in number following interventions such as lung volume reduction surgery (13) and continuous positive airway pressure (CPAP) (14). 'Hot spots' count may be used to indicate the change from turbulent to laminar airflow in response to bronchodilation. It is also unknown whether changes to small airway function post-bronchodilator, as measured with oscillometry, correlate with changes in either of the VSPECT/CT parameters.

Therefore, the aims for our study were to 1) examine the effects of bronchodilator on non-ventilated volume and 'hot spots' count in COPD with VSPECT/CT, 2) determine whether changes in non-ventilated volume and 'hot spots' relate to changes in spirometric and oscillometric measurements, 3) determine whether baseline VSPECT/CT predict changes in spirometry or oscillometry post-bronchodilator, and 4) determine whether baseline lung function predict changes in VSPECT/CT.

4.3 Methods

4.3.1 Participants and Study Design

23 participants with physician diagnosed COPD (13 men, 10 women) were recruited from the Department of Respiratory Medicine at Royal North Shore Hospital. The inclusion criteria were as follows: 18 – 80 years old, physician diagnosed COPD, and a smoking history of at least 10 pack years. Exclusion criteria were other active or chronic respiratory diseases, history of lung surgery, history of chronic kidney disease, significant cardiac disease, intensive care unit admissions in the last 12 months, and significant respiratory infection or documented exacerbation within the previous 6 weeks. All participants provided written, informed consent. The study was approved by the local Human Research Ethics Committee (Northern Sydney Local Health District, RESP/18/198)

Participants attended two visits. At the first visit, baseline lung function testing, and VSPECT/CT scans were completed as detailed in the previous chapter (Chapter 3). For the second visit, participants underwent oscillometry and spirometry testing prior to being administered 400 μg of salbutamol, followed by post-bronchodilator oscillometry and spirometry testing. The second visit concluded with a VSPECT scan but no CT scan. The VSPECT scan from the second visit was registered to the baseline CT scan. As participants were tested on two separate visits, often beyond a week apart, we required the FEV1 for both visits to be within 200 mL of each other. Participants with FEV1 difference >200 mL were excluded from analysis. Participants withheld short-acting bronchodilators for at least 6 hours and LABA and/or LAMA medication for 24 hours prior to each visit. The study design is shown in Figure 1.

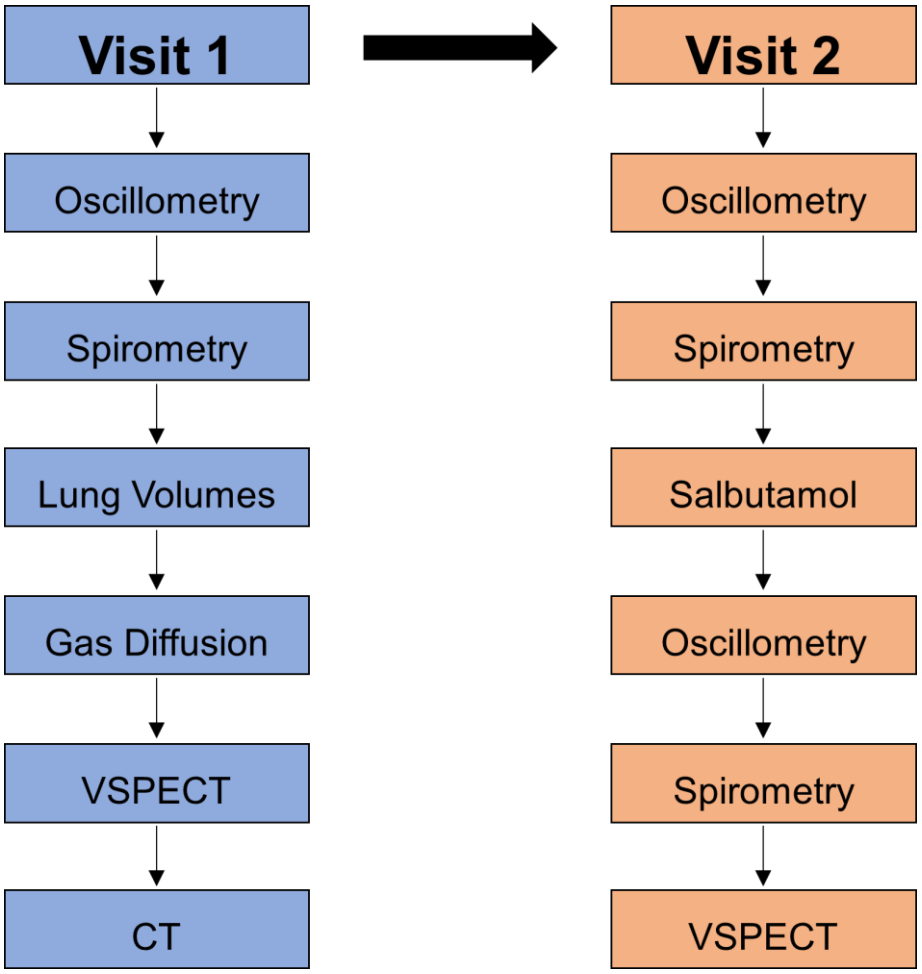


Figure 1: Study design. Visit 1 consisted of the baseline ventilation single-photon emission computed (VSPECT) and computed tomography (CT) scan. Visit 2 involved pre and post bronchodilator spirometry and oscillometry (FOT) testing, and a post-BD VSPECT scan. The VSPECT scan from Visit 2 was registered to the CT scan from the Visit 1. VSPECT = ventilation single-photon emission computed tomography; CT = computed tomography;

4.3.2 Lung Function Testing

Spirometry was performed with a MGC Diagnostics CPFS/D USB spirometer and MGC Breeze Suite interface (v. 8.6.0.56, MGC Diagnostics Corporation, Saint Paul), according to American Thoracic Society (ATS)/European Respiratory Society (ERS) criteria (15). Body plethysmography and gas diffusion (D_{LCO}) were also performed with according to ATS/ERS guidelines (16, 17).

Oscillometry was performed with the tremoFlo C-100 oscillometry system (v. 1.0.43.44, Thorasys Thoracic Medical Systems Inc, Montreal) at 5 – 37 Hz. Device calibration was performed prior to the testing session. Following the ERS technical standards (18), participants underwent at least 3 breathing measurements. For each measurement, the participant was instructed to breathe tidally in a seated position and support their cheeks for 60 seconds, whilst wearing a nose clip. The mean resistance (R5) and reactance (X5), both at 5 Hz, were then obtained. Measurements with signs of leak, coughs, swallows, or incorrect technique were excluded for quality control. A R5 coefficient of variation ≤ 10% was required for each testing session.

A significant bronchodilator response for spirometry was defined by a 200 mL and 12% increase in FEV1 or FVC as defined by ATS/ERS 2005 guidelines (19). For oscillometric parameters, significant bronchodilator response was defined as a 30% reduction (or -1.42 z-scores) for R5 or an increase of 0.57 $cmH_2O \cdot s \cdot L^{-1}$ (or 1.36 z-scores) for X5 according to Jetmalani et al. (20).

The z-scores for spirometry, body plethysmography, and diffusing capacity were determined with reference equations from the Global Lung Initiative (GLI) (21-23). Reference equations from Brown et al. instead of Oostveen et al. were used to calculate FOT z-scores (24) as one participant's weight was outside the range of the latter's reference equations.

4.3.3 Ventilation Imaging

VSPECT/CT Imaging was conducted at the Department of Nuclear Medicine, Royal North Shore Hospital, using a Siemens Symbia T16 SPECT/CT system. Technegas, consisting of 100 nm Technetium (^{99m}Tc) carbon nanoparticles, was used as the ventilation agent. The inhaled distribution of Technegas has been demonstrated to resemble gas, even in participants with severe airway obstruction (25), and its distribution should also remain fixed for at least 20 minutes after inhalation (26, 27).

Participants were required to breathe in 500 – 700 mL of Technegas from functional residual capacity (FRC) at approximately 0.5 – 1 L/sec in a seated, upright position. The volume and flow rate of each inhalation was monitored with a MGC Diagnostics CPFS/D USB spirometer and MGC Breeze Suite interface (v. 8.6.0.56, MGC Diagnostics Corporation, Saint Paul). Two to four inhalations were generally taken to achieve the required radioactivity of approximately 1.5 – 2.0 kilocounts/s, and approximately 40 mBq of Technegas was inhaled.

Since the CT scan from the first visit was registered to both baseline and post-bronchodilator VSPECT scans, participants were also administered with 400 µg of salbutamol in the first visit. However, this occurred after the participants had inhaled Technegas, preserving baseline ventilation in the 1st visit but allowing the CT scan to register with the post-bronchodilator VSPECT scan as well. Contrast bead markers placed on the suprasternal notch, xiphisternum, and 12th ribs, respectively, were used to register the scans.

Supine VSPECT and low dose CT scans (30 mA, 110 kVp, pitch 1.5, slice thickness 3 mm) were acquired with a 128 x 128 matrix and 512 x 512 matrix, respectively. Participants breathed tidally throughout the VSPECT scan, but they were then instructed to hold their breath at FRC for the CT scan. Following the settings on other human VSPECT studies (28-30), VSPECT acquisitions employed 60 stops x2 projections (total 120 projections), 15 seconds per stop, non-circular clockwise orbit and continuous acquisition.

4.3.4 Image Reconstruction and Registration

Using 128 slices, VSPECT images were reconstructed with an ordered subset expectation maximization (OSEM) Siemens Flash 3D algorithm, CT-based attenuation correction, and a Gaussian filter. CT image reconstruction was completed with a 512 x 512 matrix and OSEM Siemens Flash 3D algorithm. Both VSPECT and CT images were converted to Digital Imaging and Communication in Medicine (DICOM) file format.

VSPECT and CT scans were registered using the known, fixed spatial relationship between the VSPECT and CT scanners. The DICOM files of both scans were then transferred onto a HERMES (Nuclear Diagnostics, Stockholm, Sweden) workstation. The matrix size of the VSPECT scan was increased from 128 x 128 matrix to 512 x 512, and the original counts remained preserved. Additional three-dimensional registration was completed with the multimodality software package on HERMES by visually aligning the markers on the VSPECT and CT scans.

4.3.5 Imaging Analysis

Lung outlines on the CT scans were defined through a region growing algorithm (31) and Otsu's method (32) that had been implemented within a MATLAB script (R2019b, MathWorks, Natick) (33). The script produced a binarised mask of the lung outlines, which was applied onto the VSPECT scan (Figure 1). All VSPECT voxel activity outside of the lung borders were set to 0. VSPECT voxel data within the mask were exported onto Microsoft Excel (2021, Microsoft, Redmond).

Non-ventilated volume ($Vent_{Non}$) and 'hot spots' were defined through the same curve-fitting threshold method described in Chapter 2 and 3. To summarize, the cumulative voxel frequency was first plotted against activity, and the slopes of each data point were then calculated. The initial activity value ≥ 90% cumulative frequency with a slope ≤ 0.010 was selected as the 'slope point'. Voxels < 30% x the 'slope point' were determined to be $Vent_{Non}$. $Vent_{Non}$ was expressed as a percentage of total lung volume, which had been derived from the CT mask of the lungs. Voxels ≥ the 'slope point' were determined to be 'hot spot' activity. To count the number of 'hot

spots' in three-dimensional space, the masked VSPECT image was first opened in Fiji (National Institutes of Health, United States of America). Secondly, the VSPECT image was binarized, in which all voxel activity < the 'slope point' was set to 0 and all voxel activity ≥ the 'slope point' was set to 255 i.e., the maximum activity in an 8-bit image. Finally, the 3D Objects Counter plugin had been used to count the number of 'hot spots' in three-dimensional space.

4.3.6 Statistical Analysis

GraphPad Prism version 10.0.2 was used to analyse data and generate graphs. All data were expressed as mean ± SD unless otherwise stated. The changes in VSPECT/CT parameters post-bronchodilator were calculated as absolute changes. Normal distribution of the data was determined with a Shapiro-Wilk's test. Differences in imaging parameters and lung function measurements at baseline and post-bronchodilator were assessed with a paired Student's t-test and Wilcoxon's signed-rank test for parametric and non-parametric data, respectively. Correlations between changes in imaging parameters, $Vent_{Non}$ and 'hot spots' count, and lung function measurements post-bronchodilator were examined by Pearson's correlation coefficient. A p-value of < 0.05 was considered statistically significant.

4.4 Results

4.4.1 Participant Demographics

Participant demographics are shown in Table 1. In total, 23 participants with physician diagnosed COPD were recruited for this study. One participant was excluded from analysis as they had been unable to perform the correct inhalation manoeuvre for Technegas. Two participants were also excluded from analysis as their FEV1 differed by more than 200mL between visits.

Table 1: Participant Demographics

Participants, *n*	20
Males/females, *n*	12/8
Age, years	66.7 ± 8.7
BMI, kg/m^2	27.8 ± 6.6
Smoking history, pack years	36.2 ± 22.9
CAT	18.5 ± 6.9

Data presented as mean ± SD. BMI = body mass index; CAT = chronic obstructive pulmonary disease assessment test.

4.4.2 Effect of bronchodilator on lung function and imaging parameters

Lung function and imaging parameters at baseline and post-bronchodilator are shown in Table 2. Following bronchodilator, FEV1 z-score and FEV1/FVC z-score both improved from baseline (p = 0.003 and 0.001, respectively). However, there was no change in FVC z-score (p = 0.16). For oscillometry, there was a significant decrease in R5 z-score (p = 0.05) while there was a trend towards an improvement in X5 z-score (p = 0.06). In total, 10 participants had a significant bronchodilator response; 3 participants had only a spirometric BDR, 5 participants had only an oscillometric BDR, and 2 patients had both a spirometry and oscillometric BDR. There was no mean change in $Vent_{Non}$ or number of hot spots following bronchodilator (p = 0.29 and 0.42, respectively). However, changes in $Vent_{Vol}$ and 'hot spots' count were highly variable (Δ $Vent_{Non}$ and Δ 'hot spots' count range: -16.10 – 19.78 and -5 – 11, respectively) (Figure 2).

Table 2: Baseline and post-bronchodilator lung function and imaging measurements

	Baseline	Post-bronchodilator	p-value
FEV1, z-score	-2.7 ± 1.0	-2.5 ± 1.0	**0.003**
FVC, z-score	-0.6 ± 1.1	-0.4 ± 0.8	0.16
FEV1/FVC, %	47.1 ± 12.1	49.8 ± 13.1	**0.0002**
FEV1/FVC, z-score	-3.4 ± 1.0	-3.1 ± 1.2	**0.001**
R5, z-score	1.4 ± 1.0	1.2 ± 1.1	**0.05**
X5, z-score	-2.7 ± 0.6	-2.6 ± 0.6	0.06
$Vent_{Non}$, % #	48.2 ± 21.0	51.0 ± 19.1	0.29
'Hot spots', n #	6.0 ± 3.0	5.4 ± 3.5	0.42

Data are presented as mean ± SD. FEV1 = forced expiratory volume in 1 second; FVC = forced vital capacity; R5 = respiratory system resistance measured at 5 Hz; X5 = respiratory system reactance measured at 5 Hz; $Vent_{Non}$ = non-ventilated volume. Differences between baseline and post-bronchodilator measurements were examined with a paired Student's t-test for parametric data and Wilcoxon's signed-rank test for nonparametric data. The # symbol indicated nonparametric data.

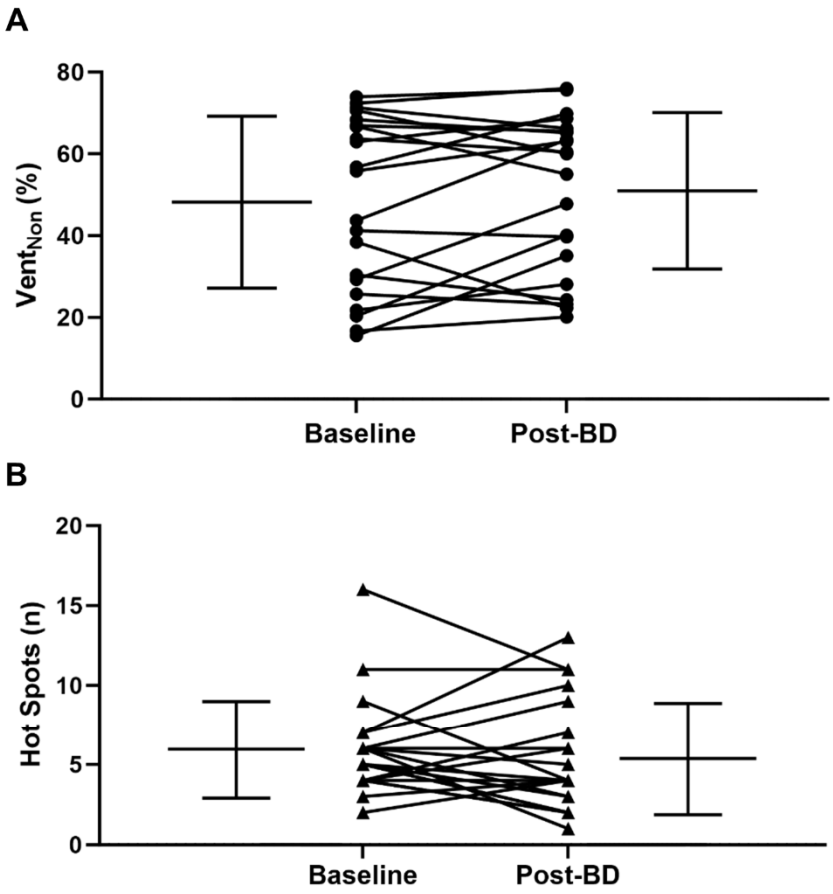


Figure 2: Non-ventilated volume ($Vent_{Non}$) (A) and 'hot spots' count (B) at baseline and bronchodilator visits. Data presented as mean ± standard deviation. Comparisons of $Vent_{Non}$ and 'hot spots' count between baseline and bronchodilator visits were completed with Wilcoxon tests. No significant differences were found for either $Vent_{Non}$ ($p = 0.29$) or 'hot spots' count ($p = 0.42$).

4.4.3 Relationships between changes in non-ventilation and hot spots

There was no correlation between the changes in $Vent_{Non}$ and changes in 'hot spot' count ($r = -0.17$, $p = 0.55$).

4.4.4 Relationships between changes in imaging parameters and lung function

The mean changes ± SD in FEV1 (%), FVC (%), and FEV1/FVC (%) were 8.53 ± 12.26, 3.16 ± 7.53, and 2.6 ± 2.5, respectively. Neither change in $Vent_{Non}$ or change in 'hot spots' count correlated with changes in spirometry measurements (Table 3). The mean changes ± SD for the oscillometric parameters, R5 ($cmH_2O.s.L^{-1}$) and X5 ($cmH_2O.s.L^{-1}$), were -0.31 ± 0.83 and 0.51 ± 0.77, respectively. Change in $Vent_{Non}$ correlated with change in R5, but there was no association between change in 'hot spots' count and change in R5. There were no correlations between changes in $Vent_{Non}$ or 'hot spots' count and change in X5.

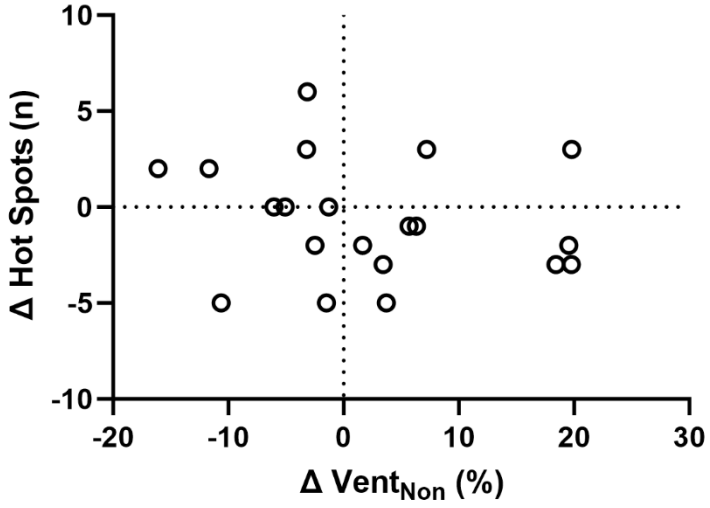


Figure 3: Relationship between changes in non-ventilated volume ($Vent_{Non}$) and 'hot spots' count.

Table 3: Univariate correlations between changes in imaging parameters and lung function measurements post-bronchodilator

	Δ $Vent_{Non}$		Δ Hot Spots	
	r	p-value	r	p-value
Δ FEV1, % #	0.22	0.36	-0.25	0.30
Δ FVC, % #	0.07	0.78	-0.22	0.36
Δ FEV1/FVC, %	0.16	0.50	0.005	0.98
Δ R5, $cmH_2O \cdot s \cdot L^{-1}$	**-0.51**	**0.02**	0.38	0.09
Δ X5, $cmH_2O \cdot s \cdot L^{-1}$	-0.12	0.59	0.14	0.55

Univariate correlations between changes in non-ventilated lung volume ($Vent_{Non}$) and 'hot spots' count and lung function post-bronchodilator using Pearson's correlation coefficient. FEV1 = forced expiratory volume in 1 second; FVC = forced vital capacity; R5 = respiratory system resistance measured at 5 Hz; X5 = respiratory system reactance measured at 5 Hz; # = Spearman's rank correlation coefficient.

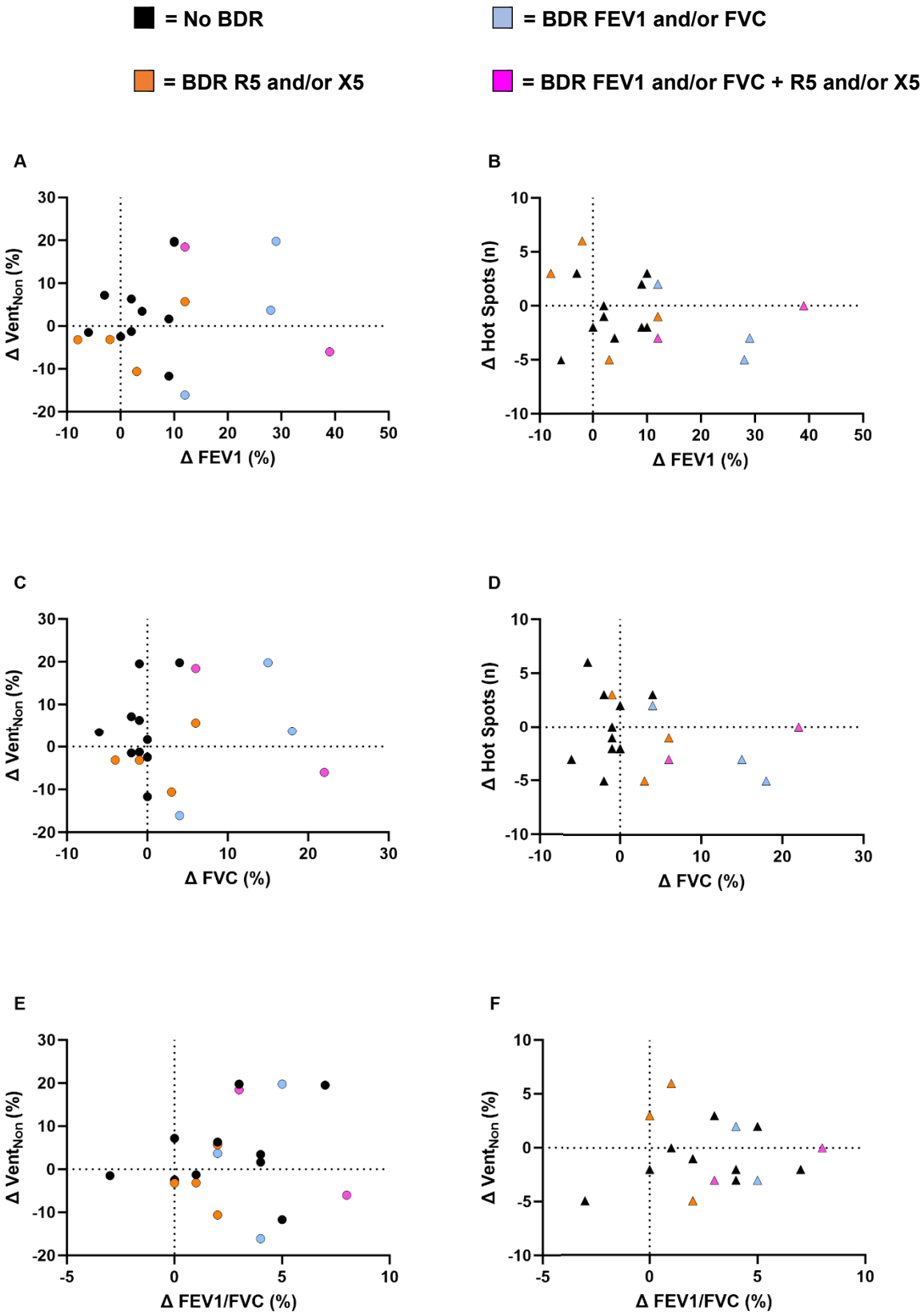

= No BDR
= BDR FEV1 and/or FVC
= BDR R5 and/or X5
= BDR FEV1 and/or FVC + R5 and/or X5
A
Δ VentNon (%)
Δ FEV1 (%)
B
Δ Hot Spots (n)
Δ FEV1 (%)
C
Δ VentNon (%)
Δ FVC (%)
D
Δ Hot Spots (n)
Δ FVC (%)
E
Δ VentNon (%)
Δ FEV1/FVC (%)
F
Δ VentNon (%)
Δ FEV1/FVC (%)

Figure 4: Relationships between changes in non-ventilated volume ($Vent_{Non}$) (A, C, and E) and 'hot spots' count (B, D, F) with changes in forced expiratory volume in 1 second (FEV1), forced vital capacity (FVC), and FEV1/FVC. BDR = significant bronchodilator response; R5 = respiratory system resistance measured at 5 Hz; X5 = respiratory system reactance measured at 5 Hz

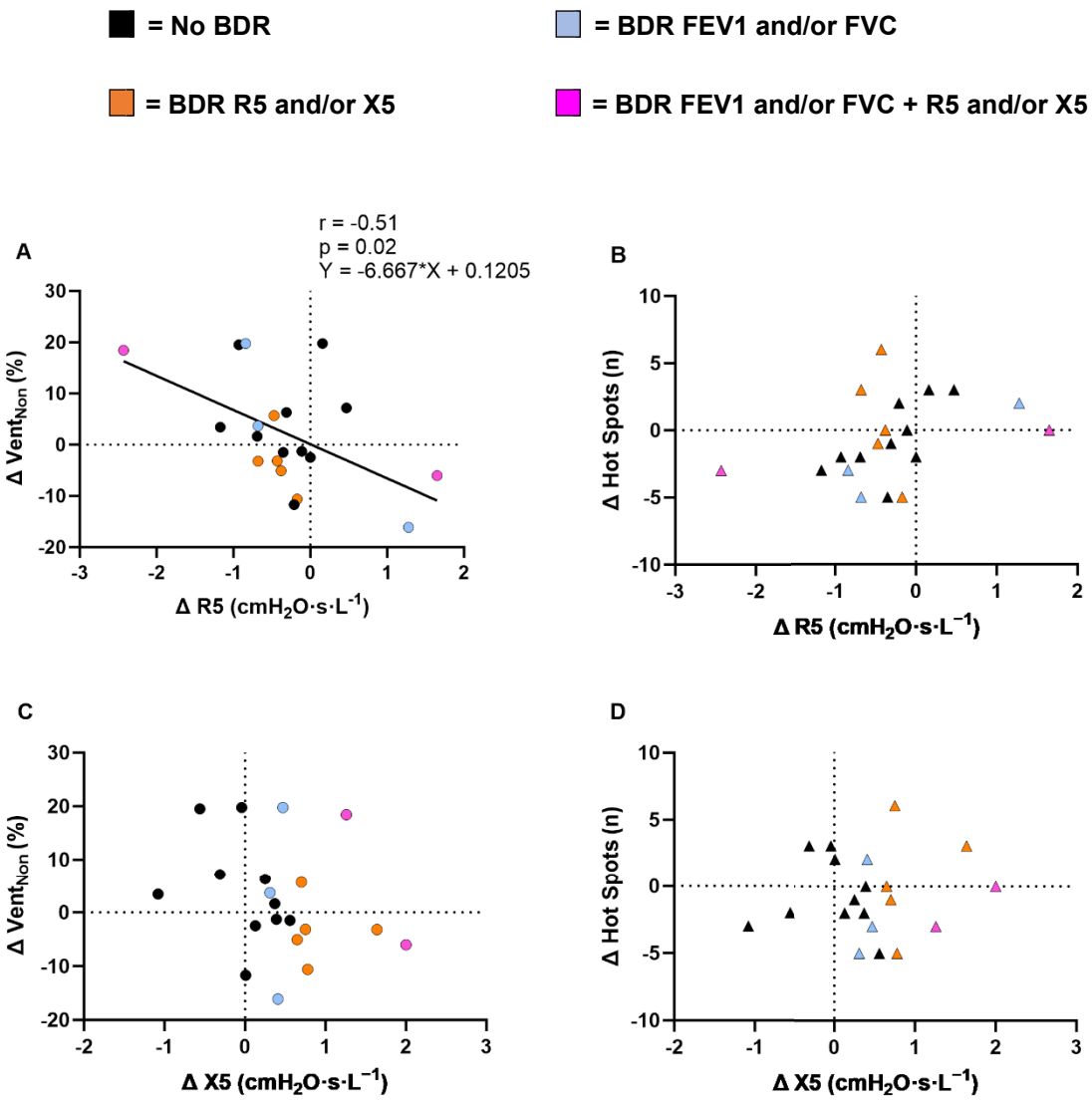


Figure 5: Relationships between changes in non-ventilated volume ($Vent_{Non}$) (A and C) and 'hot spots' count (B and D) with changes in respiratory system resistance measured at 5 Hz (R5) and respiratory system reactance measured at 5 Hz (X5). Using Pearson correlation, $Vent_{Non}$ correlated with the change in R5 (A) (r = -0.51, p = 0.02). BDR = significant bronchodilator response; FEV1 = forced expiratory volume in 1 second; FVC = forced vital capacity.

4.4.5 Relationships between baseline imaging parameters and changes in imaging parameters and lung function

Changes in VSPECT, oscillometric, spirometric parameters were unrelated to pre-bronchodilator $Vent_{Non}$ or 'hot spots' count (Table 4)

4.4.6 Relationships between changes in imaging parameters and baseline lung function

Changes in $Vent_{Non}$ and 'hot spots' count post-bronchodilator were unrelated to pre-bronchodilator lung function measurements (Table 5). The pre-bronchodilator lung function measurements for spirometry and oscillometry were from Visit 2, and lung volumes and gas diffusion measurements were from Visit 1.

Table 4: Univariate correlations between pre-bronchodilator imaging parameters and post-bronchodilator changes in lung function measurements.

	$Vent_{Non}$, % #		Hot spots, n #	
	r	p-value	r	p-value
Δ $Vent_{Non}$, % #	-0.4	0.08	0.2	0.5
Δ Hot spots, n #	-0.1	0.6	-0.2	0.4
Δ FEV1, % #	-0.18	0.46	-0.16	0.51
Δ FVC, % #	0.06	0.82	-0.09	0.72
Δ FEV1/FVC, %	-0.32	0.19	-0.32	0.19
Δ R5, $cmH_2O \cdot s \cdot L^{-1}$	0.12	0.61	-0.24	0.31
Δ X5, $cmH_2O \cdot s \cdot L^{-1}$	0.29	0.21	0.40	0.08

Univariate correlations between changes in non-ventilated lung volume ($Vent_{Non}$) and 'hot spots' count post-bronchodilator and lung function post bronchodilator using Spearman's rank correlation. # = nonparametric variable; FEV1 = forced expiratory volume in 1 second; FVC = forced vital capacity; R5 = respiratory system resistance measured at 5 Hz; X5 = respiratory system reactance measured at 5 Hz; $Vent_{Non}$ = non-ventilated volume.

Table 5: Univariate correlations between changes in imaging parameters post-bronchodilator and pre-bronchodilator lung function measurements.

	Δ $Vent_{Non}$, %		Δ Hot spots, n	
	r	p-value	r	p-value
$Vent_{Non}$, % #	-0.4	0.08	0.2	0.5
Hot spots, n #	-0.1	0.6	-0.2	0.4
FEV1, z-score	-0.2	0.5	0.2	0.3
FVC, z-score	-0.2	0.4	0.3	0.2
FEV1/FVC, %	-0.09	0.7	0.02	0.9
FEV1/FVC, z-score	-0.1	0.6	0.09	0.7
TLC, z-score	-0.05	0.8	0.3	0.3
IC, z-score	0.4	0.1	0.2	0.5
FRC, z-score	-0.2	0.3	0.3	0.3
RV, z-score	-0.2	0.3	0.2	0.3
FRC/TLC, z-score	-0.2	0.4	-0.06	0.8
RV/TLC, z-score	-0.3	0.2	-0.09	0.7
D_{LCO}, z-score	0.06	0.8	0.1	0.7
K_{CO}, z-score	0.1	0.6	-0.04	0.9
VA/TLC	0.08	0.8	0.08	0.7
R5, z-score	0.08	0.1	-0.3	0.2
X5, z-score	0.7	0.6	-0.03	0.9

Univariate correlations between changes in non-ventilated lung volume ($Vent_{Non}$) and ‘hot spots’ count post-bronchodilator and lung function post bronchodilator using Pearson’s correlation coefficient for parametric variables and Spearman’s rank correlation for nonparametric variables. # = nonparametric variable; FEV1 = forced expiratory volume in 1 second; FVC = forced vital capacity; TLC = total lung capacity; IC = inspiratory capacity; FRC = functional residual capacity; RV = residual volume; DLCO = diffusing capacity for carbon monoxide; KCO = carbon monoxide transfer coefficient; VA = alveolar volume; R5 = respiratory system resistance measured at 5 Hz; X5 = respiratory system reactance measured at 5 Hz; $Vent_{Non}$ = non-ventilated volume.

4.5 Discussion

In this study, we demonstrated that bronchodilator had no significant effect on either $Vent_{Non}$ or 'hot spots' and that changes in these parameters were unrelated to each other. However, there was a widely variable response in $Vent_{Non}$ and 'hot spots' count, and we observed that increased $Vent_{Non}$ was associated with decreased R5. Baseline imaging parameters failed to predict response in oscillometry and spirometry. Furthermore, both baseline imaging and lung function parameters were unable to predict the response in $Vent_{Non}$ or 'hot spots' count. To our present knowledge, this is the first VSPECT/CT study to assess the effects of bronchodilator on $Vent_{Non}$ and 'hot spots' in conjunction with spirometry and oscillometry.

4.5.1 The effect of bronchodilator on non-ventilation

In our study there was no significant mean change in $Vent_{Non}$ post-bronchodilator (mean Δ ± SD: 2.7 ± 10.7). This is consistently with a previous VSPECT study by Diba et al. (34) which also reported no mean change in non-ventilated volume. However, other studies that have used different ventilation imaging techniques, such as a hyperpolarised ^{3}He study from Kirby et al. (10) or a ^{129}Xe MRI conference abstract from Smith et al. (35) reported significant improvements in $Vent_{Non}$ following bronchodilator. This may be explained by the substantial differences in the properties of the ventilation agents between VSPECT and hyperpolarised MRI. Technegas is an ultrafine aerosol agent whereas MRI utilises true gas. Therefore, Technegas particles is subject to aerodynamics of airflow, aggregation, and collision, unlike ^{3}He or ^{129}Xe. And so, Technegas may be less sensitive to the effects of bronchodilator. It should also be noted that unlike VSPECT, which scans tidal ventilation (26) throughout 15

minutes, a hyperpolarised MRI scan depicts ventilation at higher lung volumes within a shorter time frame, as the scan is performed during a 10 second 1 L inhalation breath hold from FRC (36). Thus, there is likely to be greater variability in ventilation with VSPECT than MRI. Furthermore, the physiological benefits of bronchodilator on airway recruitment may compound with inspiration-induced airway distension, resulting in greater reductions to non-ventilated volume as visualised with hyperpolarised MRI. Differences in threshold techniques could be another reason why our VSPECT results conflict with the findings from hyperpolarised MRI studies. Indeed, Radadia et al. (7) demonstrated that VSPECT and MRI threshold methods produce significantly different estimations of $Vent_{Non}$ as well as different correlations with lung function and patient demographics. The differences in study protocol and specifically patient demographics could have also been a factor for the conflicting findings. For example, the hyperpolarised ^{3}He study from Kirby et al. (10) exclusively included ex-smokers, and the majority of participants, 93 out of 136, from the ^{129}Xe MRI conference abstract from Smith et al. (35) had mild FEV1 severity. The effects of bronchodilator may be greater visualised in these patient populations.

It is important to consider how the $Vent_{Non}$ threshold method categorises VSPECT data. Specifically, this approach to imaging analysis binarizes the data, defining voxels as either ventilated or non-ventilated activity. However, the binary approach to image analysis cannot distinguish between varying amounts of Technegas deposition as it recognises only the presence of Technegas through a single voxel activity threshold. If bronchodilator had reduced airway narrowing and improved ventilation in poorly ventilated lung regions, without recruiting closed lung regions, then it would not have significantly altered $Vent_{Non}$. Instead, post-bronchodilator

changes may have occurred in the voxel activities and frequencies within the 'ventilated' class, in which improved regional ventilation had increased the frequency of higher activity voxels or decreased voxel activity heterogeneity. Other VSPECT and hyperpolarised MRI studies have attempted to examine ventilation beyond binarised categories, but this involves arbitrary and unvalidated thresholds of varying levels of ventilation (28, 29, 37). Rather than categorising ventilation into 'poorly ventilated' or 'well ventilated' through additional thresholds or simply expressing non-ventilated volume as a percentage of total CT volume, Norberg et al. examined the coefficient of variation in ventilated voxel activity with VSPECT (38, 39). This alternative technique may provide complementary information on ventilation, but further studies are needed to confirm this. The lack of a significant $Vent_{Non}$ response to bronchodilators could also be due to the spatial resolution of VSPECT, which was approximately 7 mm^3. Bronchodilator may have primarily targeted the peripheral lung regions < 7 mm^3, but this is challenged by the findings from Timmins et al. (40), in which peripheral airway closure and ventilation heterogeneity, as measured by oscillometry and multiple breath nitrogen washout, respectively, were unaffected by ICS/LABA treatment in COPD patients. In the previous chapter (Chapter 3), $Vent_{Non}$ was suggested to result from the loss of airways in emphysematous COPD patients (41, 42). If $Vent_{Non}$ in COPD is primarily a result of structural pathologies, then it is not surprising that we would see no significant differences following bronchodilator.

Despite no mean change in $Vent_{Non}$ in the current study, there was very large variability in response, with a maximum increase of 19.78 and maximum decrease of 28.19. This variability contributed to a significant correlation between the change in $Vent_{Non}$ and change in R5. A reduction in $Vent_{Non}$ was associated with an increase in

R5 (i.e. worsening), whereas an increase in $Vent_{Non}$ was associated with a decrease in R5. While seemingly counterintuitive, this relationship may indicate two different physiological responses to bronchodilator, as illustrated in Figure 6. The first response involves the recruitment of airways that had been completely obstructed at baseline, which might reduce $Vent_{Non}$, provided if the dilation was sufficient for stable Technegas deposition from inhalation to scanning. As those airways were closed prior to bronchodilator, they would not have contributed to the measurement of R5. However, if a significant amount of previously obstructed airways were recruited following bronchodilator, thus becoming assessable to 5 Hz pressure waves, but were nonetheless narrow or if they introduced substantial regions or clusters of airway narrowing to FOT, $Vent_{Non}$ and R5 might have decreased and increased, respectively. Both Milne et al. (43) and Baldi et al. (44) have also reported there to be increased airway recruitment and possibly greater ventilated lung volume, post-bronchodilator in COPD. Additionally, bronchodilator, which should typically produce greater dilation and thus reduced R5 by relaxing airway smooth muscle, may have instead caused some airways to partially collapse, thereby increasing R5 but still allowing Technegas deposition. The partial collapse of airways could be attributed to low radial traction from emphysematous destruction of lung parenchyma (45). On the other hand, if bronchodilator caused dilation of narrowed airways that were already ventilated at baseline, both R5 and hyperinflation may be reduced (improve), barring airway collapse. This could lead to greater lung emptying at end-expiratory lung volume. Since $Vent_{Non}$ is calculated as a percent of total lung volume at FRC, then a reduction in hyperinflation with no change in airway closure would lead to an increase of $Vent_{Non}$ and reduced R5. The correlation between improved R5 and reduced hyperinflation, measured with the inspiratory capacity/total lung capacity

ratio (IC/TLC), following bronchodilator in COPD patients has been observed by Milne et al. (43). Previous studies have suggested that the bronchodilator response in COPD may primarily involve the reduction of hyperinflation and gas trapping instead of improvements to FEV1 (5, 6). Both O'Donnell et al. (2) and Belman et al. (46) reported associations between this response and improvements to dyspnoea and exercise endurance. Further studies will be required to confirm the relationship between increased $Vent_{Non}$ and reduced hyperinflation following bronchodilator.

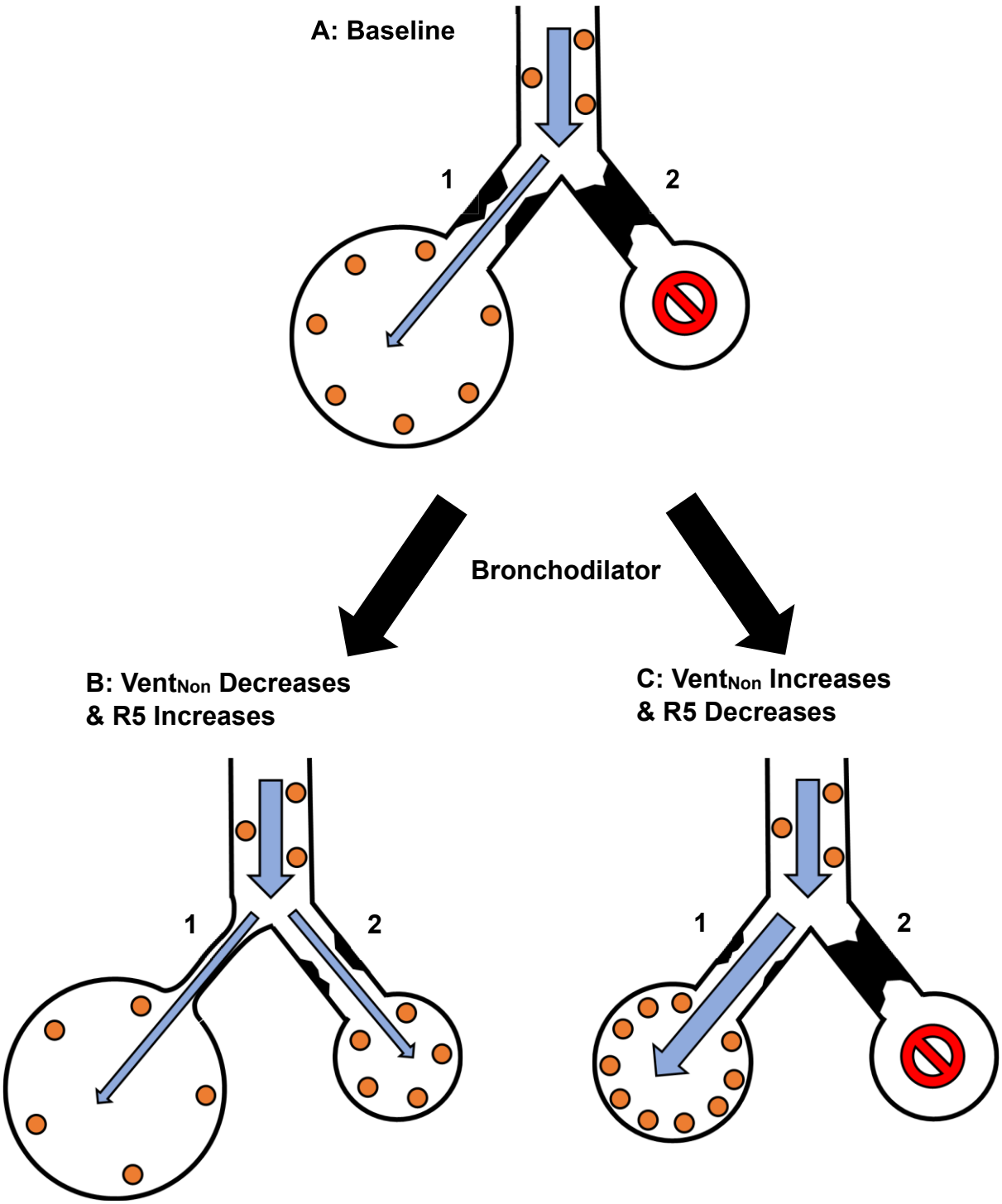


Figure 6: Technegas deposition in airways and alveoli at baseline (A) and two possible outcomes for Technegas deposition post-bronchodilator (B and C). (A) Baseline, one airway (airway 1) is narrowed but ventilated, and the lung region is hyperinflated. The second airway (airway 2) is severely narrowed or completely closed, resulting in a trapped lung region. As airway 2 is closed and the lung region

is trapped, there is no contribution to the measurement of respiratory system resistance (R5). Thus Technegas (depicted with orange circles) is deposited through airway 1 exclusively at baseline. (B) Post-bronchodilator, the narrowing in airway 2 has reduced, leading to ventilation and Technegas deposition. This results in decreased $Vent_{Non}$. However, due to reduced radial traction, the relaxation of airway smooth muscle resulted in airway 1 to partially collapse, decreasing airway lumen diameter. Consequently, airways 1 and 2 and their lung regions contribute to the measurement of R5, and R5 is then increased. The lung region for airway 1 remains hyperinflated. (C) Post-bronchodilator, airway 2 is still closed and non-ventilated, and they do not contribute to the measurement of R5. However, airway 1 becomes further dilated, reducing R5, and its lung region is deflated. As the lung region decreases in size, there is a smaller ventilated space in comparison to baseline. Thus, $Vent_{Non}$ becomes increased.

4.4.2 The effect of bronchodilator on hot spots count

Like $Vent_{Non}$, 'hot spots' count did not significantly change post-bronchodilator (mean Δ ± SD: -0.6 ± 3.0) and the response was also variable (range: 11). Additionally, we found that the change in 'hot spots' count had no relation with change in lung function and that there were no correlations between change in 'hot spots' count and baseline imaging parameters or lung function measurements. To our knowledge, this has been the first study to examine the effects of bronchodilator on 'hot spots' count with VSPECT. We believe that measuring the total 'hot spots' count without topographical analysis is unhelpful for assessing bronchodilator response,

Regarding the increase in 'hot spots' count in some of our participants, we had observed that a large 'hot spot' at baseline occasionally appeared to increase in number by subdividing into smaller 'hot spots' within the approximately same region post-bronchodilator. In these participants, the more numerous but smaller 'hot spots' likely reflect reduced Technegas deposition due to an incomplete transition from turbulent to laminar flow following airway dilation. Additional 'hot spots' were also observed when new lung regions became ventilated post-bronchodilator. Therefore, these additional 'hot spots' could then be markers of ventilation redistribution through recruited airways that were inaccessible at baseline and non-ventilation improving to poor ventilation. Topographical analysis of 'hot spots' following bronchodilator may be used to reveal greater 'penetration' of 'hot spots' into the peripheral lung regions.

We speculate that reduced 'hot spots' count had likely resulted from airway dilation. The dilation of proximal airways would improve airflow and consequently reduce

Technegas aggregation and both ‘hot spot’ count and size. Furthermore, we previously discussed the possible transition from completely or severely obstructed airways to open but narrowed airways following bronchodilator administration (Figure 6). Using positron emission tomography (PET) on asthmatic patients in addition to a computational model of a 12-generation airway tree, Venegas et al. reported that bronchoconstriction had led to large peripheral clusters of ventilation defects (47). This mechanism may also apply to COPD. If so, peripheral clusters of narrowed airways may have been formed post-bronchodilator, and ‘hot spots’ count could have then been reduced as a result from laminar airflow and reduced airflow velocity. Furthermore, the formation of these peripheral clusters could have also improved Technegas penetration into distal lung regions and reduced deposition within the central airways, which are the typical location for ‘hot spots’ (48). In the observed cases of singular ‘hot spots’ segmenting into multiple smaller ‘hot spots’, thereby increasing total ‘hot spots’ count, we speculate that this resulted from narrowed airways ‘de-clustering’ post-bronchodilator. A single ‘hot spot’ within a cluster could be transformed into smaller ‘hot spots’ in different airways once the cluster was removed with bronchodilation. It is interesting to note that both reduced ‘hot spots’ count and size in proximal lung regions and the addition of ‘hot spots’ in new lung regions were occasionally observed in the same participant.

4.4.3 Limitations

One of the limitations for our study was the lack of lung volume measurements post-bronchodilator. This would have allowed us to confirm whether the paradoxical increase of $Vent_{Non}$ was associated with reduced hyperinflation. Additionally, we had

not assessed dyspnoea. The relationships between VSPEST imaging parameters and dyspnoea measurements such as the modified Borg dyspnoea scale are currently unknown, and it is possible that the changes in $Vent_{Non}$ and 'hot spots' could have correlated with changes to dyspnoea. Thus, we cannot conclusively decide whether these VSPECT parameters possess clinical utility. There is also no information on variability in either $Vent_{Non}$ or 'hot spots' count for VSPECT, and therefore, we were unable to determine whether the large variability was due to natural variability or true changes from bronchodilator.

4.4.4 Conclusion

In summary, our study observed that there were no significant changes in non-ventilated volume or 'hot spots' from bronchodilator. The variability in response for both parameters could have resulted from the complex physiology involved in the response to bronchodilator in patients with COPD. Along with airway dilation, ventilation imaging is likely sensitive to redistribution of ventilation and airway recruitment. Instead of solely using global measurements of non-ventilated volume and 'hot spots' count', topographical analysis may be used to assess peripheral changes in ventilation. Alternative VSPECT parameters, such as ventilation heterogeneity, could also provide further insight on the effect of bronchodilator in COPD.

4.6 References

1. (GOLD) GIfCOLD. Global strategy for the diagnosis, management, and prevention of chronic obstructive lung disease (2024 Report) 2024 [Available from: https://goldcopd.org/2024-gold-report/.
2. O'DONNELL DE, LAM M, WEBB KA. Measurement of Symptoms, Lung Hyperinflation, and Endurance during Exercise in Chronic Obstructive Pulmonary Disease. American Journal of Respiratory and Critical Care Medicine. 1998;158(5):1557-65.
3. Borrill ZL, Houghton CM, Woodcock AA, Vestbo J, Singh D. Measuring bronchodilation in COPD clinical trials. Br J Clin Pharmacol. 2005;59(4):379-84.
4. Saadeh C, Saadeh C, Cross B, Gaylor M, Griffith M. Advantage of impulse oscillometry over spirometry to diagnose chronic obstructive pulmonary disease and monitor pulmonary responses to bronchodilators: An observational study. SAGE Open Med. 2015;3:2050312115578957.
5. Newton MF, O'Donnell DE, Forkert L. Response of Lung Volumes to Inhaled Salbutamol in a Large Population of Patients With Severe Hyperinflation. CHEST. 2002;121(4):1042-50.
6. D.E O, Donnell, Forkert L, Webb KA. Evaluation of bronchodilator responses in patients with “irreversible” emphysema. European Respiratory Journal. 2001;18(6):914.
7. Radadia N, Friedlander Y, Priel E, Konyer NB, Huang C, Jamal M, Farncombe T, Marriott C, Finley C, Agzarian J, Dolovich M, Noseworthy MD, Nair P, Shargall Y, Svenningsen S. Comparison of ventilation defects quantified by Technegas SPECT and hyperpolarized 129Xe MRI. Frontiers in Physiology. 2023;14.
8. Bajc M, Markstad H, Jarenbäck L, Tufvesson E, Bjermer L, Jögi J. Grading obstructive lung disease using tomographic pulmonary scintigraphy in patients with chronic obstructive pulmonary disease (COPD) and long-term smokers. Ann Nucl Med. 2015;29(1):91-9.
9. Bajc M, Chen Y, Wang J, Li XY, Shen WM, Wang CZ, Huang H, Lindqvist A, He XY. Identifying the heterogeneity of COPD by V/P SPECT: a new tool for improving the diagnosis of parenchymal defects and grading the severity of small airways disease. Int J Chron Obstruct Pulmon Dis. 2017;12:1579-87.
10. Kirby M, Mathew L, Heydarian M, Etemad-Rezai R, McCormack DG, Parraga G. Chronic Obstructive Pulmonary Disease: Quantification of Bronchodilator Effects by Using Hyperpolarized He MR Imaging. Radiology. 2011;261(1):283-92.
11. Kirby M, Heydarian M, Wheatley A, McCormack DG, Parraga G. Evaluating bronchodilator effects in chronic obstructive pulmonary disease using diffusion-weighted hyperpolarized helium-3 magnetic resonance imaging. Journal of Applied Physiology. 2011;112(4):651-7.
12. Mummy DG, Coleman EM, Wang Z, Bier EA, Lu J, Driehuys B, Huang YC. Regional Gas Exchange Measured by (129) Xe Magnetic Resonance Imaging Before and After Combination Bronchodilators Treatment in Chronic Obstructive Pulmonary Disease. J Magn Reson Imaging. 2021;54(3):964-74.
13. Imai T, Sasaki Y, Shinkai T, Ohishi H, Nezu K, Nishimoto Y, Ichiba N, Yamane T, Yoshikawa M, Narita N, Uchida H. Clinical evaluation of99mTc-Technegas SPECT in thoracoscopic lung volume reduction surgery in patients with pulmonary emphysema. Annals of Nuclear Medicine. 2000;14(4):263-70.
14. Paludan JPD, Andresen SR, Abrahamsen J, Petersen LJ, Høyer C. Improvement in image quality of Tc-99m-based ventilation/perfusion single-photon emission computed tomography in patients with chronic obstructive pulmonary disease through pretest continuous positive airway pressure treatment. World J Nucl Med. 2019;18(2):185-6.
15. Graham BL, Steenbruggen I, Miller MR, Barjaktarevic IZ, Cooper BG, Hall GL, Hallstrand TS, Kaminsky DA, McCarthy K, McCormack MC, Oropez CE, Rosenfeld M, Stanojevic S, Swanney MP, Thompson BR. Standardization of Spirometry 2019 Update. An Official American Thoracic Society and

European Respiratory Society Technical Statement. American Journal of Respiratory and Critical Care Medicine. 2019;200(8):e70-e88.
16. Wanger J, Clausen JL, Coates A, Pedersen OF, Brusasco V, Burgos F, Casaburi R, Crapo R, Enright P, van der Grinten CPM, Gustafsson P, Hankinson J, Jensen R, Johnson D, MacIntyre N, McKay R, Miller MR, Navajas D, Pellegrino R, Viegi G. Standardisation of the measurement of lung volumes. European Respiratory Journal. 2005;26(3):511-22.
17. Graham BL, Brusasco V, Burgos F, Cooper BG, Jensen R, Kendrick A, MacIntyre NR, Thompson BR, Wanger J. 2017 ERS/ATS standards for single-breath carbon monoxide uptake in the lung. European Respiratory Journal. 2017;49(1):1600016.
18. King GG, Bates J, Berger KI, Calverley P, Melo PLd, Dellacà RL, Farré R, Hall GL, Ioan I, Irvin CG, Kaczka DW, Kaminsky DA, Kurosawa H, Lombardi E, Maksym GN, Marchal F, Oppenheimer BW, Simpson SJ, Thamrin C, Berge Mvd, Oostveen E. Technical standards for respiratory oscillometry. European Respiratory Journal. 2020;55(2):1900753.
19. Pellegrino R, Viegi G, Brusasco V, Crapo RO, Burgos F, Casaburi R, Coates A, Grinten CPMvd, Gustafsson P, Hankinson J, Jensen R, Johnson DC, MacIntyre N, McKay R, Miller MR, Navajas D, Pedersen OF, Wanger J. Interpretative strategies for lung function tests. European Respiratory Journal. 2005;26(5):948.
20. Jetmalani K, Brown NJ, Boustany C, Toelle BG, Marks GB, Abramson MJ, Johns DP, James AL, Hunter M, Musk AW, Berend N, Farah CS, Chapman DG, Thamrin C, King GG. Normal limits for oscillometric bronchodilator responses and relationships with clinical factors. ERJ Open Res. 2021;7(4).
21. Philip HQ, Sanja S, Tim JC, Xaver B, Graham LH, Bruce HC, Paul LE, John LH, Mary SMI, Jinping Z, Janet S, the ERSGLFI. Multi-ethnic reference values for spirometry for the 3–95-yr age range: the global lung function 2012 equations. European Respiratory Journal. 2012;40(6):1324.
22. Graham LH, Nicole F, Gregg R, Tolu O, Bruce T, Jane K, Irene S, Brendan GC, Sanja S, on behalf of the contributing GLINm. Official ERS technical standard: Global Lung Function Initiative reference values for static lung volumes in individuals of European ancestry. European Respiratory Journal. 2021;57(3):2000289.
23. “Official ERS technical standards: Global Lung Function Initiative reference values for the carbon monoxide transfer factor for Caucasians.” Sanja Stanojevic, Brian L. Graham, Brendan G. Cooper, Bruce R. Thompson, Kim W. Carter, Richard W. Francis and Graham L. Hall on behalf of the Global Lung Function Initiative T_{LCO} working group. Eur Respir J 2017; 50: 1700010. European Respiratory Journal. 2020;56(4):1750010.
24. Brown NJ, Xuan W, Salome CM, Berend N, Hunter ML, Musk AW, James AL, King GG. Reference equations for respiratory system resistance and reactance in adults. Respiratory Physiology & Neurobiology. 2010;172(3):162-8.
25. Crawford AB, Davison A, Amis TC, Engel LA. Intrapulmonary distribution of 99mtechnetium labelled ultrafine carbon aerosol (Technegas) in severe airflow obstruction. Eur Respir J. 1990;3(6):686-92.
26. Amis TC, Crawford AB, Davison A, Engel LA. Distribution of inhaled 99mtechnetium labelled ultrafine carbon particle aerosol (Technegas) in human lungs. European Respiratory Journal. 1990;3(6):679.
27. Lemb M, Oei T, Eifert H, Günther B. Technegas: a study of particle structure, size and distribution. European journal of nuclear medicine. 1993;20:576-9.
28. Farrow CE, Salome CM, Harris BE, Bailey DL, Bailey E, Berend N, Young IH, King GG. Airway closure on imaging relates to airway hyperresponsiveness and peripheral airway disease in asthma. J Appl Physiol (1985). 2012;113(6):958-66.
29. Farrow CE, Salome CM, Harris BE, Bailey DL, Berend N, King GG. Peripheral ventilation heterogeneity determines the extent of bronchoconstriction in asthma. Journal of Applied Physiology. 2017;123(5):1188-94.

30. Rutting S, Mahadev S, Tonga KO, Bailey DL, Dame Carroll JR, Farrow CE, Thamrin C, Chapman DG, King GG. Obesity alters the topographical distribution of ventilation and the regional response to bronchoconstriction. Journal of Applied Physiology. 2019;128(1):168-77.
31. Kroon D-J. Region Growing: MATLAB Central File Exchange; 2008 [Available from: https://au.mathworks.com/matlabcentral/fileexchange/19084-region-growing.
32. Otsu N. A Threshold Selection Method from Gray-Level Histograms. IEEE Transactions on Systems, Man, and Cybernetics. 1979;9(1):62-6.
33. Koltai H. Novel 3D Segmentation Methods for SPECT Images of Airway Disease: The University of Sydney; 2021.
34. Diba C, Salome CM, Berend N, Harris B, Bailey D, King GG. Effect of Bronchodilator on Ventilation Heterogeneity in COPD. D28 IMAGING OBSTRUCTIVE LUNG DISEASES I. American Thoracic Society International Conference Abstracts: American Thoracic Society; 2009. p. A5577.
35. Laurie S, Helen M, Alberto B, Guilhem C, Ho-Fung C, Dave C, Jody B, Demi J, Laura S, Joshua A, Bilal T, Ryan M, Oliver R, James B, Paul H, Smitha R, Andy S, Neil S, Graham N, Martin B, Leanne A, Latife H, Titti F-W, Rod H, Jim W. Xe-MRI bronchodilator response to assess disease severity in patients with asthma and/or COPD. European Respiratory Journal. 2023;62(suppl 67):PA4500.
36. Gregory GK, Catherine EF, David GC. Dismantling the pathophysiology of asthma using imaging. European Respiratory Review. 2019;28(152):180111.
37. He M, Zha W, Tan F, Rankine L, Fain S, Driehuys B. A Comparison of Two Hyperpolarized (129)Xe MRI Ventilation Quantification Pipelines: The Effect of Signal to Noise Ratio. Acad Radiol. 2019;26(7):949-59.
38. Norberg P, Persson HL, Carlsson GA, Bake B, Kentson M, Sandborg M, Gustafsson A. Quantitative lung SPECT applied on simulated early COPD and humans with advanced COPD. EJNMMI Res. 2013;3(1):28.
39. Norberg P, Persson HL, Schmekel B, Carlsson GA, Wahlin K, Sandborg M, Gustafsson A. Does quantitative lung SPECT detect lung abnormalities earlier than lung function tests? Results of a pilot study. EJNMMI Res. 2014;4(1):39-.
40. Timmins SC, Diba C, Schoeffel RE, Salome CM, King GG, Thamrin C. Changes in oscillatory impedance and nitrogen washout with combination fluticasone/salmeterol therapy in COPD. Respiratory Medicine. 2014;108(2):344-50.
41. Hogg JC, McDonough JE, Sanchez PG, Cooper JD, Coxson HO, Elliott WM, Naiman D, Pochettino M, Horng D, Gefter WB, Wright AC. Micro-computed tomography measurements of peripheral lung pathology in chronic obstructive pulmonary disease. Proc Am Thorac Soc. 2009;6(6):546-9.
42. Diaz AA, Valim C, Yamashiro T, Estépar RSJ, Ross JC, Matsuoka S, Bartholmai B, Hatabu H, Silverman EK, Washko GR. Airway Count and Emphysema Assessed by Chest CT Imaging Predicts Clinical Outcome in Smokers. Chest. 2010;138(4):880-7.
43. Milne S, Hammans C, Watson S, Farah CS, Thamrin C, King GG. Bronchodilator Responses in Respiratory Impedance, Hyperinflation and Gas Trapping in COPD. COPD: Journal of Chronic Obstructive Pulmonary Disease. 2018;15(4):341-9.
44. Baldi S, Dellacà R, Govoni L, Torchio R, Aliverti A, Pompilio P, Corda L, Tantucci C, Gulotta C, Brusasco V, Pellegrino R. Airway distensibility and volume recruitment with lung inflation in COPD. Journal of Applied Physiology. 2010;109(4):1019-26.
45. Verbeken EK, Cauberghs M, van de Woestijne KP. Membranous bronchioles and connective tissue network of normal and emphysematous lungs. J Appl Physiol (1985). 1996;81(6):2468-80.
46. Belman MJ, Botnick WC, Shin JW. Inhaled bronchodilators reduce dynamic hyperinflation during exercise in patients with chronic obstructive pulmonary disease. American Journal of Respiratory and Critical Care Medicine. 1996;153(3):967-75.
47. Venegas JG, Winkler T, Musch G, Vidal Melo MF, Layfield D, Tgavalekos N, Fischman AJ, Callahan RJ, Bellani G, Harris RS. Self-organized patchiness in asthma as a prelude to catastrophic shifts. Nature. 2005;434(7034):777-82.

48. Cabahug CJ, McPeck M, Palmer LB, Cuccia A, Atkins HL, Smaldone GC. Utility of technetium-99m-DTPA in determining regional ventilation. J Nucl Med. 1996;37(2):239-44.

Chapter 5 – Effects of methacholine on Single Photon Emission Computed Tomography Ventilation Imaging in COPD

5.1 Abstract

Introduction: Whilst airway hyperresponsiveness (AHR) is traditionally thought to be a marker for asthma, it is also common in COPD. However, the physiological mechanisms for AHR and bronchoconstriction in COPD is thought to be different from those in asthma. Our objective was to examine the effects of bronchoconstriction on non-ventilated volume and 'hot spots' count in COPD with VSPECT/CT.

Methods: 7 COPD participants underwent a baseline VSPECT/CT scan. On the second visit, the participants underwent pre- and post-methacholine spirometry and oscillometry, and a post-methacholine VSPECT/CT scan was completed. Non-ventilated volume ($Vent_{Non}$) and 'hot spots' were defined with the curve-fitting threshold method.

Results: $Vent_{Non}$ and 'hot spots' count did not significantly increase post-methacholine, and the responses for both were variable. Neither VSPECT/CT parameter predicted AHR. There was a trend towards a relationship between increased 'hot spots' count and reduced $Vent_{Non}$ post-methacholine ($r = -0.67$; $p = 0.10$). Increased FVC z-score at baseline predicted greater 'hot spots' count post-methacholine ($r = 0.82$; $p = 0.02$). Increased $Vent_{Non}$ at baseline predicted a lower closing index ($r = -0.76$; $p = 0.05$) and reduced conductance at 5 Hz (G5) ($r = -0.83$; $p = 0.04$) post-methacholine.

Conclusion: Contrary to results from VSPECT/CT asthma studies, airway closure and airway narrowing did not seem to occur concurrently. Instead, bronchoconstriction appeared to be characterised with greater ventilation heterogeneity and hyperinflation or airway closure and reduced ventilation.

5.2 Introduction

Airway hyperresponsiveness (AHR) is the increased sensitivity to excessive narrowing or closure in response to inhaled stimulus and is considered a hallmark characteristic for asthma. However, AHR also appears to be a common feature in chronic obstructive pulmonary disease (COPD), with studies reporting AHR to occur in 23 – 50% of COPD patients (1-3). COPD patients with AHR have accelerated decline in lung function (4) and increased risk of mortality (5). Although the physiological mechanisms behind AHR in COPD remain elusive, some evidence appears to suggest that they differ from AHR asthma.

In asthma, studies have shown AHR to be predicted by increased gas trapping and increased ventilation heterogeneity at baseline (6, 7). According to a computational modelling study by Venegas et al. (8), heterogeneity in the bronchial tree predisposes the airways to catastrophic formation of poorly ventilated lung regions following smooth muscle activation. Although ventilation heterogeneity and gas trapping are common in COPD as well, Hardaker et al. (9) instead observed that AHR in COPD had been predicted by decreased ventilation heterogeneity and increased airway closure, as measured by forced vital capacity (FVC) (10). Additionally, COPD participants with AHR were reported to have significantly increased gas diffusion, and thus less evidence of emphysema, compared to those without AHR. The authors thus speculated that COPD patients with the airway disease phenotype may be more susceptible to AHR than those with emphysema. These findings by Hardaker et al. (9) suggest that despite physiological similarities between asthma and COPD patients with AHR, such as severe airway narrowing

(11-13), AHR may be ultimately determined by physiological mechanisms that are unique to each disease.

The effects of bronchoconstriction on ventilation, as visualised and assessed with three-dimensional imaging techniques, and relationships between AHR and ventilation have been previously examined in asthma patients. Despite differences in imaging techniques and analysis methods, bronchoconstriction is consistently demonstrated to increase the extent of non-ventilated volume (14-16). Utilising ventilation single-photon emission tomography/computed tomography (VSPECT/CT), Farrow et al. (17) reported a correlation between more severe AHR and increased non-ventilated volume due to airway closure following the bronchial challenge in asthma. Like previous asthma studies, Farrow et al. also noted there to be correlations between increased ventilation heterogeneity at baseline and more severe AHR and a greater loss of ventilation. In another VSPECT/CT asthma study by Farrow et al. (16), the development of poorly ventilated lung regions from airway narrowing was predicted by greater ventilation heterogeneity at the acinar lung regions. These findings are strongly aligned with the observations made by Hardaker et al. (7) and Venegas et al. (8). However, the findings from Hardaker et al. (10) suggest that these effects and relationships observed by Farrow et al. in asthma patients (16, 17) may not apply to COPD patients. For COPD, reduced non-ventilated volume at baseline, potentially indicative of reduced emphysematous destruction, may be predictive of more severe AHR and greater airway closure following the bronchial challenge.

In Chapter 2, we demonstrated that popular analysis methods for VSPECT, which include the one used by Farrow et al. (16), fail to provide accurate estimations of non-ventilated volume in lungs with heterogeneous imaging data. This makes the findings of previous VSPECT studies possibly suspect. In comparison, our novel 'curve-fitting' analysis method was shown to be significantly more accurate despite varying extents of image data heterogeneity. In addition to estimating non-ventilated volume, we also developed a technique that analyses the number of 'hot spots' in the image, which results from the particles of Technegas ventilation agent aggregating or 'clumping' in lung regions with abnormal airflow and airway narrowing (18, 19). These two parameters, non-ventilated volume and 'hot spots' count, were demonstrated to provide complementary information on lung function in a previous chapter (Chapter 3). 'Hot spots' count has not been previously utilised to investigate AHR and bronchoconstriction with three-dimensional VSPECT imaging. In a scintigraphic VSPECT study in asthma patients, the number of 'hot spots' were noted by Pellegrino et al. (19) to be increased following a bronchial challenge test. However, the exact number of 'hot spots' at baseline nor the change in 'hot spots' count in all asthma participants were not presented. We hypothesize that bronchoconstriction would increase both non-ventilated volume and 'hot spots' count. However, we also hypothesize that more severe AHR in COPD is predicted by reduced non-ventilated and greater 'hot spots' at baseline. For this study, our primary objectives were to 1) examine the effects of bronchoconstriction on non-ventilated volume and 'hot spots' count, 2) determine whether changes in VSPECT/CT parameters correlate with AHR and changes in lung function, 3) determine whether baseline lung function predicts change in VSPECT/CT parameters, and 4) determine whether baseline VSPECT/CT parameters predict AHR and change in lung function.

5.3 Methods

5.3.1 Participants and Study Design

Out of 22 participants with physician diagnosed COPD recruited from the Department of Respiratory Medicine at Royal North Shore Hospital, only 10 (13 men, 10 women) met inclusion criteria for bronchial challenge testing. The inclusion criteria were as follows: 18 – 80 years old, physician diagnosed COPD, a smoking history of at least 10 pack years, and FEV1 greater than or equal to 40% of the predicted value. Exclusion criteria were other active or chronic respiratory diseases, history of lung surgery, history of chronic kidney disease, significant cardiac disease, intensive care unit admissions in the last 12 months, and significant respiratory infection or documented exacerbation within the previous 6 weeks. All participants provided written, informed consent. The study was approved by the local Human Research Ethics Committee (Northern Sydney Local Health District, RESP/18/198)

Participants attended two visits. The first visit involved baseline lung function testing and a VSPECT/CT scan as noted in Chapter 3. For the second visit, participants performed oscillometry and spirometry before undergoing a methacholine challenge test using spirometry only. Oscillometry was performed at the end of the challenge which was then immediately followed by the post-methacholine VSPECT/CT scan. Participants with > 200 mL FEV1 difference between the two visits were excluded from the study so that lung function was consistent throughout the study. Prior to each visit, the participants withheld short-acting bronchodilators for 6 hours and LABA and/or LAMA medication for 24 hours.

5.3.2 Lung Function Testing

Spirometry was performed with a MGC Diagnostics CPFS/D USB spirometer and MGC Breeze Suite interface (v. 8.6.0.56, MGC Diagnostics Corporation, Saint Paul), according to American Thoracic Society (ATS)/European Respiratory Society (ERS) criteria (20).

Oscillometry was performed with the tremoFlo C-100 oscillometry system (v. 1.0.43.44, Thorasys Thoracic Medical Systems Inc, Montreal) at 5 – 37 Hz. The device calibration was performed prior to the testing session. Following the ERS technical standards, participants underwent at least 3 breathing measurements. For each measurement, the participant was instructed to breathe tidally in a seated position and support their cheeks for 60 seconds, whilst wearing a nose clip. The mean respiratory system resistance (R5), respiratory system conductance (inverse of resistance, G5), and respiratory system reactance (X5), which had all been measured at 5 Hz, were then obtained. Measurements with signs of leak, coughs, swallows, or incorrect technique were excluded for quality control. A R5 coefficient of variation ≤ 10% was required for each testing session.

The z-scores for spirometry, body plethysmography, and diffusing capacity were determined with reference equations from the Global Lung Initiative (GLI) (21-23). Reference equations from Brown et al. instead of Oostveen et al. were used to calculate oscillometry z-scores (24) as one participant's weight was outside the range of the latter's reference equations.

5.3.3 Methacholine Challenge Test

The methacholine challenge test was conducted by administering cumulative methacholine doses, which ranged from 0.08 to 48.5 µmol, with the Koko dosimeter (PDS Instrumentation, Louisville, KY). Participants performed a minimum of two spirometry measurements after methacholine was administered. The test concluded if FEV1 decreased by at least 20% or after giving the maximum dose. Airway hyperresponsiveness was defined by dose response slope for FEV1 (DRS_{FEV1}) ≥ 8 (% decrease in FEV1/µmol in methacholine + 3), (DRS_{G5}) ≥ 9.75 (% decrease in G5/µmol in methacholine + 3), or ≥ 3.23 DRS_{X5} (decrease in X5/ µmol in methacholine + 3) (25, 26). The cutoffs for these dose response slopes were equivalent to a ≥ 20% reduction in FEV1, ≥ 27% reduction in G5, and ≥ 0.93 $cmH_2O.L.s^{-1}$ reduction in X5 at 4 µmol cumulative dose of methacholine. The closing index (%ΔFVC/%ΔFEV1) was calculated to determine the proportion of change in FEV1 from airway closure (27).

5.3.4 Ventilation Imaging

VSPECT/CT Imaging was conducted at the Department of Nuclear Medicine, Royal North Shore Hospital, using a Siemens Symbia T16 SPECT/CT system. Technegas, consisting of 100 nm Technetium (^{99m}Tc) carbon nanoparticles, was used as the ventilation agent. The inhaled distribution of Technegas has been demonstrated to resemble gas, even in participants with severe airway obstruction (28), and its distribution should also remain fixed for at least 20 minutes after inhalation (29, 30).

Participants were required to breathe in 500 – 700 mL of Technegas from functional residual capacity (FRC) at approximately 0.5 – 1 L/sec in a seated, upright position. The volume and flow rate of each inhalation was monitored with a MGC Diagnostics CPFS/D USB spirometer that had been connected to the Technegas patient administration kit and MGC Breeze Suite interface (v. 8.6.0.56, MGC Diagnostics Corporation, Saint Paul). Two – four inhalations were generally taken to achieve the required radioactivity of approximately 1.5 – 2.0 kilocounts/s, and approximately 40 mBq of Technegas was inhaled. Following Technegas inhalation, 400 µg of salbutamol was administered to the participants. As noted in the previous chapters (3 and 4), the baseline CT scan was also registered to post-bronchodilator VSPECT scan. This ensured that CT scans for all visits were post-bronchodilator scans.

Supine VSPECT and low dose CT scans (30 mA, 110 kVp, pitch 1.5, slice thickness 3 mm) were acquired with a 128 x 128 matrix and 512 x 512 matrix, respectively. Participants breathed tidally throughout the VSPECT scan, but they were then instructed to hold their breath at FRC for the CT scan. Following the settings on other human VSPECT studies (16, 17, 31), VSPECT acquisitions employed 60 stops x2 projections (total 120 projections), 15 seconds per stop, non-circular clockwise orbit and continuous acquisition.

5.3.5 Image Reconstruction and Registration

Using 128 slices, VSPECT images were reconstructed with an ordered subset expectation maximization (OSEM) Siemens Flash 3D algorithm, CT-based attenuation correction, and a Gaussian filter. CT image reconstruction was completed with a 512 x 512 matrix and OSEM Siemens Flash 3D algorithm. Both VSPECT and CT images were converted to Digital Imaging and Communication in Medicine (DICOM) file format.

VSPECT and CT scans were registered using the known, fixed spatial relationship between the VSPECT and CT scanners. The DICOM files of both scans were then transferred onto a HERMES (Nuclear Diagnostics, Stockholm, Sweden) workstation. The matrix size of the VSPECT scan was increased from 128 x 128 matrix to 512 x 512, and the original counts remained preserved. Additional three-dimensional registration was completed with the multimodality software package on HERMES by visually aligning the markers on the VSPECT and CT scans.

5.3.6 Imaging Analysis

Lung outlines on the CT scans were defined through Otsu's method (32) for thresholding and a region growing algorithm (33) that had been implemented within a MATLAB script (R2019b, MathWorks, Natick) (34). The script produced a binarised mask of the lung outlines, which was applied onto the VSPECT scan. All VSPECT voxel activity outside of the lung borders were set to 0. VSPECT voxel data within the mask were exported onto Microsoft Excel (2021, Microsoft, Redmond).

Non-ventilated volume ($Vent_{Non}$) and 'hot spots' were defined through the same curve-fitting threshold method, as described in Chapter 2 and 3 (Figure 1). To summarize, the cumulative voxel frequency was first plotted against activity, and the slopes of each data point were then calculated. The initial activity value ≥ 90% cumulative frequency with a slope ≤ 0.010 was selected as the 'slope point'. Voxels < 30% x the 'slope point' were determined to be $Vent_{Non}$. $Vent_{Non}$ was expressed as a percentage of total lung volume, which had been derived from the CT mask of the lungs. Voxels ≥ the 'slope point' were determined to be 'hot spot' activity. To count the number of 'hot spots' in three-dimensional space, the masked VSPECT image was first opened in Fiji (National Institutes of Health, United States of America). Secondly, the VSPECT image was binarized, in which all voxel activity < the 'slope point' was set to 0 and all voxel activity ≥ the 'slope point' was set to 255 i.e., the maximum activity in an 8-bit image. Finally, the 3D Objects Counter plugin had been used to count the number of 'hot spots' in three-dimensional space.

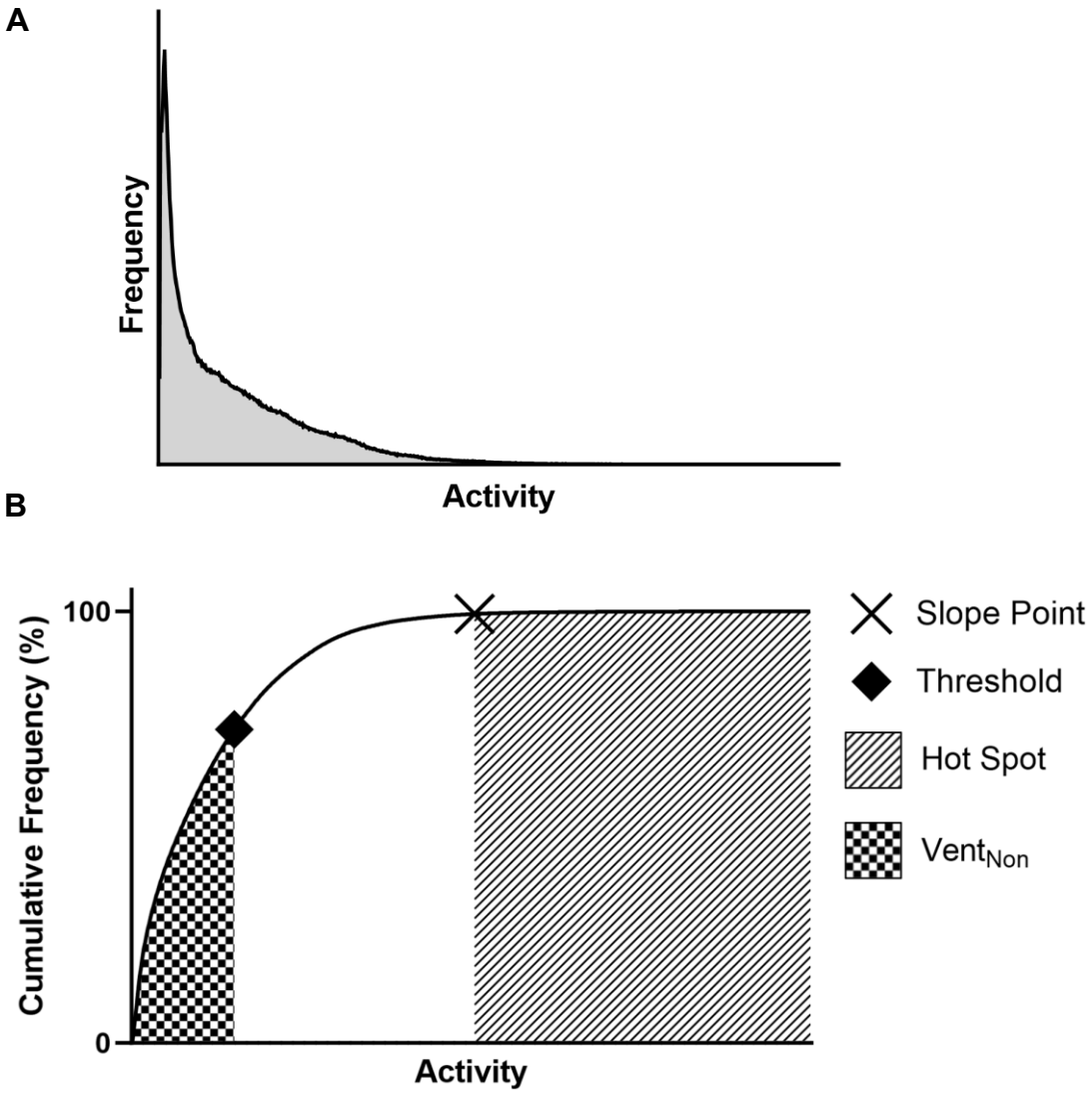


Figure 1: Curve-fitting threshold method for ventilation single-photon emission computed tomography (VSPECT)/computed tomography (CT) scan. (A) Voxel activity – frequency plot of masked VSPECT/CT scan; (B) Voxel activity – cumulative frequency plot with curve-fitting threshold method. Slope Point = initial activity value ≥ 90% cumulative frequency with ≤ 0.010 slope; Threshold = 30% x 'slope point'; $Vent_{Non}$ = non-ventilated volume

5.3.7 Statistical Analysis

GraphPad Prism version 10.0.2 was used to analyse data and generate graphs. All data were expressed as mean ± SD unless otherwise stated. The changes in imaging parameters post-methacholine were calculated as absolute changes. Normal distribution of the data was determined with a Shapiro-Wilk's test. Differences in imaging parameters between at baseline and post-methacholine were assessed with Wilcoxon's signed-rank test. Correlations between changes in imaging parameters, $Vent_{Non}$ and 'hot spots' count, and lung function measurements post-methacholine were examined by Pearson's correlation coefficient and Spearman's rank correlation coefficient for parametric and non-parametric data, respectively. A p-value of < 0.05 was considered statistically significant.

5.4 Results

5.4.1 Participant Demographics

Participant demographics and baseline spirometry, oscillometry, and VSPECT/CT measurements are displayed in Table 1. The baseline spirometric and oscillometric measurements were from the second visit. 10 participants with physician diagnosed COPD were recruited for the study, but 3 were excluded as the difference in FEV1 between visit 1 and visit 2 was > 200 mL. 1 participant did not perform oscillometry during the methacholine visit. However, all participants completed the Technegas inhalation manoeuvre successfully. On average, participants were overweight (BMI: 30.9 ± 7.4), and their wellbeing was moderately impacted by COPD (CAT: 16.1 ± 5.7). Additionally, participants were mildly obstructed (FEV1/FVC z-score: -3.0 ± 1.0, FEV1 z-score: -2.0 ± 0.8). R5 was within normal range (R5 z-score: 0.9 ± 1.5), but X5 was more negative (X5 z-score: -1.7 ± 1.8). $Vent_{Non}$ and 'hot spots' from the first visit were 42.8 ± 20.4 and 4 ± 1, respectively.

Table 1: Participant demographics and baseline measurements of lung function, non-ventilated volume, and 'hot spots'.

Participants, *n*	7
Males/females, *n*	6/1
Age, years	61.3 ± 7.8
Height, m	1.8 ± 0.06
BMI, kg/m^2	30.9 ± 7.4
Smoking history, pack years	35.2 ± 27.7
CAT	16.1 ± 5.7
FEV1, z-score	-2.4 ± 0.8
FVC, z-score	-0.5 ± 1.0
FEV1/FVC, %	54.0 ± 8.6
FEV1/FVC, z-score	-3.0 ± 1.0
R5, z-score	0.9 ± 1.5
X5, z-score	-1.7 ± 1.8
G5, $s.L.cmH_2O^{-1}$	0.2 ± 0.1
$Vent_{Non}$, %	42.8 ± 20.4
Hot spots, n	4 ± 1

BMI = body mass index; CAT = chronic obstructive pulmonary disease assessment test; FEV1 = forced expiratory volume in 1 second; FVC = forced vital capacity; R5 = respiratory system resistance measured at 5 Hz; X5 = respiratory system reactance measured at 5 Hz; $Vent_{Non}$ = non-ventilated volume. Data are mean +/- SD.

5.4.2 Airway hyperresponsiveness and changes in lung function, non-ventilated volume, and hot spots

Changes in spirometric, oscillometric, and VSPECT/CT parameters post-methacholine, in addition to dose response slopes and closing indexes are shown in Table 2. In total, 6 participants were determined to have AHR, with 4 of them according to FEV1, G5, and X5 dose response slopes. 1 participant possessed AHR as defined by FEV1 and X5 dose response slopes, and another participant had AHR defined by their FEV1 dose response slope. FEV1 and FVC decreased by 24.9% ± 5.7 and 19.14% ± 9 respectively. The mean absolute changes for R5 and X5 were 0.6 ± 0.6 and -1.7 ± 1.5, respectively. The mean closing index, 0.77 ± 0.29, indicated that the reduction in FEV1 was mostly due to airway closure.

There were no significant changes in $Vent_{Non}$ and 'hot spots' count (p-values = 0.3 and 0.2, respectively), although responses for both VSPECT/CT parameters were variable, with the ranges for $Vent_{Non}$ and 'hot spots' count responses being -9.65 – 9.52 and -3 – 9, respectively. The relationship between changes in $Vent_{Non}$ and 'hot spots' are shown in Figure 3. There was a trend towards a correlation between increased 'hot spots' count and reduced $Vent_{Non}$ post-methacholine (r = -0.67, p-value = 0.10).

Table 2: Post-methacholine dose response slopes and changes in lung function, non-ventilated volume, and ‘hot spots’

Δ FEV1, L	-0.4 ± 0.4
Δ FEV1, %	-24.9 ± 5.7
Δ FVC, L	-0.5 ± 0.6
Δ FVC, %	-19.1 ± 9.0
Δ R5, $cmH_2O.s.L^{-1}$	0.6 ± 0.6
Δ R5, %	23.3 ± 24.9
Δ G5, $L/cmH_2O.s^{-1}$	-0.04 ± 0.06
Δ G5, %	-13.2 ± 12.8
Δ X5, $cmH_2O.s.L^{-1}$	-1.7 ± 1.5
Δ X5, %	-76.5 ± 32.4
DRS_{FEV1}, % decrease FEV1/µmol +3^	27.77 (9.47 – 81.45)
DRS_{G5}, % decrease G5/µmol +3^	16.69 (3.67 – 75.99)
DRS_{X5}, decrease X5/µmol +3^	5.66 (3.05 – 10.51)
Closing index, %ΔFVC/%ΔFEV1	0.77 ± 0.29
Δ $Vent_{Non}$, %	3.0 ± 7.4
Δ Hot spots, n	3 ± 4

FEV1 = forced expiratory volume in 1 second; FVC = forced vital capacity; DRS_{FEV1} = dose response slope for FEV1; R5 = respiratory system resistance at 5 Hz; G5 = respiratory system conductance; DRS_{G5} = dose response slope for G5; X5 = respiratory system reactance measured at 5 Hz; DRS_{X5} = dose response slope for X5; $Vent_{Non}$ = non-ventilated volume. Data are mean ± SD. ^ = geometric mean (95% confidence interval).

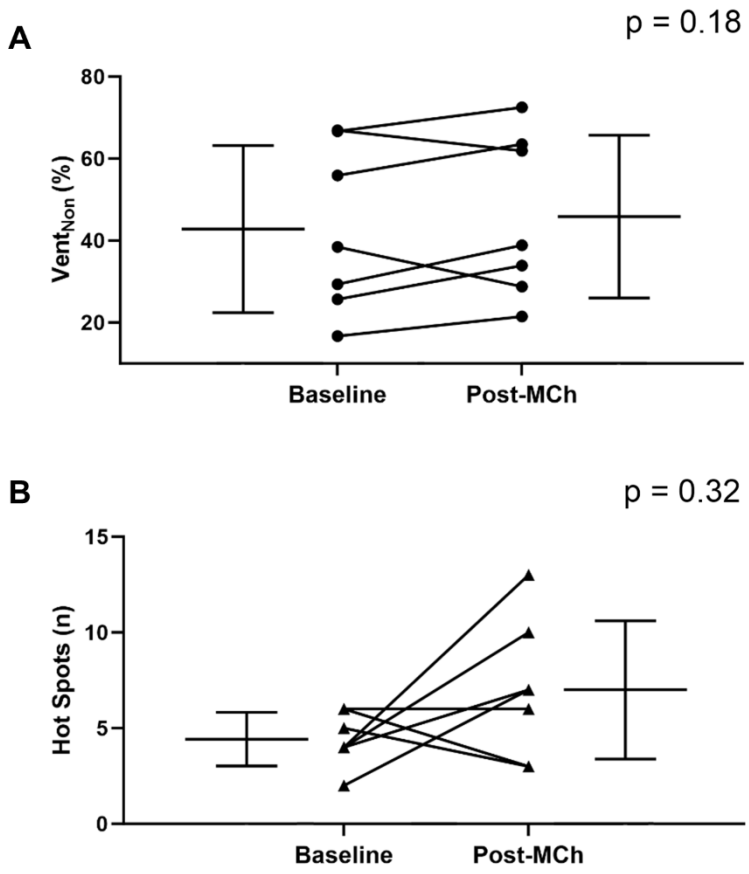


Figure 1: Pre- and post-methacholine measurements of non-ventilated volume (A) and 'hot spots' count (B). Comparisons between pre- and post-methacholine measurements were done with paired Student's t-test. $Vent_{Non}$ = non-ventilated volume.

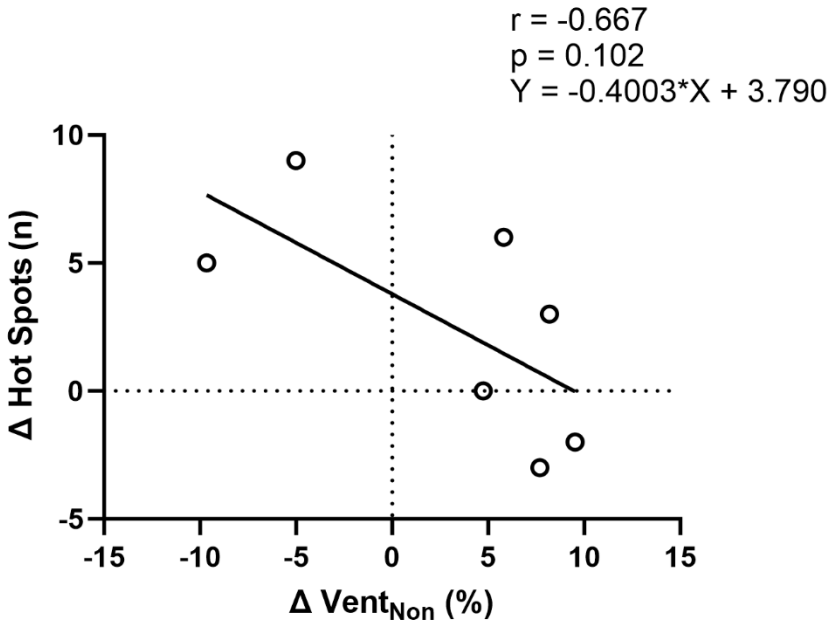


Figure 3: Relationship between post-methacholine changes in non-ventilated volume ($Vent_{Non}$) and 'hot spots' count. There was a trend towards a significant correlation between increased $Vent_{Non}$ and reduced 'hot spots' count change post-methacholine.

5.4.3 Relationships between imaging parameters and airway hyperresponsiveness and closing index

Relationships between changes in imaging parameters post-methacholine and dose response slopes are shown in Figure 4. There was a trend towards a relationship between change in $Vent_{Non}$ and DRS_{FEV1} (r = 0.70, p-value = 0.08) but change in $Vent_{Non}$ did not correlate with the other dose response slopes. There were no correlations between change in 'hot spots' count and all dose response slopes. The relationships between changes in imaging parameters and closing index is displayed in Figure 5. Although there was no relationship between change in $Vent_{Non}$ and closing index, there was a trend towards a significant correlation between reduced 'hot spots' count and increased closing index.

5.4.4 Relationships between changes in imaging parameters and lung function

The relationships between changes in $Vent_{Non}$ and 'hot spots' count and changes in spirometric and oscillometric measurements are shown in Figures 6 and 7, respectively. There were no correlations between changes in imaging parameters and change in spirometric and oscillometric parameters.

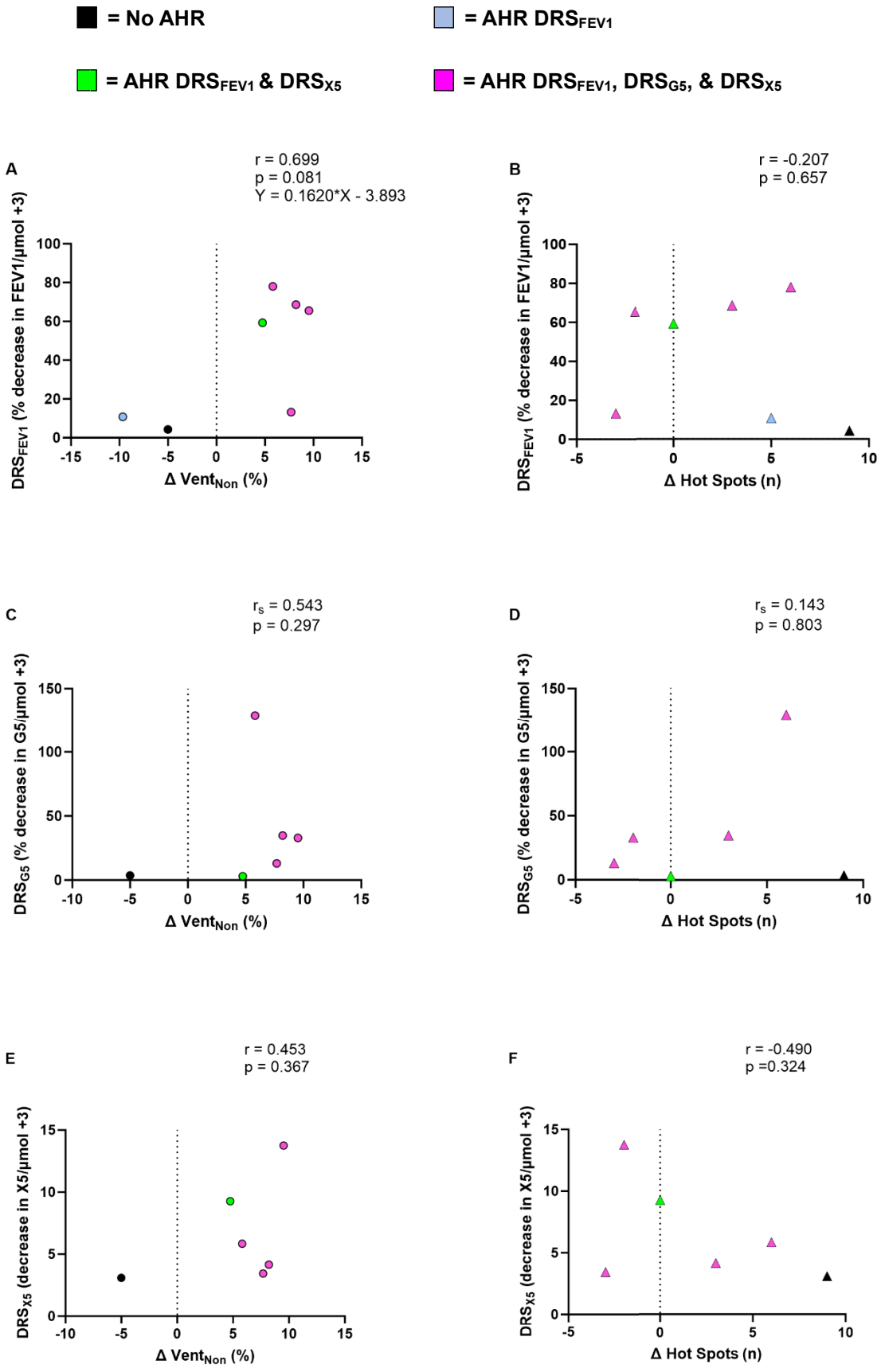

= No AHR
= AHR DRS$_{FEV1}$
= AHR DRS$_{FEV1}$ & DRS$_{X5}$
= AHR DRS$_{FEV1}$, DRS$_{G5}$, & DRS$_{X5}$
A
r = 0.699
p = 0.081
Y = 0.1620*X - 3.893
DRS$_{FEV1}$ (% decrease in FEV1/µmol +3)
Δ Vent$_{Non}$ (%)
B
r = -0.207
p = 0.657
DRS$_{FEV1}$ (% decrease in FEV1/µmol +3)
Δ Hot Spots (n)
C
r$_S$ = 0.543
p = 0.297
DRS$_{G5}$ (% decrease in G5/µmol +3)
Δ Vent$_{Non}$ (%)
D
r$_S$ = 0.143
p = 0.803
DRS$_{G5}$ (% decrease in G5/µmol +3)
Δ Hot Spots (n)
E
r = 0.453
p = 0.367
DRS$_{X5}$ (decrease in X5/µmol +3)
Δ Vent$_{Non}$ (%)
F
r = -0.490
p =0.324
DRS$_{X5}$ (decrease in X5/µmol +3)
Δ Hot Spots (n)

Figure 4: Relationships between post-methacholine changes in non-ventilated volume ($Vent_{Non}$) and 'hot spots' count and dose response slopes. AHR = airway hyperresponsiveness; FEV1 = forced expiratory volume in 1 second; DRS_{FEV1} = dose response slope for FEV1; G5 = respiratory system conductance measured at 5 Hz; DRS_{G5} = dose response slope for G5; X5 = respiratory system reactance measured at 5 Hz; DRS_{X5} = dose response slope for X5; $Vent_{Non}$ = non-ventilated volume; r_s = Spearman's rank correlation

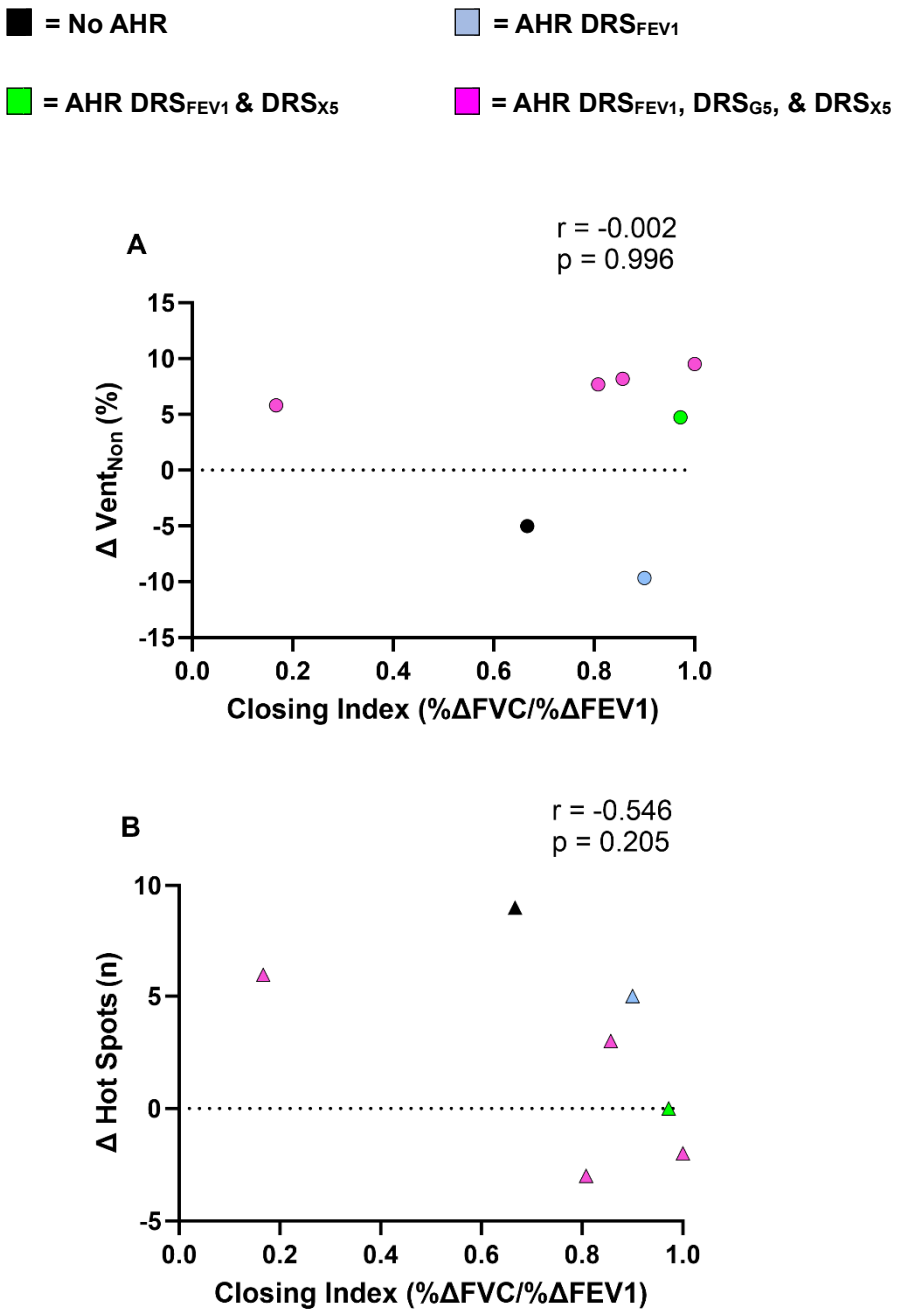


Figure 5: Relationships between post-methacholine changes in non-ventilated volume ($Vent_{Non}$) and 'hot spots' count and closing index. AHR = airway hyperresponsiveness; FEV1 = forced expiratory volume in 1 second; FVC = forced vital capacity; DRS_{FEV1} = dose response slope for FEV1; G5 = respiratory system conductance measured at 5 Hz; DRS_{G5} = dose response slope for G5; X5 = respiratory system reactance measured at 5 Hz; DRS_{X5} = dose response slope for X5; $Vent_{Non}$ = non-ventilated volume.

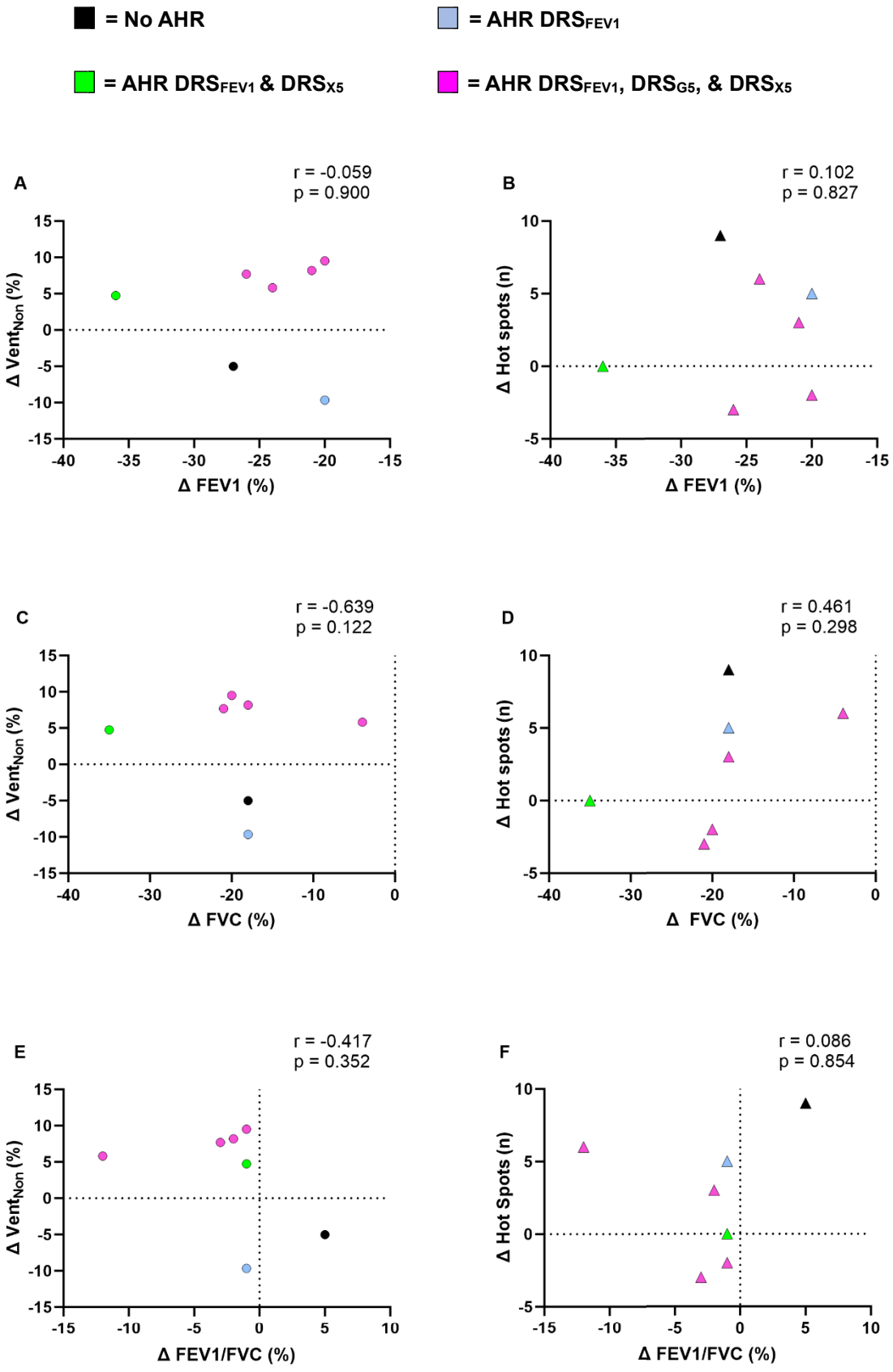

= No AHR
= AHR DRS$_{FEV1}$
= AHR DRS$_{FEV1}$ & DRS$_{X5}$
= AHR DRS$_{FEV1}$, DRS$_{G5}$, & DRS$_{X5}$
A
r = -0.059
p = 0.900
Δ Vent$_{Non}$ (%)
Δ FEV1 (%)
B
r = 0.102
p = 0.827
Δ Hot spots (n)
Δ FEV1 (%)
C
r = -0.639
p = 0.122
Δ Vent$_{Non}$ (%)
Δ FVC (%)
D
r = 0.461
p = 0.298
Δ Hot spots (n)
Δ FVC (%)
E
r = -0.417
p = 0.352
Δ Vent$_{Non}$ (%)
Δ FEV1/FVC (%)
F
r = 0.086
p = 0.854
Δ Hot Spots (n)
Δ FEV1/FVC (%)

Figure 6: Relationships between post-methacholine changes in non-ventilated volume ($Vent_{Non}$) and 'hot spots' count and changes in spirometric measurements. AHR = airway hyperresponsiveness; FEV1 = forced expiratory volume in 1 second; FVC = forced vital capacity; DRS_{FEV1} = dose response slope for FEV1; G5 = respiratory system conductance measured at 5 Hz; DRS_{G5} = dose response slope for G5; X5 = respiratory system reactance measured at 5 Hz; DRS_{X5} = dose response slope for X5; $Vent_{Non}$ = non-ventilated volume.

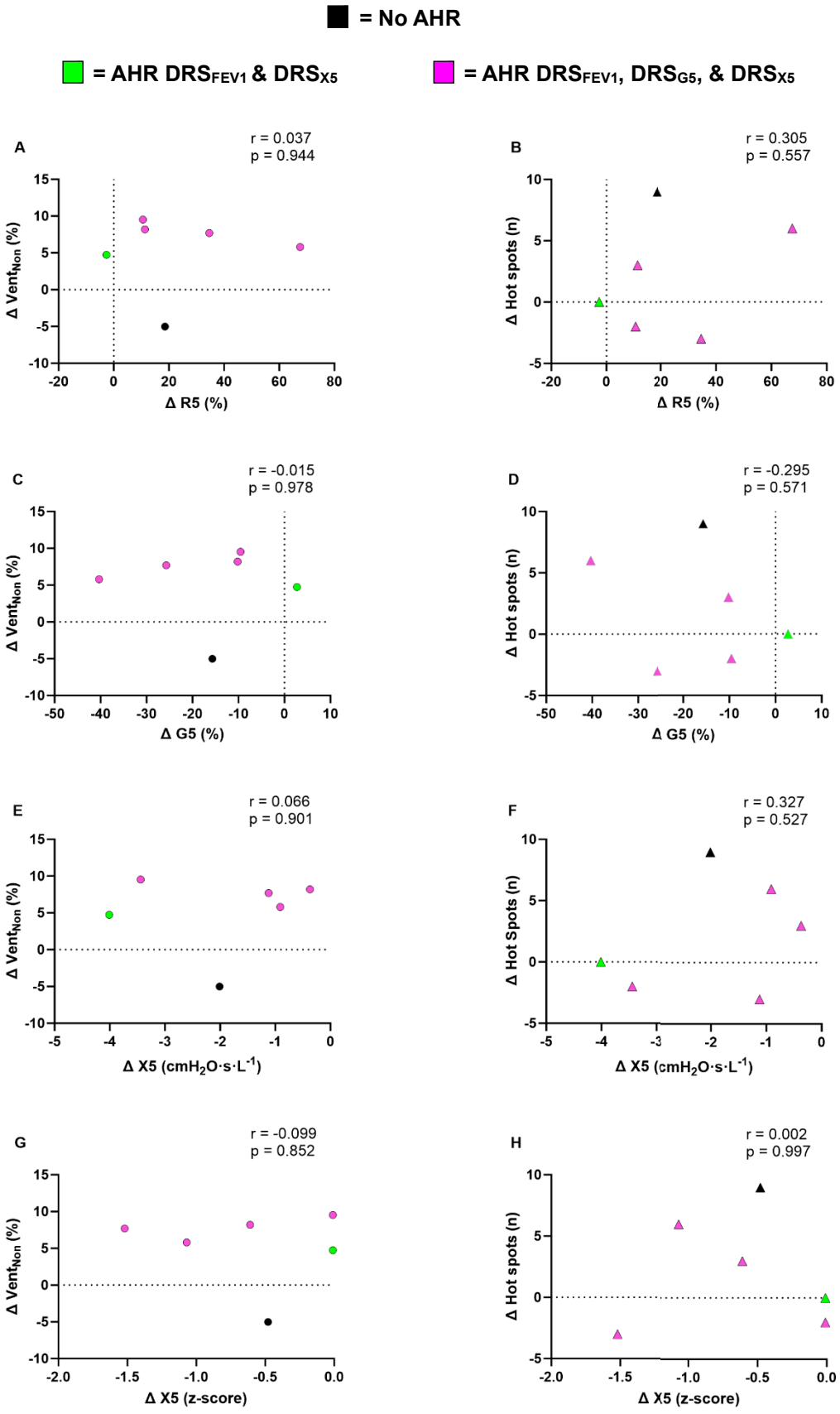

■ = No AHR
■ = AHR DRSFEV1 & DRSX5
■ = AHR DRSFEV1, DRSG5, & DRSX5
A
r = 0.037
p = 0.944
Δ VentNon (%)
Δ R5 (%)
B
r = 0.305
p = 0.557
Δ Hot spots (n)
Δ R5 (%)
C
r = -0.015
p = 0.978
Δ VentNon (%)
Δ G5 (%)
D
r = -0.295
p = 0.571
Δ Hot spots (n)
Δ G5 (%)
E
r = 0.066
p = 0.901
Δ VentNon (%)
Δ X5 (cmH2O·s·L-1)
F
r = 0.327
p = 0.527
Δ Hot Spots (n)
Δ X5 (cmH2O·s·L-1)
G
r = -0.099
p = 0.852
Δ VentNon (%)
Δ X5 (z-score)
H
r = 0.002
p = 0.997
Δ Hot spots (n)
Δ X5 (z-score)

Figure 7: Relationships between post-methacholine changes in non-ventilated volume ($Vent_{Non}$) and 'hot spots' count and changes in oscillometry measurements. AHR = airway hyperresponsiveness; FEV1 = forced expiratory volume in 1 second; FVC = forced vital capacity; DRS_{FEV1} = dose response slope for FEV1; R5 = respiratory system resistance measured at 5 Hz; G5 = respiratory system conductance measured at 5 Hz; DRS_{G5} = dose response slope for G5; X5 = respiratory system reactance measured at 5 Hz; DRS_{X5} = dose response slope for X5; $Vent_{Non}$ = non-ventilated volume.

5.4.5 Predictors of changes in non-ventilated volume and 'hot spots'

Relationships between changes in $Vent_{Non}$ and 'hot spots' count and baseline lung function measurements are summarised in Table 3. There was a trend towards an association between an increase in $Vent_{Non}$ post-methacholine with increased baseline 'hot spots' count ($r = 0.72$, p-value = 0.07) (Figure 8C). There was also a trend towards a significant relationship between increased 'hot spots' count post-methacholine and reduced 'hot spots' count at baseline (Figure 8D). Increased baseline FVC z-score was associated with a greater increase in 'hot spots' count post-methacholine ($r = 0.82$, p-value = 0.02) (Figure 9).

Table 3: Univariate correlations between post-methacholine changes in non-ventilated volume and 'hot spots' and baseline lung function measurements.

	Δ $Vent_{Non}$, %		Δ Hot spots (n)	
	r	p-value	r	p-value
$Vent_{Non}$, %	-0.26	0.58	0.51	0.25
Hot spots, n	0.72	0.07	-0.69	0.09
FEV1, z-score	-0.004	0.99	0.46	0.29
FVC, z-score	-0.31	0.49	**0.82**	**0.02**
FEV1/FVC, %	0.18	0.70	-0.35	0.44
FEV1/FVC, z-score	0.12	0.79	-0.17	0.71
TLC, z-score	-0.03	0.95	0.39	0.39
IC, z-score	-0.23	0.63	0.59	0.17
FRC, z-score	0.17	0.72	0.09	0.86
RV, z-score	0.25	0.58	0.04	0.94
FRC/TLC, z-score	0.41	0.36	-0.35	0.44
RV/TLC, z-score	0.24	0.61	0.27	0.56
D_{LCO}, z-score	0.03	0.96	-0.37	0.41
K_{CO}, z-score	0.06	0.90	-0.40	0.38
VA/TLC, z-score	-0.25	0.59	-0.31	0.49
R5, z-score	-0.13	0.81	-0.13	0.79
G5, $L.cm.H_2O.s^{-1}$	0.08	0.88	0.23	0.67
X5, z-score	-0.46	0.30	0.22	0.64

$Vent_{Non}$ = non-ventilated volume; FEV1 = forced expiratory volume in 1 second; FVC = forced vital capacity; TLC = total lung capacity; IC = inspiratory capacity; FRC = functional residual capacity; RV = residual volume; DL_{CO} = diffusing capacity for carbon monoxide; K_{CO} = carbon monoxide transfer coefficient; VA = alveolar volume; R5 = respiratory system resistance at 5 Hz; G5 = respiratory system conductance; X5 = respiratory system reactance measured at 5 Hz

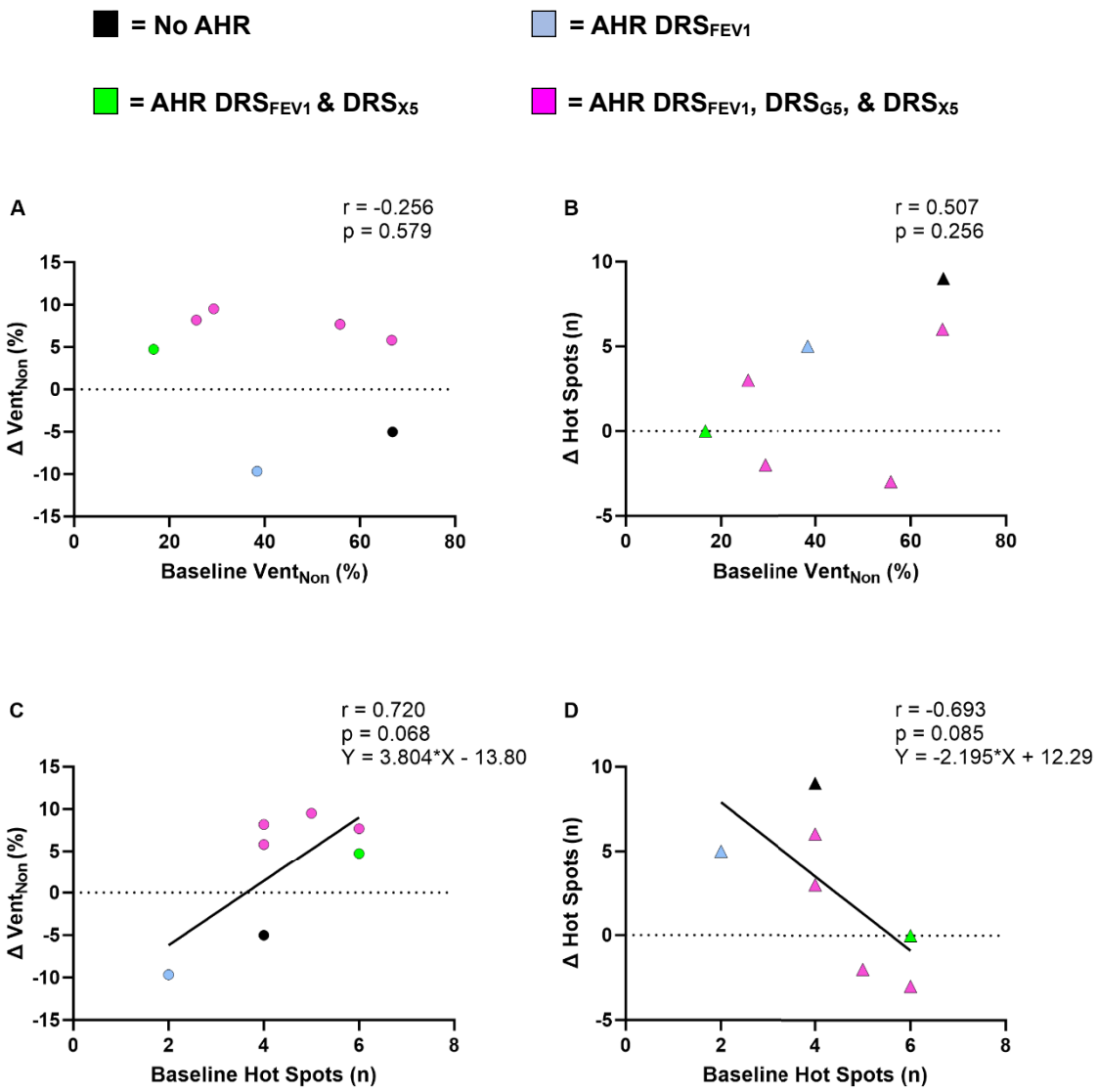


Figure 8: Relationships between post-methacholine changes in non-ventilated volume ($Vent_{Non}$) and 'hot spots' count and baseline $Vent_{Non}$ and 'hot spots'. AHR = airway hyperresponsiveness; FEV1 = forced expiratory volume in 1 second; FVC = forced vital capacity; DRS_{FEV1} = dose response slope for FEV1; G5 = respiratory system conductance measured at 5 Hz; DRS_{G5} = dose response slope for G5; X5 = respiratory system reactance measured at 5 Hz; DRS_{X5} = dose response slope for X5; $Vent_{Non}$ = non-ventilated volume.

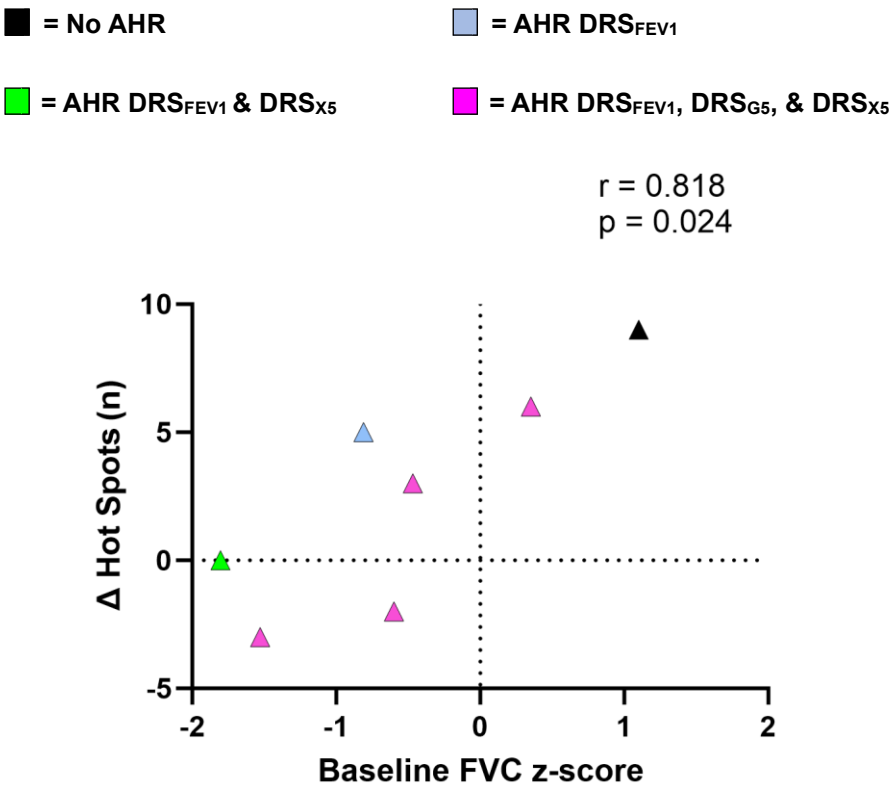


Figure 9: Relationship between post-methacholine change in 'hot spots' count and baseline forced vital capacity (FVC) z-score. AHR = airway hyperresponsiveness; FEV1 = forced expiratory volume in 1 second; FVC = forced vital capacity; DRS_{FEV1} = dose response slope for FEV1; G5 = respiratory system conductance measured at 5 Hz; DRS_{G5} = dose response slope for G5; X5 = respiratory system reactance measured at 5 Hz; DRS_{X5} = dose response slope for X5; $Vent_{Non}$ = non-ventilated volume.

5.4.6 Relationships between baseline imaging parameters and changes in lung function

The relationships between baseline $Vent_{Non}$ and 'hot spots' count and changes in lung function are shown in Table 4. Decreased baseline $Vent_{Non}$, and thus greater ventilation, predicted a greater closing index (r = -0.76, p-value = 0.05) (Figure 10B). There was a trend towards a relationship between baseline $Vent_{Non}$ and a greater increase in R5 post-methacholine (r = 0.78, p-value = 0.07) (Figure 10C). Additionally, increased $Vent_{Non}$ at baseline was associated with a larger reduction of G5 post-methacholine (r = -0.83, p-value = 0.04) (Figure 10D).

Table 5: Univariate correlations between baseline non-ventilated volume and 'hot spots' count and changes in lung function

	$Vent_{Non}$, %		Hot spots (n)	
	r	p-value	r	p-value
Δ FEV1, %	0.13	0.78	-0.62	0.14
Δ FVC, %	0.69	0.08	-0.51	0.24
Δ FEV1/FVC, %	-0.21	0.66	-0.01	0.98
Δ FEV1/FVC, z-score #	-0.61	0.17	-0.06	0.93
Δ R5, %	0.78	0.07	-0.35	0.50
Δ G5, %	**-0.83**	**0.04**	0.36	0.48
Δ X5, $cm.H_2O.s.L^{-1}$	0.50	0.31	-0.53	0.28
Δ X5, z-score	-0.66	0.16	-0.004	0.99
DRS_{FEV1}, % decrease FEV1/μmol +3	-0.39	0.39	0.23	0.63
DRS_{G5}, % decrease G5/μmol +3 #	0.20	0.71	-0.59	0.23
DRS_{X5}, decrease X5/μmol +3	-0.58	0.23	0.30	0.56
Closing index, %ΔFVC/%ΔFEV1	**-0.76**	**0.05**	0.19	0.68

$Vent_{Non}$ = non-ventilated volume; FEV1 = forced expiratory volume in 1 second; FVC = forced vital capacity; R5 = respiratory system resistance at 5 Hz; G5 = respiratory system conductance; X5 = respiratory system reactance measured at 5 Hz; DRS_{FEV1} = dose response slope for FEV1; DRS_{G5} = dose response slope for G5; DRS_{X5} = dose response slope for X5; # = Spearman's rank correlation coefficient

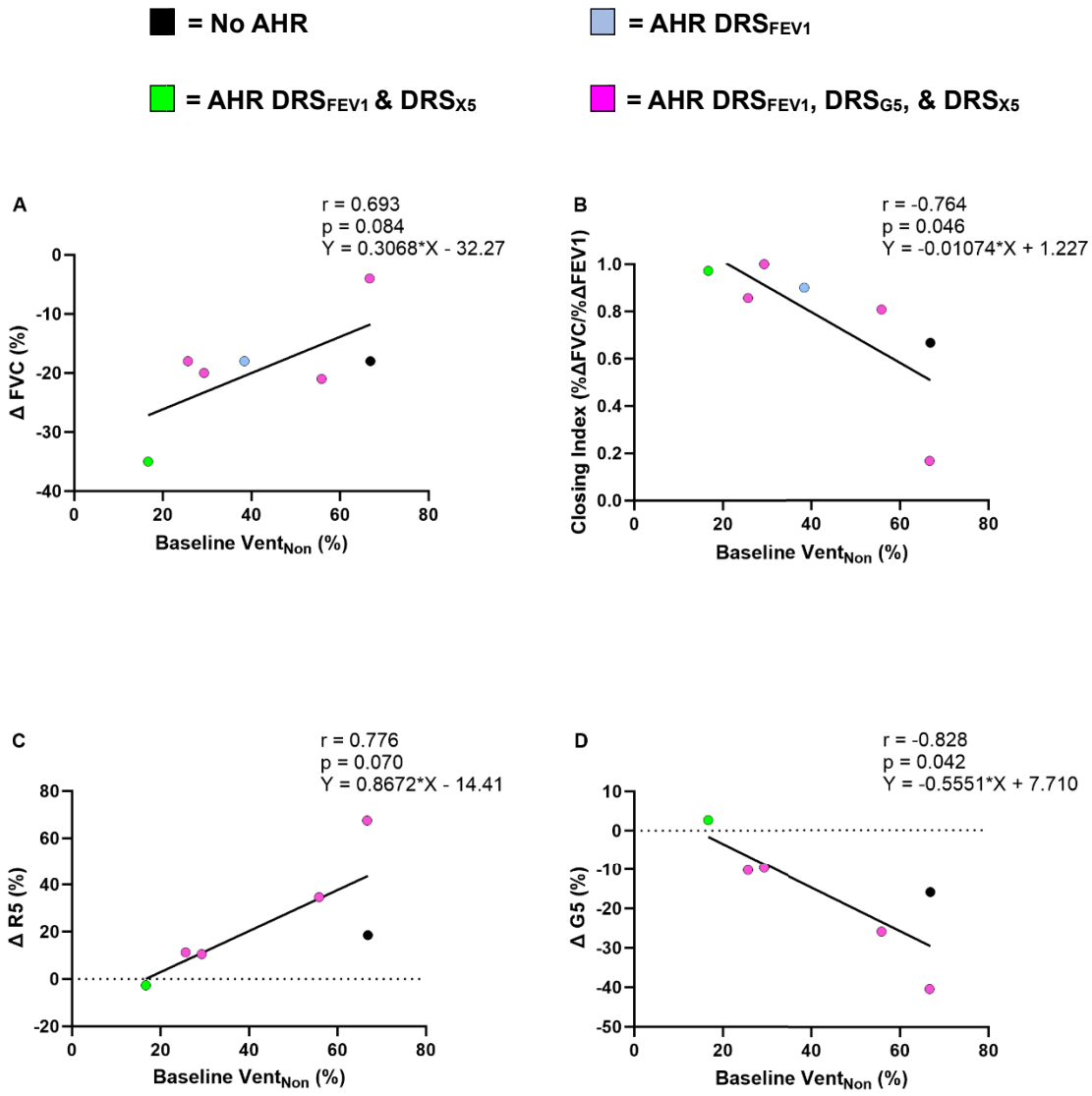


Figure 10: Relationships between baseline non-ventilated volume ($Vent_{Non}$) and change in forced vital capacity (FVC), closing index, change in respiratory system resistance at 5 Hz (R5), and change in respiratory system conductance at 5 Hz (G5) post-methacholine. AHR = airway hyperresponsiveness; FEV1 = forced expiratory volume in 1 second; FVC = forced vital capacity; DRS_{FEV1} = dose response slope for FEV1; G5 = respiratory system conductance measured at 5 Hz; DRS_{G5} = dose response slope for G5; X5 = respiratory system reactance measured at 5 Hz; DRS_{X5} = dose response slope for X5; $Vent_{Non}$ = non-ventilated volume.

5.5 Discussion

To our current knowledge, this has been the first study to investigate the effects of bronchoconstriction in COPD patients with VSPECT/CT. We observed that despite some similarities to the results of VSPECT asthma studies, there were noted differences in how ventilation was affected post-methacholine in COPD patients. Firstly, bronchoconstriction did not significantly reduce $Vent_{Non}$ and 'hot spots' count, and responses for both parameters appeared to be variable (change in $Vent_{Non}$ and 'hot spots' count ranges: -9.65 – 9.53 and -3 – 9, respectively). Overall, the high closing index indicated that airway closure had predominately contributed to the fall in FEV1. The increased closing index could have been due to the generally high BMI (mean ± SD: 30.9 ± 7.4) of the participants (27). Contrary to our hypothesis, neither baseline $Vent_{Non}$ nor 'hot spots' count predicted AHR severity. Although our previous chapters (3 and 4) demonstrated no correlations between $Vent_{Non}$ and 'hot spots' count at baseline nor post-bronchodilator, we showed that there was a trend towards reduced $Vent_{Non}$ and increased 'hot spots' post-methacholine. This may indicate that bronchoconstriction had either primarily caused airway narrowing ('hot spots' count) or airway closure ($Vent_{Non}$) but not both. Our findings support the idea that AHR in COPD to be mechanistically distinct from AHR in asthma.

5.5.1 The effects of methacholine on non-ventilated volume

We observed there to be a trend towards a significant relationship between more severe AHR, as measured by DRS_{FEV1}, and greater loss of ventilation post-methacholine ($r = 0.70$, p-value = 0.08). As the study from Farrow et al. (17) reported a r value of 0.56, our result is likely have been due to the low number of participants in the study. Thus, in both asthma and COPD, those with more severe AHR appear to have experienced extensive airway closure and loss of ventilation.

Unlike bronchoconstriction in asthma, which has been shown to both significantly decrease ventilation (17) and increase poor ventilation (16) from airway closure and airway narrowing, respectively, we observed that the $Vent_{Non}$ response post-methacholine in COPD to be highly variable. Although asthma methacholine challenge studies have utilised similar methacholine cumulative dose ranges to our study, they consistently reported significant increases in $Vent_{Non}$ despite similar changes in FEV1 (14, 15, 17). Although the physiological mechanisms behind AHR in asthma and COPD are suspected to differ, it was still surprising to observe the lack of a significant change in $Vent_{Non}$ and the variability in response. Of course, this may be at least partially attributed to the low participant number and the noise of repeated measurements. Whilst we previously demonstrated there to be issues regarding accuracy and robustness with the threshold method utilised by Farrow et al. (17) in Chapter 2, it is unlikely to have been responsible for our conflicting results. In fact, their method had probably underestimated the loss of ventilation and the extent of airway closure post-methacholine (Chapter 2). As Verhoeven et al. (13) observed no relationships between AHR and parameters relating to parenchymal damage and

gas transfer in COPD patients, it is unlikely that emphysematous changes alone to the lung parenchyma are responsible for the variable $Vent_{Non}$ response. As suggested by Hardaker et al. (10), small airways disease processes specific to COPD, such as extensive airway pruning (35), may have been responsible for the variability in $Vent_{Non}$ response. As a result of small airway obliteration and obstruction in COPD (36, 37), there is greater ventilation throughout collateral airways to preserve gas exchange (35). Thus, it is possible that through recruitment of narrow collateral airways and redistributing ventilation that two of our COPD patients resisted airway closure and ventilation loss.

To explain further, there appears to be primarily two different physiological responses to methacholine that either increased or decreased $Vent_{Non}$, but the changes for both responses were relatively low compared to $Vent_{Non}$ at baseline (mean ± SD: 42.8 ± 20.4). For five of our participants, the mean ± SD increase in $Vent_{Non}$ post-methacholine was 7.91 ± 1.91. This likely reflects the loss of ventilation and Technegas deposition due to airway closure in participants with AHR, and this is supported by the trend towards an association between increase in $Vent_{Non}$ and increased DRS_{FEV1} (Figure 4A). Conversely, the mean ± SD change in $Vent_{Non}$ post-methacholine in the remaining two participants was -7.33 ± 3.28. Rather than an 'improvement' in ventilation, these participants may have primarily responded to methacholine through hyperinflation, thereby protecting airways from closure. This distinct and opposite response was observed and discussed by Osorio-Valencia et al. (38) in their high-resolution CT study on asthmatic and non-asthmatic participants. Indeed, increase in lung volume was found to be inversely associated with airway luminal area narrowing post-methacholine. The trend towards an inverse

correlation between changes in $Vent_{Non}$ and ‘hot spots’ count post-methacholine (Figure 3) suggest an additional physiological mechanism: ventilation redistribution. Participants who responded to methacholine with hyperinflation and decreased $Vent_{Non}$, ventilation could have also redistributed through newly dilated airways (8) that were either severely narrowed or closed at baseline and with collateral airways, thus increasing overall ventilation heterogeneity. These airways may have dilated enough for ventilation and Technegas deposition to occur but not to the extent to avoid turbulent airflow and Technegas aggregation or collision. Redistribution of ventilation may have occurred as a way of avoiding lung regions with poor ventilation or simply due to expanded airspace. For participants that experienced airway closure and increased $Vent_{Non}$, the reduction of ‘hot spots’ count is likely to indicate towards decruitment of airways, and thus, the removal of areas with turbulent or abnormal airflow, rather than reduced airway narrowing. Therefore, the two distinct and opposite responses to methacholine, airway closure and hyperinflation, may be accompanied by reduced ventilation heterogeneity and ventilation redistribution, respectively. As with investigating bronchodilator effects with VSPECT/CT, regional analysis should provide further information on ventilation redistribution.

5.5.2 The effects of methacholine on hot spots

Like the results with $Vent_{Non}$, ‘hot spots’ count did not significantly change post-methacholine, and the response was again variable. As there has only been other VSPECT study (although scintigraphic) that utilised quantitative ‘hot spot’ analysis, comparisons are somewhat difficult to make. Our findings are contradictory to the observations made by Pellegrino et al. (19) in their scintigraphic VSPECT study with

asthma patients, in which ‘hot spots’ count had reportedly increased. As we believe that ‘hot spots’ are representative of airway abnormalities in narrowed airways as suggested by Jobse et al. (18) and Pellegrino et al. (19), some further comparisons could be made with studies by Farrow et al. (16) and Tzeng et al. (39), as they had also examined airway narrowing by measuring poor or patchy ventilation. Although Farrow et al. (16) determined poor ventilation via a threshold and Tzeng et al. (39) utilised coefficient of variation around each voxel to determine patchy ventilation, these measurements were thought to reflect airway narrowing and not airway closure. Contrary to our results again, both Farrow et al. (16) and Tzeng et al. (39) reported significant increases in poor or patchy ventilation after inducing bronchoconstriction. Furthermore, not only did both poor ventilation and $Vent_{Non}$ significantly increase in the studies by Farrow et al. (16, 17), the changes in poor ventilation and $Vent_{Non}$ had correlated positively with each other, i.e. greater airway narrowing coincided with greater airway closure (16).

Like the $Vent_{Non}$ response, the change in ‘hot spots’ count was variable. As indicated by Figure 3, the inverse relationship between changes in ‘hot spot’ count and $Vent_{Non}$ post-methacholine again suggests the idea that COPD patients had either resisted airway closure with airway recruitment and hyperinflation (at the cost of increasing ventilation heterogeneity and ‘hot spots’) or failed to recruit airways, consequently experiencing extensive airway closure and ventilation loss. Whilst no change in ‘hot spots’ count likely reflects the lack of new regions with airway narrowing, the reduction of ‘hot spots’ may be indicative of airway closure and decruitment. This is further supported by the trend towards a significant relationship between increased ‘hot spots’ count and reduced closing index post-methacholine as shown in Figure

5B. As discussed previously, this somewhat binary response in COPD could have resulted from extensive small airway damage and increased collateral ventilation.

5.5.3 Predictors of change in non-ventilated volume, hot spots, and lung function

Baseline ‘hot spots’ count trended toward positive and negative correlations with changes in $Vent_{Non}$ and ‘hot spots’ count, respectively. These trends indicate that increased airflow abnormalities at baseline due to greater airway narrowing or ventilation heterogeneity predicted a greater increase in $Vent_{Non}$ from airway closure. The increased ‘hot spots’ count at baseline may have reflected a greater number of narrowed airways that were unstable and therefore close to the ‘critical point’ of catastrophic airway narrowing and closure. The idea of a ‘critical point’ in airway narrowing that leads to airway instability and airway closure has long been examined within the context of asthma. In a computational 12-generation bronchial tree model, Venegas et al. (8) simulated bronchoconstriction with smooth muscle activation, and they initially observed that the airways had homogeneously constricted. However, once smooth muscle activation and airway resistance increased past a ‘critical point’, a positive feedback loop was formed, consequently leading to distinct clusters of severely constricted airways and large ventilation defects. The authors noted that prior to reaching this ‘critical point’ large, distinct clusters of ventilation defects did not occur. Using the same bronchial model, Winkler and Venegas (40) again observed the ‘critical point’ between homogenous airway narrowing and catastrophic airway closure (and ventilation defects, particularly in the peripheral airways). Past the critical point, the authors also observed complex behaviours to emerge such as

greater ventilation heterogeneity and dilation of other airways in the bronchial tree due to serial and parallel airway interdependence. In another bronchial tree model study, Winkler et al. (41) demonstrated that the ‘critical point’ could be substantially reduced (reached with lower levels of airway smooth muscle activation) if airway wall thickness had increased. Furthermore, a regional increase in airway thickness resulted in a lower ‘critical point’ than homogenous, global airway thickening. And so, as previously stated, the ‘hot spots’ at baseline may have represented regions of narrowed or thickened small airways that were close to a potentially reduced ‘critical point’. Once these unstable airways were provoked by methacholine, they reached the ‘critical point’ and closed, thereby increasing $Vent_{Non}$ and reducing ‘hot spots’ count, respectively.

We found that increased $Vent_{Non}$ at baseline predicted greater airway narrowing, as measured by reduction in G5, increase in R5, and a lower closing index. These results altogether suggest that greater airway closure or absent ventilation prior to methacholine leads to a post-methacholine response involving greater airway narrowing (42). Conversely, this also indicates that in participants with reduced airway closure, their response to methacholine had almost exclusively involved airway closure instead of airway narrowing. The functional loss of terminal bronchioles or perhaps large, proximal airways as a result of emphysema may have limited the propagation of airway closure to other connected airways in the bronchial tree (8). Alternatively, airway narrowing and closure following bronchoprovocation is thought to mostly occur within the small airways (43), but this may not take place in emphysematous participants who have undergone substantial small airway pruning. Airway narrowing and methacholine deposition might have been primarily localised

within the larger proximal airways, which were demonstrated in a simulation study by Winkler and Venegas (40) to be resistant against near or complete airway closure compared to smaller, peripheral airways. Therefore, the reduced proportion of airway closure in emphysematous patients following bronchoprovocation may simply be because of the reduced availability of smaller peripheral airways.

We also observed that FVC z-score had exclusively predicted the response in 'hot spots' count. We speculate that a larger FVC z-score could indicate towards a greater availability of airways that were not severely narrowed and were thus resistant to closure or collapse during the forced expiratory manoeuvre (44, 45). These relatively 'healthier' small airways with a higher 'critical point' than narrowed airways may have been more susceptible to narrowing than complete closure, hence the increase of 'hot spots' count post-methacholine. Conversely, if there was a greater proportion of small airways that were severely narrowed at baseline with a lower 'critical point', methacholine may have induced complete closure, thereby ceasing airflow entirely. This would result in the reduction of 'hot spots' count.

5.5.4 Limitations

Our study was limited by the small number of participants, so all interpretations of results were made with caution. The variable length of time between the baseline and methacholine visits was another limitation, and although a FEV1 difference > 200 mL excluded participants from analysis, ventilation may not have remained consistent. Changes in hyperinflation, such as IC, were not measured in this study so we could only speculate on the role of hyperinflation. Furthermore, improvements

in dyspnoea had not been measured and redistributions of $Vent_{Non}$ or ‘hot spots’ into new locations in the lung had not been assessed.

5.5.5 Conclusion

To summarise, we found that non-ventilated volume and ‘hot spots’ count had not changed significantly post-methacholine, although changes in both parameters appeared to be variable, which could indicate distinctly different responses. Neither of the VSPECT/CT parameters predicted AHR. Participants with greater non-ventilated volume at baseline were more predisposed to airway narrowing. Furthermore, reduced gas trapping at baseline was associated with an increase in ‘hot spots’ count. When assessing post-methacholine responses with VSPECT/CT, parameters that assess regional changes in non-ventilated volume or distribution of ventilation and ‘hot spots’ may provide further insight.

5.6 References

1. Scichilone N, Battaglia S, La Sala A, Bellia V. Clinical implications of airway hyperresponsiveness in COPD. Int J Chron Obstruct Pulmon Dis. 2006;1(1):49-60.
2. Yan K, Salome CM, Woolcock AJ. Prevalence and Nature of Bronchial Hyperresponsiveness in Subjects with Chronic Obstructive Pulmonary Disease. American Review of Respiratory Disease. 1985;132(1):25-9.
3. Tashkin DP, Altose MD, Bleecker ER, Connett JE, Kanner RE, Lee WW, Wise R, 4 TLHSRG. The Lung Health Study: Airway Responsiveness to Inhaled Methacholine in Smokers with Mild to Moderate Airflow Limitation. American Review of Respiratory Disease. 1992;145(2_pt_1):301-10.
4. Tashkin DP, Altose MD, Connett JE, Kanner RE, Lee WW, Wise RA. Methacholine reactivity predicts changes in lung function over time in smokers with early chronic obstructive pulmonary disease. The Lung Health Study Research Group. American Journal of Respiratory and Critical Care Medicine. 1996;153(6):1802-11.
5. Tkacova R, Dai DLY, Vonk JM, Leung JM, Hiemstra PS, van den Berge M, Kunz L, Hollander Z, et al. Airway hyperresponsiveness in chronic obstructive pulmonary disease: A marker of asthma-chronic obstructive pulmonary disease overlap syndrome? Journal of Allergy and Clinical Immunology. 2016;138(6):1571-9.e10.
6. Downie SR, Salome CM, Verbanck S, Thompson B, Berend N, King GG. Ventilation heterogeneity is a major determinant of airway hyperresponsiveness in asthma, independent of airway inflammation. Thorax. 2007;62(8):684-9.
7. Hardaker KM, Downie SR, Kermode JA, Farah CS, Brown NJ, Berend N, King GG, Salome CM. Predictors of Airway Hyperresponsiveness Differ Between Old and Young Patients With Asthma. Chest. 2011;139(6):1395-401.
8. Venegas JG, Winkler T, Musch G, Vidal Melo MF, Layfield D, Tgavalekos N, Fischman AJ, Callahan RJ, et al. Self-organized patchiness in asthma as a prelude to catastrophic shifts. Nature. 2005;434(7034):777-82.
9. Jarenbäck L, Ankerst J, Bjermer L, Tufvesson E. Acinar ventilation heterogeneity in COPD relates to diffusion capacity, resistance and reactance. Respir Med. 2016;110:28-33.
10. Hardaker KM, Downie SR, Kermode JA, Berend N, King GG, Salome CM. Ventilation heterogeneity is associated with airway responsiveness in asthma but not COPD. Respiratory Physiology & Neurobiology. 2013;189(1):106-11.
11. Kanner RE, Connett JE, Altose MD, Buist AS, Lee WW, Tashkin DP, Wise RA. Gender difference in airway hyperresponsiveness in smokers with mild COPD. The Lung Health Study. American Journal of Respiratory and Critical Care Medicine. 1994;150(4):956-61.
12. Koyama H, Nishimura K, Ikeda A, Sakai N, Mishima M, Izumi T. Influence of baseline airway calibre and pulmonary emphysema on bronchial responsiveness in patients with chronic obstructive pulmonary disease. Respiratory Medicine. 1996;90(6):323-8.
13. Verhoeven GT, Verbraak AFM, Boere-van der Straat S, Hoogsteden HC, Bogaard JM. Influence of Lung Parenchymal Destruction on the Different Indexes of the Methacholine Dose-Response Curve in COPD Patients. Chest. 2000;117(4):984-90.
14. COSTELLA S, KIRBY M, MAKSYM GN, MCCORMACK DG, PATERSON NAM, PARRAGA G. Regional pulmonary response to a methacholine challenge using hyperpolarized 3He magnetic resonance imaging. Respirology. 2012;17(8):1237-46.
15. Samee S, Altes T, Powers P, de Lange EE, Knight-Scott J, Rakes G, Mugler Iii JP, Ciambotti JM, et al. Imaging the lungs in asthmatic patients by using hyperpolarized helium-3 magnetic resonance: Assessment of response to methacholine and exercise challenge. Journal of Allergy and Clinical Immunology. 2003;111(6):1205-11.

16. Farrow CE, Salome CM, Harris BE, Bailey DL, Berend N, King GG. Peripheral ventilation heterogeneity determines the extent of bronchoconstriction in asthma. Journal of Applied Physiology. 2017;123(5):1188-94.
17. Farrow CE, Salome CM, Harris BE, Bailey DL, Bailey E, Berend N, Young IH, King GG. Airway closure on imaging relates to airway hyperresponsiveness and peripheral airway disease in asthma. J Appl Physiol (1985). 2012;113(6):958-66.
18. Jobse BN, Rhem RG, McCurry CA, Wang IQ, Labiris NR. Imaging lung function in mice using SPECT/CT and per-voxel analysis. PLoS One. 2012;7(8):e42187.
19. Pellegrino R, Biggi A, Papaleo A, Camuzzini G, Rodarte JR, Brusasco V. Regional expiratory flow limitation studied with Technegas in asthma. Journal of Applied Physiology. 2001;91(5):2190-8.
20. Graham BL, Steenbruggen I, Miller MR, Barjaktarevic IZ, Cooper BG, Hall GL, Hallstrand TS, Kaminsky DA, et al. Standardization of Spirometry 2019 Update. An Official American Thoracic Society and European Respiratory Society Technical Statement. American Journal of Respiratory and Critical Care Medicine. 2019;200(8):e70-e88.
21. Philip HQ, Sanja S, Tim JC, Xaver B, Graham LH, Bruce HC, Paul LE, John LH, et al. Multi-ethnic reference values for spirometry for the 3–95-yr age range: the global lung function 2012 equations. European Respiratory Journal. 2012;40(6):1324.
22. Graham LH, Nicole F, Gregg R, Tolu O, Bruce T, Jane K, Irene S, Brendan GC, et al. Official ERS technical standard: Global Lung Function Initiative reference values for static lung volumes in individuals of European ancestry. European Respiratory Journal. 2021;57(3):2000289.
23. "Official ERS technical standards: Global Lung Function Initiative reference values for the carbon monoxide transfer factor for Caucasians." Sanja Stanojevic, Brian L. Graham, Brendan G. Cooper, Bruce R. Thompson, Kim W. Carter, Richard W. Francis and Graham L. Hall on behalf of the Global Lung Function Initiative T_{LCO} working group. Eur Respir J 2017; 50: 1700010. European Respiratory Journal. 2020;56(4):1750010.
24. Brown NJ, Xuan W, Salome CM, Berend N, Hunter ML, Musk AW, James AL, King GG. Reference equations for respiratory system resistance and reactance in adults. Respiratory Physiology & Neurobiology. 2010;172(3):162-8.
25. Peat JK, Salome CM, Berry G, Woolcock AJ. Relation of Dose-Response Slope to Respiratory Symptoms and Lung Function in a Population Study of Adults Living in Busselton, Western Australia. American Review of Respiratory Disease. 1992;146(4):860-5.
26. McClean MA, Htun C, King GG, Berend N, Salome CM. Cut-points for response to mannitol challenges using the forced oscillation technique. Respiratory Medicine. 2011;105(4):533-40.
27. Chapman DG, Berend N, King GG, Salome CM. Increased airway closure is a determinant of airway hyperresponsiveness. European Respiratory Journal. 2008;32(6):1563-9.
28. Crawford AB, Davison A, Amis TC, Engel LA. Intrapulmonary distribution of 99mtechnetium labelled ultrafine carbon aerosol (Technegas) in severe airflow obstruction. Eur Respir J. 1990;3(6):686-92.
29. Amis TC, Crawford AB, Davison A, Engel LA. Distribution of inhaled 99mtechnetium labelled ultrafine carbon particle aerosol (Technegas) in human lungs. European Respiratory Journal. 1990;3(6):679.
30. Lemb M, Oei T, Eifert H, Günther B. Technegas: a study of particle structure, size and distribution. European journal of nuclear medicine. 1993;20:576-9.
31. Rutting S, Mahadev S, Tonga KO, Bailey DL, Dame Carroll JR, Farrow CE, Thamrin C, Chapman DG, et al. Obesity alters the topographical distribution of ventilation and the regional response to bronchoconstriction. Journal of Applied Physiology. 2019;128(1):168-77.
32. Otsu N. A Threshold Selection Method from Gray-Level Histograms. IEEE Transactions on Systems, Man, and Cybernetics. 1979;9(1):62-6.
33. Kroon D-J. Region Growing: MATLAB Central File Exchange; 2008 [Available from: https://au.mathworks.com/matlabcentral/fileexchange/19084-region-growing.

34. Koltai H. Novel 3D Segmentation Methods for SPECT Images of Airway Disease: The University of Sydney; 2021.
35. Hogg JC, Chu F, Utokaparch S, Woods R, Elliott WM, Buzatu L, Cherniack RM, Rogers RM, et al. The Nature of Small-Airway Obstruction in Chronic Obstructive Pulmonary Disease. New England Journal of Medicine. 2004;350(26):2645-53.
36. Morrell NW, Wignall BK, Biggs T, Seed WA. Collateral ventilation and gas exchange in emphysema. Am J Respir Crit Care Med. 1994;150(3):635-41.
37. Terry PB, Traystman RJ, Newball HH, Batra G, Menkes HA. Collateral Ventilation in Man. New England Journal of Medicine. 1978;298(1):10-5.
38. Osorio-Valencia JS, Wongviriyawong C, Winkler T, Kelly VJ, Harris RS, Venegas JG. Elevation in lung volume and preventing catastrophic airway closure in asthmatics during bronchoconstriction. PLoS One. 2018;13(12):e0208337.
39. Tzeng Y-S, Lutchen K, Albert M. The difference in ventilation heterogeneity between asthmatic and healthy subjects quantified using hyperpolarized 3He MRI. Journal of Applied Physiology. 2009;106(3):813-22.
40. Winkler T, Venegas JG. Complex airway behavior and paradoxical responses to bronchoprovocation. Journal of Applied Physiology. 2007;103(2):655-63.
41. Winkler T, Thamrin C, Farah CS, King GG. Regional Increase in Airway Wall Thickness Could Explain Increase in Ventilation Defects (VDefs) and Heterogeneity in Ventilation in Asthma. D97 IMAGING AND MODELING: INSIGHTS INTO LUNG STRUCTURE AND FUNCTION. p. A7524-A.
42. Irvin CG. Chapter 5 - Pulmonary Physiology. In: Barnes PJ, Drazen JM, Rennard SI, Thomson NC, editors. Asthma and COPD (Second Edition). Oxford: Academic Press; 2009. p. 53-69.
43. Beigelman-Aubry C, Capderou A, Grenier PA, Straus C, Becquemin M-H, Similowski T, Zelter M. Mild Intermittent Asthma: CT Assessment of Bronchial Cross-sectional Area and Lung Attenuation at Controlled Lung Volume. Radiology. 2002;223(1):181-7.
44. Chan ED, Irvin CG. The Detection of Collapsible Airways Contributing to Airflow Limitation. CHEST. 1995;107(3):856-9.
45. Chhabra SK. Forced Vital Capacity, Slow Vital Capacity, or Inspiratory Vital Capacity: Which Is the Best Measure of Vital Capacity? Journal of Asthma. 1998;35(4):361-5.

Chapter 6 – General Discussion & Conclusion

6.1 Results Summary

This thesis presents the following findings regarding ventilation single-photon emission computed tomography/computed tomography (VSPECT/CT) imaging analysis and its parameters in COPD participants.

- In Chapter 2, we developed a novel 'curve-fitting' threshold method for VSPECT/CT that sought to accurately define non-ventilated volume ($Vent_{Non}$). Using physical lung phantom models, we also assessed and compared the 'curve-fitting' threshold method to three existing methods that were either commonly used in computer vision (Otsu's method) or in previous VSPECT studies. The 'curve-fitting' threshold method was determined to be the ideal threshold method for VSPECT/CT analysis as it possessed superior accuracy and robustness against image data heterogeneity compared to the other methods. Additionally, the accuracy of existing VSPECT/CT threshold methods were significantly affected by image data heterogeneity.

- In Chapter 3, we applied VSPECT/CT and the 'curve-fitting' threshold method on COPD participants. In addition to the $Vent_{Non}$, we also measured 'hot spots' count, which detected instances of exaggerated Technegas deposition. Our results showed that both imaging parameters provided distinct, complementary information on lung function. $Vent_{Non}$ mostly related with lung function measurements that were associated with emphysema, whilst 'hot spots' count primarily related with lung function measurements that indicated airflow impairment, likely from airway narrowing, and ventilation heterogeneity. $Vent_{Non}$ and 'hot spots' count were not related to each other.

- In Chapter 4, we examined the effects of bronchodilator with the VSPECT/CT parameters, $Vent_{Non}$ and 'hot spots' count. Although there was no significant change in either VSPECT/CT parameter, the responses for both were variable. Furthermore, change in $Vent_{Non}$ was inversely related to change in respiratory system resistance measured at 5 Hz (R5). We speculated that increased R5 and decreased $Vent_{Non}$ indicated a bronchodilator response involving airway recruitment, thereby also increasing global ventilation. Conversely, reduced R5 and increased $Vent_{Non}$ was suggested to reflect dilated airways and decreased hyperinflation. 'Hot spots' were occasionally observed to subdivide, thereby increasing overall count, or relocate into different lung regions in some COPD participants. Applying topographical analysis on the VSPECT/CT parameters in addition to assessing ventilation quality may provide further information on the bronchodilator response in COPD.

- In Chapter 5, we examined AHR and the effects of bronchoconstriction via methacholine on $Vent_{Non}$ and 'hot spots' count in COPD. Like the effects of bronchodilation, responses for both VSPECT/CT parameters were variable and not significant, and neither of the VSPECT/CT parameters predicted AHR. However, we observed a trend towards a relationship between increased $Vent_{Non}$ post-methacholine and AHR, which suggested that COPD patients with AHR experienced greater airway closure and loss of ventilation. Furthermore, there was another trend towards an inverse correlation between changes in 'hot spots' count and $Vent_{Non}$. Thus, we speculated that there were two distinct responses to methacholine: airway closure and hyperinflation, in

conjunction with decreased and increased ventilation heterogeneity (possibly from ventilation redistribution), respectively. Additionally, COPD patients with extensive airway closure at baseline appeared less likely to experience airway closure post-methacholine. This may have been a consequence of extensive destruction or complete obstruction of the small airways.

6.2 The utility of measuring global estimates of non-ventilated volume and 'hot spots' count

6.2.1 Non-ventilated volume in COPD and possible utility

Throughout this thesis, we attempted to examine COPD with the use of quantitative VSPECT/CT imaging and their relationships with various lung function measurements. Measuring the global estimate of non-ventilated volume has now long been a mainstay for ventilation imaging analysis, but only a few quantitative VSPECT studies have used it to examine COPD. Qualitative studies had consistently reported there to be a substantial loss of ventilation and reduced Technegas deposition in severe COPD patients with emphysema. Furthermore, the relationships between lung function measurements, such as spirometry or lung volumes or oscillometry, and $Vent_{Non}$ have been either inconsistent or unknown.

We were able to confirm the visual observations made in older qualitative VSPECT studies as COPD participants with evidence of emphysema, as determined by poor gas transfer, did indeed possess highly increased $Vent_{Non}$. The loss of Technegas deposition, and thus ventilation, had been speculated by some authors, such as Milne et al. (1), to occur primarily from the loss of diffusive flow within peripheral lung regions. But $Vent_{Non}$ in some COPD patients were highly extensive, and $Vent_{Non}$ regions were observed in proximal lung regions, which suggested the loss of larger airways with convective flow.

Despite the use of an accurate and validated threshold method, our studies involving bronchodilator and bronchoconstriction responses in COPD on $Vent_{Non}$ revealed there to be great variability and no significant changes. These findings suggest limited utility of $Vent_{Non}$ for measuring bronchodilator response and bronchoconstriction in COPD. Whether changes in $Vent_{Non}$ correlate with changes in hyperinflation or gas trapping or dyspnoea is unknown, and further study is warranted. Nonetheless, measuring global $Vent_{Non}$ may still be of use. With quantitative CT imaging analysis, increased global estimations of emphysema (LAA%) has been shown to predict important clinical outcomes, such as mortality (2) and exacerbations (3). Thus, $Vent_{Non}$ could also potentially be used to predict clinical outcomes and assess disease severity in conjunction with traditional methods (e.g., spirometry and symptom severity).

6.2.2 'Hot spots' in COPD and possible utility

The common theme across multiple VSPECT studies was that 'hot spots', which were typically determined through qualitative methods, appeared to form in participants that were more obstructed. But as previously stated, the actual number of 'hot spots', the relationships between 'hot spots' count and $Vent_{Non}$ and lung function measurements were not reported. Additionally, the response in 'hot spots' count to bronchodilator and bronchoconstriction in COPD had not been examined before. This thesis has been the first to provide an in-depth examination of 'hot spots' count with quantitative VSPECT/CT. Surprisingly, we found that 'hot spots' count and $Vent_{Non}$ were unrelated to each other, and the parameters may have related to different physiological mechanisms. Whereas $Vent_{Non}$ appeared to largely reflect

catastrophic damage such as airway destruction or complete airway obstruction, ‘hot spots’ count was speculated to not only reflect instances of airway narrowing and turbulent airflow but also ventilation heterogeneity and unstable airways at risk of closure if provoked by bronchoconstriction. $Vent_{Non}$ and ‘hot spots’ count may have indicated patients who were either predominately affected by emphysema or airways disease, respectively. This may suggest a potential use for these VSPECT parameters as phenotypical markers.

Like $Vent_{Non}$, the response in ‘hot spots’ count to bronchodilator and methacholine were variable, and we speculated that this was due to heterogeneous airway dilation, ventilation redistribution, and airway recruitment/decruitment. However, regional analysis was not included in this thesis, and we could not confirm whether changes in count (or no change) were truly related to those physiological mechanisms. Like $Vent_{Non}$, it appears that measuring total ‘hot spots’ count is unsuitable when analysing response to either bronchodilator treatment or methacholine due to variability in response.

6.3 Future directions for quantitative ventilation imaging analysis

6.3.1 Limitations and possible improvements to the measurement of non-ventilation

In this thesis, $Vent_{Non}$ was an equivalent to ventilation defect percent (VDP), which is a term commonly used in quantitative imaging studies. It should be noted that they measure both hypo-ventilated and unventilated lung volumes. We visually observed this in our lung phantom study since small regions external to the containers without Technetium solution were sometimes classified as $Vent_{Non}$. This was most likely due to the tight spaces restricting Technetium deposition. Nonetheless, binarily categorising all voxel activity as either $Vent_{Non}$/VDP or ventilated activity is likely to be too simple. For example, bronchodilator treatment may predominately improve the quality of ventilation in COPD patients by further dilating airways instead of recruiting previously hypo-ventilated or unventilated lung regions. It is therefore unsurprising to observe recent ventilation studies, whether with VSPECT/CT or hyperpolarised noble gas magnetic resonance imaging (MRI), supplementing the traditional threshold method with additional thresholds for subjectively determined ventilation qualities. Typically, poorly ventilated volume is defined with a strict cut-off above the $Vent_{Non}$ threshold i.e., poorly ventilated volume threshold > $Vent_{Non}$ threshold. Likewise, another ventilation category such as well-ventilated volume is then defined with a cut-off above the threshold for poorly ventilated volume, resulting in $Vent_{Non}$ < poorly ventilated volume < well-ventilated volume thresholds. These additional thresholds for either ‘poorly ventilated’ and ‘well ventilated’ volumes can easily be used with the ‘curve-fitting’ threshold method. The ‘curve-fitting’ method

technically defines ventilated voxel activity as the range between the $Vent_{Non}$ threshold (30% of 'slope point') and the 'slope point', the approximate border between ventilated and 'hot spot' activity. Ventilated activity may be simply categorised into two classes, 'poorly' and 'well', and the voxel activity threshold that divides these two classes could be calculated as the mid-point between the $Vent_{Non}$ threshold and 'slope point'. Of course, the inherent issue with this concept is the arbitrary classification of 'poorly' and 'well' ventilated voxel activities, but we believe that assessing the change in ventilated activity, measured as % of total CT volume, following bronchodilation or bronchoconstriction is still worth investigating. One method of validating this idea of additional thresholds to the 'curve-fitting' threshold method would be by further modifying the lung phantom design in Chapter 2. To briefly reiterate what was stated in that chapter's discussion, one of the limitations to the lung phantoms was their homogenous Technetium (Tc^{99m}) solution concentrations for $Vent_{Vol}$ regions. For example, the Tc^{99m} concentration for a lung phantom contained only one of three (0.04, 0.06, 0.08 mBq/mL) solutions. A relatively easy modification would be to have a lung phantom contain at least two Tc^{99m} concentrations, 0.04 and 0.08 mBq/mL, to simulate 'poorly' and 'well' ventilated lung volumes respectively.

6.3.2 Limitations and possible improvements to the measurement of 'hot spots'

Compared to $Vent_{Non}$, we believe the response in 'hot spots' count to be far more variable. The 'hot spots' were frequently observed to substantially change positions (either more proximally or peripherally in three-dimensional space), size, volume, and shape in the same participant following bronchodilation or bronchoconstriction.

In Chapter 3, we had mentioned there were instances of a large ‘hot spot’ segmenting into multiple smaller ‘hot spots’ following bronchodilation, possibly due to heterogeneous dilation introducing laminar airflow within an airway that had been consistently turbulent at baseline (Figure 1). Alternatively, the locations of ‘hot spots’ were also observed to change drastically without any change in ‘hot spots’ count. The sheer variability of the response in ‘hot spots’ makes interpretation of global measurements such as ‘hot spots’ count difficult. Like $Vent_{Non}$, topographical analysis of ‘hot spots’ may be highly useful.

As discussed in Chapter 3, we suggested analysing the topography of VSPECT/CT parameters by segmenting the lung into proximal and peripheral regions of interest either through traditional segmentation methods (e.g., subjectively determine the border and volume of the peripheral/proximal lung space) or airway generation (e.g., regions beyond the 12^{th} generation of airways is classified as peripheral). The former is a common, regional analysis technique for $Vent_{Non}$: $Vent_{Non}$ within the total lung space is categorised as either proximal or peripheral (or alternatively: upper, middle, or lower) $Vent_{Non}$ (4). If this technique was applied to ‘hot spots’, the overall ‘hot spots’ count could be categorised into proximal or peripheral ‘hot spot’ counts. However, these regions are still too large to examine the highly variable topographical changes in ‘hot spots’. For example, a ‘hot spot’ in an anteriorly peripheral region may have moved significantly more peripherally or posteriorly, but with $Vent_{Non}$ regional analysis techniques, there would be no detected change in location. Indeed, changes in location would only be detected if the ‘hot spot(s)’ crossed the border between the lung regions of interest. A simple solution would be to create multiple regions of interest (> 2) such as central, middle, and outer ‘shells’

of the lung. Another but more complication solution would be to measure the average position of all ‘hot spots’ relative to a single ‘centre’ point in three-dimensional space between the lungs. The benefit of this more complicated technique would be the lack of the arbitrary number of lung regions. As mentioned previously, airway generation in addition to segmenting the lungs into lobes may also be used to analyse the topography of ‘hot spots’.

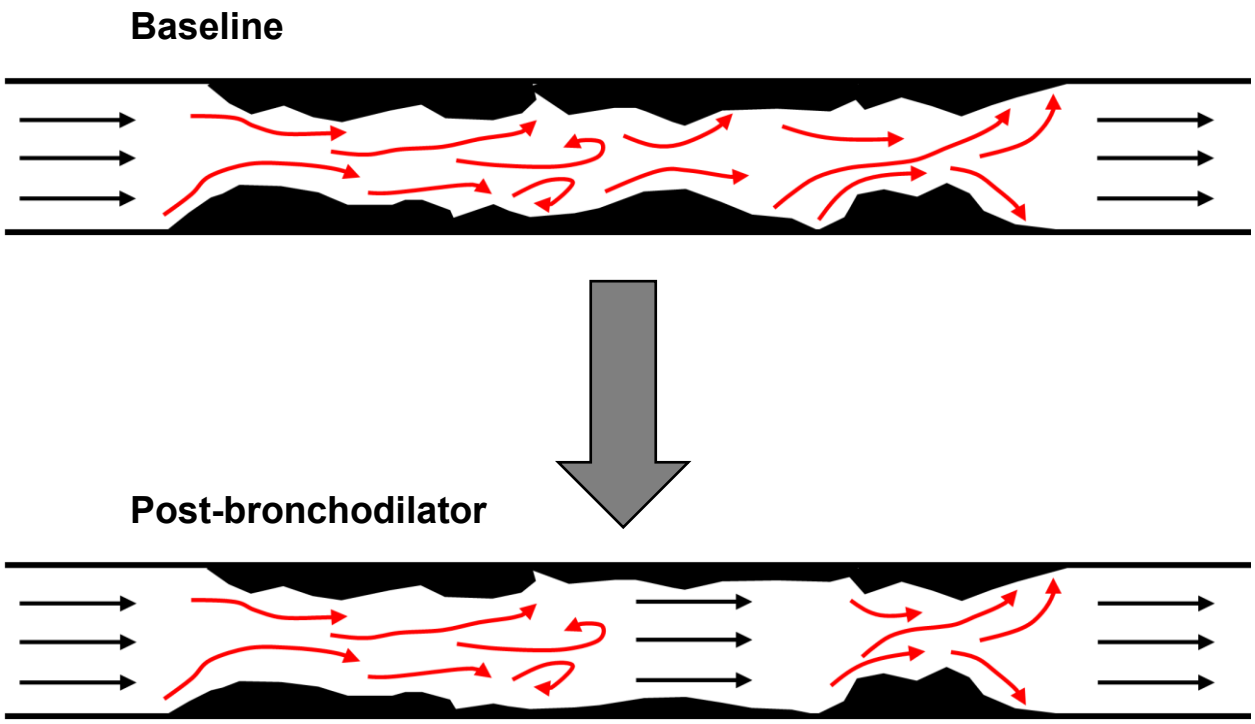


Figure 1: Schematics of airway and airflow at baseline and post-bronchodilator. Smooth or laminar flow is depicted in black arrows. Turbulent airflow is depicted in red arrows. At baseline, consistent airway narrowing results in continuous turbulent airflow. Technegas aggregation would occur within this unbroken section of turbulent airflow, producing one large ‘hot spot’ in the image. Post-bronchodilator, turbulent airflow is no longer consistent due to bronchodilation, and the airflow within the ‘middle’ section is now laminar. As there are now two sections of turbulent airflow and Technegas aggregation, two ‘hot spots’ would then be visible in the image despite airway dilation and improvement of airflow.

6.3.4 Ventilation heterogeneity and analysis without thresholds

Aside from measuring $Vent_{Non}$ and 'hot spots' count, VSPECT/CT could also be used to analyse ventilation heterogeneity. There have been a variety of possible methods to do this. Previously, Nagao et al. (5) combined fractal analysis with ventilation SPECT to investigate examine the visually observable heterogeneous distribution of Technegas (i.e., heterogeneous ventilation) in COPD patients with emphysema. By delineating ventilated voxel activity with five thresholds, which were 15%, 20%, 25%, and 30% of maximum activity, they had calculated the fractal dimension from the slope of the linear regression equation between the total number of voxels and the five thresholds transformed into logarithms. Their results showed that the fractal dimensions, and thus heterogeneous Technegas distribution, had increased with increasing severity of emphysema possibly resulting from parenchyma destruction and small airway narrowing. This technique was suggested by the authors to be a potentially helpful tool in clinical use for quantifying emphysema severity and assessing emphysematous progression. Since there are accuracy issues with percentage of maximum thresholds for delineating ventilated activity, fractal analysis could be applied to the curve fitting threshold method instead by applying additional thresholds above the non-ventilated volume threshold.

Norberg et al. (6) developed another technique for measuring ventilation heterogeneity, and it was named the density curve method. They had calculated the coefficient of variation (CoV) from overlapping cubic volumes of 1 cm^3 on the three-dimensional VSPECT/CT lung image. After compensating the CoV values for the variation in activity uptake between participants, the compensated CoV values were

then plotted as density curves with an area under the curve (AUC) of 100%. Two AUC thresholds were selected: 9.5% and 20%. In a pilot study, the authors reported that increased AUCs above the 20% threshold were found in a patient with asthma and alpha-1 antitrypsin deficiency and another patient with COPD. Increased AUCs above the 20% threshold, and so mild ventilation heterogeneity, were also observed in ‘healthy’ participants with normal lung function and/or possible early signs of emphysema. And so, measuring ventilation heterogeneity with SPECT/CT may be useful in identifying patients with small airway abnormalities earlier than standard lung function tests.

Heterogeneous ventilation could alternatively be assessed by simply measuring CoV in the SPECT/CT image without any threshold. This would avoid the complications inherent to thresholding heterogeneous voxel data in SPECT or complex imaging analysis. Gibson et al. (7) utilised this approach in their asthma ventilation SPECT/CT study (7), and it was observed that ventilation heterogeneity, as measured with CoV, had significantly improved following monoclonal antibody treatment in patients with severe asthma. This simpler CoV analysis technique may be used to examine COPD severity and investigate treatment response.

6.4 Conclusion

For the first time, we have assessed current threshold methods for quantitative VSPECT/CT analysis and demonstrated there to be critical issues. However, we also validated a novel ‘curve-fitting’ threshold method, which had been demonstrated to be superior in both accuracy and robustness to existing methods. This simple method was also used to identify the number of ‘hot spots’ in COPD. This thesis has extensively examined not only relationships of non-ventilated volume and ‘hot spots’ count with each other but also their relationships with a wide variety of lung function measurements and their responses to bronchodilator and bronchoconstriction in COPD. These parameters may be useful as physiological markers or predictors for poor clinical outcomes. For future studies, the novel ‘curve-fitting’ method may be modified further to assess ventilation quality in addition to non-ventilated volume. It may also be used conjunctively with topographical analysis to better understand regional changes in ventilation and to identify patients who fail to respond to treatment.

6.5 References

1. Milne S, King GG. Advanced imaging in COPD: insights into pulmonary pathophysiology. J Thorac Dis. 2014;6(11):1570-85.
2. Johannessen A, Skorge TD, Bottai M, Grydeland TB, Nilsen RM, Coxson H, Dirksen A, Omenaas E, et al. Mortality by level of emphysema and airway wall thickness. Am J Respir Crit Care Med. 2013;187(6):602-8.
3. Han MK, Kazerooni EA, Lynch DA, Liu LX, Murray S, Curtis JL, Criner GJ, Kim V, et al. Chronic obstructive pulmonary disease exacerbations in the COPDGene study: associated radiologic phenotypes. Radiology. 2011;261(1):274-82.
4. Rutting S, Chapman DG, Thamrin C, Tang FSM, Dame Carroll JR, Bailey DL, Trifunovic M, Magnussen JS, et al. Effect of combination inhaled therapy on ventilation distribution measured by SPECT/CT imaging in uncontrolled asthma. J Appl Physiol (1985). 2021;131(2):621-9.
5. Nagao M, Murase K, Yasuhara Y, Ikezoe J. Quantitative analysis of pulmonary emphysema: three-dimensional fractal analysis of single-photon emission computed tomography images obtained with a carbon particle radioaerosol. AJR Am J Roentgenol. 1998;171(6):1657-63.
6. Norberg P, Persson HL, Carlsson GA, Bake B, Kentson M, Sandborg M, Gustafsson A. Quantitative lung SPECT applied on simulated early COPD and humans with advanced COPD. EJNMMI Res. 2013;3(1):28.
7. Gibson PG, Urroz Guerrero PD, Poon C, Rutherford N, Brooker B, Smith A, Grainge C, Wark PAB, et al. Ventilation Heterogeneity Is a Treatable Trait in Severe Asthma. The Journal of Allergy and Clinical Immunology: In Practice. 2024;12(4):929-35.e4.